

**Dissertation zur Erlangung des Doktorgrades
der Fakultät für Chemie und Pharmazie
der Ludwig-Maximilians-Universität München**

**The PIP1 protein expression is positively
regulated by PIP2;1 and PIP2;2 in
*Arabidopsis thaliana***

Chen Liu

aus

Shuangfeng, Hunan, China

2015

Erklärung

Diese Dissertation wurde im Sinne von § 7 der Promotionsordnung vom 28. November 2011 von PD Dr. Anton Schäffner betreut.

Eidesstattliche Versicherung

Diese Dissertation wurde eigenständig und ohne unerlaubte Hilfe erarbeitet.

München, am 26.02.2015

(Chen Liu)

Dissertation eingereicht am	26.02.2015
1. Gutachter:	PD Dr. Anton Schäffner
2. Gutachter:	Prof. Dr. Jörg Durner
Mündliche Prüfung am	15.04.2015

ABSTRACT

Aquaporins are water channel proteins ubiquitously present in all kingdoms. In plants, plasma membrane intrinsic proteins (PIPs) are aquaporins which are considered to be important for a tight and rapid control of membrane water permeability in response to various environmental stimuli. The model plant *Arabidopsis thaliana* harbours two subfamilies comprising five PIP1 and eight PIP2 isoforms. Although the regulation of single PIP isoforms by activation, relocalization and post-translational modification has been studied, the interaction and regulation between PIP1s and PIP2s remain mostly obscure. In a previous study in our laboratory, *pip2;2* and *pip2;1 pip2;2* loss-of-function lines led to an additional repression of PIP1 protein expression in the roots. However, due to the lack of specific antibodies a detailed quantification in different tissues and the identification of the affected PIP1 isoform(s) was missing and the mechanism underlying this regulation remained unknown.

This work shows that PIP1 protein expression is dependent on both PIP2;1 and PIP2;2 in the rosettes and roots, respectively. The *pip2;1 pip2;2* double mutant exhibited an additive, but stable reduction of PIP1 protein in both rosettes and roots, indicating the dependence of PIP1 expression on PIP2;1 and PIP2;2. A general reduction of all five PIP1 isoforms was identified in the *pip2;1 pip2;2* double mutant by quantitative mass spectrometry. The reduction of specific PIP1 isoforms (PIP1;1 and PIP1;2) was further determined by quantitatively comparing the PIP1 protein levels between *pip1* single mutants and *pip1* mutations introgressed into *pip2;1 pip2;2*. This result was independently supported by EGFP- and HA- tagged transgenic PIP1;1- and PIP1;2-expressing lines. The repression of PIP1 protein was not due to the downregulation of transcription and translation; all five *PIP1* genes were properly transcribed and PIP1 proteins were synthesized in the *pip2;1 pip2;2* double mutant based on transcriptional and translational analyses. Thus, PIP1s were obviously degraded via a so far not yet unravelled process. Preliminary

ABSTRACT

experiments, including co-immunoprecipitation and transient expression in protoplasts, indicate that PIP1;1 or PIP1;2 interacts with the immunologically related PIP2;1/PIP2;2/PIP2;3 and that the trafficking and/or stability of PIP1;1 or PIP1;2 is affected in the absence of PIP2;1 and PIP2;2. These observations suggest that PIP2;1 or PIP2;2 may work as indispensable partners of PIP1s, form a heterotetramer not only for the correct targeting of PIP1s, but also for stabilizing PIP1 proteins. These findings demonstrate a novel regulatory mechanism between PIP1s and PIP2s. The dependence of PIP1 protein expression on PIP2;1 and PIP2;2 may reveal a new aspect of a rapid control of the water conductivity and may provide a means to control the channel selectivity or other related functions by coupling the regulation of the abundance of PIP1 and PIP2 in response to different environmental challenges or specific plant development stages.

CONTENTS

ABSTRACT	I
CONTENTS	III
ABBREVIATIONS	IX
FIGURES AND TABLES	XI
1. INTRODUCTION	1
1.1. Aquaporins in plants	1
1.1.1. General overview and importance	1
1.1.2. Classification of aquaporins in plants	2
1.1.3. Structure and transport selectivity of aquaporins.....	3
1.1.4. Expression of aquaporins in plants.....	6
1.1.5. Interaction and trafficking of PIPs aquaporins in plants.....	8
1.1.6. Function and regulation of PIPs aquaporins in plants	9
1.1.7. PIP2;2-dependent repression of PIP1 protein	13
1.2. Aims of this work	16
2. RESULTS	17
2.1. The PIP1 protein level is dependent on both PIP2;1 and PIP2;2...	17
2.1.1. The PIP1 protein level is repressed in the <i>pip2;1</i> mutant, the <i>pip2;2</i> mutant and the <i>pip2;1 pip2;2</i> double mutant.....	17
2.1.2. Recovery of PIP1 protein level in <i>pip2;1</i> and <i>pip2;2</i> lines complemented with wild-type genes.....	20
2.2. The PIP1 protein level is enhanced by Hybrid-expression of PIP2;3	22
2.3. A general reduction of all five PIP1 isoforms is identified in the <i>pip2;1 pip2;2</i> double mutant by quantitative mass spectrometry	24
2.4. Specific PIP1 isoforms are affected in the <i>pip2;1</i> mutant, the <i>pip2;2</i> mutant and the <i>pip2;1 pip2;2</i> double mutant	25

2.4.1. Isolation and molecular characterization of <i>pip1</i> insertional mutants.....	25
2.4.2. The relative contribution of each PIP1 isoform to total PIP1 protein level is deduced from loss-of-function <i>pip1</i> mutant lines	27
2.4.3. Loss-of-function <i>pip1</i> mutant lines reveal that PIP1;1 and PIP1;2 isoforms are both affected in the <i>pip2;1 pip2;2</i> double mutant.....	29
2.4.3.1. The PIP1;1 protein level is affected in the <i>pip2;1 pip2;2</i> double mutant	30
2.4.3.2. The PIP1;2 protein level is affected in the <i>pip2;1 pip2;2</i> double mutant	31
2.4.4. Tagged <i>PIP1</i> transgenic lines further confirm the reduction of PIP1;1 and PIP1;2 protein in the <i>pip2;1</i> mutant, the <i>pip2;2</i> mutant and the <i>pip2;1 pip2;2</i> double mutant	34
2.4.4.1. Production and characterization of EGFP-tagged and HA-tagged PIP1;1 and PIP1;2.....	34
2.4.4.2. Quantitative analysis of tagged <i>PIP1;1</i> transgenic lines confirms the reduction of PIP1;1 protein level.....	39
2.4.4.3. Quantitative analysis of tagged <i>PIP1;2</i> transgenic lines verifies the reduction of PIP1;2 protein level.....	56
2.5. All five <i>PIP1</i> genes are not changed at the transcriptional level ..	72
2.6. All five <i>PIP1</i> transcripts are not affected at the translational level	74
2.7. PIP1;1 and PIP1;2 may physically interact with PIP2;1/PIP2;2/PIP2;3.....	78
2.8. Trafficking and/or stability of PIP1;1 and PIP1;2 proteins are influenced by PIP2;1 or PIP2;2.....	80
2.9. Pilot experiments to address the degradation analysis of PIP1 protein in the <i>pip2;1 pip2;2</i> double mutant	91
2.9.1. Co-localization analysis of EGFP-PIP1;1 fluorescence with different compartments	91
2.9.2. Pilot experiment to check whether the ubiquitin-26S proteasome system is involved in the degradation of PIP1 protein.....	94
2.9.3. Preliminary investigation of the degradation of the PIP1;1 and PIP1;2 protein	96

3. DISCUSSION	102
3.1. Reduction of the PIP1 protein level in <i>pip2</i> mutants depends mainly on PIP2;1 and PIP2;2	102
3.1.1. PIP1 expression is dependent on both PIP2;1 and PIP2;2	102
3.1.2. Multiple lines of evidence reveal that PIP1 isoforms are reduced in the <i>pip2;1 pip2;2</i> double mutant.....	104
3.2. Possible mechanisms underlying the PIP2;1/PIP2;2-dependence of PIP1 expression	106
3.2.1. Potential interaction between PIP1s and PIP2s may be involved in regulation of PIP2;1/PIP2;2-dependence of PIP1 expression.....	106
3.2.2. Possible mechanisms underlying the dependence of PIP1 expression on PIP2;1 and PIP2;2	111
3.3. Possible timing and localization of PIP1 protein degradation	118
3.3.1. ER-associated degradation or ER-phagy-related degradation of PIP1s in the <i>pip2;1 pip2;2</i> double mutant.....	118
3.3.2. Vesicle-associated vacuolar degradation of PIP1s in the <i>pip2;1 pip2;2</i> double mutant	123
3.4. Possible physiological role of dependence of PIP1s on PIP2;1 and PIP2;2	125
3.4.1. The dependence of PIP1s on PIP2;1 and PIP2;2 may prevent the ER stress	125
3.4.2. The dependence of PIP1s on PIP2;1 and PIP2;2 may influence water permeability or transport of other molecules (CO ₂ , NO, H ₂ O ₂ or NH ₃) in plants.....	126
4. MATERIALS AND METHODS	130
4.1. Materials	130
4.1.1. Plant materials.....	130
4.1.2. Vectors	134
4.1.3. Plasmids.....	135
4.1.4. Bacterial strains.....	135
4.1.5. Antibiotics.....	136
4.1.6. Chemicals.....	136

CONTENTS

4.1.7. Medium and solutions	136
4.1.8. Oligonucleotide primers.....	137
4.2. Methods	140
4.2.1. Plant methods	140
4.2.1.1. Growth conditions	140
4.2.1.2. Plant growth on soil.....	140
4.2.1.3. Seed surface sterilization.....	140
4.2.1.4. Sterile culture on solid medium.....	140
4.2.1.5. Plant growth in hydroponic culture	141
4.2.1.6. Generation of double/triple/quadruple mutants and backcrossing of single mutants	141
4.2.1.7. Production and/or characterization of transgenic lines.....	142
4.2.1.8. Seed harvesting and storage	143
4.2.2. Microbiological methods	143
4.2.2.1. Competent cells of <i>E. coli</i>	143
4.2.2.2. Heat shock transformation of <i>E. coli</i>	144
4.2.2.3. Competent cells of <i>Agrobacterium tumefaciens</i>	144
4.2.2.4. Electroporation of competent <i>Agrobacterium tumefaciens</i> cells ...	144
4.2.2.5. <i>Agrobacterium tumefaciens</i> mediated plant transformation	145
4.2.2.6. Miniprep plasmid DNA preparation	146
4.2.2.7. Midiprep plasmid DNA preparation	146
4.2.3. Molecular biology methods.....	146
4.2.3.1. PCR (Polymerase Chain Reaction)	146
4.2.3.2. PCR-based joining of fragments	147
4.2.3.3. PCR-based genotyping.....	148
4.2.3.4. Molecular cloning using single fragment or multisites two fragment Gateway™ recombination technology	148
4.2.3.5. DNA gel electrophoresis	149
4.2.3.6. Purification of PCR product and DNA gel extraction	150
4.2.3.7. Determination of nucleic acids concentration.....	150
4.2.3.8. Digestion by restriction endonucleases.....	150
4.2.3.9. DNA sequencing	151
4.2.3.10. Isolation of total RNA using Qiagen RNeasy Plant Mini Kit.....	151

4.2.3.11. Affinity isolation of ribosomes and extraction of RNA.....	151
4.2.3.12. Reverse Transcription Polymerase Chain Reaction (RT-PCR)	153
4.2.3.13. Quantitative real time polymerase chain reaction (qRT-PCR).....	154
4.2.3.14. Protoplast isolation and PEG-mediated transient expression.....	156
4.2.4. Protein methods	157
4.2.4.1. Whole protein extraction	157
4.2.4.2. RC-DC for determination of protein concentration	158
4.2.4.3. Microsomal fractions preparation	158
4.2.4.4. Bradford determination of protein concentration	159
4.2.4.5. LC-MS and LC-MS/MS-based label-free quantification	159
4.2.4.6. SDS polyacrylamide gel electrophoresis (SDS-PAGE).....	160
4.2.4.7. Western blot.....	161
4.2.4.8. Enzyme-linked immunosorbent assay (ELISA).....	163
4.2.4.9. Co-Immunoprecipitation.....	164
4.2.4.10. Degradation assay	165
4.2.5. Microscopy	166
5. REFERENCES	168
ACKNOWLEDGEMENTS.....	183
CURRICULUM VITAE	185

ABBREVIATIONS

ABRC	<i>Arabidopsis</i> Biological Resource Center
ABTS	2, 2'-azinobis(3-ethylbenzothiazoline-6-sulfonic acid)-diammonium salt
AGI	<i>Arabidopsis</i> Genome Initiative
ar/R	aromatic/Arg
BFA	Brefeldin A
BHT	3,5-Di-tert-4-butylhydroxytoluene
BSA	Bovine Serum Albumin
C	carboxyl
cDNA	complementary DNA
CHX	Cycloheximide
CLSM	Confocal Laser Scanning Microscope
COPII	Coat protein complex II
ddH ₂ O	double distilled water
DEPC	Diethylpyrocarbonate
DMSO	Dimethyl sulfoxide
DNA	Deoxyribonucleic acid
dNTPs	deoxynucleotide-5'-triphosphates
DOC	Sodium deoxycholate
DTT	Dithiothreitol
<i>E. coli</i>	<i>Escherichia coli</i>
EDTA	Ethylene Diamine Tetra-acetic Acid
EGFP	Enhanced Green Fluorescent Protein
EGTA	Ethylene glycol tetraacetic acid
ELISA	Enzyme-linked immunosorbent assay
ER	Endoplasmic Reticulum
ERAD	ER associated degradation
ERQC	ER quality control
GIP	GlpF-like Intrinsic Protein
GM	Germination medium
GUS	β-glucuronidase
h	hour
HA	Hemagglutinin
HIP	Hybrid Intrinsic Protein
kb	kilo base pair
kDa	kiloDalton
LB	Lysogeny broth
LC-MS	Liquid Chromatography-Mass Spectrometry
MES	2-(N-Morpholino)-ethanesulfonic acid
min	minute

ABBREVIATIONS

MIP	Major Intrinsic Protein
MS	Murashige and Skoog
MVBs	Multivesicular bodies
N	amino
NASC	Nottingham <i>Arabidopsis</i> Stock Center
NIP	Nodulin-26-like Intrinsic Protein
NPA	Asparagine-Proline-Alanine
OD	Optical Density
OSER	Organized Smooth Endoplasmic Reticulum
PAGE	Polyacrylamide gel electrophoresis
PBS	Phosphate-buffered saline
PCR	Polymerase Chain Reaction
PEB	Polysome Extraction Buffer
PEG	Polyethylene glycol
PIP	Plasma membrane Intrinsic Protein
PM	Plasma membrane
PMSF	Phenylmethylsulfonyl fluoride
PTE	Polyoxyethylene 10 tridecyl ether
PVC	Prevacuolar compartments
RC-DC	Reducing agent compatible detergent compatible
RIN	RNA Integrity Number
RNA	Ribonucleic acid
rpm	revolutions per minute
RT-PCR	Reverse Transcription Polymerase Chain Reaction
RT-qPCR	Real-time quantitative PCR
SD	Standard Deviation
SDS	Sodium Dodecyl Sulfate
SIP	Small basic Intrinsic Protein
SNARE	Soluble N-ethylmaleimide-sensitive factor attachment protein receptor
TAE	Tris-acetate-EDTA
TAIR	The <i>Arabidopsis</i> Information Resource
TBS	Tris-buffered saline
T-DNA	Transfer-DNA
TEMED	N,N,N',N'- Tetramethylethylenediamine
TIP	Tonoplast Intrinsic Protein
TRAP	Translating ribosome affinity innunopurification
UPS	Ubiquitin-26S Proteasome System
v/v	volume per volume
w/v	weight per volume
Wm	Wortmannin

FIGURES AND TABLES

FIGURES

Figure 1. Phylogenetic tree of 35 aquaporin homologues in <i>Arabidopsis thaliana</i> and their clustering in four subgroups.	3
Figure 2. Membrane topology of an aquaporin monomer.	5
Figure 3. Histochemical expression pattern of <i>PIP2;1</i> and <i>PIP2;2</i> in vegetative tissues.	8
Figure 4. PIP1 protein and PIP2 protein level in <i>pip1</i> mutants and <i>pip2</i> mutants.	14
Figure 5. Repression of PIP1 level in the <i>pip2;2</i> mutant and the <i>pip2;1 pip2;2</i> double mutant.	14
Figure 6. PIP1 protein level is reduced in the <i>pip2;1</i> mutant, the <i>pip2;2</i> mutant, and the <i>pip2;1 pip2;2</i> double mutant.	18
Figure 7. Reduction of PIP1 protein level in the <i>pip2;1 pip2;2</i> double mutant is independent of stage and tissue.	19
Figure 8. Recovery of total PIP1 protein level in <i>pip2;1</i> , <i>pip2;2</i> , <i>pip2;1 pip2;2</i> lines complemented with wild-type genes.	21
Figure 9. The relative PIP1 protein level is enhanced by hybrid-expression of <i>PIP2;3</i>	23
Figure 10. Molecular characterization of <i>pip1</i> mutants after backcrossing.	26
Figure 11. Relative contribution of each PIP1 isoform of PIP1 protein level.	27
Figure 12. Relative contribution of each PIP1 isoform to the PIP1 protein level in both the rosettes and roots.	28
Figure 13. Relative PIP1 protein levels in both the rosettes and roots of the <i>pip1;1</i> mutant and of <i>pip1;1</i> -related multiple mutants.	31
Figure 14. Relative PIP1 protein levels in both the rosettes and roots of the <i>pip1;2</i> mutant and of <i>pip1;2</i> -related multiple mutants.	32
Figure 15. Relative PIP1 protein levels in both the rosettes and roots of the <i>pip1;1 pip1;2</i> double mutant and of multiple mutants.	33
Figure 16. Illustration of the constructs for EGFP-tag fusion using GATEWAY™ two-fragment vector recombination method.	36
Figure 17. Subcellular localization of EGFP fusion transgenic lines.	37
Figure 18. Regenerated transgenic lines by crossing and genotyping.	37
Figure 19. Immunoblot analysis and fluorescence quantification of EGFP-PIP1;1 fusion protein in mesophyll protoplasts of transgenic lines.	41
Figure 20. Different regions of the root for quantification of fluorescence signal of EGFP-fusion protein.	42
Figure 21. Fluorescence signals of EGFP-PIP1;1 fusion protein in different root zones and quantification of fluorescence signals in the root zone IV.	43
Figure 22. Unknown compartments of EGFP-PIP1;1 were observed in the root maturation zone of two transgenic lines.	45

FIGURES AND TABLES

Figure 23. Fluorescence signals of the PIP1;1-EGFP fusion protein in different root zones and quantification of fluorescence signals in the root zone IV.	46
Figure 24. Immunoblot analysis and ELISA quantification of HA-PIP1;1 fusion protein in transgenic lines.	48
Figure 25. Fluorescence quantification of the EGFP-PIP1;1 fusion protein from mesophyll protoplasts of four different transgenic lines.....	50
Figure 26. Fluorescence quantification of the PIP1;1-EGFP fusion protein from mesophyll protoplasts of four different transgenic lines.....	52
Figure 27. Fluorescence signals of EGFP-PIP1;1 in root zone IV and quantification of fluorescence signals in four different backgrounds.	54
Figure 28. Fluorescence signals of PIP1;1-EGFP in root zone IV and quantification of fluorescence signals in four different backgrounds.	55
Figure 29. Immunoblot analysis and fluorescence quantification of EGFP-PIP1;2 fusion proteins in mesophyll protoplasts from two transgenic lines.	57
Figure 30. Immunoblot analysis and fluorescence quantification of PIP1;1-EGFP fusion protein in mesophyll protoplasts of two transgenic lines.....	59
Figure 31. Fluorescence signals of the EGFP-PIP1;2 fusion protein in different root zones and quantification of fluorescence signals in root zone IV.	61
Figure 32. Unknown compartments of EGFP-PIP1;2 were observed in the root maturation zone of two transgenic lines.	62
Figure 33. Fluorescence signals of PIP1;2-EGFP fusion protein in different root zones and quantification of fluorescence signal in root zone IV.....	63
Figure 34. Immunoblot analysis and ELISA quantification of the HA-PIP1;2 fusion protein in transgenic lines.	65
Figure 35. Fluorescence quantification of the EGFP-PIP1;2 fusion protein from mesophyll protoplasts of four different transgenic lines.....	67
Figure 36. Fluorescence quantification of the PIP1;2-EGFP fusion protein from mesophyll protoplasts of four different transgenic lines.....	68
Figure 37. Fluorescence signals of EGFP-PIP1;2 in root zone IV and quantification of fluorescence signals in four different backgrounds.	70
Figure 38. Fluorescence signals of PIP1;2-EGFP in root zone IV and quantification of fluorescence signals in four different backgrounds.	71
Figure 39. <i>PIP1</i> transcript levels were not altered in <i>pip2</i> mutants as shown by quantitative real-time PCR analysis.	73
Figure 40. Immunopurification of ectopically expressed HIS-FLAG-tagged ribosomal proteins driven by <i>PIP2;2</i> promoter.....	75
Figure 41. Quality control of total RNA and immunopurified polysomal RNA isolated from rosettes of transgenic lines by Bioanalyser™.	75
Figure 42. Transcriptional analysis of <i>PIP1s</i> and <i>PIP2s</i> of total RNA and immunopurified polysomal RNA from <i>PIP2;2</i> -expressing cells.	76
Figure 43. The Co-Immunoprecipitation experiment revealed the interaction between HA-PIP1;1 or HA-PIP1;2 and PIP2;1/PIP2;2/PIP2;3	79

Figure 44. Transient expression of *EGFP-PIP1;1* singly (left) or co-expressed *EGFP-PIP1;1* with *35S_{pro}:PIP2;2* (right) in mesophyll protoplasts of different mutants. 81

Figure 45. Transient expression of *EGFP-PIP1;2* singly (left) or co-expressed *EGFP-PIP1;2* with *35S_{pro}:PIP2;2* (right) in mesophyll protoplasts of different mutants. 82

Figure 46. Localization and expression analysis of *EGFP-PIP1;1* in protoplasts of *PIP2;1-mCherry* line..... 84

Figure 47. Time-lapse images of two different shapes and movements of fluorescence compartments of *EGFP-PIP1;1* in mesophyll protoplasts. 85

Figure 48. Confocal pictures of *pip1;1 pip2;1 pip2;2* triple mutant protoplasts 14 h and 20 h after transformation. 87

Figure 49. The stability of *EGFP-PIP1;1* was influenced by the constitutive expression of *PIP2;1* and *PIP2;2*. 88

Figure 50. The stability of *EGFP-PIP1;2* was influenced by the constitutive expression of *PIP2;1* and *PIP2;2*. 89

Figure 51. Co-localization analysis with Wave 13R (trans-Golgi network/early endosome) and Wave 27R (Post-Golgi/endosomal) and *EGFP-PIP1;1*. 92

Figure 52. Co-localization analysis of Wave 7R (Late endosome/pre-vacuolar compartment) and *EGFP-PIP1;1*. 93

Figure 53. Live-cell fluorescence microscopy of co-localization analysis of Wave 11R (Late endosome/ Vacuole) and *EGFP-PIP1;1*..... 94

Figure 54. Immunoblotting and quantification analysis of MG132 treatment with mesophyll protoplasts of the wild-type line and the *pip2;1 pip2;2* double mutant..... 95

Figure 55. Confocal observation of BFA-induced compartments in the root elongation zones and the maturation zones of different transgenic lines. 98

Figure 56. Confocal observation of Wortmannin-induced compartments (*EGFP-PIP1;1*) in the root elongation zones and the maturation zones of different transgenic lines. 99

Figure 57. Confocal observation of Wortmannin-induced compartments (*PIP1;2-EGFP*) in root maturation zone of different transgenic lines..... 100

Figure 58. Relative protein abundance profile of five *PIP1*s and eight *PIP2*s in leaf and root of *Arabidopsis*. 104

Figure 59. Coexpression analyses of aquaporin transcripts and protein-protein interaction (ATTED-II) and Genevestigator analysis of *PIPs* gene expression in different tissues..... 109

Figure 60. Protein-protein interaction network. 110

Figure 61. Protein-protein binding site prediction according to ISIS2 analysis..... 116

Figure 62. Clustal W multiple sequence alignment of *PIP* isoforms. 117

Figure 63. Protein-protein interaction analysis with membrane-based interactome database. 120

TABLES

Table 1. A general reduction of five PIP1 isoforms was identified in the *pip2;1 pip2;2* double mutant by LC-MS/MS-based label-free quantification. 24

Table 2. *Arabidopsis* PIP single mutants backcrossed and used in this study. 25

Table 3. *pip1* single and multiple mutants used in this work. 26

Table 4. List of expression constructs in binary vectors and the name of transgenic lines generated in this work..... 37

Table 5. The EGFP fusion of transgenic lines in different mutant backgrounds and their names used in this work..... 38

Table 6. The HA fusion of transgenic lines in different mutant backgrounds and their names used in this work..... 38

Table 7. List of transgenic lines of tagged-PIP1;1 generated in this work. 131

Table 8. List of transgenic lines of tagged-PIP1;2 generated in this work. 132

Table 9. List of transgenic lines of hybrid-lines and inducible-lines in different mutant backgrounds generated in this work..... 133

Table 10. List of transgenic lines selected and used for translatoe analysis. 133

Table 11. Vectors 134

Table 12. Plasmids generated in this work..... 135

Table 13. Bacterial strains..... 135

Table 14. Antibiotics..... 136

Table 15. Chemicals 137

Table 16. The primers used for the characterization of mutants. 137

Table 17. The primer sequences of reference genes used for RT-qPCR. 138

Table 18. The primers used for the production of transgenic lines using Gateway™ recombination 138

Table 19. The primers used for the production of PIP2;1/PIP2;2-cDNA constructs using Gateway™ recombination. 139

1. INTRODUCTION

1.1. Aquaporins in plants

1.1.1. General overview and importance

Water, as a solvent and reactant, is a basic requirement for all living organisms. Many functionalities of molecules, cells and organs are dependent on water (Alleva *et al.*, 2012). The necessity of a tight and accurate regulation of water flow invoked a broad range of investigations addressing the question of how water could rapidly pass through biological membranes. Subsequently, these studies contributed to the discovery of aquaporins (Ray, 1960; Agre *et al.*, 1987). CHIP28 from erythrocytes was the first aquaporin characterized as having water channel activity in *Xenopus* oocytes or inserted in proteoliposomes, respectively. Water permeation is passive and driven by osmotic or hydraulic pressure gradients (Agre *et al.*, 1987; Preston and Agre, 1991; Preston *et al.*, 1992). This remarkable breakthrough sparked a great number of studies on aquaporins. In the last twenty years, the characterization of aquaporins in different phylogenetic kingdoms and the establishment of their relationship with the cell water homeostasis were the main targets of this research field.

Plants as sessile organisms have to take up water from the surrounding environment mainly via their root system. Once water is absorbed by the roots, its transport and distribution in the plant body relies on three distinct and co-existing pathways: the extracellular apoplastic path around the protoplast, the symplastic path with the cytoplasmatically connected cells through plasmodesmata, and the transcellular path across the cell membranes (Steudle and Peterson, 1998; Steudle, 2001). The involvement of aquaporins in the transcellular path is essential for plants when an apoplast barrier exists in certain tissues, such as the exodermis and endodermis of roots or the suberized bundle sheath cells of leaves (Schäffner, 1998; Suga *et al.*, 2003; Vandeleur *et al.*, 2009; Hachez *et al.*, 2012; Prado *et al.*, 2013) or

when high rates of transcellular water transport are required by plants. Recent investigations have also focussed on the diversity of the transport selectivity of aquaporins including water and other small, uncharged molecules, suggesting their involvement in many other physiological processes (Bienert *et al.*, 2008; Gomes *et al.*, 2009).

Furthermore, many studies tackle a wide range of regulations of aquaporins in plants. The existence and control of channel gating or localization studies in resting or stress conditions, for instance, are also intensively explored. These recent discoveries about aquaporins bring new insights about their regulatory network and shed new light on their physiological roles in plants (Hachez and Chaumont, 2010; Luu and Maurel, 2013; Li *et al.*, 2014).

1.1.2. Classification of aquaporins in plants

Aquaporins belong to the major intrinsic protein (MIP) family, which are ubiquitously present in all kingdoms. Plants exhibit a higher multiplicity of isoforms, including 30 to more than 70 homologues in monocots and eudicots in comparison to only 10 to 13 different aquaporins in mammals (Verkman and Mitra, 2000; Chaumont and Tyerman, 2014). Plant aquaporins are divided into four subfamilies based on sequence similarity, which basically correlates to their specific membrane localization. The model plant *Arabidopsis thaliana* harbours 35 MIP homologues (Johanson *et al.*, 2001; Quigley *et al.*, 2002), divided into 13 plasma membrane intrinsic proteins (PIPs), which can be further split into PIP1 (five isoforms) and PIP2 (eight isoforms) subfamilies, ten tonoplast intrinsic proteins (TIPs), nine nodulin-26-like intrinsic proteins (NIPs), which have been reported to be localized both at the plasma membrane and at intracellular membranes (Mizutani *et al.*, 2006; Takano *et al.*, 2006), and three small basic intrinsic proteins (SIPs), which are mainly localized in the endoplasmic reticulum (ER) (Johanson *et al.*, 2001; Johanson and Gustavsson, 2002; Ishikawa *et al.*, 2005) (Figure 1).

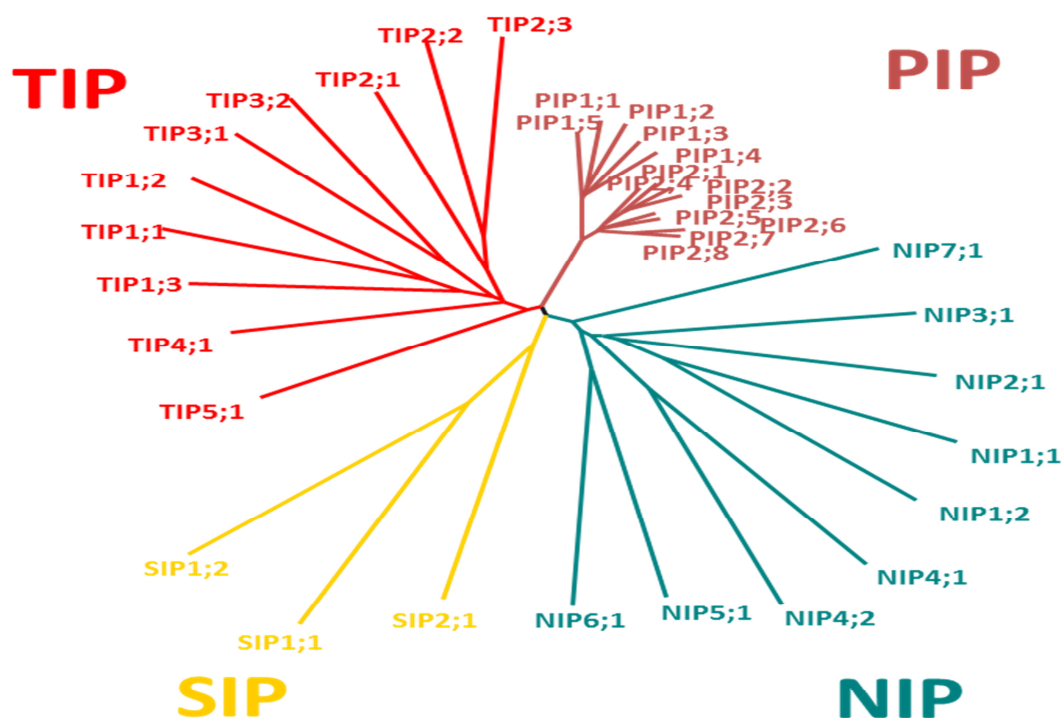


Figure 1. Phylogenetic tree of 35 aquaporin homologues in *Arabidopsis thaliana* and their clustering in four subgroups.

In addition, three other aquaporin subfamilies have been identified: the GlpF-like intrinsic proteins (GIPs), the hybrid intrinsic proteins (HIPs), which have been found in the moss *Physcomitrella patens* (Gustavsson *et al.*, 2005; Danielson and Johanson, 2008), and the uncategorized X intrinsic proteins (XIPs), which have been identified in a wide variety of non-vascular and vascular plants (Borstlap, 2002; Danielson and Johanson, 2008; Gupta and Sankararamakrishnan, 2009; Sade *et al.*, 2009; Park *et al.*, 2010; Bienert *et al.*, 2011; Lopez *et al.*, 2012).

1.1.3. Structure and transport selectivity of aquaporins

In 1999, the first high-resolution three-dimensional structure of AQP1 at 4.5 Å resolution revealed how water molecules move through the channel (Mitsuoka *et al.*, 1999). Aquaporins are small transmembrane proteins (21-34 kDa) which exhibit conserved structural features in all living organisms. Typically an aquaporin monomer contains six transmembrane α -helices connected by five loops (A to E), with N- and C-terminal domains protruding into the cytosol. Two highly conserved

asparagine-proline-alanine (NPA) motifs, which are localized at the relatively hydrophobic cytosolic loop B and the extracytosolic loop E, respectively, inserted halfway into the membrane from opposite sides participating in forming a pore with high selectivity (Figure 2). The pore consists of a size exclusion zone, together with an aromatic/Arg (ar/R) constriction called selectivity filter, which contributes to the substrate selectivity and controls water molecules passing the channel in a single-file manner (Murata *et al.*, 2000; Fujiyoshi *et al.*, 2002). By electron microscopy and X-ray crystallography, the structure of yeast aquaporin1 has been recently determined at a sub-Ångstrom resolution (0.8 Å). This further revealed that water molecules flow through an aquaporin channel in a pairwise manner (Kosinska Eriksson *et al.*, 2013).

Aquaporins form homo- and/or hetero-tetramers in the membrane. An AQP1 monomer interacts with two neighbouring monomers via membrane spanning with α -helices and loops that contribute to tetramer stability, wherein each monomer works as a functional unit (Murata *et al.*, 2000; Sui *et al.*, 2001; Fetter *et al.*, 2004; Yaneff *et al.*, 2014). Homo- and/or hetero-tetramers could form a fifth pore, known as the central pore, which is considered to be a pathway facilitating the transport of ions (K^+ , Cs^+ , Na^+ and Me_4N^+) or gases (CO_2 , O_2 , NH_3) across the membrane (Muller *et al.*, 2002; Yool and Weinstein, 2002; Kruse *et al.*, 2006; Bertl and Kaldenhoff, 2007; Wang *et al.*, 2007).

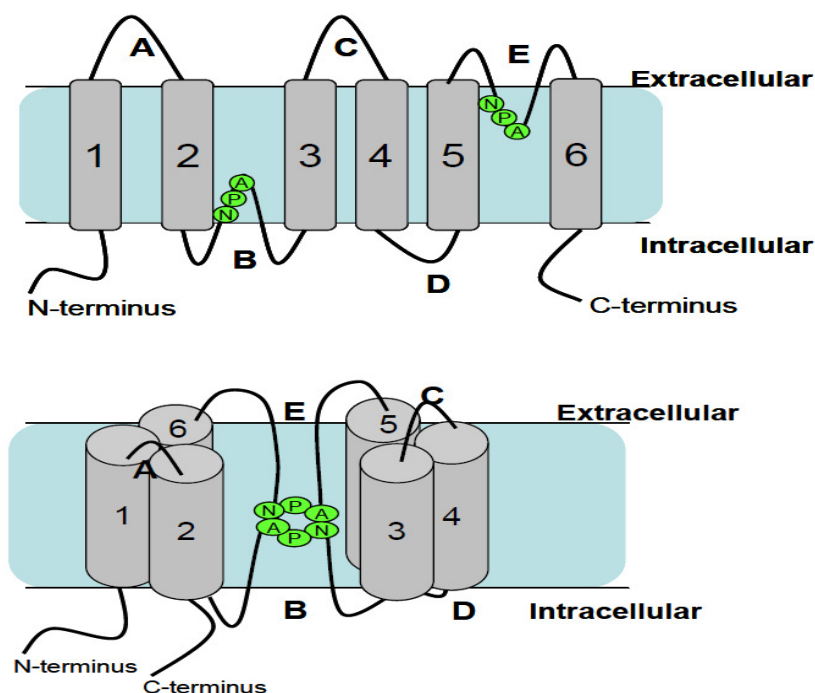


Figure 2. Membrane topology of an aquaporin monomer.

Six trans-membrane α -helices (1 to 6) are connected by five loops (A to E). N- and C-terminal domains are localized in the cytosol. The loop B and loop E both containing the highly conserved NPA motifs are folded halfway into the membrane from opposite sides, forming a single aqueous pore with high selectivity.

As indicated, aquaporins were initially regarded as water channels, yet a constantly increasing number of studies have demonstrated that some aquaporin isoforms are multifunctional channels with a growing range of substrates (Bienert *et al.*, 2007; Bienert *et al.*, 2008; Gomes *et al.*, 2009). Some homologues have been shown to facilitate the transport of other small uncharged molecules, including urea (Gerbeau *et al.*, 1999), glycerol (Biela *et al.*, 1999), carbon dioxide (Uehlein *et al.*, 2003), ammonia (Holm *et al.*, 2005), hydrogen peroxide (Bienert *et al.*, 2007; Dynowski *et al.*, 2008), boric acid (Takano *et al.*, 2006), silicic acid (Ma *et al.*, 2006) and arsenic acid (Bienert and Jahn, 2010). These findings indicate that aquaporins may participate in various physiological processes not only related to water homeostasis, but also involved in nutrient acquisition, nitrogen and carbon fixation, or signalling processes (Maurel, 2007).

1.1.4. Expression of aquaporins in plants

In plants, aquaporins have been reported to be highly expressed in the places where a high rate of cell to cell water transport is required (Javot *et al.*, 2003; Hachez *et al.*, 2008; Da Ines *et al.*, 2010). The expression levels of aquaporins at different developmental stages and in different tissues and organs may provide first hints for their physiological role. The transcript abundance of *PIPs* and *TIPs* at different ages and in different organs has been examined in *Arabidopsis*. The relatively high abundance of *PIPs* and *TIPs* as compared to other *MIP* homologues highlights their importance in transcellular water transport and cell osmoregulation (Jang *et al.*, 2004; Alexandersson *et al.*, 2005; Boursiac *et al.*, 2005; Alexandersson *et al.*, 2010). High expression levels of *TIP3;1*, *TIP3;2*, and *TIP5;1*, along with low gene expression of the whole *PIP* family have been revealed in dry seeds. Transcript levels of *TIP1s*, *TIP2s* and *PIPs* subfamily (especially *PIP1;2*) are highly induced during the seedling developmental stages (Vander Willigen *et al.*, 2006). In two-week-old *Arabidopsis* seedlings, *PIP1;1*, *PIP1;2* and *PIP2;7* show higher transcript levels both in aerial parts and in roots as compared to other *PIP* isoforms (Jang *et al.*, 2004). In fully developed *Arabidopsis* plants at the vegetative state (four- to five-week-old), *PIP1;2*, *PIP2;1* are highly expressed both in leaves and in roots, *PIP2;6* is highly expressed in leaves, *PIP1;1*, *PIP2;2*, *PIP2;4* are other genes with a dominant expression in roots (Alexandersson *et al.*, 2005). In addition to gene expression, the protein abundance of *PIPs* in roots and leaves has been quantitatively determined in *Arabidopsis*. The protein amount of *PIP1;1*, *PIP1;2*, *PIP2;1* shows dominant expression in rosettes and roots. *PIP2;7* exhibits a high abundance in rosettes, *PIP2;2* and *PIP2;4* exhibit a high abundance in roots (Monneuse *et al.*, 2011). *PIP2;6* exhibits high transcript level in leaves, but with a relative low amount of protein in developing stages (Jang *et al.*, 2004; Monneuse *et al.*, 2011). The transcript level and protein levels of remaining *PIP* isoforms and other *MIP* genes are lower in roots, leaves and flowers (Alexandersson *et al.*, 2005;

Monneuse *et al.*, 2011). Interestingly, the transcript and protein levels of *PIPs* are more abundant in the roots than in the leaves (Alexandersson *et al.*, 2005). Some aquaporin isoforms with a lower abundance but expressed in a specific cell type could play an essential role with regard to plant water relations, for instance, in guard cells or bundle sheath cells.

Taking advantage of the promoter driven β -glucuronidase (GUS) reporter, the spatial expression pattern of specific aquaporin isoforms has also been analysed (Javot *et al.*, 2003; Da Ines, 2008; Alexandersson *et al.*, 2010; Da Ines *et al.*, 2010; Postaire *et al.*, 2010; Peret *et al.*, 2012; Prado *et al.*, 2013; Zhao *et al.*, 2013). These studies on specific aquaporin isoforms confirmed their differential expression in different organs, and revealed additional information regarding the putative functional identity of the isoforms. For instance, staining of GUS fusion lines in combination with their cross-sections have shown that PIP1;1, PIP1;2, PIP2;1, PIP2;2, PIP2;4 and PIP2;7 are highly expressed in the roots. Interestingly, PIP1;1 and PIP2;4 are observed exclusively in the outer layers (from pericycle to epidemis). PIP2;1 and PIP2;2 are highly expressed in the stele and less in outer layers. PIP1;2 and PIP2;7 are expressed both in the outer layers and the stele (Zhao *et al.*, 2013). The distinct connection between expression pattern, protein abundance, and function could be further highlighted by the following examples: the promoter fusion line *PIP2;1_{pro}:GUS* fusion shows intense staining of vascular tissue, endodermal cells and bundle sheath cells. *PIP2;2_{pro}:GUS* fusion, on the other hand, is observed to be highly expressed in endodermis and stele (Figure 3). The cross-section of GUS-stained roots further reveal that PIP2;1, PIP2;2 are both highly expressed at the xylem poles and adjacent pericycle cells where lateral root primordium originates (Zhao *et al.*, 2013). Loss of function in PIP2;1 and PIP2;2 both result in retarded lateral root emergence and exhibit a reduced water flux from roots to leaves, emphasizing the role of both isoforms in plant development and water transport (Da Ines *et al.*, 2010; Peret *et al.*, 2012).

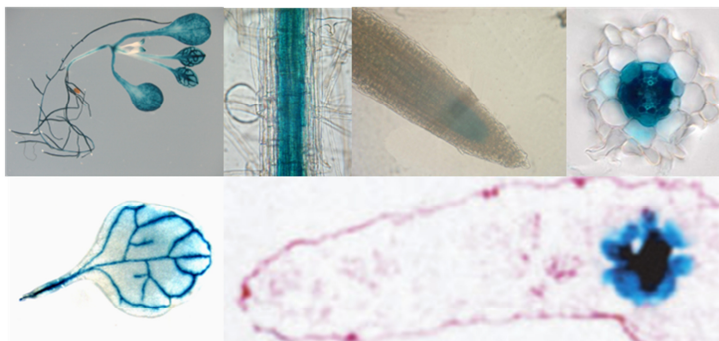
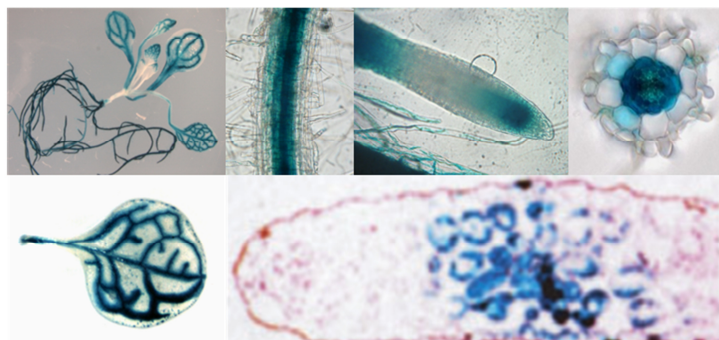
PIP2;1_{pro}:GUS***PIP2;2_{pro}:GUS***

Figure 3. Histochemical expression pattern of *PIP2;1* and *PIP2;2* in vegetative tissues.

The figures of *PIP2;1_{pro}:GUS* fusion and *PIP2;2_{pro}:GUS* fusion were combined from (Da Ines, 2008; Da Ines *et al.*, 2010) (Zhao, Dissertation, 2013).

1.1.5. Interaction and trafficking of PIPs aquaporins in plants

In plants, aquaporins are synthesized in the endoplasmic reticulum and specifically targeted to certain membranes via the classical secretory pathway (Hachez *et al.*, 2013; Luu and Maurel, 2013). Since the cellular membrane permeability largely depends on the density and activity of channels in the membrane, the trafficking of aquaporins is widely regarded as a critical point in regulating aquaporin expression and function. Recent studies have been mainly focussed on PIPs, revealing several mechanisms related to PIP trafficking. In yeast, a diacidic motif DXE (Asp-X-Glu) acts as an ER export signal interacting with Sec24p, the main cargo selection protein of the coat protein complex II (COPII) (Miller *et al.*, 2003). This interaction promotes the trafficking of the channels to the plasma membrane. Mutation of this motif in PIP2s from *Zea mays* and *Arabidopsis thaliana* leads to ER-retained ZmPIP2s or ER-retained AtPIP2s (Zelazny *et al.*, 2009; Sorieul *et al.*, 2011). The

determination of a new motif LXXXA in the transmembrane helix3 reveals a novel anterograde signal for ZmPIP2;5 export from the endoplasmic reticulum and targeting to the plasma membrane (Chevalier *et al.*, 2014). However, this motif is also not sufficient to mediate a plasma localization for ZmPIP1;2, indicating the existence of other retention signals which retain ZmPIP1;2 in the endoplasmic reticulum (Chevalier *et al.*, 2014). More interestingly, a growing number of experimental studies have demonstrated that ER-retained PIP1s could be targeted to the plasma membrane by physically interacting with PIP2s via forming hetero-oligomers (Fetter *et al.*, 2004; Zelazny *et al.*, 2007; Chen *et al.*, 2013; Jozefkowicz *et al.*, 2013; Yaneff *et al.*, 2014). More recently, the post-Golgi trafficking of PIPs has been shown to depend on the physical interaction with syntaxin of plants (ZmPIP2;5 with SYP121, AtPIP2;7 with SYP61 and SYP121), which are Qa-soluble *N*-ethylmaleimide-sensitive factor attachment protein receptors (SNAREs) known to mediate vesicular trafficking (Geelen *et al.*, 2002; Besserer *et al.*, 2012; Hachez *et al.*, 2014). In addition, BEX5 (BFA-visualized exocytotic trafficking defective) has also been identified as a new protein regulating post-Golgi trafficking of PIPs (Feraru *et al.*, 2012). The endocytosis and enhanced recycling of PIPs during salt stress or enhanced cellular H₂O₂ condition indicate that relocalization of PIPs from the plasma membrane could be an important mean to rapidly respond to changing environments (Boursiac *et al.*, 2008; Luu *et al.*, 2012; Martiniere *et al.*, 2012). The relocalization of specific PIPs will be further discussed below in the context of regulation studies. Even though the targeting of PIPs to the plasma membrane still leaves open questions, the importance of PIP trafficking and recycling for transmembrane water movement is conclusive (Hachez *et al.*, 2013).

1.1.6. Function and regulation of PIPs aquaporins in plants

In plants, activation and relocalization of aquaporins are considered to be important for a rapid control of cellular membrane water permeability (Chaumont *et al.*, 2005; Maurel *et al.*, 2008). On another level of regulation, post-translational modifications

are crucial for aquaporin function, for instance, phosphorylation (Johansson *et al.*, 1998; Santoni *et al.*, 2003; Daniels and Yeager, 2005; Prak *et al.*, 2008), methylation (Santoni *et al.*, 2006), deamidation, acetylation (di Pietro *et al.*, 2013), ubiquitylation (Lee *et al.*, 2009), disulfide bond formation (Bienert *et al.*, 2012), heteromerization (Fetter *et al.*, 2004; Yaneff *et al.*, 2014), protonation (Törnroth-Horsefield *et al.*, 2006), glycosylation, or palmitoylation (Hemsley *et al.*, 2013). These multiple post-translational regulation mechanisms are involved in processes which could regulate aquaporin gating, localization and stability in response to different environmental conditions and hormonal stimuli (di Pietro *et al.*, 2013).

Gating of PIPs has been reported to be controlled by protons and/ or Ca^{2+} but also by phosphorylation as an important regulation of the channel's closed and open conformation, thereby modulating the channel activity (Gerbeau *et al.*, 2002; Tournaire-Roux *et al.*, 2003; Törnroth-Horsefield *et al.*, 2006; Verdoucq *et al.*, 2008; Nyblom *et al.*, 2009; Frick *et al.*, 2013).

Relocalization of PIPs may provide another essential way to rapidly regulate the channel abundance and activity in their target membrane as a quick response to a changing environment. Hetero-oligomerization has been reported as a possible strategy to regulate the activity or trafficking of oligomeric protein complexes. Although some aquaporins are considered to form homotetramers by structural studies (Fu *et al.*, 2000; Murata *et al.*, 2000; Fotiadis *et al.*, 2001). Some plant PIPs have been demonstrated to form heterotetramers (Harvengt *et al.*, 2000; Fetter *et al.*, 2004; Zelazny *et al.*, 2007; Yaneff *et al.*, 2014). The importance of oligomerisation for the functionality of plant aquaporins is supported by experimental data. Plant PIP2s generally display high water channel activity in *Xenopus oocytes*, yeast and plant protoplasts. However, PIP1s are sometimes inactive or have a lower water channel activity as compared to PIP2s when they are transiently expressed alone in those expression systems (Johansson *et al.*, 1998; Chaumont *et al.*, 2000; Temmei *et al.*, 2005). In maize protoplasts, endoplasmic reticulum retention of ZmPIP1;2 is

observed unless it is coexpressed with ZmPIP2, which restores the plasma membrane targeting, a finding further supported by experiments proving the physical interaction of those proteins (Zelazny *et al.*, 2007). In addition to the relocalization effect of ZmPIP2s on ZmPIP1;2 in maize protoplasts, a synergistic activation effect is observed in *Xenopus oocytes*. When ZmPIP1;2 was co-expressed with ZmPIP2s, the membrane water permeability was enhanced compared to expression of ZmPIP2s alone (Fetter *et al.*, 2004). This phenomenon has been supported by experiments in various species (Mut *et al.*, 2008; Matsumoto *et al.*, 2009; Vandeleur *et al.*, 2009; Chen *et al.*, 2013; Yaneff *et al.*, 2014), suggesting that heteromerization may not only influence the targeting of PIP1s to the plasma membrane but also modulate or enhance the intrinsic activity of the channel (Fetter *et al.*, 2004; Yaneff *et al.*, 2014). Despite the effect of PIP2s on PIP1s trafficking, their mutual regulation remains unclear.

Relocalization of PIPs from the plasma membrane into endosomes exhibit another essential way to control the abundance of channels in the plasma membrane in response to osmotic and salt stress (Boursiac *et al.*, 2005; Boursiac *et al.*, 2008; Luu *et al.*, 2012). In *Arabidopsis thaliana*, AtPIP2;1 is endocytosed into the cytosol either via clathrin-coated vesicles under resting conditions (Dhonukshe *et al.*, 2007), or in a raft-associated manner in response to salt stress (Li *et al.*, 2011). Accordingly, there are at least two co-existing pathways involved in regulating the PIPs abundance in the plasma membrane depending on environmental conditions. The constitutive cycling of AtPIP2;1 is significantly enhanced in response to salt stress and high cellular H₂O₂ concentration (Luu *et al.*, 2012). Phosphorylation and dephosphorylation of the C-terminus of AtPIP2;1 has been shown to regulate the localization in these conditions (Prak *et al.*, 2008). Stress-induced PIP internalization is often associated with a strong decrease of root water uptake or permeability (Boursiac *et al.*, 2008; Prak *et al.*, 2008), suggesting that the plant could rapidly and reversibly modulate the cellular water homeostasis by regulating

the PIPs abundance in the plasma membrane or in the whole cell level. With regards to the relocalization and life cycle of PIPs, protein degradation might be another important factor in stress-invoked fast regulation of PIP activity.

Surprisingly, a significant decrease in the abundance of AtPIP1 proteins is observed in whole-cell extracts half an hour after salt exposure, whereas the transcriptional level remains unchanged (Boursiac *et al.*, 2005). Downregulation of AtPIP1 protein may interfere with the function of PIP2s through relocalization, possibly causing the rapid inhibition of root water permeability response after stress (Boursiac *et al.*, 2005). The underlying mechanisms of the downregulation of PIP1 have not been elucidated so far. Furthermore, overexpressed ER-retained AtPIP2;1 colocalized with AtPIP1;4 and AtPIP2;1, which may suggest that ER-retained AtPIP2;1 interacts with other PIPs to interfere with their proper trafficking or stability, thus causing the inhibition of root cell hydraulic conductivity (Sorieul *et al.*, 2011). However, whether the interplay between PIP1 and PIP2 truly relies on their interaction and whether this interaction further influences their stability still remains poorly understood in *Arabidopsis*.

In general, there are two pathways for cellular protein degradation of membrane proteins: polyubiquitylation with subsequent targeting to the proteasome or vesicle-associated vacuolar degradation in an endocytotic process. AtPIP2;1 was shown to be polyubiquitylated by the pepper ubiquitin ligase Rma1H1 in the endoplasmic reticulum, followed by degradation via the proteasome (Lee *et al.*, 2009). The transgenic line overexpressing Rma1H1 exhibited enhanced drought tolerance, suggesting that degradation of AtPIP2;1 may play a role in regulating the cellular mechanism underlying drought tolerance. The fate of endocytosed PIPs is still in debate. Either the proteins could be directly recycled back to the plasma membrane or they are directed to multivesicular bodies (MVBs) to be recycled or degraded (Dhonukshe *et al.*, 2007). In addition, a vacuole-associated accumulation of AtPIP2;1-GFP signal was observed after dark treatment in combination with lytic

vacuole inhibitor treatment experiments. This indicates that AtPIP2;1-GFP like other plasma membrane proteins PIN2 and BRI1 are targeted to the vacuole for degradation in resting conditions (Kleine-Vehn *et al.*, 2008). Both pathways lead to the degradation of AtPIP2;1, suggesting the existence of alternative mechanisms regulating the PIPs protein level in the target membrane and in the cell. The degradation pathways of other PIPs remain unknown. The existence of ER-associated or autophagy-related degradation in PIPs has not yet been verified.

Deciphering the network of mechanisms that modulate PIP activity, localization, and stability in the whole cell is essential to improve the current knowledge on PIP regulation and function (Hachez *et al.*, 2013).

1.1.7. PIP2;2-dependent repression of PIP1 protein

Previous analyses in our lab had shown that PIP1 protein was expressed at a lower level in the root of *pip2;2* mutants (*pip2;2-3* and *pip2;2-4*) and especially prominent in the root of the *pip2;1 pip2;2* double mutant, but not in the other *pip2* loss-of-function mutants of *Arabidopsis thaliana*. On the other hand, no significant repression of PIP2 protein (PIP2;1/PIP2;2/PIP2;3) had been observed in the *pip1;1* and *pip1;2* mutants (Da Ines, 2008; Da Ines and Geist, unpublished; Figure 4). Moreover, no concomitant down-regulation of *PIP1* transcripts of *pip2;2* mutants had been observed using an Affymetrix ATH microarray, indicating that the interference should occur at the post-transcriptional level (Da Ines, 2008). The repression of PIP1 might indicate that the stability of PIP1 protein is altered in the loss-of-function mutant of *PIP2;2*. Instead of being retained in the endoplasmic reticulum or mistargeted to other membranes, PIP1 protein may be degraded by a yet unknown mechanism. The dependence of PIP1 protein on the *PIP2;2* possibly indicates a novel regulation between PIP1 and PIP2 subfamilies. This PIP1 repression was observed both in the microsomal fraction and in the plasma membrane.

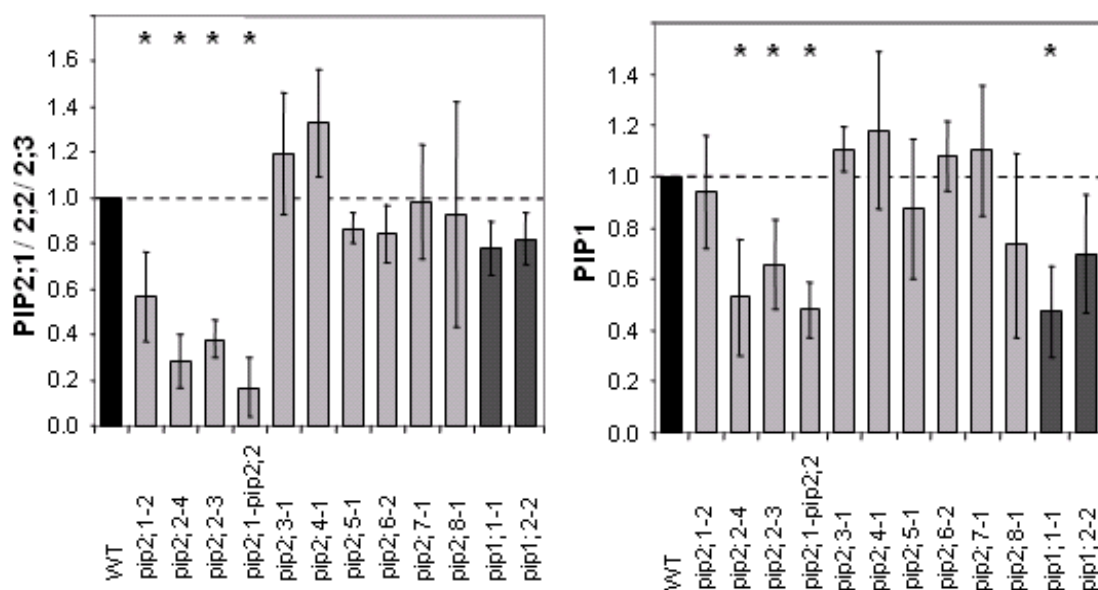


Figure 4. PIP1 protein and PIP2 protein level in *pip1* mutants and *pip2* mutants.

PIP1 and PIP2 protein levels were determined by immunoblotting using anti-PIP1 and anti-PIP2;1/PIP2;2/PIP2;3 antibodies (Da Ines and Geist, unpublished). Anti-PIP1 antiserum recognizes all five PIP1 members, which are highly similar; Anti-PIP2;1/2;2/2;3 antiserum specifically recognizes these three PIP2 isoforms. Error bars are \pm SD.

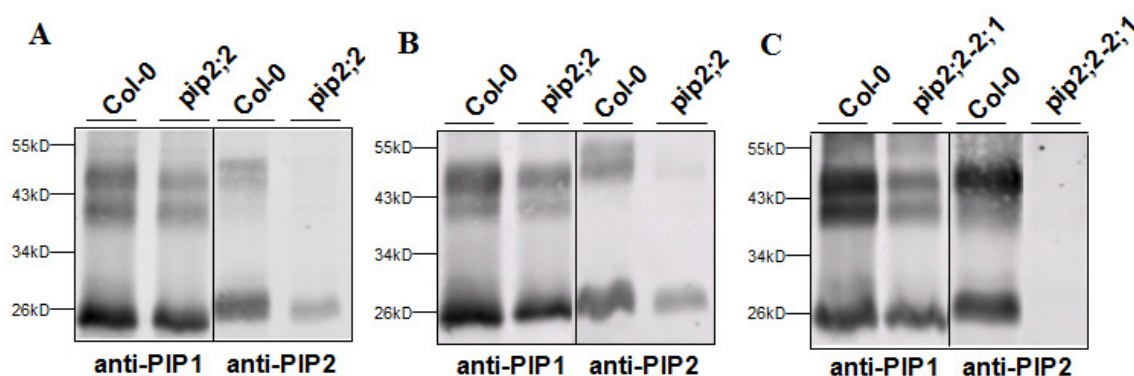


Figure 5. Repression of PIP1 level in the *pip2;2* mutant and the *pip2;1 pip2;2* double mutant.

Microsomal fraction (A) and plasma membrane (B and C) were isolated and used for immunoblotting with the same antibodies described above (Zhao, unpublished).

Microsomal fraction (containing intracellular membranes and the plasma membrane) and plasma membrane proteins were analyzed by immunoblotting using anti-PIP1 or anti-PIP2;1/PIP2;2/PIP2;3 antibodies, respectively, which exhibited 20-50% repression of PIP1 level in the *pip2;2* mutant and the *pip2;1 pip2;2* double mutant as compared to the wild type (Zhao, unpublished; Figure 5). Since the anti-PIP1

antiserum detects all five isoforms, the affected individual *PIP1* isoforms cannot be deduced from this study.

The repression of PIP1 might indicate that the stability of PIP1 proteins is altered in the loss-of-function mutant of *PIP2;2*. Instead of being retained in the endoplasmic reticulum or mistargeted to other membranes, PIP1 proteins may be degraded by a yet unknown mechanism. The dependence of PIP1 proteins on PIP2;2 possibly indicates a novel regulation between PIP1 and PIP2 subfamilies.

1.2. Aims of this work

The goal of this work was to gain further insight into the interaction and mutual regulation between PIP1s and PIP2s and the mechanisms involved therein.

To examine the PIP1 repression in *pip2* mutants in detail, PIP1 protein was quantitatively determined in *pip2;1*, *pip2;2* and *pip2;1 pip2;2* double mutant at different developmental stages both in root and rosette. Their corresponding complementation lines should further deepen our understanding of the interplay between these two subfamilies.

To assess which *PIP1* isoform is affected, the total PIP1 protein levels will be quantitatively compared between *pip1* single mutants and *pip1* mutations introgressed into *pip2;1 pip2;2* to estimate the specific PIP1 isoform influenced by the *pip2* mutants. Enhanced green fluorescent protein (EGFP) - or hemagglutinin (HA) - tagged *PIP1* isoforms will be expressed in different mutant backgrounds to further quantitatively determine reduction of specific PIP1 isoforms and to explore the potential mechanism of this regulation.

Furthermore, this work aimed at investigating the mechanism underlying the PIP2-dependent PIP1 protein repression, namely

- 1) to determine at which stage the PIP1 protein level is affected by transcriptional and translational analyses;
- 2) to unravel whether a physical interaction between PIP1 isoforms and PIP2;1/PIP2;2/PIP2;3 exists using co-immunoprecipitation;
- 3) to explore whether the trafficking and/or stability of PIP1s is affected by PIP2;1/PIP2;2;
- 4) to reveal the functional similarity of PIP2;2 and PIP2;3 in the regulation of PIP1 protein;
- 5) to illuminate whether the degradation is involved in this regulatory process;

2. RESULTS

2.1. The PIP1 protein level is dependent on both PIP2;1 and PIP2;2

2.1.1. The PIP1 protein level is repressed in the *pip2;1* mutant, the *pip2;2* mutant and the *pip2;1 pip2;2* double mutant

Previous studies showed that the PIP1 protein repression was observed in the roots of the *pip2;2* mutant and of the *pip2;1 pip2;2* double mutant by immunoblotting (Danes and Geist, unpublished; Figure 4). Microsomal membrane fractions were isolated and analyzed by enzyme-linked immunosorbent assay (ELISA) quantification (described in 4.2.4.9) in order to investigate whether different levels of repression of PIP1 protein level could be observed in specific tissues or at different developmental stages comparing *pip2* mutants with the wild-type plants.

To investigate the contribution of single *pip2* mutants (*pip2;1* and *pip2;2*) to the PIP1 protein repression, microsomal membrane fractions from 35-day-old plants were first examined. A substantial reduction of the PIP1 protein level was observed in the rosettes of the *pip2;1* mutant (Figure 6A). Conversely, a significant reduction of the PIP1 protein level was found in the roots of the *pip2;2* mutant (Figure 6A). Despite no statistically significant change, the tendency of PIP1 protein repression was present in the roots of the *pip2;1* mutant (24%) and the rosettes of the *pip2;2* mutant (14%) (Figure 6A).

In addition, the statistically significant reduction of PIP1 protein in the rosette of *pip2;1* was independently verified in 28-day-old plants grown on soil (Figure 6B). Collectively, the *pip2;1* mutant showed a dominant role of repression in the rosettes of 35-day-old and 28-day-old plants, whereas the *pip2;2* mutant exhibited the main contribution to PIP1 protein repression in the roots of 35-day-old plants.

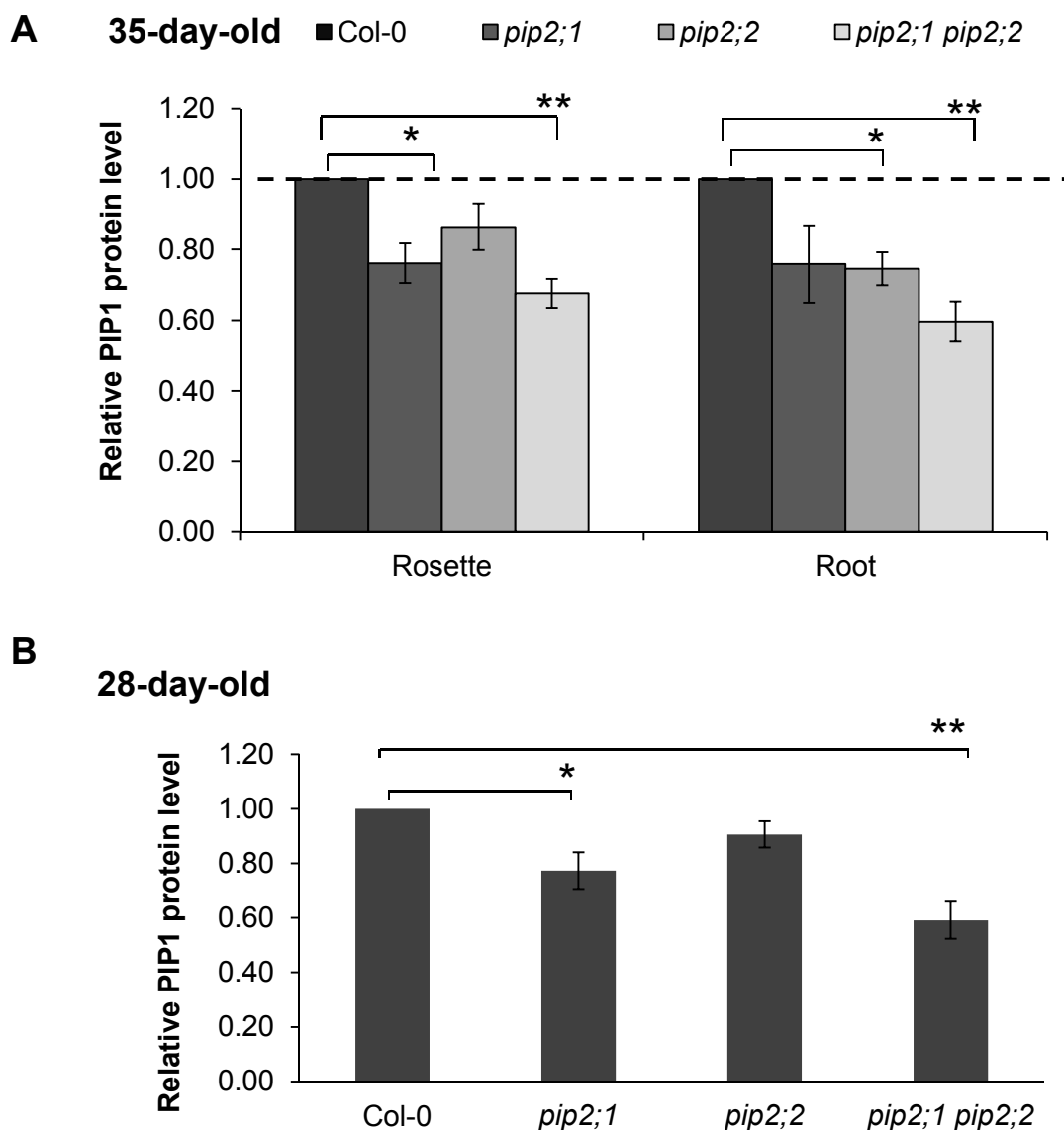


Figure 6. PIP1 protein level is reduced in the *pip2;1* mutant, the *pip2;2* mutant, and the *pip2;1 pip2;2* double mutant.

(A) Total PIP1 protein levels of wild type (Col-0) and *pip2* mutants were determined in the microsomal membrane fraction obtained from 35-day-old plants grown in the hydroponic culture system (approximately 10-20 plants were pooled in one biological sample) and (B) 28-day-old plants (rosette) grown on soil (approximately 10-20 plants were pooled in one biological sample) by an ELISA assay using an anti-PIP1 antiserum (as described in 4.2.4.9). All results were relative to the wild type line (set to 1) in each ELISA measurement. Data were the means of three independent experiments with multiple technical replicates. Error bars represent standard deviation (SD), $n = 3$ independent experiments. The asterisks denote significance between pairs indicated with brackets. ** $p < 0.01$, * $p < 0.05$. P values were derived from a two-tailed one-sample Student's *t* test.

The statistically significant repression of PIP1 protein level was stably observed in the *pip2;1 pip2;2* double mutant when compared to the wild-type plants, not only in the rosettes and roots of 35-day-old plants but also in the rosettes of 28-day-old plants (Figure 6). In addition, microsomal membrane fractions from seven-day-old and 14-day-old plants were examined once. Despite the diverse cultivation of plants (seven-day-old and 14-day-old plants grown on half strength MS plates, 28-day-old plants grown on soil and 35-day-old plants grown in a hydroponic system) and non-uniform chamber conditions, the relative PIP1 protein level showed the same tendency of repression at all the different developmental stages and in specific tissues (rosette and root), indicating that the reduction of PIP1 protein level in the *pip2;1 pip2;2* double mutant is independent of stage and tissue (Figure 7).

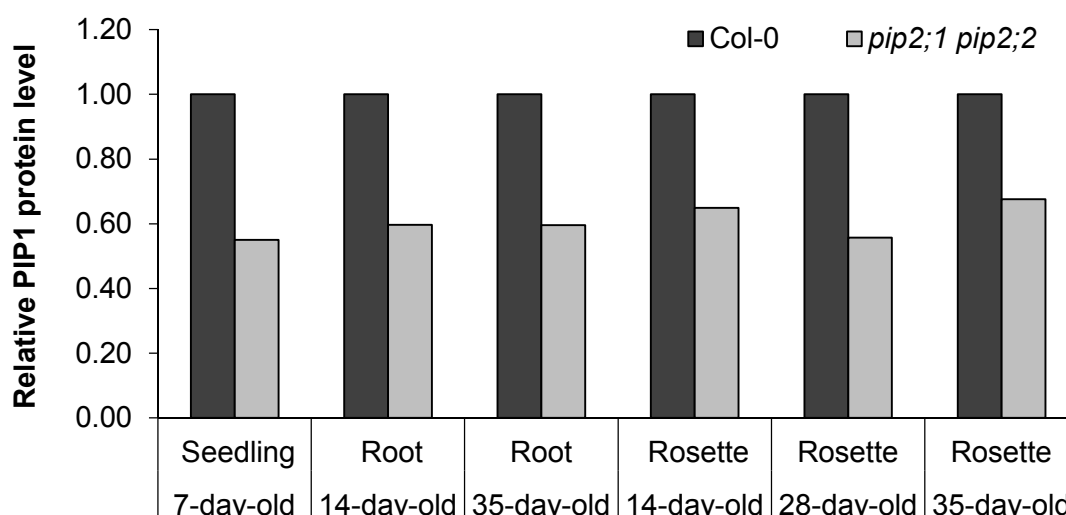


Figure 7. Reduction of PIP1 protein level in the *pip2;1 pip2;2* double mutant is independent of stage and tissue.

Total PIP1 protein levels of wild-type plants (Col-0) and *pip2;1 pip2;2* double mutant were determined in the microsomal fractions obtained from different developmental stages and tissues by ELISA assay using anti-PIP1 antiserum (as described). All results were relative to wild type (set to 1) in each ELISA measurement. The results of seven-day-old (approximately 100 seedlings pooled together) and 14-day-old (approximately 60 plants pooled together) grown on half strength MS plates were the means of three technical replicates. The results of 28-day-old and 35-day-old were the means of three biological replicates (shown in Figure 6, combined here to get a more complete picture).

2.1.2. Recovery of PIP1 protein level in *pip2;1* and *pip2;2* lines complemented with wild-type genes

The microsomal membrane fractions of complementation lines expressing rescue constructs under control of their native promoters were analyzed by ELISA quantification once in order to confirm that PIP1 protein repression was indeed caused by the T-DNA insertional mutation of *PIP2;1* and *PIP2;2*. The relative PIP1 protein level was increased in complementation lines of *pip2;1* mutant and *pip2;2* mutant (Figure 8A). Similarly, the PIP1 protein level was enhanced in the *pip2;1 pip2;2* double mutant, which had been complemented with *PIP2;2*. This *pip2;1* mutant-like transgenic line exhibited an PIP1 protein level similar to the authentic *pip2;1* mutant (Figure 8A). Additionally, the PIP2 protein (*PIP2;1/PIP2;2/PIP2;3*) level was examined by ELISA quantification. The PIP2 protein level was accordingly increased in the complementation lines of *pip2;1*, *pip2;2* and *pip2;1 pip2;2* double mutant which had been complemented with *PIP2;2* (Figure 8B).

In summary, the repression of PIP1 protein was quantified in *pip2;1* and *pip2;2* in the rosettes and roots of 35-day-old plants and the rosettes of 28-day-old plants, indicating the dominant contribution to PIP1 repression had been caused by loss of *PIP2;1* or *PIP2;2* in specific tissues. In agreement with previous findings (Da Ines and Geist, Figure 4), PIP1 protein level was reduced in the *pip2;1 pip2;2* double mutant as compared to the wild-type plants in roots as well as rosettes of 35-day-old plants. Furthermore, the repression of PIP1 protein was evident in different developmental stages and specific tissues in the *pip2;1 pip2;2* double mutant as compared to the wild-type plants, indicating that the loss of PIP2 protein (*PIP2;1* and *PIP2;2*) has a negative impact on the PIP1 protein level.

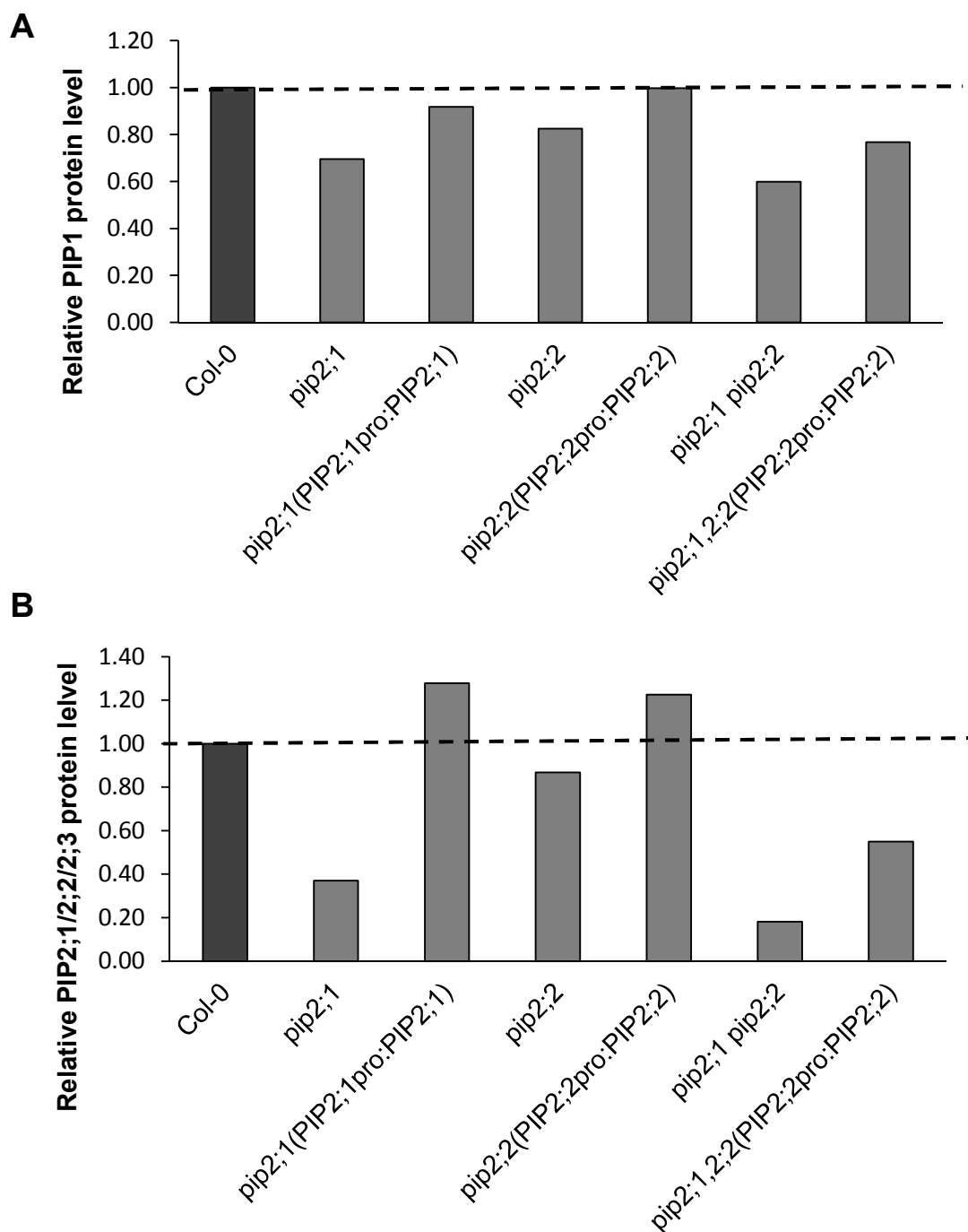


Figure 8. Recovery of total PIP1 protein level in *pip2;1*, *pip2;2*, *pip2;1 pip2;2* lines complemented with wild-type genes.

(A) Total PIP1 protein levels of wild-type plants (Col-0), *pip2* mutants and their complementation lines were determined in the microsomal membrane fractions obtained from 28-day-old plants grown on soil (approximately 10-20 plants (rosettes) were pooled in one biological sample) for an ELISA assay using an anti-PIP1 antiserum (B) using an anti-PIP2 (PIP2;1/PIP2;2/PIP2;3) antiserum for the same samples. All values were relative to wild-type plants (set to 1) in each ELISA measurement. The values were the means of three technical replicates. This experiment was repeated with 14-day-old plants yielding similar results with the help of Jessica Lutterbach.

2.2. The PIP1 protein level is enhanced by Hybrid-expression of *PIP2;3*

The synthesis of the PIP1 protein could be re-initiated in *pip2;1*, *pip2;2* and *pip2;1 pip2;2* mutants by expressing *PIP2;1* or *PIP2;2*. This is an important evidence that the PIP1 protein level is indeed affected by *PIP2;1* or *PIP2;2* (Figure 8).

Due to the high similarities of *PIP2;1*, *PIP2;2*, and *PIP2;3* (especially *PIP2;2* and *PIP2;3* share 96.8% identity at the amino acid level), it is possible that these PIPs exhibit similar functions (Javot *et al.*, 2003). However, based on the Western blot analysis of the PIP1 protein level in *pip2* mutants, there was no apparent repression of the PIP1 protein level in *pip2;3* mutant (Da Ines and Geist, unpublished; Figure 4). One simple explanation for this observation might be the low abundance of the transcript and protein levels of *PIP2;3* in comparison to *PIP2;1* and *PIP2;2* (Jang *et al.*, 2004; Alexandersson *et al.*, 2005; Monneuse *et al.*, 2011) and thus, a minor impact on PIP1 expression. Alternatively, *PIP2;3* could have functions different from those of *PIP2;1* and *PIP2;2*. To assess the functional similarity of *PIP2;3* gene and to investigate whether there is any specific requirement for *PIP2;2* or *PIP2;3* action on PIP1 protein expression, *PIP2;3* was ectopically expressed under the control of *PIP2;2* 5'- and 3'-sequences to determine whether this would be able to complement the loss of *PIP2;2*.

A construct containing the coding sequence of *PIP2;3* gene under the control of a 2000bp *PIP2;2* promoter and *PIP2;2*-3'-UTR sequences was transformed into the *pip2;2* mutant and the *pip2;1 pip2;2* double mutant (see 4.2.1.7 and 4.2.2.5), respectively. Three independent homozygous lines of each mutant background with single transgene insertion were selected (Table 9). From these, two single insertion lines from each mutant background were chosen for further ELISA quantification. The PIP1 protein level was increased to wild-type level in the rosettes of the *pip2;2* mutant transformed with hybrid-construct (*PIP2;2_{pro}:PIP2;3:tPIP2;2*) (Figure 9). The

tendency of a PIP2;3-dependent complementation of PIP1 expression in the *pip2;2* mutant background could be substantiated in the *pip2;1 pip2;2* background (Figure 9). The PIP1 protein level was enhanced in two independent transgenic lines (Figure 9). At a preliminary level, this indicated that ectopically expressed PIP2;3 could functionally complement the repression of PIP1 protein in the *pip2;1 pip2;2* double mutant.

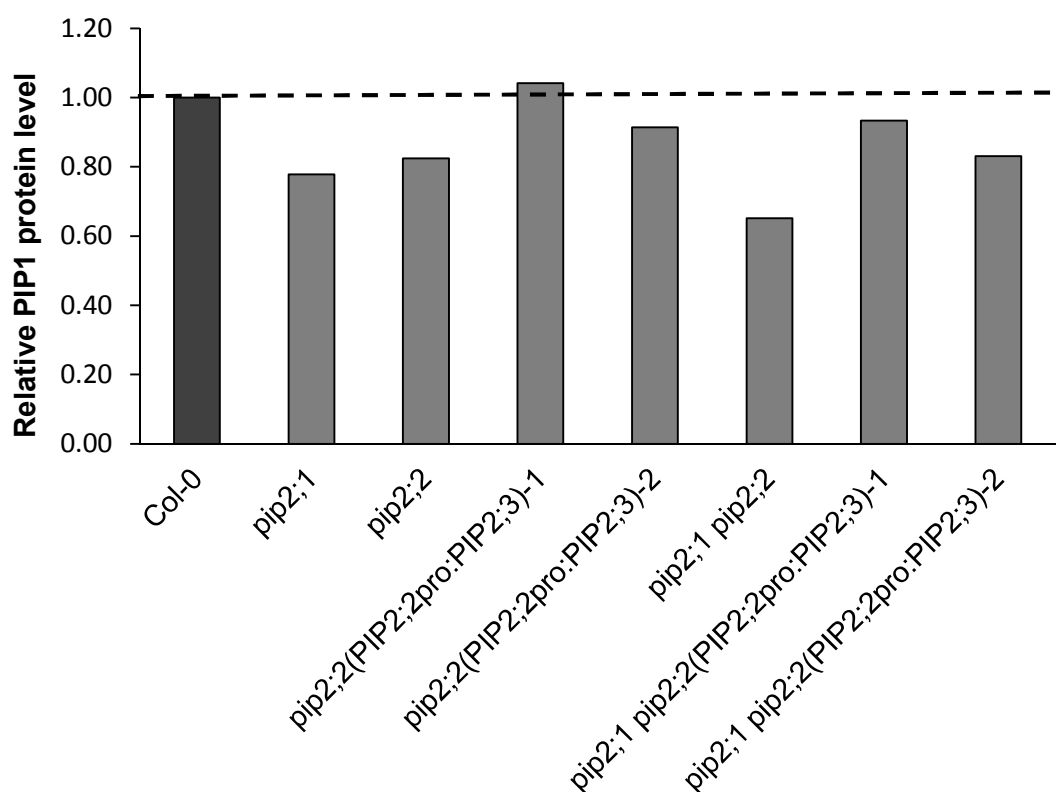


Figure 9. The relative PIP1 protein level is enhanced by hybrid-expression of PIP2;3.

Total PIP1 protein levels of wild-type plants (Col-0), *pip2* mutants and the corresponding hybrid transgenic lines contained *PIP2;2_{pro}:PIP2;3:tPIP2;2* were determined by the microsomal membrane fractions obtained from the rosettes of 28-day-old plants grown on soil for an ELISA assay using an anti-PIP1 antiserum as described. Expression levels were relative to the levels quantified for wild-type plants (Col-0). The values were the means calculated from three technical replicates. This experiment was repeated with 14-day-old plants yielding similar results with the help of Jessica Lutterbach.

2.3. A general reduction of all five PIP1 isoforms is identified in the *pip2;1 pip2;2* double mutant by quantitative mass spectrometry

A proteomics approach using isolated microsomal membrane fractions from the rosettes of 28-day-old wild-type plants and *pip2;1 pip2;2* double mutant has been launched first to identify which PIP1 isoform was affected in *pip2;1 pip2;2* double mutant as compared to the wild type by LC-MS/MS-based label-free quantification together with Jin Zhao and Juliane Merl-Pham (Helmholtz München Zentrum). Statistic analysis of the proteomic data was performed by Georgii Elisabeth (Helmholtz München Zentrum). All five PIP1 isoforms were identified during the long gradient elution process (5 h) performed by mass spectrometry. A general reduction (43%-65%) of all five PIP1 isoforms was revealed and all five PIP1 proteins showed significant changes when normalized abundance comparisons (peptide peak intensity) were utilized for quantification of individual PIP1 proteins in the *pip2;1 pip2;2* double mutant as compared to the wild-type line.

Table 1. A general reduction of five PIP1 isoforms was identified in the *pip2;1 pip2;2* double mutant by LC-MS/MS-based label-free quantification.

Isoform	Accession	Fold change	Raw p_value	Adjusted p_value	Unique peptide
PIP1;1	AT3G61430	0.34	0.000107571	0.000537853	1
PIP1;2	AT2G45960	0.56	0.000584756	0.000709464	3
PIP1;3	AT1G01620	0.57	0.00286656	0.000974595	1
PIP1;4	AT4G00430	0.50	0.000822942	0.001028678	1
PIP1;5	AT4G23400	0.50	0.000283786	0.00286656	2

Fold change represented the means of four replicates of normalized abundance of the *pip2;1 pip2;2* double mutant as compared to the wild type. Raw p values and adjusted p values (after multiple testing correction) were derived from a paired sample test that has been designed for count data (Pham and Jimenez, 2012). More unique peptides detected by mass spectrometry indicated the more reliable protein identification.

2.4. Specific PIP1 isoforms are affected in the *pip2;1* mutant, the *pip2;2* mutant and the *pip2;1 pip2;2* double mutant

2.4.1. Isolation and molecular characterization of *pip1* insertional mutants

The application of loss-of-function *pip1* mutants could be an important experimental tool to assess the relative content of individual PIP1 proteins compared to wild-type plants when there is no isoform-specific PIP1 antibody. To obtain the information on the protein levels of individual PIP1 isoforms in *Arabidopsis*, a collection of T-DNA insertion mutants were isolated and characterized (Table 2). Publicly accessible seed collections (NASC, INRA and GABI) were screened for available T-DNA insertion lines. PIP1 isoform single mutants were obtained in our lab except for *pip1;5*, which is currently not available. All mutant lines were verified by PCR genotyping and sequencing and further confirmed by RT-PCR analysis. *pip1;1-1* was verified as a knockdown mutant. Other mutants were knockout mutants (a weak band was always detected in the *pip1;2-1* mutant) (Figure 10). All *pip1* mutant lines listed in Table 2 were backcrossed at least three times to the wild type to purify the insertion background in this work. Later, one single mutant from each PIP1 isoform (Table 3) was chosen for further experimental analysis.

Table 2. *Arabidopsis* PIP single mutants backcrossed and used in this study.

AGI Code	Mutant	Line	Ecotype	Reference	Molecular Characterization
At3g61430	<i>pip1;1-1</i>	GABI_437B11	Col-0	(Da Ines, 2008)	Knockdown
At2g45960	<i>pip1;2-1</i>	SALK_145347	Col-0	(Postaire <i>et al.</i> , 2010)	Knockout
	<i>pip1;2-2</i>	SALK_019794	Col-0	(Postaire <i>et al.</i> , 2010)	Knockout
At1g01620	<i>pip1;3-1</i>	SALK_051107	Col-0	This work	Knockout
At4g00430	<i>pip1;4-2</i>	SAIL_808_A10	Col-0	This work	Knockout
	<i>pip1;4-4</i>	GABI_412E06	Col-0	This work	Knockout
At3g53420	<i>pip2;1-2</i>	SM_3_35928	Col-0	(Da Ines,2008)*	Knockout
At2g37170	<i>pip2;2-3</i>	SAIL_169A03	Col-0	(Da Ines,2008)*	Knockout

* indicate that these *pip2* mutants were backcrossed by a colleague Ming Jin.

RESULTS

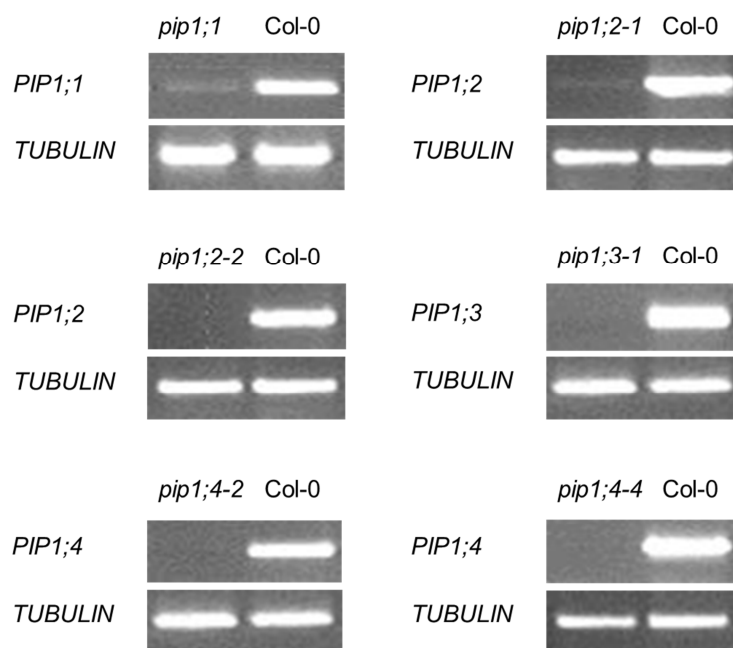


Figure 10. Molecular characterization of *pip1* mutants after backcrossing.

RT-PCR analysis of *PIP1* transcript levels in mutants compared to wild-type plants (Col-0). *TUBULIN9* (At4g20890) transcript levels were assessed as a control.

Table 3. *pip1* single and multiple mutants used in this work.

Mutant name	Mutant name in this work
<i>pip1;1-1</i>	<i>pip1;1</i>
<i>pip1;2-2</i>	<i>pip1;2</i>
<i>pip1;3-1</i>	<i>pip1;3</i>
<i>pip1;4-2</i>	<i>pip1;4</i>
<i>pip2;1-2</i>	<i>pip2;1</i>
<i>pip2;2-3</i>	<i>pip2;2</i>
<i>pip1;1-1 pip1;2-2</i>	<i>pip1;1 pip1;2</i>
<i>pip2;1-2 pip2;2-3</i> (Da Ines, 2008)	<i>pip2;1 pip2;2</i>
<i>pip1;1-1 pip2;1-2 pip2;2-3</i>	<i>pip1;1 pip2;1 pip2;2</i>
<i>pip1;2-2 pip2;1-2 pip2;2-3</i>	<i>pip1;2 pip2;1 pip2;2</i>
<i>pip1;1-1 pip1;2-2 pip2;1-2 pip2;2-3</i>	<i>pip1;1 pip1;2 pip2;1 pip2;2</i>

T-DNA inserted mutant lines were of Columbia (Col-0) background and used for generating the multiple mutants.

2.4.2. The relative contribution of each PIP1 isoform to total PIP1 protein level is deduced from loss-of-function *pip1* mutant lines

The total PIP1 protein level could be relatively measured by an immunoassay using an anti-PIP1 antiserum detecting all five PIP1 isoforms. To deduce the portion of each PIP1 isoform, the total PIP1 protein level was examined in individual *pip1* single mutants and wild-type plants by an ELISA assay as described (see 4.2.4.9).

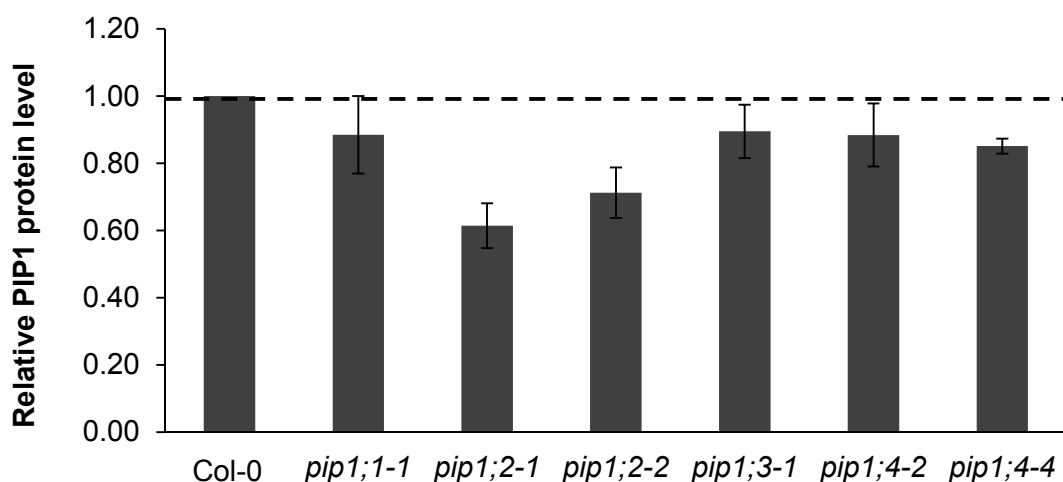


Figure 11. Relative contribution of each PIP1 isoform of PIP1 protein level.

Total PIP1 protein levels of wild-type plants (Col-0), *pip1* mutants were determined using the microsomal fractions obtained from rosettes of 28-day-old plants grown on soil by an ELISA assay using an anti-PIP1 antiserum as described. All results were relative to wild-type plants (set to 1) in each ELISA measurement. The values displayed were means of three biological replicates, except for *pip1;2-1* and *pip1;4-4* were means of two biological replicates obtained.

The PIP1 protein content of *pip1;2* mutant was approximately 30% less than that of wild-type in rosettes of 28-day-old plants, showing a dominant profile in the overall PIP1 protein level (Figure 11). Due to the *pip1;1* mutant being a knockdown and the lack of an available *pip1;5* mutant, the PIP1 protein expression levels of PIP1;1 and PIP1;5 could not be determined absolutely. The study of mutants further revealed that both, PIP1;3 (10%) and PIP1;4 (12%-15%) contributed approximately 10% to the whole protein abundance. For PIP1;2 and PIP1;4, two mutant alleles were

RESULTS

tested and no apparent differences between the PIP1 protein expressions were present in these alleles. Therefore, *pip1;2-2* and *pip1;4-2* were chosen for further analysis (listed in Table 3).

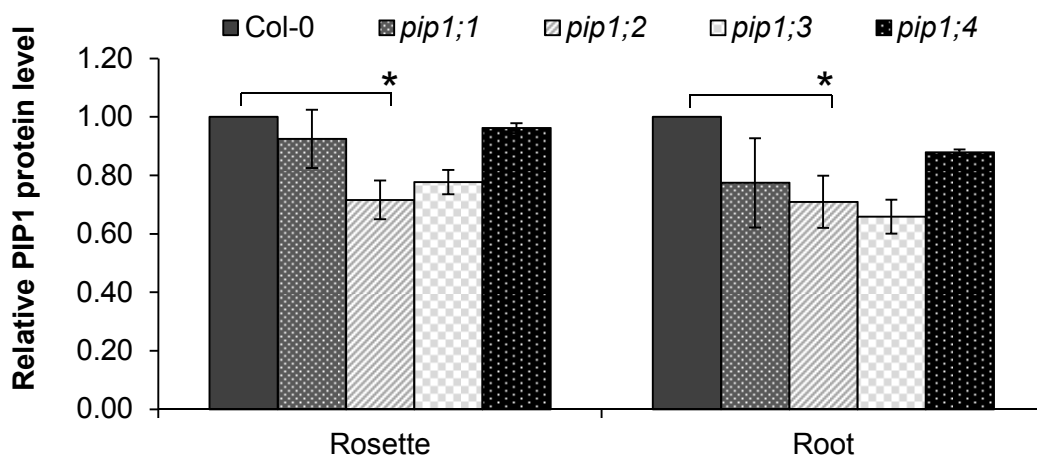


Figure 12. Relative contribution of each PIP1 isoform to the PIP1 protein level in both the rosettes and roots.

Total PIP1 protein levels of wild-type plants (Col-0), *pip1* mutants were determined using the microsomal fractions obtained from 35-day-old plants grown in the hydroponic culture system by an ELISA assay using an anti-PIP1 antiserum as described. All results were relative to the wild-type plants (set to 1) in each ELISA measurement. Error bars represent standard deviation (SD). $n = 2$ or 3 from independent experiments. The values of *pip1;3* and *pip1;4* were the means of two biological replicates, the rest of the values were the means of three biological replicates. The asterisks denote statistically significant differences from wild-type plants. * $p < 0.05$. P values were derived from a two-tailed one-sample Student's *t* test (only for the data obtained from three experiments).

To allow the assessment of the PIP1 protein level in both, the rosettes and roots of individual PIP1 isoforms, the plant materials from hydroponic culture were used for an ELISA assay. The quantitative ELISA revealed that the *pip1;2* mutant exhibited 28% (Figure 12) less PIP1 protein than the wild-type plants in the rosettes of 35-day-old plants, confirming the results of 28-day-old plants grown on soil (Figure 11).

In addition, *pip1;2* showed 29% less PIP1 protein than wild-type in the roots of 35-day-old plants (Figure 12), indicating that PIP1;2 is a major isoform in both the rosettes and roots of 35-day-old plants. The PIP1 protein content of *pip1;1*

knockdown mutant was found to be 8% less in the rosettes and 23% less than in the roots of the wild-type plants (Figure 12), suggesting that PIP1;1 is a major isoform in the roots of 35-day-old plants. PIP1 protein levels of *pip1;3* and *pip1;4* were estimated from two biological experiments. The PIP1 protein content of the *pip1;3* mutant was 22% less in the rosettes and 34% less in the roots as compared to wild-type plants, indicating that PIP1;3 may be a major isoform of the PIP1 subfamily. The PIP1 protein content of *pip1;4* was in agreement with the result of 28-day-old plants.

2.4.3. Loss-of-function *pip1* mutant lines reveal that PIP1;1 and PIP1;2 isoforms are both affected in the *pip2;1 pip2;2* double mutant

To determine which PIP1 isoform was affected in *pip2* mutants, the total amount of PIP1 protein was compared between the *pip1* single mutant and its multiple mutants, also taking into account combinations with loss-of-function of PIP2;1 and PIP2;2, e.g. *pip1;1* and *pip1;1 pip2;1 pip2;2*.

In these multiple mutants, further repression of PIP1 protein compared to the protein levels of the corresponding single mutants revealed that four other PIP1 isoforms potentially contributed to the PIP1 repression in the *pip2* mutants (or were affected by the loss-of-function of PIP2;1 and PIP2;2). In contrast, no further reduction of PIP1 protein quantity in this comparison indicated that this specific PIP1 isoform had already been affected in the *pip2;1 pip2;2* double mutant.

Previous studies on the transcriptional and proteomic analysis of aquaporins in *Arabidopsis* (Alexandersson *et al.*, 2005; Monneuse *et al.*, 2011) indicated that PIP1;1 and PIP1;2 were major isoforms of the PIP1 subfamily. The PIP1;3 may be another major isoform according to the PIP1 content analysis of knockout mutants (Figure 12). However, the construction of multiple mutants of *pip1;3* with the combination of *pip2s* (*pip2;1 pip2;2*) is still ongoing. Therefore, the studies focus on

their attention on the *pip1;1* and *pip1;2* single mutants and their multiple mutants for PIP1 protein analysis (Table 3).

2.4.3.1. The PIP1;1 protein level is affected in the *pip2;1 pip2;2* double mutant

PIP1 protein levels of *pip1;1*, *pip2;1 pip2;2* and *pip1;1 pip2;1 pip2;2* were determined in order to assess whether PIP1;1 was affected in the *pip2;1 pip2;2* double mutant, and compared accordingly to investigate the influence of loss-of-function of PIP2;1 and PIP2;2 on the PIP1;1 isoform. As shown before (Figure 12), the results indicated that in a *pip1;1* knockdown line, PIP1;1 contributed at least 8% of the total amount of the PIP1 protein in 35-day-old rosettes. No further reduction of the PIP1 protein level of *pip1;1 pip2;1 pip2;2* as compared to *pip2;1 pip2;2* was observed in the rosettes of 35-day-old plants (Figure 13). This suggested that the PIP1;1 isoform had already been reduced in the rosettes of *pip2;1 pip2;2*. Moreover, the PIP1;1 isoform made up at least 23% of the total amount of the PIP1 protein in the roots (Figure 13). No statistically significant reduction of PIP1 protein of *pip1;1 pip2;1 pip2;2* as compared to *pip2;1 pip2;2* strongly indicated that the PIP1;1 isoform had already been reduced in the roots of *pip2;1 pip2;2*. The further reduction tendency of the PIP1 protein observed in *pip1;1 pip2;1 pip2;2* as compared to *pip1;1* in both the rosettes and roots, implied that other PIP1 isoforms were also affected in the *pip2;1 pip2;2* double mutant. However, since the *pip1;1* is a knockdown line as mentioned above, the possibility that further PIP1 repression in *pip1;1 pip2;1 pip2;2* might due to the reduction of PIP1;1 protein cannot be excluded.

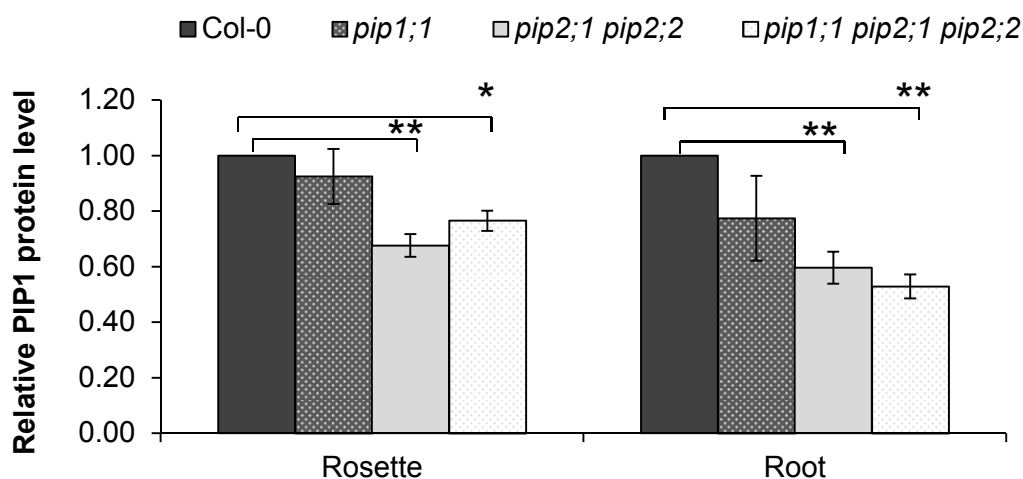


Figure 13. Relative PIP1 protein levels in both the rosettes and roots of the *pip1;1* mutant and of *pip1;1*-related multiple mutants.

Total PIP1 protein levels of wild-type lines (Col-0), *pip1* and *pip2* mutants were determined with the microsomal fractions obtained from 35-day-old plants grown in the hydroponic culture system by ELISA assay using an anti-PIP1 antiserum as described. All results were relative to wild-type lines (set to 1) in each ELISA measurement. Data were the means of three independent experiments with multiple technical replicates. Error bars represent standard deviation (SD). $n = 3$ independent experiments. The asterisks denote significance between pairs indicated with brackets. $**p < 0.01$, $*p < 0.05$. P values were derived from a two-tailed one-sample Student's *t* test.

2.4.3.2. The PIP1;2 protein level is affected in the *pip2;1 pip2;2* double mutant

PIP1 protein levels of *pip1;2*, *pip2;1 pip2;2* and *pip1;2 pip2;1 pip2;2* were determined and to assess whether PIP1;2 was affected in the *pip2;1 pip2;2* double mutant, and compared accordingly to investigate the influence of absence of PIP2;1 and PIP2;2 on the PIP1;2 isoform. According to the analysis of PIP1 protein contents in *pip1* mutants above, PIP1;2 contributes around 28% of the total amount of PIP1 protein in the rosettes of 35-day-old plants (Figure 12). No statistically significant reduction of PIP1 protein in *pip1;2 pip2;1 pip2;2* as compared to *pip2;1 pip2;2* was observed in the rosettes of 35-day-old plants (Figure 14). This suggested that the PIP1;2 isoform had already been reduced in the rosettes of *pip2;1 pip2;2*. Besides, the PIP1;2 isoform contributed roughly 29% to the total amount PIP1 protein in the roots (Figure 12). No statistically significant reduction of the PIP1

RESULTS

protein in *pip1;2 pip2;1 pip2;2* as compared to *pip2;1 pip2;2* strongly indicated that the PIP1;2 isoform had already been reduced in the roots of *pip2;1 pip2;2*. Moreover, no further reduction of PIP1 protein in *pip1;2 pip2;1 pip2;2* as compared to *pip1;2* in the rosettes indicated that PIP1;2 as a major isoform of the PIP1 subfamily had been dominantly affected in the rosettes of *pip2;1 pip2;2* (Figure 14). The further strong reduction of PIP1 protein in the roots of *pip1;2 pip2;1 pip2;2* as compared to *pip1;2* was revealed, suggesting that other PIP1 isoforms were affected in the roots of *pip2;1 pip2;2*. In addition, the tendency of further reduction (14%) of PIP1 protein in *pip1;2 pip2;1 pip2;2* as compared to *pip2;1 pip2;2* implied that PIP1;2 was partially affected in the roots of the *pip2;1 pip2;2* double mutant.

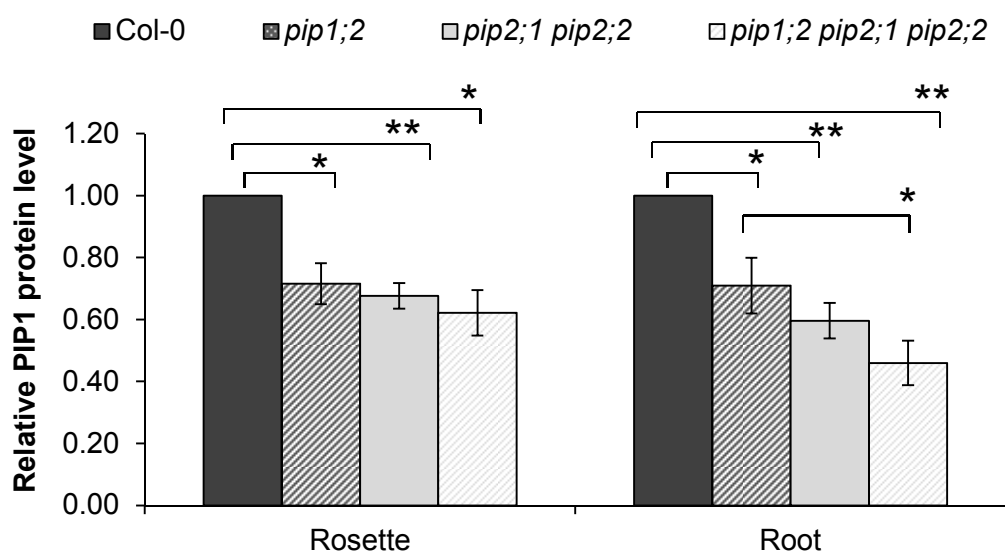


Figure 14. Relative PIP1 protein levels in both the rosettes and roots of the *pip1;2* mutant and of *pip1;2*-related multiple mutants.

Total PIP1 protein levels of wild-type plants (Col-0), *pip1* and *pip2* mutants were determined with the microsomal fractions obtained from 35-day-old grown in the hydroponic culture system by ELISA assay using an anti-PIP1 antiserum. All results were relative to wild-type plants (set to 1) in each ELISA measurement. Data were the means of three independent experiments with multiple technical replicates. Error bars represent standard deviation (SD). $n = 3$ independent experiments. The asterisks denote significance between pairs indicated with brackets. ** $p < 0.01$, * $p < 0.05$. P values were derived from a two-tailed one-sample Student's *t* test.

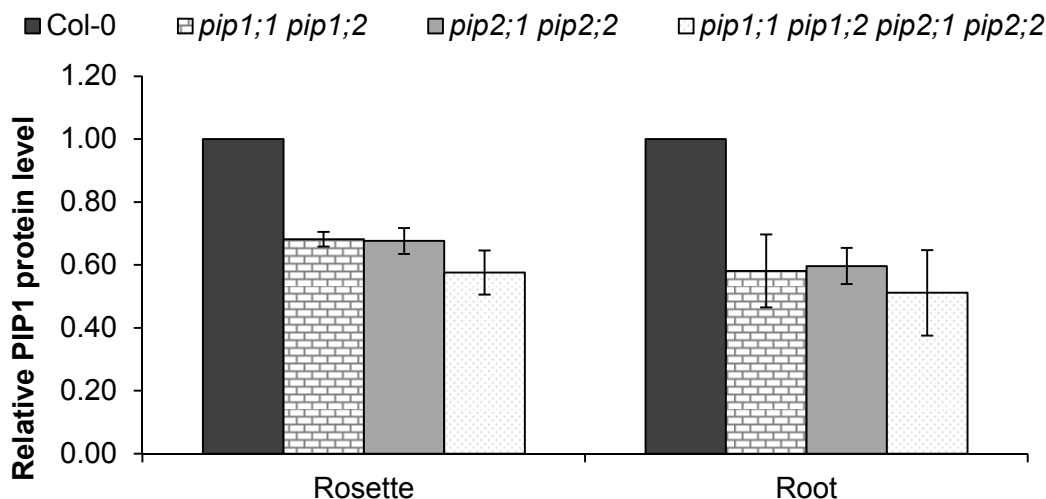


Figure 15. Relative PIP1 protein levels in both the rosettes and roots of the *pip1;1 pip1;2* double mutant and of multiple mutants.

Total PIP1 protein levels of wild-type plants (Col-0), *pip1* and *pip2* mutants were determined with the microsomal membrane fractions obtained from 35-day-old grown in the hydroponic culture system by ELISA assay using an anti-PIP1 antiserum as described. All results were relative to wild-type plants (set to 1) in each ELISA measurement. The values were means from two biological replicates, $n = 2$ independent experiments. Two experiments yielded similar results.

The PIP1 protein content of the *pip1;1 pip1;2* double mutant was 32% less than of the wild-type in the rosettes of 35-day-old plants. No strong reduction of the total PIP1 protein of *pip1;1 pip1;2 pip2;1 pip2;2* as compared to *pip2;1 pip2;2* suggested that PIP1;1 and PIP1;2 as the major PIP1 isoforms were reduced in the rosettes of *pip2;1 pip2;2* (Figure 15). In addition, the same tendency was detected in the roots of 35-day-old plants, suggesting that PIP1;1 and PIP1;2 were reduced in the roots of *pip2;1 pip2;2*. These results confirmed the data mentioned above (Figure 13 and 14). Furthermore, the further tendency of reduction of PIP1 protein in *pip1;1 pip1;2 pip2;1 pip2;2* as compared to *pip2;1 pip2;2* suggested that the other PIP1 isoforms might also be affected in both the rosettes and roots of the *pip2;1 pip2;2* double mutant (Figure 15).

2.4.4. Tagged *PIP1* transgenic lines further confirm the reduction of PIP1;1 and PIP1;2 protein in the *pip2;1* mutant, the *pip2;2* mutant and the *pip2;1 pip2;2* double mutant

2.4.4.1. Production and characterization of EGFP-tagged and HA-tagged PIP1;1 and PIP1;2

The deduction of the isoform contributions to the total protein abundance via mutant lines remains an indirect tool. To obtain independent evidence for the reduction of PIP1 proteins at the genetic and cell biological level, epitope tagged PIP1;1 and PIP1;2 by hemagglutinin (HA) or enhanced green fluorescent protein (EGFP) in different mutant backgrounds were generated. Hemagglutinin was used because it generally has no effect on the biological function of the tagged protein and because of its small size. In addition, enhanced green fluorescent protein was employed for better visualization of tagged proteins. By selecting independent transgenic lines after transformation and subsequently crossing with corresponding multiple mutants, the tagged version replaced the endogenous gene and therefore regenerated the wild-type situation, the *pip2;1* mutant, the *pip2;2* mutant and the *pip2;1 pip2;2* double mutant with tagged PIP1;1 or PIP1;2 (Table 5 and 6). The whole process would be further elucidated in detailed below (Figure 16, 17 and 18). Therefore, the expression of PIP1;1 and PIP1;2 could be specifically and quantitatively measured by immunological assays using the antisera against the EGFP or HA tags or visualized by confocal microscopy.

Constructs containing N- or C-terminal fusions of EGFP- or HA-tag to *PIP1;1* and *PIP1;2* coding sequences under the control of the *PIP1s* endogenous promoters and 3'-UTRs were generated by using PCR-based joining of fragments (see 4.2.3.2 and 4.2.3.4) and a GATEWAY™ two-fragment vector recombination method (Karimi *et al.*, 2005) (Figure 16). This method could reduce the misfolding influence of att recombination sites existing in the GATEWAY™ multiple fragments vector system,

thereby ensuring the proper folding of both the protein of interest and the fluorescent protein.

Figure 16 shows the scheme of N-terminal and C-terminal fusions of EGFP with the *PIP1;1* gene, which were being transferred into the binary destination vector (pPm42GW inserted with seed coat specifically expressed GFP as a selection marker-fragment cloned from pAlligator2) (see 4.2.3.4). The HA-fusion constructs of the *PIP1;1* gene and the EGFP-fusion and HA-fusion constructs of the *PIP1;2* gene were generated using the same strategy. These constructs were transformed into the *pip1;1* or *pip1;2* single mutants, respectively (Table 4).

For N- and C- terminal EGFP fusions of *PIP1;1* or *PIP1;2*, three independent transgenic lines were examined for their expected plasma membrane localization of protoplasts and roots by an fluorescence microscopy (see 4.2.5). One transgenic line of each (Figure 17) was crossed with the *pip1;1 pip2;1 pip2;2* triple mutant or the *pip1;2 pip2;1 pip2;2* triple mutant, respectively. The homozygous lines possessed the same single insertion site of these fusion constructs in different backgrounds were selected from the segregating populations derived from crosses by PCR-based genotyping (see 4.2.3.3), thus regenerated the wild-type line, the *pip2;1* mutant, the *pip2;2* mutant, and the *pip2;1 pip2;2* double mutant with the expression of tagged PIP1;1 or PIP1;2 (Figure 18). Therefore, the protein expression of PIP1;1 or PIP1;2 could be directly compared among these different backgrounds.

For the HA-tag fusion transgenic lines, two independent lines of N-terminal fusion were selected for crossing and genotyping to create the different backgrounds with the same insertion site situation since the transgenic lines of C-terminal EGFP fusions of PIP1;1 and PIP1;2 both exhibited relatively low fluorescence signal as compared to the transgenic lines of N-terminal EGFP fusions of PIP1;1 and PIP1;2.

Table 4. List of expression constructs in binary vectors and the name of transgenic lines generated in this work.

Construct	Mutant	Name in this work
<i>PIP1;1_{pro}:EGFP-PIP1;1:tPIP1;1</i>	<i>pip1;1</i>	<i>pip1;1</i> (EGFP-PIP1;1)
<i>PIP1;1_{pro}:PIP1;1-EGFP:tPIP1;1</i>	<i>pip1;1</i>	<i>pip1;1</i> (PIP1;1-EGFP)
<i>PIP1;1_{pro}:HA-PIP1;1:tPIP1;1</i>	<i>pip1;1</i>	<i>pip1;1</i> (HA-PIP1;1)
<i>PIP1;1_{pro}:PIP1;1-HA:tPIP1;1</i>	<i>pip1;1</i>	<i>pip1;1</i> (PIP1;1-HA)
<i>PIP1;2_{pro}:EGFP-PIP1;2:tPIP1;2</i>	<i>pip1;2</i>	<i>pip1;2</i> (EGFP-PIP1;2)
<i>PIP1;2_{pro}:PIP1;2-EGFP:tPIP1;2</i>	<i>pip1;2</i>	<i>pip1;2</i> (PIP1;2-EGFP)
<i>PIP1;2_{pro}:HA-PIP1;2:tPIP1;2</i>	<i>pip1;2</i>	<i>pip1;2</i> (HA-PIP1;2)
<i>PIP1;2_{pro}:PIP1;2-HA:tPIP1;2</i>	<i>pip1;2</i>	<i>pip1;2</i> (PIP1;2-HA)

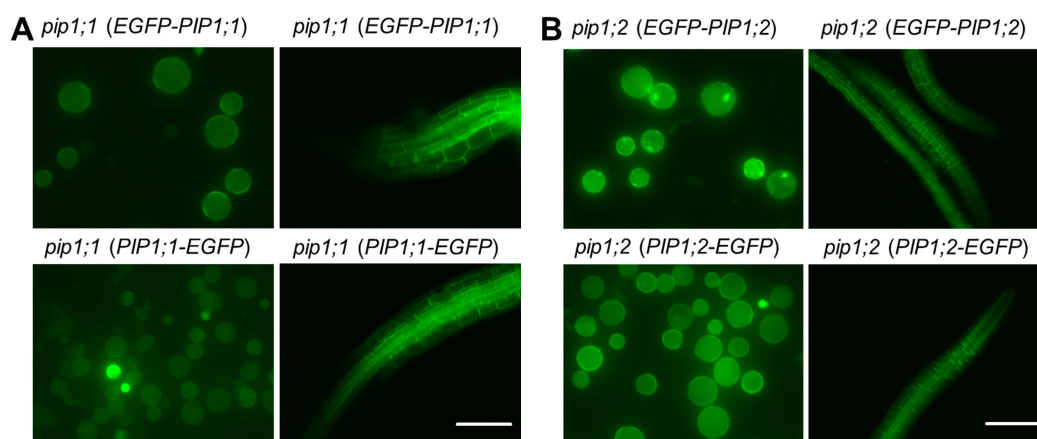


Figure 17. Subcellular localization of EGFP fusion transgenic lines.

(A) The expression pattern of N- and C-terminal EGFP fusion to PIP1;1 in mesophyll protoplasts and in roots. (B) The expression pattern of N- and C-terminal EGFP fusion to PIP1;2 in mesophyll protoplasts and in roots. Bars = 100 μ m.

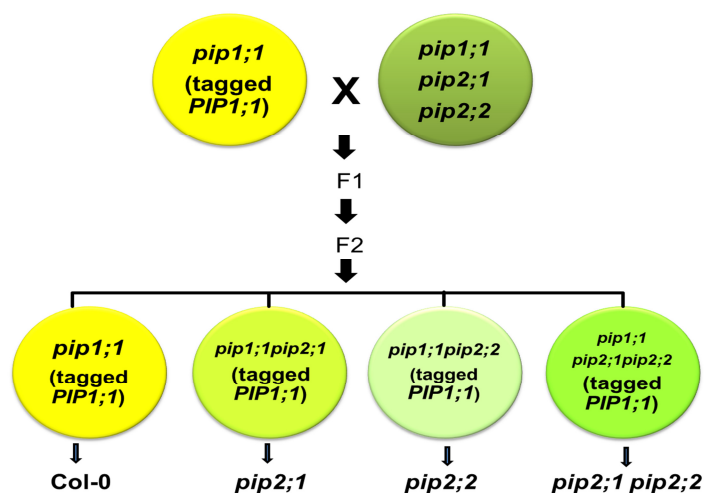


Figure 18. Regenerated transgenic lines by crossing and genotyping.

RESULTS

Table 5. The EGFP fusion of transgenic lines in different mutant backgrounds and their names used in this work.

Transgenic line	Mutant background	Name in this work
<i>pip1;1</i> (EGFP-PIP1;1)	<i>pip1;1</i>	<i>pip1;1</i> (EGFP-PIP1;1)
	<i>pip1;1 pip2;1</i>	<i>pip1;1 pip2;1</i> (EGFP-PIP1;1)
	<i>pip1;1 pip2;2</i>	<i>pip1;1 pip2;2</i> (EGFP-PIP1;1)
	<i>pip1;1 pip2;1 pip2;2</i>	<i>pip1;1 pip2;1 pip2;2</i> (EGFP-PIP1;1)
<i>pip1;1</i> (PIP1;1-EGFP)	<i>pip1;1</i>	<i>pip1;1</i> (PIP1;1-EGFP)
	<i>pip1;1 pip2;1</i>	<i>pip1;1 pip2;1</i> (PIP1;1-EGFP)
	<i>pip1;1 pip2;2</i>	<i>pip1;1 pip2;2</i> (PIP1;1-EGFP)
	<i>pip1;1 pip2;1 pip2;2</i>	<i>pip1;1 pip2;1 pip2;2</i> (PIP1;1-EGFP)
<i>pip1;2</i> (EGFP-PIP1;2)	<i>pip1;2</i>	<i>pip1;2</i> (EGFP-PIP1;2)
	<i>pip1;2 pip2;1</i>	<i>pip1;2 pip2;1</i> (EGFP-PIP1;2)
	<i>pip1;2 pip2;2</i>	<i>pip1;2 pip2;2</i> (EGFP-PIP1;2)
	<i>pip1;2 pip2;1 pip2;2</i>	<i>pip1;2 pip2;1 pip2;2</i> (EGFP-PIP1;2)
<i>pip1;2</i> (PIP1;2-EGFP)	<i>pip1;2</i>	<i>pip1;2</i> (PIP1;2-EGFP)
	<i>pip1;2 pip2;1</i>	<i>pip1;2 pip2;1</i> (PIP1;2-EGFP)
	<i>pip1;2 pip2;2</i>	<i>pip1;2 pip2;2</i> (PIP1;2-EGFP)
	<i>pip1;2 pip2;1 pip2;2</i>	<i>pip1;2 pip2;1 pip2;2</i> (PIP1;2-EGFP)

Table 6. The HA fusion of transgenic lines in different mutant backgrounds and their names used in this work.

Transgenic line	Mutant background	Name in this work
<i>pip1;1</i> (HA-PIP1;1)-7	<i>pip1;1</i>	<i>pip1;1</i> (HA-PIP1;1)-7
	<i>pip1;1 pip2;1</i>	<i>pip1;1 pip2;1</i> (HA-PIP1;1)-7
	<i>pip1;1 pip2;2</i>	<i>pip1;1 pip2;2</i> (HA-PIP1;1)-7
	<i>pip1;1 pip2;1 pip2;2</i>	<i>pip1;1 pip2;1 pip2;2</i> (HA-PIP1;1)-7
<i>pip1;1</i> (HA-PIP1;1)-19	<i>pip1;1</i>	<i>pip1;1</i> (HA-PIP1;1)-19
	<i>pip1;1 pip2;1</i>	<i>pip1;1 pip2;1</i> (HA-PIP1;1)-19
	<i>pip1;1 pip2;2</i>	<i>pip1;1 pip2;2</i> (HA-PIP1;1)-19
	<i>pip1;1 pip2;1 pip2;2</i>	<i>pip1;1 pip2;1 pip2;2</i> (HA-PIP1;1)-19
<i>pip1;2</i> (HA-PIP1;2)-4	<i>pip1;2</i>	<i>pip1;2</i> (HA-PIP1;2)-4
	<i>pip1;2 pip2;1</i>	<i>pip1;2 pip2;1</i> (HA-PIP1;2)-4
	<i>pip1;2 pip2;2</i>	<i>pip1;2 pip2;2</i> (HA-PIP1;2)-4
	<i>pip1;2 pip2;1 pip2;2</i>	<i>pip1;2 pip2;1 pip2;2</i> (HA-PIP1;2)-4
<i>pip1;2</i> (HA-PIP1;2)-5	<i>pip1;2</i>	<i>pip1;2</i> (HA-PIP1;2)-5
	<i>pip1;2 pip2;1</i>	<i>pip1;2 pip2;1</i> (HA-PIP1;2)-5
	<i>pip1;2 pip2;2</i>	<i>pip1;2 pip2;2</i> (HA-PIP1;2)-5
	<i>pip1;2 pip2;1 pip2;2</i>	<i>pip1;2 pip2;1 pip2;2</i> (HA-PIP1;2)-5

2.4.4.2. Quantitative analysis of tagged *PIP1;1* transgenic lines confirms the reduction of *PIP1;1* protein level

2.4.4.2.1 The *PIP1;1* protein level is reduced in the *pip2;1 pip2;2* double mutant

Homozygous transgenic lines which harboured tagged *PIP1;1* (listed in Table 5 and 6) were employed for visualization, quantification and analysis to investigate to what extent the *PIP1;1* is affected in the *pip2;1 pip2;2* double mutant as compared to the wild-type line.

Microsomal membrane fractions from different transgenic lines which expressed the same construct of *EGFP-PIP1;1* (in a thereby regenerated wild type line and *pip2;1 pip2;2* double mutant) were first isolated and analyzed by immunoblotting using an antibody against GFP and an antibody against PIP1 proteins, respectively.

In the anti-GFP Western blot analysis, it showed the correct size of the fusion protein: around 55 kDa (EGFP: 26.9 kDa, *PIP1;1*: 28 kDa) in both transgenic lines. It demonstrated that the immunoblotting signal of *EGFP-PIP1;1* from *pip2;1 pip2;2* was apparently weaker than the signal from the corresponding wild-type line (Figure 19A). This clearly indicated that *PIP1;1* had been affected in the *pip2;1 pip2;2* double mutant.

The tendency of less PIP1 protein in the *pip2;1 pip2;2* double mutant as compared to the wild-type line was observed in the anti-PIP1 Western blot analysis, despite the fact that it was difficult to distinguish the *EGFP-PIP1;1* fusion protein from the PIP1 dimer band because of the similar sizes of the protein bands (around 55 kDa) in transgenic lines (Figure 19A). In addition, the less abundant immunoblotting signal of the monomer (between 25-35 kDa) position suggested that the other four PIP1 isoforms may also be affected in the *pip2;1 pip2;2* double mutant compared to the corresponding wild-type line (Figure 19A). These two Western blot analyses

RESULTS

together confirmed the result which was deduced from the analysis of loss-of-function *pip1* mutants (Figure 13).

Quantitative live-cell imaging was applied to mesophyll protoplasts isolated from 28-day-old plants (grown on soil) by using confocal microscopy to visualize correct plasma membrane targeting of EGFP-PIP1;1. EGFP-PIP1;1 localized at the plasma membrane in both the wild-type and in the *pip2;1 pip2;2* double mutant background (Figure 19B). The EGFP fluorescence signals in the protoplasts of *pip2;1 pip2;2* were weaker than those in the wild-type background. To gain more detailed data about the reduction of PIP1;1 protein in the *pip2;1 pip2;2* double mutant, fluorescence signals of EGFP-PIP1;1 from individual protoplasts were quantitatively analyzed from confocal pictures using Image J software. Relative quantification of the mean and the total fluorescence signals (to eliminate the size effect of individual protoplasts) of EGFP-PIP1;1 derived from individual protoplasts both revealed the significant reduction of the EGFP-PIP1;1 fluorescence signal (40-50%) of the *pip2;1 pip2;2* double mutant as compared to the wild type (Figure 19C) (The total fluorescence signal = mean fluorescence intensity of each protoplast × area of individual protoplast).

In addition, the transgenic lines which possessed the same C-terminal fluorescence fusion (*PIP1;1-EGFP*) in different genotype backgrounds were also utilized for visualization and quantitative analysis. Despite the fact that the fluorescence signal of PIP1;1-EGFP was weaker than of those of *EGFP-PIP1;1* transgenic lines, the reduction of the fluorescence signal of PIP1;1-EGFP was still observed in *pip2;1 pip2;2* as compared to the wild-type background. This part will be further described later (in 2.4.4.2.2).

In summary, the results from N- and C-terminal EGFP fusions of *PIP1;1* transgenic lines both revealed that PIP1;1 protein is reduced in the rosettes of the *pip2;1 pip2;2* double mutant.

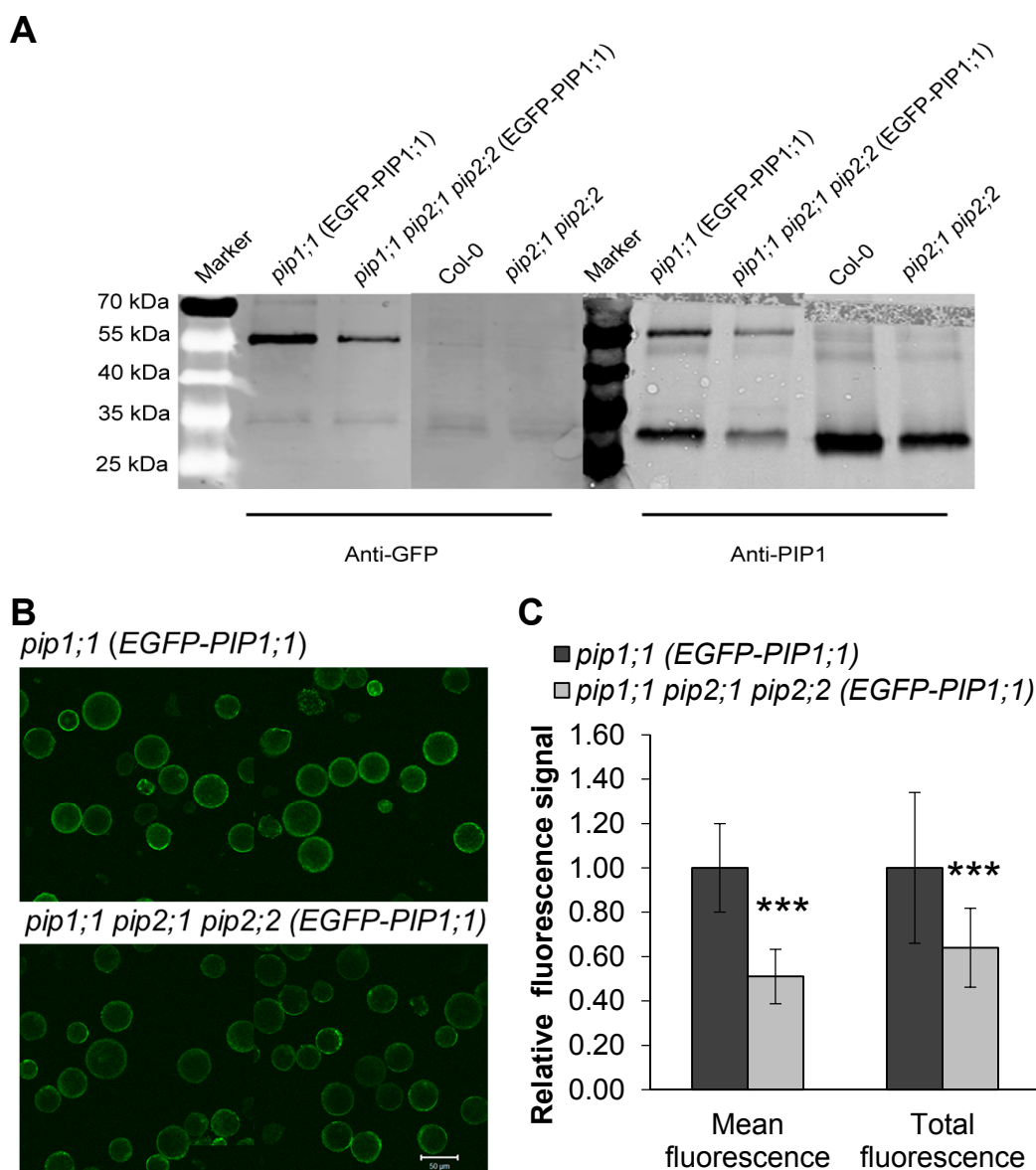


Figure 19. Immunoblot analysis and fluorescence quantification of EGFP-PIP1;1 fusion protein in mesophyll protoplasts of transgenic lines.

(A) Immunoblot analysis of microsomal membrane fractions from rosettes of transgenic lines (14-day-old plants grown on half strength MS plates) using an anti-GFP and an anti-PIP1 antibody. Col-0 and the *pip2;1 pip2;2* double mutant served as a negative control in anti-HA immunoblotting and as a positive control in an anti-PIP1 immunoblotting, respectively. (B) Confocal pictures of mesophyll protoplasts of two transgenic lines. (C) Relative quantification of the mean and the total fluorescence signal of EGFP-PIP1;1 fusion protein from individual protoplasts by Image J software (The total fluorescence signal = mean fluorescence level (mean grey value) × area of individual protoplasts). Expression levels relative to the levels quantified for wild type (mean values of at least 25 protoplast cells from three different pictures of the same setting in confocal microscopy). The asterisks denote statistically significant differences between samples (***) $p < 0.001$; two-tailed t test). Bars = 50 μ m. The experiment was independently repeated with similar result.

RESULTS

Seven-day-old seedlings of transgenic lines which had been studied above were examined by confocal microscopy to investigate that whether PIP1;1 protein repression was affected in the roots of the *pip2;1 pip2;2* double mutant. The roots were divided into four different zones: root zone I (meristematic/transition zone), root zone II (elongation zone), root zone III (maturation zone I), and root zone IV (maturation zone II-lateral root initiation zone) for better quantification analysis (Figure 20). Localization profiles of transgenic lines showed that the EGFP-PIP1;1 fluorescence signals were present at a rather low level in the root meristematic/transition zone. The fluorescence signal of EGFP-PIP1;1 increased in the root elongation zone, whereas it was decreased in the root maturation zone (Figure 21A).

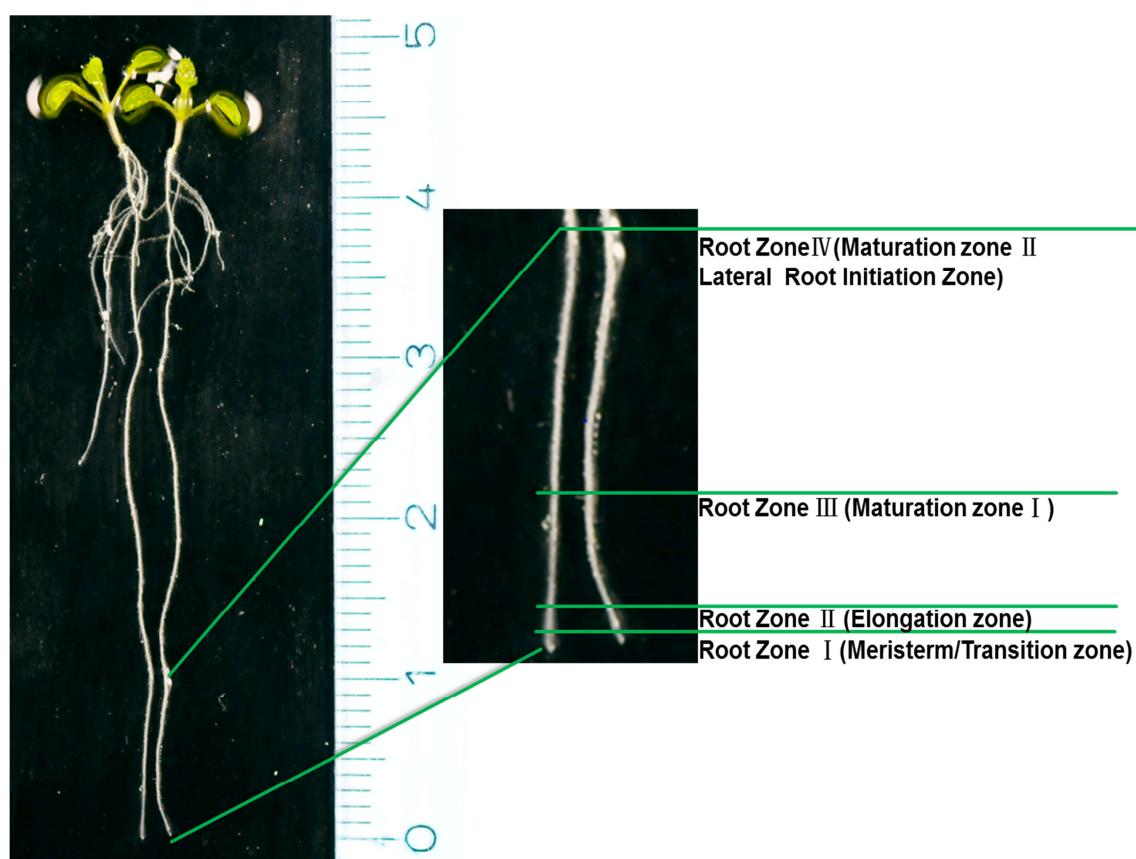


Figure 20. Different regions of the root for quantification of fluorescence signal of EGFP-fusion protein.

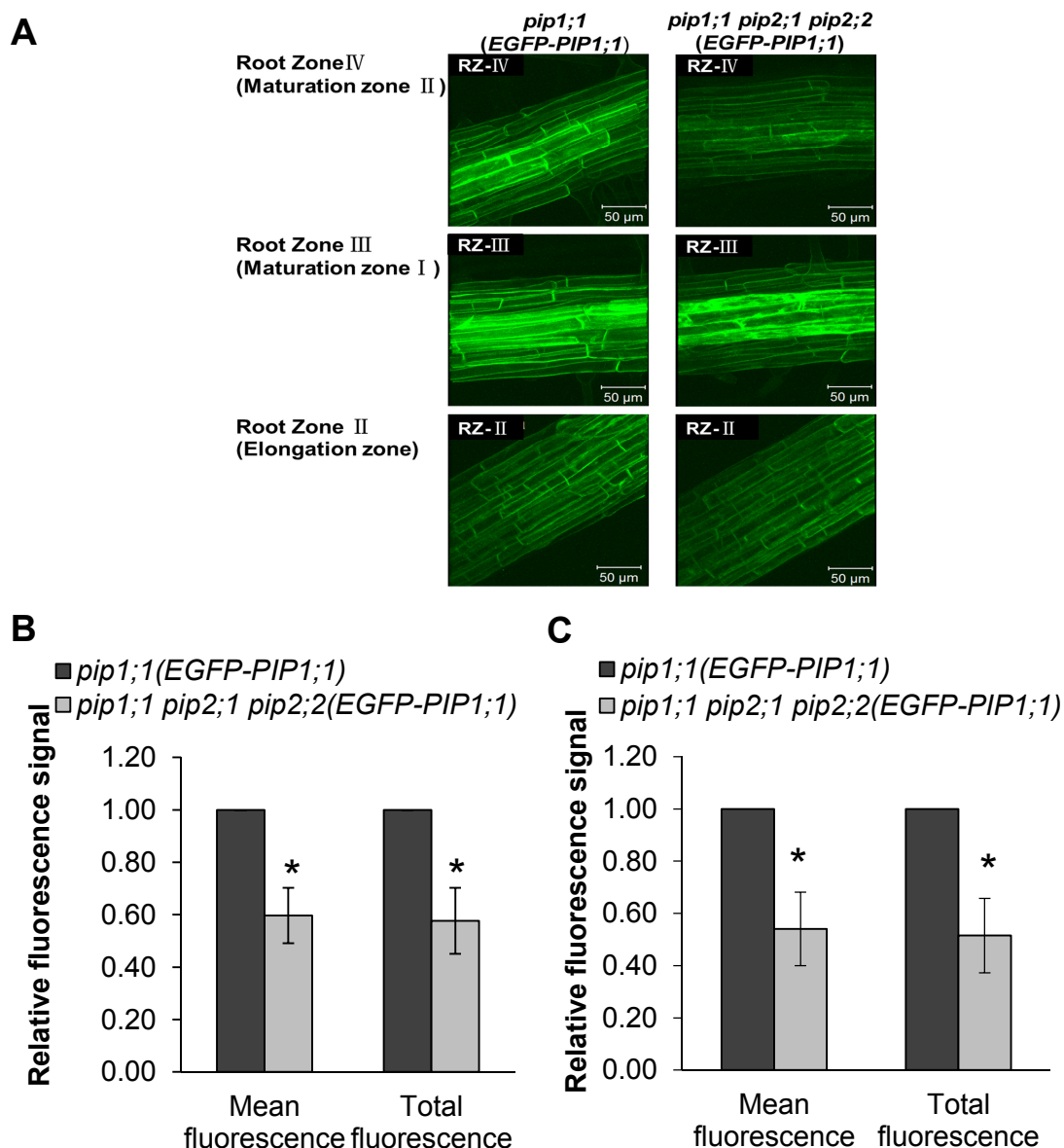


Figure 21. Fluorescence signals of EGFP-PIP1;1 fusion protein in different root zones and quantification of fluorescence signals in the root zone IV.

(A) Overlapped 40 Z-stack pictures of different root zones in seven-day-old seedlings of *pip1;1 (EGFP-PIP1;1)* and *pip1;1 pip2;1 pip2;2 (EGFP-PIP1;1)* utilizing the Maximum-intensity-projection function of the Zen software (1 μm interval per Z-stack). (B) Quantification of EGFP-PIP1;1 fluorescence intensity in the root zone IV by using overlapped pictures as shown in A by Image J software as described for the quantification in protoplasts. (C) Quantification of EGFP-PIP1;1 fluorescence signals from single Z-stack pictures of around 20 μm below the upper surface of the root zone IV. The data represent the mean ± SD of at least three independent samples. Expression levels relative to the levels quantified for wild-type line. The asterisks denote statistically significant differences between samples (* $p < 0.05$, two-tailed t test). Bars = 50 μm. The experiment was independently repeated with similar results.

RESULTS

By comparing different root zones at identical root length, the Z-stack confocal pictures of EGFP-PIP1;1 fluorescence signals from different transgenic lines were collected and quantitatively analyzed. The overlapped Z-stack pictures displayed the overview of the fluorescence signal of EGFP-PIP1;1 using the maximum-intensity-projection function of the Zen software. The EGFP-PIP1;1 fusion protein could be targeted to the plasma membrane in both cases, similarly with regard to its localization in mesophyll protoplasts. However, EGFP-PIP1;1 fluorescence signals exhibited fuzzy patterns and several unknown compartments were observed in the root zone III and root zone IV of the *pip2;1 pip2;2* double mutant (Figure 21A and 22). There was no significant difference between *pip2;1 pip2;2* and the wild-type line with regard to the fluorescence signal of EGFP-PIP1;1 in the root zone II (elongation zone). The fluorescence signal of EGFP-PIP1;1 fusion protein, however, became well visible in the root zone III (maturation zone I). A strong reduction of the fluorescence signal of the EGFP-PIP1;1 fusion protein was exhibited in the root zone IV of the *pip2;1 pip2;2* double mutant as compared to the wild-type line (Figure 21A). Similar distributions of fluorescence signals were observed in the independent transgenic lines of PIP1;1-EGFP (Figure 23A).

Relative quantification of the mean and the total fluorescence signal of overlapped Z-stack pictures or single pictures in a similar position from the root zone IV demonstrated the statistically significant reduction of the EGFP-PIP1;1 fusion protein in the *pip2;1 pip2;2* double mutant as compared to wild-type line (approximately 40-50% in Figure 21B and 21C). In addition, the statistically significant reduction of PIP1;1-EGFP was determined in the transgenic lines of PIP1;1-EGFP by the same quantification method (Figure 23B and 23C). These observations strongly suggested that PIP1;1 was repressed in the roots of the *pip2;1 pip2;2* double mutant as compared to the wild-type line. This effect was evident in the root maturation zone, but not obvious in the root elongation zone.

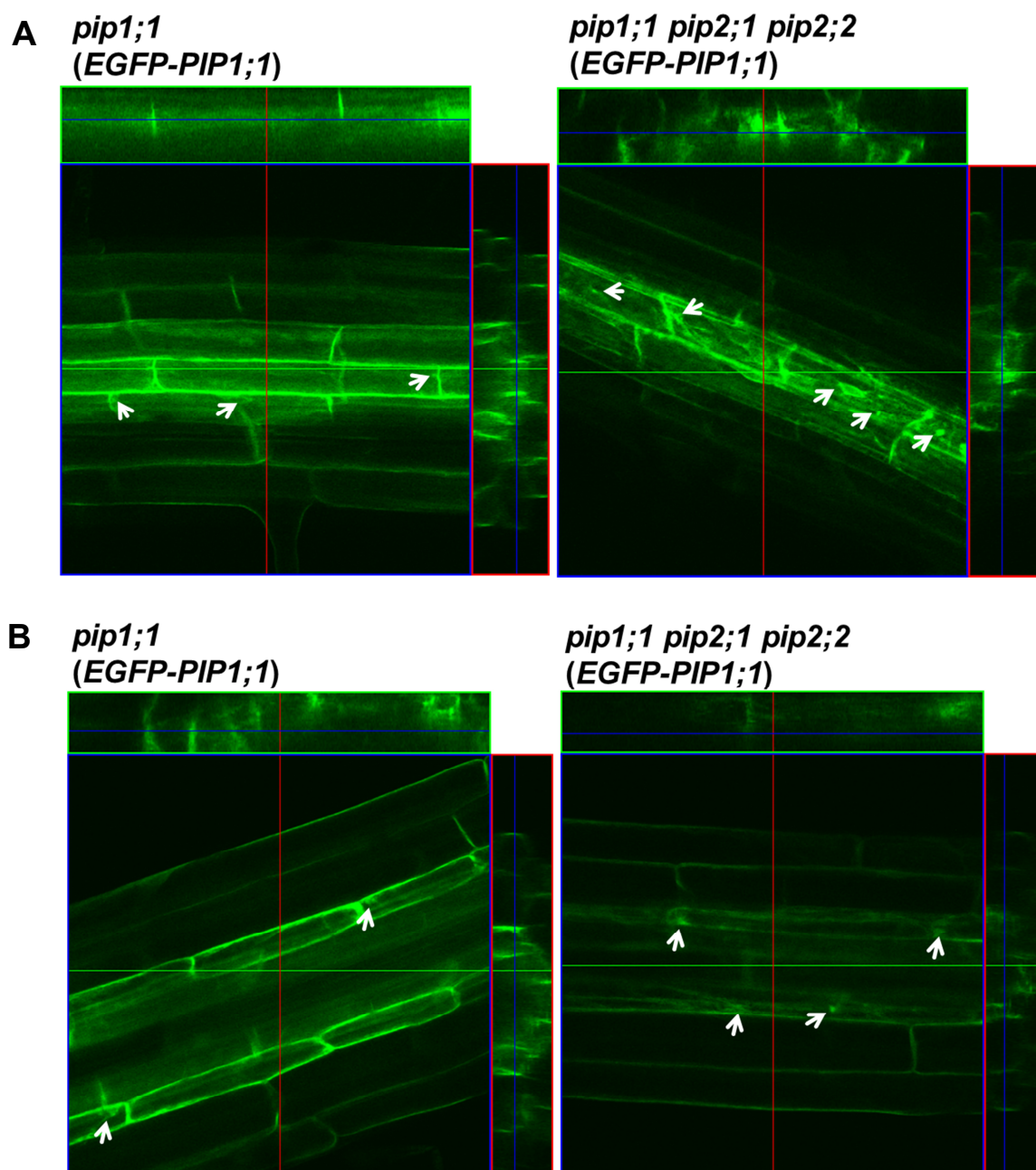


Figure 22. Unknown compartments of EGFP-PIP1;1 were observed in the root maturation zone of two transgenic lines.

(A) (B) EGFP-PIP1;1 fluorescence signal of the root maturation zone of two independent lines (seven-day-old seedlings) from different positions. The images were selected from a Z-stack obtained in a similar position of *pip1;1* (EGFP-PIP1;1) and of *pip1;1 pip2;1 pip2;2* (EGFP-PIP1;1).

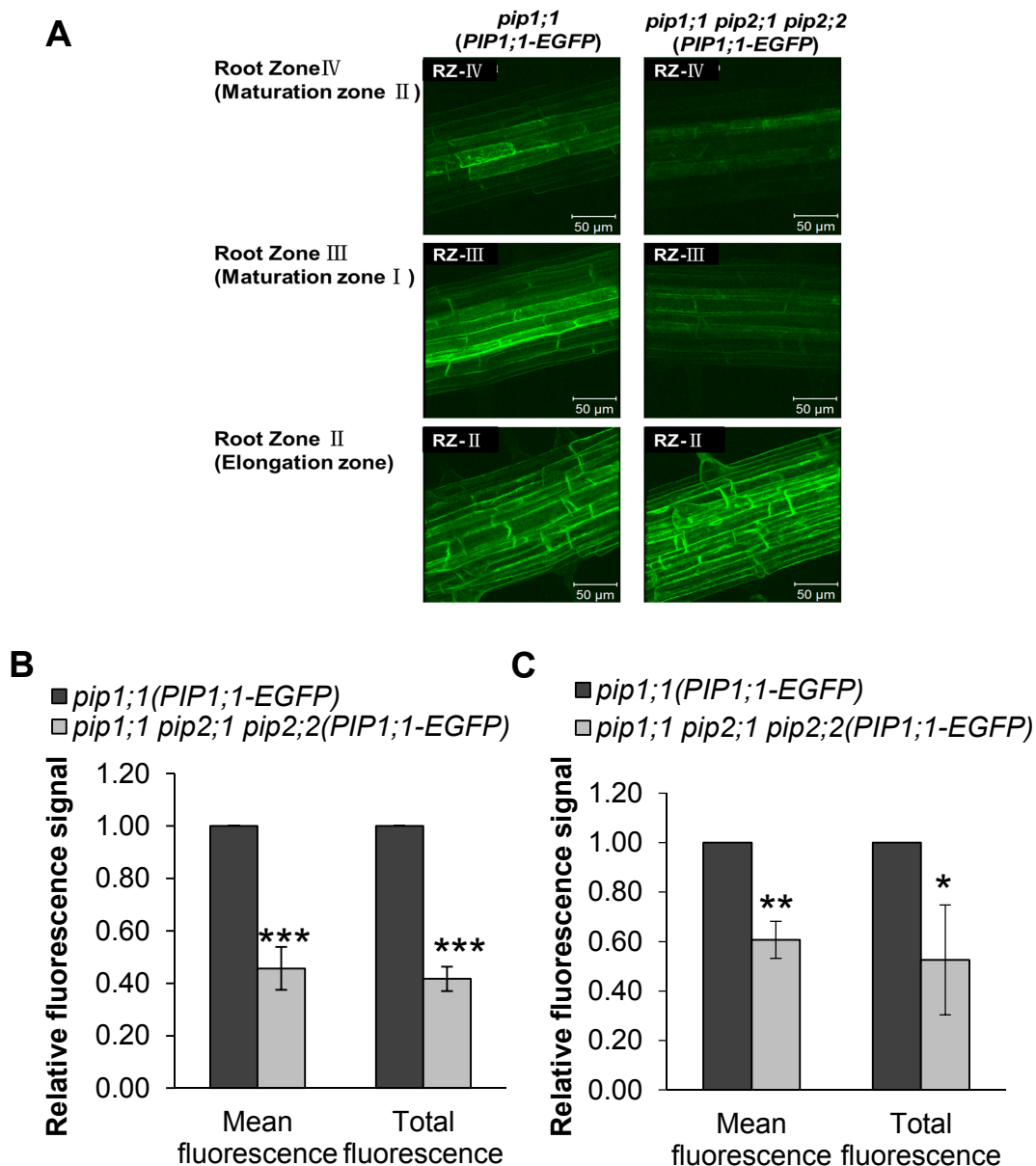


Figure 23. Fluorescence signals of the PIP1;1-EGFP fusion protein in different root zones and quantification of fluorescence signals in the root zone IV.

(A) Overlapped 40 Z-stack pictures of different root zones in seven-day-old seedlings of *pip1;1* (*PIP1;1-EGFP*) and *pip1;1 pip2;1 pip2;2* (*PIP1;1-EGFP*) utilizing the Maximum-intensity-projection function of the Zen software (1 μ m interval per Z-stack). (B) Quantification of PIP1;1-EGFP fluorescence intensity in the root zone IV by using overlapped pictures as shown in A. (C) Quantification of PIP1;1-EGFP fluorescence signals from single Z-stack pictures of around 20 μ m below the upper surface of the root zone IV. The data represent the mean \pm SD of at least three independent samples. Expression levels relative to the levels quantified for wild-type line. The asterisks denote statistically significant differences between samples (*** p < 0.001, ** p < 0.01, * p < 0.05; two-tailed t test). Bars = 50 μ m. The experiment was independently repeated with similar results.

Moreover, the transgenic lines which possessed the small hemagglutinin (HA) tag fusion to PIP1;1 were examined as an independent source of evidence determining whether PIP1;1 protein was affected in the *pip2;1 pip2;2* double mutant. The N-terminal fusion (*HA-PIP1;1*) construct was chosen due to the weak fluorescence signal of PIP1;1-EGFP. Two sets of independent transgenic lines (listed in Table 6) were generated and employed in the subsequent analyses.

Two lines which expressed the same transgenic insertion of HA-PIP1;1 (in a thereby complemented/regenerated-wild type and *pip2;1 pip2;2* double mutant background) were examined by immunoblotting using an antibody against HA and an antibody against the PIP1 protein, respectively. Western blot analysis revealed the correct size of the fusion protein: around 35 kDa (3xHA tag: 4 kDa, PIP1;1: 28 kDa) in both transgenic lines (Figure 24A). The immunoblotting signal of HA-PIP1;1 from *pip2;1 pip2;2* was much weaker than the signals from the wild-type line (Figure 24A), indicating that PIP1;1 was affected in the *pip2;1 pip2;2* double mutant in an anti-HA Western blot analysis. Furthermore, a weak immunoblotting signal in the monomer position (between 25-35 kDa marker) suggested that the other four PIP1 isoforms may be affected in the *pip2;1 pip2;2* double mutant as compared to the corresponding wild-type line in an anti-PIP1 Western blot analysis (Figure 24A).

ELISA quantification analyses of two independent sets of transgenic lines were conducted to experimentally verify the immunoblotting results and to evaluate to what extent the repression level in *pip2;1 pip2;2* as compared to the wild-type line. The strong reduction of two independent HA-PIP1;1 fusion proteins was detected in the rosettes of *pip2;1 pip2;2* as compared to the wild-type line (50-60%) (Figure 24B). However, the repression of the HA-PIP1;1 fusion protein was less affected in roots (20-40%) (Figure 24B). In summary, these results together firmly established that HA-PIP1;1 was strongly reduced in the *pip2;1 pip2;2* double mutant as compared to the wild-type line, especially in the rosettes.

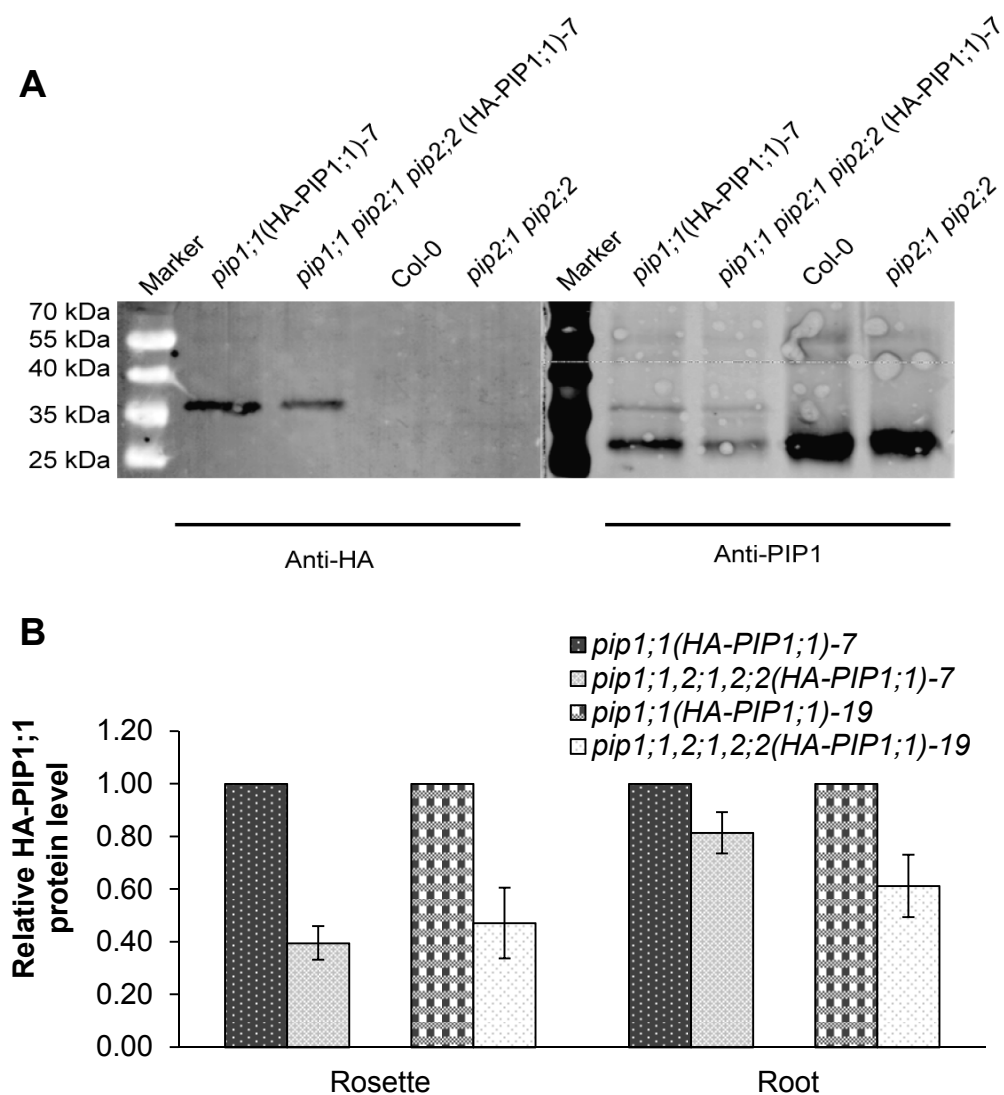


Figure 24. Immunoblot analysis and ELISA quantification of HA-PIP1;1 fusion protein in transgenic lines.

(A) Immunoblot analysis of microsomal fractions from the rosettes of 14-day-old transgenic lines by an anti-HA and an anti-PIP1. Col-0 and the *pip2;1 pip2;2* double mutant as a negative control in anti-HA immunoblotting and as a positive control in anti-PIP1 immunoblotting, respectively. (B) ELISA quantification of microsomal fractions from 14-day-old rosettes and roots of independent transgenic lines (60 seedlings pooled together for each line) (with the help of Jessica Lutterbach). Expression levels relative to the levels quantified for pseudowild-type line *pip1;1 (HA-PIP1;1)*. The data represent the means of three technical replicates. The experiment was independently repeated with similar results.

In summary, it can be stated that these data provided strong experimental evidence that PIP1;1 was subject to significant reduction in both the rosettes and the root maturation zone of the *pip2;1 pip2;2* double mutant.

2.4.4.2.2 The PIP1;1 protein level is differently affected in specific tissues of the *pip2;1* and the *pip2;2* mutants

It has been demonstrated that the total PIP1 protein is significantly reduced in the rosettes of the *pip2;1* mutant and in the roots of the *pip2;2* mutant by ELISA quantification (Figure 6). To assess whether PIP1;1 is differently affected in the rosettes and the roots of the *pip2;1* and the *pip2;2* mutants, the transgenic lines which harboured the same *EGFP-PIP1;1* or *PIP1;1-EGFP* construct (listed in Table 5, regenerated the *pip2;1* mutant and the *pip2;2* mutant) were utilized for observation of subcellular localization and for quantification of the fluorescence signals. The corresponding wild-type line and the *pip2;1 pip2;2* double mutant were used here as relative controls and for verification of the results above (2.4.4.2.1).

The 28-day-old rosettes of four different transgenic lines which harboured the same insertion site of *EGFP-PIP1;1* were examined first. To visualize the subcellular localization of EGFP-PIP1;1, mesophyll protoplasts from different transgenic line backgrounds were isolated and analyzed by using confocal microscopy. The confocal images showed that EGFP-PIP1;1 was mainly located at the plasma membrane in four different backgrounds, with few punctate fluorescence signals inside the protoplast cells (Figure 25A). More importantly, EGFP-PIP1;1 protein showed evident repression in the *pip2;1* mutant, but less strong reduction in the *pip2;2* mutant (Figure 25A-[b], [c]), as compared to the wild-type line and the *pip2;1 pip2;2* double mutant (Figure 25A-[a], [d]). Relative quantification of the mean and the total fluorescence signals (as described before) from the individual protoplasts demonstrated the statistically significant reduction of EGFP-PIP1;1 in the *pip2;1* mutant, the *pip2;2* mutant and the *pip2;1 pip2;2* double mutant compared to the wild-type line (Figure 25B). However, the repression of the EGFP-PIP1;1 fluorescence signal in the *pip2;1* mutant was stronger than in the *pip2;2* mutant.

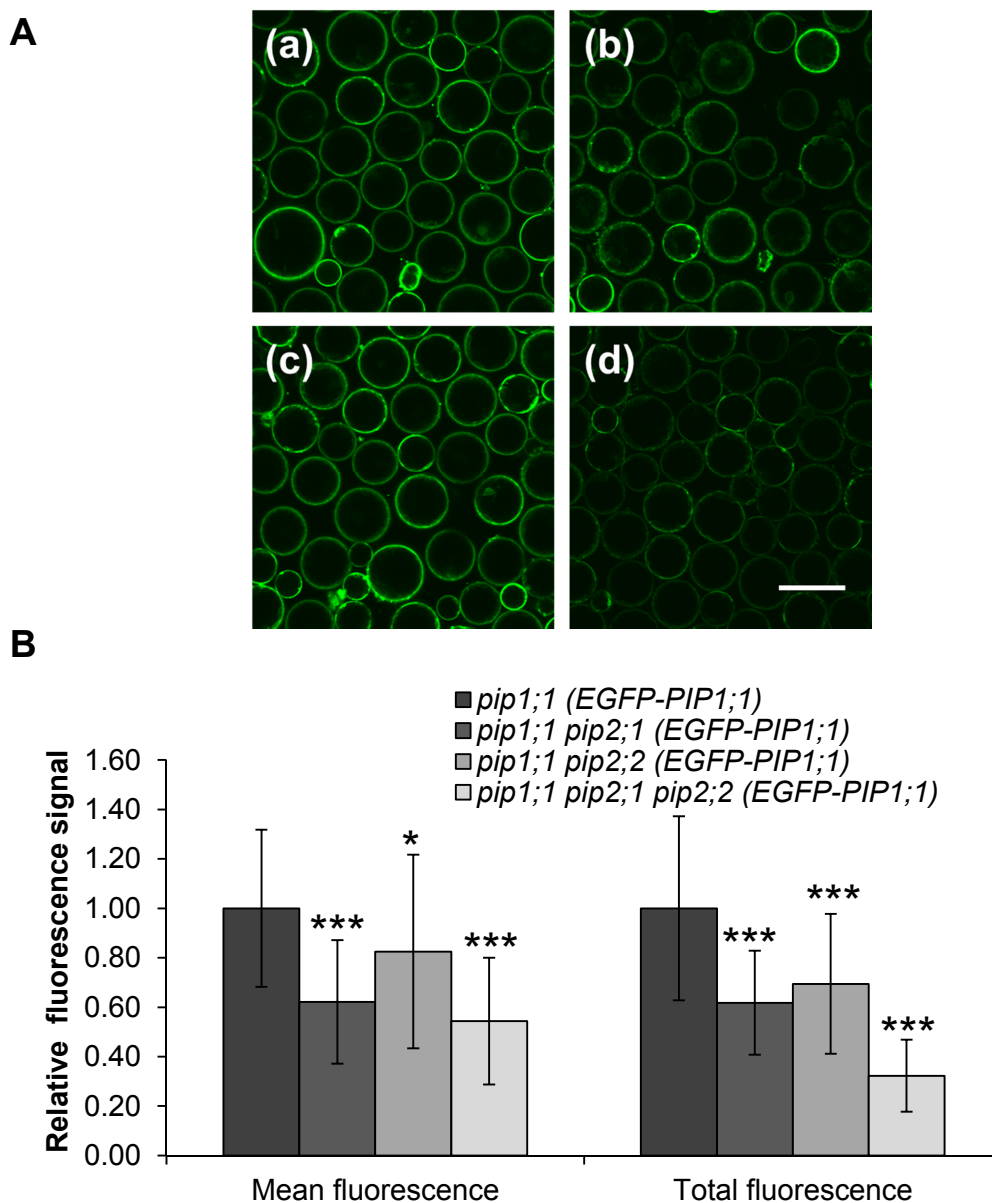


Figure 25. Fluorescence quantification of the EGFP-PIP1;1 fusion protein from mesophyll protoplasts of four different transgenic lines.

(A) Confocal pictures of mesophyll protoplasts from four different genotype backgrounds (a) *pip1;1* (EGFP-PIP1;1), (b) *pip1;1 pip2;1* (EGFP-PIP1;1), (c) *pip1;1 pip2;2* (EGFP-PIP1;1), (d) *pip1;1 pip2;1 pip2;2* (EGFP-PIP1;1). (B) Quantification of the mean and the total fluorescence signals of EGFP-PIP1;1 from individual protoplasts by Image J software (as described before). Expression levels relative to the levels quantified for wild type (mean values of at least 40 protoplast cells from three different confocal pictures with the same settings). The asterisks denote statistically significant differences between pseudowild-type line and corresponding mutant lines (***) $p < 0.001$, * $p < 0.05$; two-tailed t test). Bar = 50 μm . The experiment was independently repeated with similar results.

Quantification of the mean fluorescence signals of EGFP-PIP1;1 in confocal pictures revealed that PIP1;1 was slightly repressed in leaf cells of the *pip2;2* mutant (18%), but strongly repressed in the *pip2;1* mutant (38%) and the *pip2;1 pip2;2* double mutant (46%) (Figure 25B). A similar result was obtained by quantification of the total fluorescence signals of EGFP-PIP1;1 (Figure 25B).

As an independent evidence, the transgenic lines with the same insertion site of C-terminal fluorescence fusion (*PIP1;1-EGFP*) in the four different genotype backgrounds were utilized for the same experiment and analysis. Mesophyll protoplasts of these transgenic lines were isolated and analyzed by confocal microscopy.

Despite the fact that the fluorescence signals of PIP1;1-EGFP were weaker than those of EGFP-PIP1;1, even in the wild-type background, an evident repression of PIP1;1-EGFP was observed in the *pip2;1* mutant and the *pip2;1 pip2;2* double mutant (Figure 26A). The relative quantification of the mean fluorescence signal from the confocal images verified the result of repression of PIP1;1 from the EGFP-PIP1;1 transgenic lines, showing a reduction of PIP1;1-EGFP in *pip2;2* by about 15%, in *pip2;1* by about 30% and in *pip2;1 pip2;2* by about 30-40% as compared with wild-type background (Figure 26B). However, there was no change in the quantity of the total fluorescence signal of the *pip2;2* mutant as compared to the wild-type line.

Based on the quantitative results of EGFP-PIP1;1 and PIP1;1-EGFP in different mutant backgrounds, it became clear that PIP1;1 was significantly reduced in the rosettes of the *pip2;1* mutant. The repression of PIP1;1 was observed in the rosettes of the *pip2;2* mutant, however, not as pronounced as in the *pip2;1* mutant.

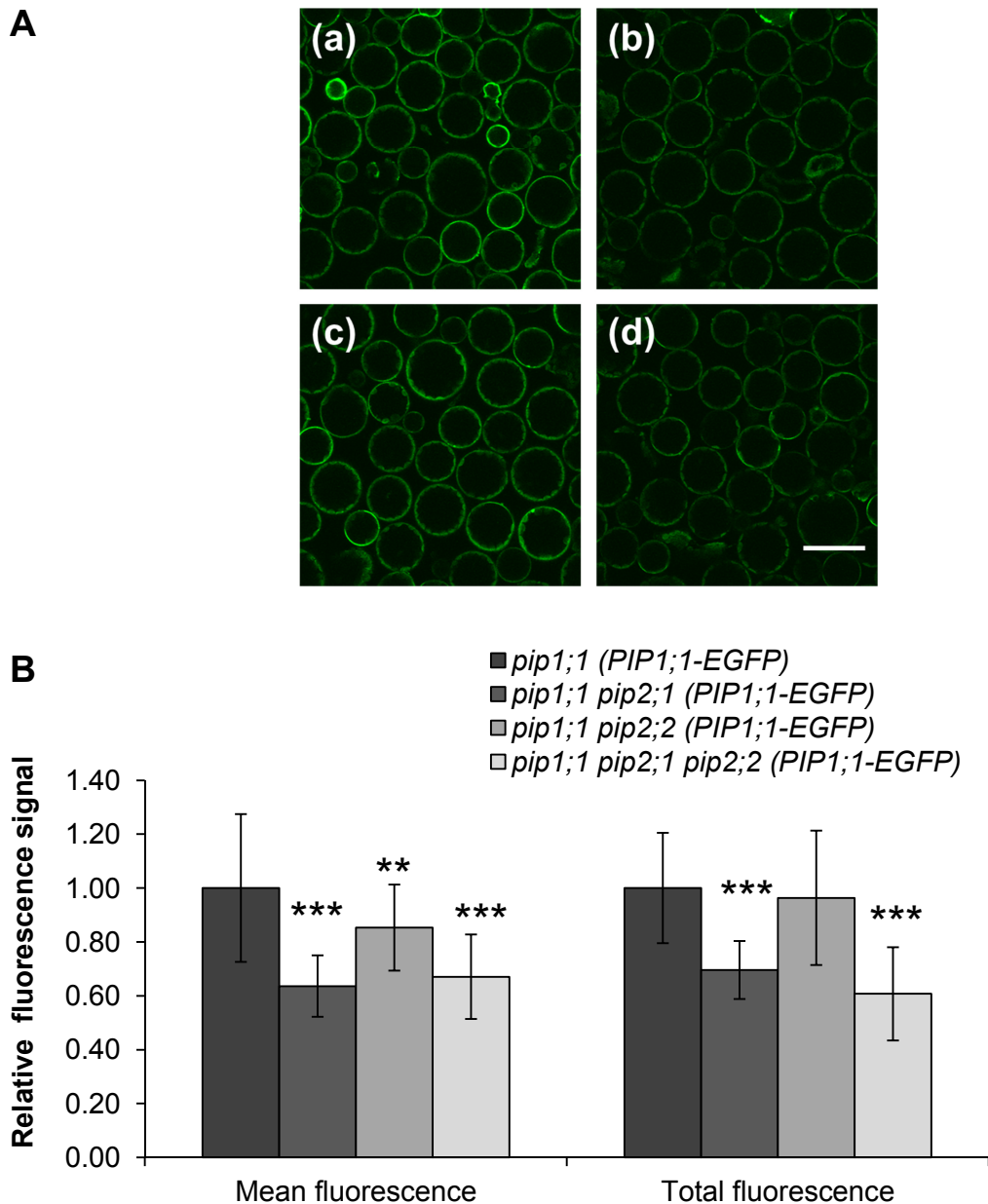


Figure 26. Fluorescence quantification of the PIP1;1-EGFP fusion protein from mesophyll protoplasts of four different transgenic lines.

(A) Confocal pictures of mesophyll protoplasts from four different genotype backgrounds (a) *pip1;1* (*PIP1;1-EGFP*), (b) *pip1;1 pip2;1* (*PIP1;1-EGFP*), (c) *pip1;1 pip2;2* (*PIP1;1-EGFP*), (d) *pip1;1 pip2;1 pip2;2* (*PIP1;1-EGFP*). (B) Quantification of the mean and the total fluorescence signals of PIP1;1-EGFP from individual protoplasts by Image J software (as described before). Expression levels relative to the levels quantified for wild type (mean value of at least 40 protoplast cells from three different confocal pictures with the same settings). The asterisks denote statistically significant differences between pseudowild-type line and corresponding mutant lines (***) $p < 0.001$, ** $p < 0.01$; two-tailed *t* test). Bar = 50 μm . The experiment was independently repeated with similar results.

In addition, the root (seven-day-old seedlings) of four different backgrounds of transgenic lines expressing *EGFP-PIP1;1* or *PIP1;1-EGFP* were utilized for localization and fluorescence signal quantification analysis as before (2.4.4.2.1). Based on the observation of the EGFP-PIP1;1 fluorescence signal in the different root zones (Figure 21A), the root zone IV (maturation zone II) of these transgenic lines was selected for further investigation. Confocal microscopy observation of the root maturation zone in the wild-type line showed that the EGFP-PIP1;1 was highly expressed in the epidermis, cortex, endodermis, less expressed in the pericycle and in vascular tissue, mainly located in the plasma membrane (Figure 27A [a]). The single picture from Z-stack of *pip2;1* mutant showed a slightly reduced fluorescence signal of EGFP-PIP1;1 in the epidermis and cortex (Figure 27A [b]). The reduction was more pronounced in the *pip2;2* mutant not only in its epidermis and cortex, but also in the endodermis and vascular tissue (Figure 27A [c]). The decrease of fluorescence signal of EGFP-PIP1;1 in the *pip2;1 pip2;2* double mutant was similar like that of the *pip2;2* mutant (Figure 27A [d]). The fluorescence signal of EGFP-PIP1;1 displayed in a fuzzy pattern in *pip2* mutants, especially evident in *pip2;1 pip2;2* double mutant background when the multiple Z-stack pictures were overlapped (Figure 27B). In addition, these overlapped pictures of all four different backgrounds were used for further quantification analysis. Relative quantification of the mean and the total fluorescence signal from the overlapped pictures demonstrated the statistically significant reduction of EGFP-PIP1;1 in the *pip2;1* mutant, the *pip2;2* mutant and the *pip2;1 pip2;2* double mutant as compared to the wild-type background. This result revealed that PIP1;1 was reduced in the root maturation zone of the *pip2;1* mutant by about 30-40%, in the *pip2;2* mutant by about 50% and in the *pip2;1 pip2;2* double mutant by about 60% as compared to the wild-type background (Figure 27C). A similar result was observed in independent *PIP1;1-EGFP* transgenic lines, confirming the result which was demonstrated above (Figure 28).

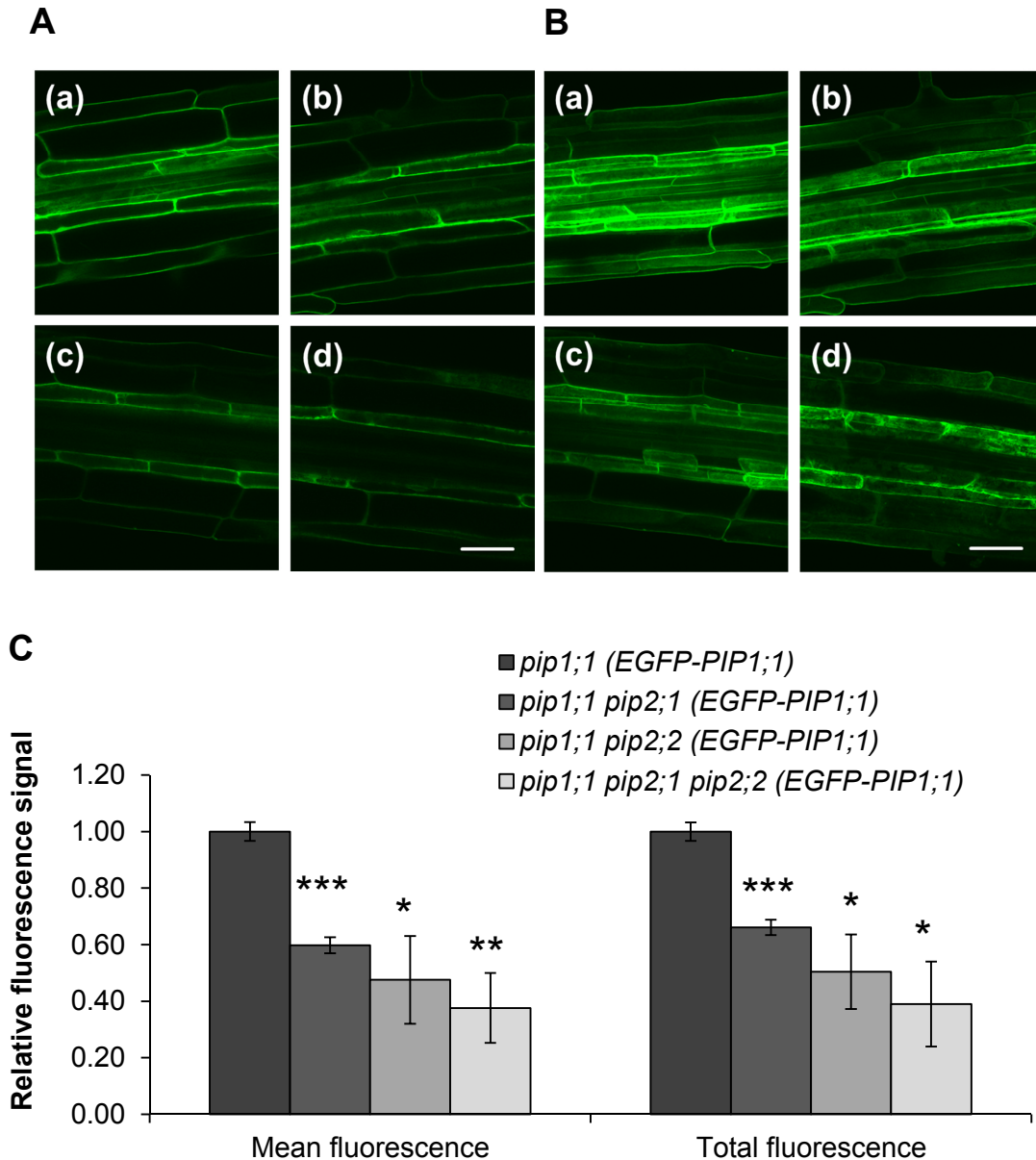


Figure 27. Fluorescence signals of EGFP-PIP1;1 in root zone IV and quantification of fluorescence signals in four different backgrounds.

(A) EGFP-PIP1;1 fluorescence of the root maturation zone of seven-day-old seedlings. The images were selected from a Z-stack from a similar position in (a) *pip1;1* (EGFP-PIP1;1), (b) *pip1;1 pip2;1* (EGFP-PIP1;1), (c) *pip1;1 pip2;2* (EGFP-PIP1;1), (d) *pip1;1 pip2;1 pip2;2* (EGFP-PIP1;1). (B) Maximum-intensity-projection of 17 Z-stack pictures of the root maturation zone of EGFP-PIP1;1 in transgenic lines as in A (1 μ m interval per Z-stack). (C) Quantification of fluorescence of images as presented in B. The data represent the mean \pm SD of at least three independent seedlings. The asterisks denote statistically significant differences between pseudowild-type line and corresponding mutant lines (***) $p < 0.001$, ** $p < 0.01$, * $p < 0.05$; two-tailed t test). Bars = 50 μ m.

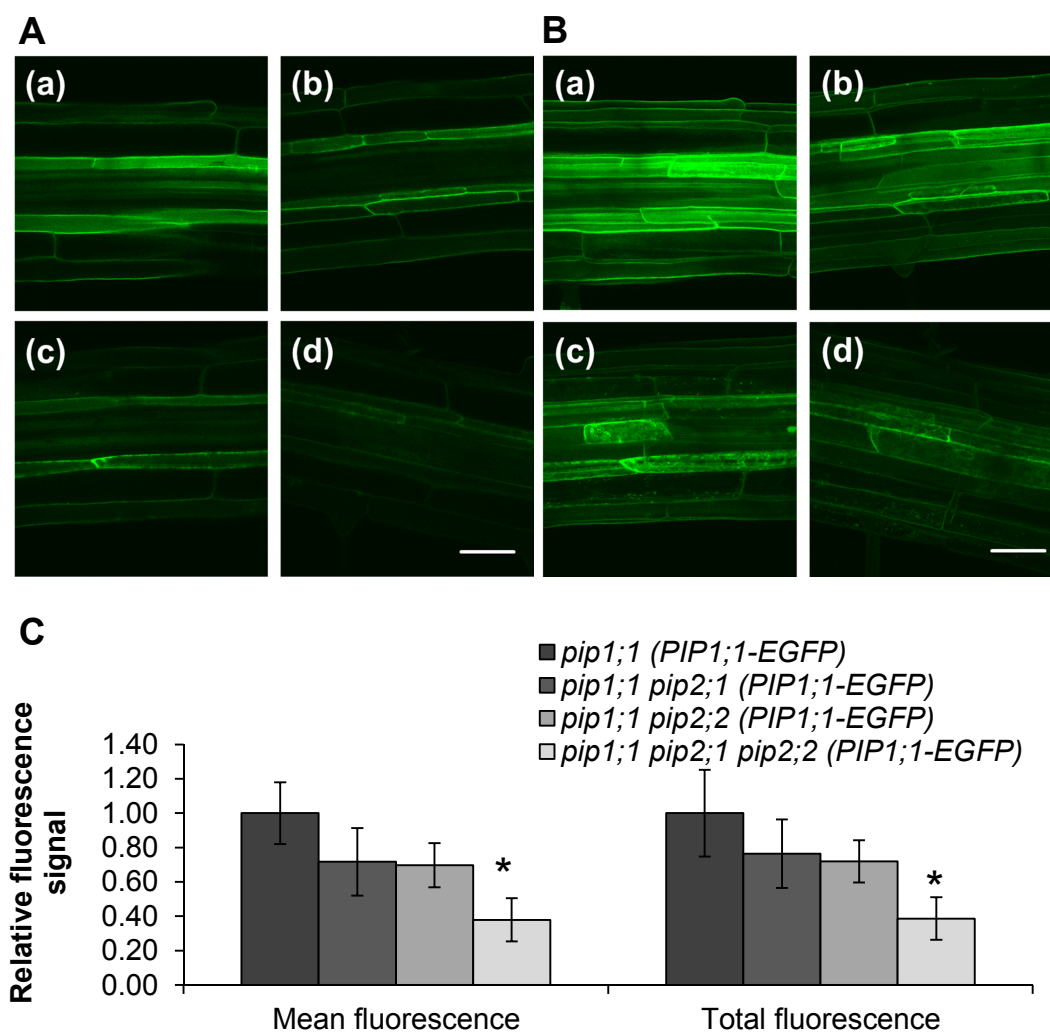


Figure 28. Fluorescence signals of PIP1;1-EGFP in root zone IV and quantification of fluorescence signals in four different backgrounds.

(A) PIP1;1-EGFP fluorescence of the root maturation zone of seven-day-old seedlings. The images were selected from a Z-stack from a similar position in (a) *pip1;1* (PIP1;1-EGFP), (b) *pip1;1 pip2;1* (PIP1;1-EGFP), (c) *pip1;1 pip2;2* (PIP1;1-EGFP), (d) *pip1;1 pip2;1 pip2;2* (PIP1;1-EGFP). (B) Maximum-intensity-projection of 26 Z-stack pictures of root maturation zone of EGFP-PIP1;1 in transgenic lines as in A (1 μm interval per Z-stack). (C) Quantification of fluorescence in the root maturation zone of Maximum intensity projection of 26 Z-stacks pictures (1 μm interval per Z-stack). Quantification of fluorescence of images as presented in B. The data represent the mean \pm SD of at least three independent seedlings. The asterisks denote statistically significant differences between pseudowild-type line and corresponding mutant lines (* $p < 0.05$; two-tailed t test). Bars = 50 μm .

Based upon the data described above, it could be concluded that PIP1;1 was more reduced in the rosette of the *pip2;1* mutant and as well reduced in the root maturation zone of the *pip2;1* mutant and the *pip2;2* mutant.

2.4.4.3. Quantitative analysis of tagged *PIP1;2* transgenic lines verifies the reduction of *PIP1;2* protein level

A similar strategy as in the previous *PIP1;1* part was followed to investigate to what extent the *PIP1;2* was affected in *pip2;1*, *pip2;2* and *pip2;1 pip2;2*. Homozygous transgenic lines which possessed the equivalent EGFP and HA tagged *PIP1;2* fusion constructs in the genome of four different genotype backgrounds were employed for analysis.

2.4.4.3.1 The *PIP1;2* protein level is reduced in the *pip2;1 pip2;2* double mutant

These transgenic lines which expressed EGFP-*PIP1;2* or *PIP1;2*-EGFP were first examined by immunoblotting using an antibody against GFP and an antibody against *PIP1* proteins, respectively.

The anti-GFP Western blot analysis, yielded the correct size of the fusion protein: around 55 kDa (EGFP: 26.9 kDa, *PIP1;1*: 28 kDa) in both transgenic lines (Figure 29A and 30A). It demonstrated that the immunoblotting signal of EGFP-*PIP1;2* and *PIP1;2*-EGFP from *pip2;1 pip2;2* was apparently weaker than the signals from the corresponding wild-type line (Figure 29A and 30A), indicating that *PIP1;2* had been affected in the *pip2;1 pip2;2* double mutant. In the anti-*PIP1* Western blot analysis, despite that it is difficult to distinguish the EGFP-*PIP1;2* and *PIP1;2*-EGFP fusion proteins from the *PIP1* dimer band because of the similar sizes of the protein bands (around 55 kDa) in transgenic lines (Figure 29A and 30A), the tendency of less *PIP1* protein in *pip2;1 pip2;2* as compared to the wild-type line was observed. Moreover, the less abundant immunoblotting signal of the monomer position (between 25-35 kDa) suggested that the other four *PIP1* isoforms may also be affected in the *pip2;1 pip2;2* double mutant as compared to the corresponding wild-type line (Figure 29A). These two Western blot analyses together confirmed the result which was deduced from loss-of-function *pip1* mutants analysis (Figure 14).

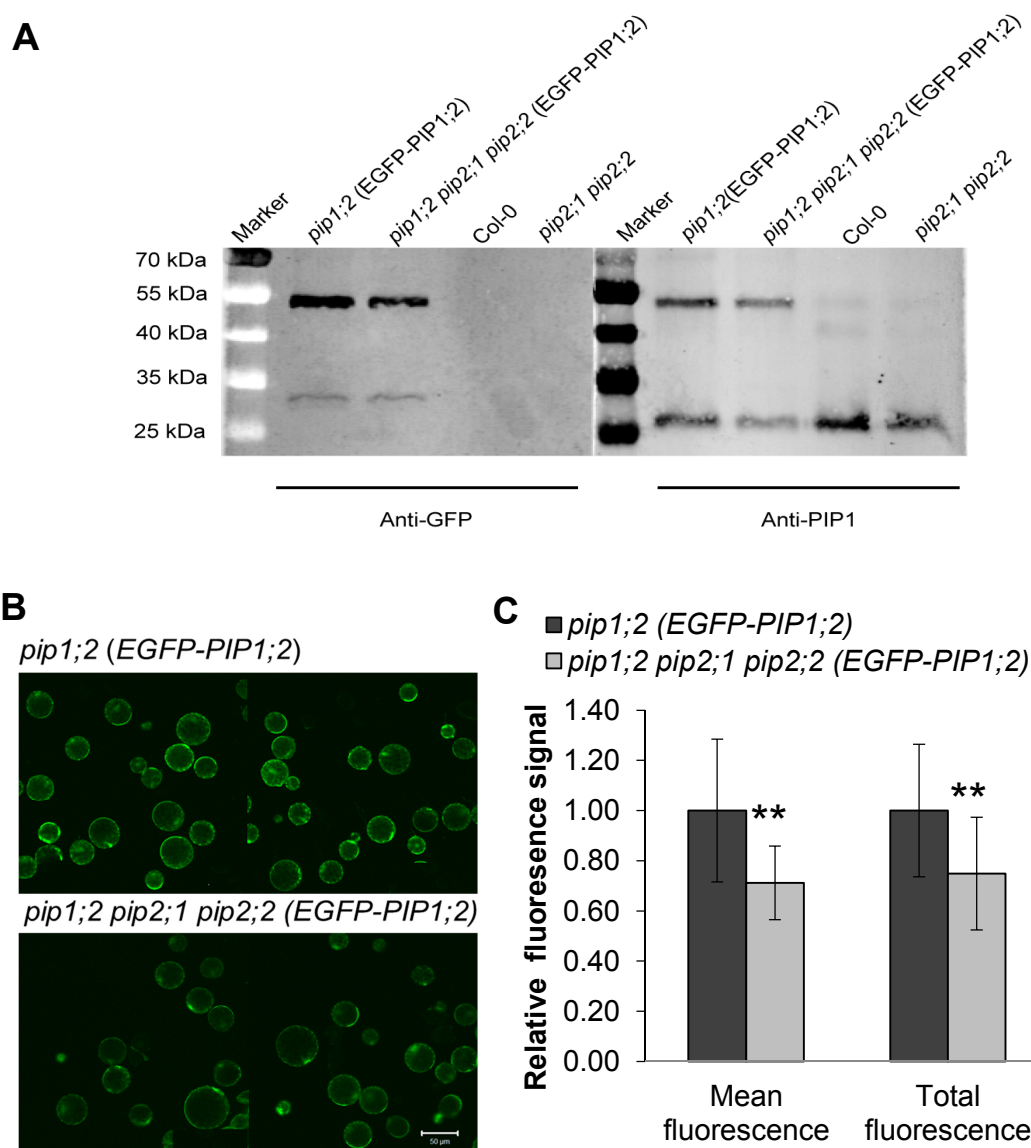


Figure 29. Immunoblot analysis and fluorescence quantification of EGFP-PIP1;2 fusion proteins in mesophyll protoplasts from two transgenic lines.

(A) Immunoblot analysis of microsomal membrane fractions from rosettes of transgenic lines (14-day-old plants grown on half strength MS plates) using an anti-GFP and an anti-PIP1 antibody. Col-0 and the *pip2;1 pip2;2* double mutant as the negative control in anti-GFP immunoblotting, and as the positive control in anti-PIP1 immunoblotting, respectively. (B) Confocal pictures of mesophyll protoplasts from two transgenic lines. (C) Relative quantification of the mean and the total fluorescence signals of EGFP-PIP1;2 fusion protein from individual protoplasts by Image J software (as described before). Expression levels relative to the levels quantified for the wild-type line (mean values of at least 25 protoplast cells from three different pictures of the same setting in confocal microscopy). The asterisks denote statistically significant differences between samples (** $p < 0.01$; two-tailed t test). Bars = 50 μm . The experiment was independently repeated with similar results.

RESULTS

To visualize the correct plasma membrane targeting of PIP1;2, quantitative live-cell imaging was also applied to mesophyll protoplasts using confocal microscopy. EGFP-PIP1;2 and PIP1;2-EGFP localized at the plasma membrane in both the wild-type and the *pip2;1 pip2;2* double mutant background (Figure 29B and 30B). The EGFP fluorescence signal in the protoplasts of *pip2;1 pip2;2* were clearly weaker than those in the wild-type background (Figure 29B and 30B). To gain more detailed data about the reduction of PIP1;2 in *pip2;1 pip2;2* as compared to wild type, fluorescence signals of the EGFP-PIP1;2 and PIP1;2-EGFP from individual protoplasts were quantitatively analyzed using Image J software. Relative quantification of the mean and the total fluorescence signals of EGFP-PIP1;2 from individual protoplasts both revealed the significant reduction of the EGFP-PIP1;2 (30%) and of PIP1;2-EGFP (50%) fluorescence signals in *pip2;1 pip2;2* as compared to the corresponding wild-type lines (Figure 29C and 30C). In summary, the results from N- and C-terminal EGFP fusions of *PIP1;2* transgenic lines both revealed that the PIP1;2 protein was affected in the rosettes of the *pip2;1 pip2;2* double mutant.

Seven-day-old seedlings of transgenic lines were examined by confocal microscopy to investigate that whether PIP1;2 protein repression was affected in the roots of the *pip2;1 pip2;2* double mutant following the same strategy as that for the *PIP1;1* transgenic lines (Figure 20). Localization profiles of transgenic lines showed that EGFP-PIP1;2 and PIP1;2-EGFP fluorescence signals could be targeted to the plasma membrane in both cases (Figure 31A and 33A). EGFP-PIP1;2 and PIP1;2-EGFP fusion proteins were visible in the root of the meristematic/transition zone. The fluorescence signal increased in the root elongation zone, whereas it was decreased in the root maturation zone (Figure 31A and 33A) of both transgenic lines.

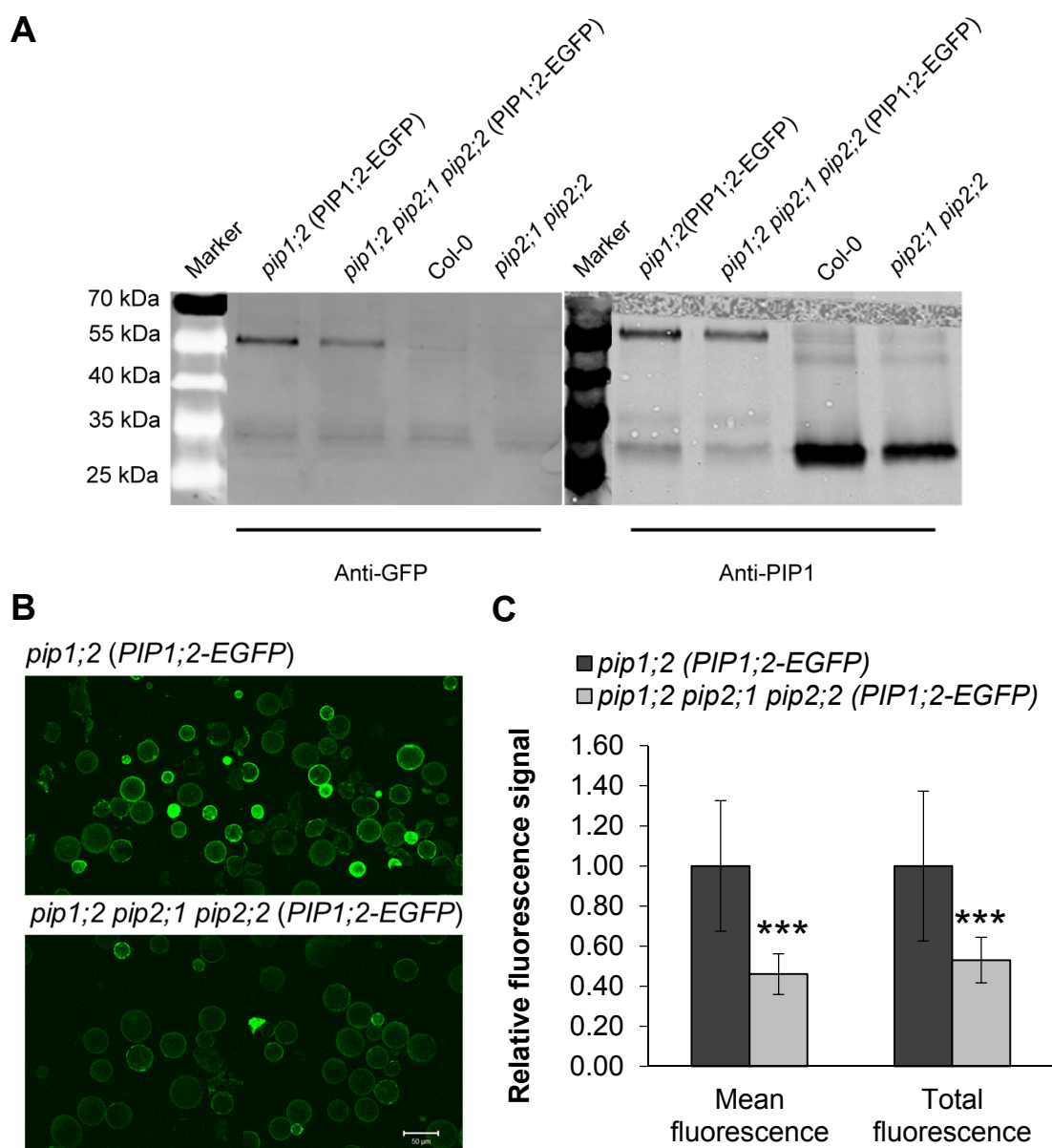


Figure 30. Immunoblot analysis and fluorescence quantification of PIP1;1-EGFP fusion protein in mesophyll protoplasts of two transgenic lines.

A) Immunoblot analysis of transgenic lines using an anti-GFP and an anti-PIP1 antibody. Col-0 and the *pip2;1 pip2;2* double mutant were the negative control in anti-GFP immunoblotting and the positive control in anti-PIP1 immunoblotting, respectively. B) Confocal pictures of mesophyll protoplasts of two transgenic lines. C) Relative quantification of the mean and the total fluorescence signals of the PIP1;2-EGFP fusion protein of individual protoplasts by Image J software (as described before). Expression levels relative to the levels quantified for the wild-type line (mean value of at least 25 protoplast cells from three different pictures of the same setting in confocal microscopy). The asterisks denote statistically significant differences between samples (***) $p < 0.001$; two-tailed t test). Bars = 50 μm . The experiment was independently repeated with similar results.

RESULTS

The Z-stack confocal pictures of EGFP-PIP1;2 and PIP1;2-EGFP fluorescence signals from different transgenic lines were collected and quantitatively analyzed, comparing different root zones at identical root length. The overlapped Z-stack pictures displayed the overview of fluorescence signals of EGFP-PIP1;2 or PIP1;2-EGFP using the Maximum-intensity-projection function of the Zen software. There was no significant difference of the fluorescence signal of EGFP-PIP1;2 or PIP1;2-EGFP of the root zone II (elongation zone) between *pip2;1 pip2;2* and the wild-type line (Figure 31A and 33A). The differences of fluorescence signals of EGFP-PIP1;2 or PIP1;2-EGFP fusion proteins became visible in root zone III (maturation zone I). A strong reduction of the fluorescence signals of EGFP-PIP1;2 or PIP1;2-EGFP fusion proteins was observed in root zone IV of the *pip2;1 pip2;2* double mutant as compared to the wild-type line (Figure 31A and 33A). More unknown fluorescence compartments were observed in the root zone IV of the *pip2;1 pip2;2* double mutant as compared to the wild-type line (Figure 32).

Relative quantification of the mean and the total fluorescence signals of overlapped Z-stack pictures or single pictures in similar position from the root zone IV demonstrated the statistically significant reduction of EGFP-PIP1;2 fusion protein in the *pip2;1 pip2;2* double mutant as compared to the wild-type line by about 30-40% (Figure 31B). In addition, a statistically significant reduction of PIP1;2-EGFP (50-60%) was determined in the *pip2;1 pip2;2* double mutant by the same quantification method (Figure 33B), confirming the results derived from *EGFP-PIP1;2* transgenic lines.

These observations strongly suggested that PIP1;2 was repressed in the roots of the *pip2;1 pip2;2* double mutant as compared to the wild-type line. This effect was evident in the root maturation zone, but not very obvious in the root elongation zone.

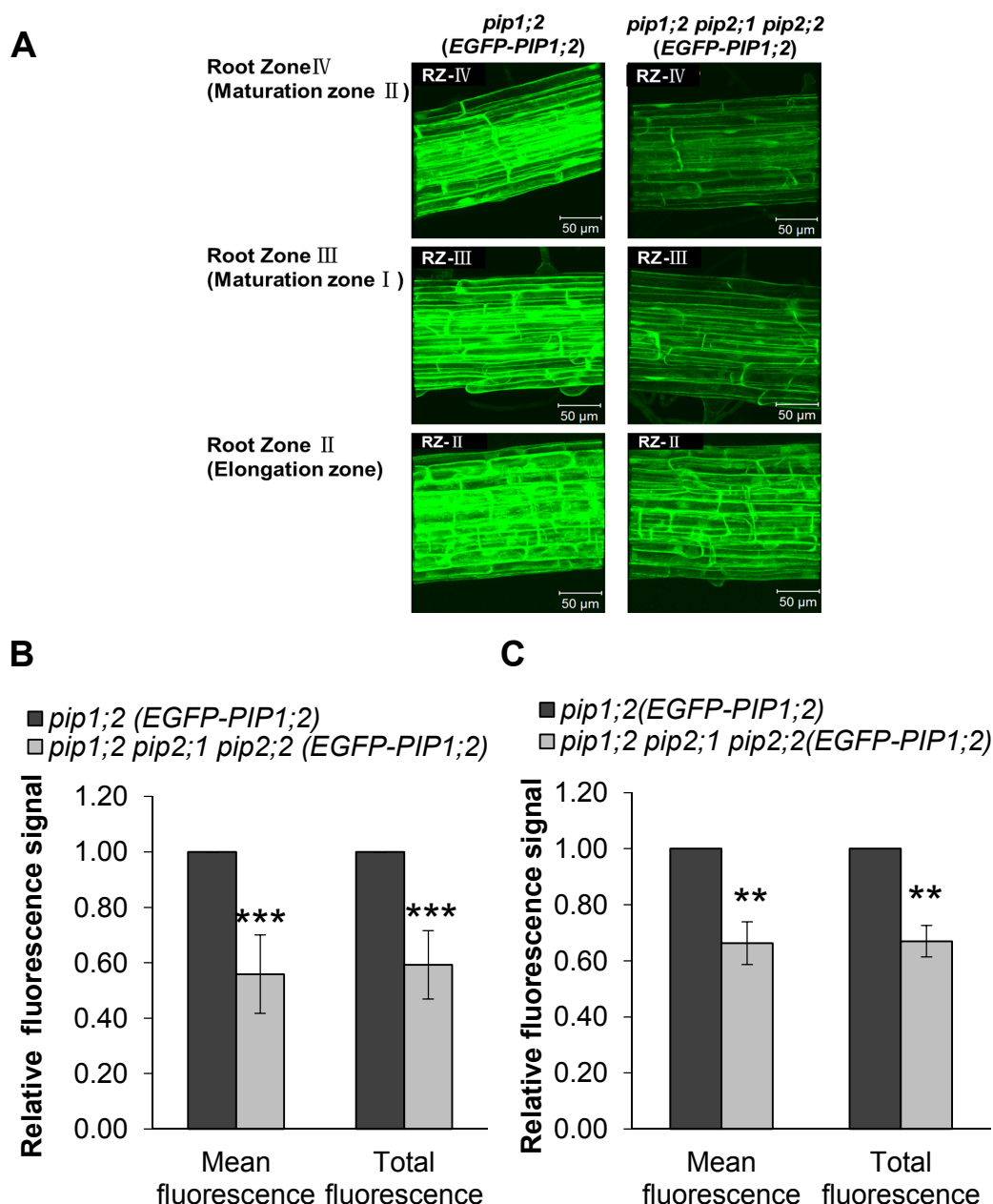


Figure 31. Fluorescence signals of the EGFP-PIP1;2 fusion protein in different root zones and quantification of fluorescence signals in the root zone IV.

(A) Overlapped 40 Z-stack pictures of different root zones in seven-day-old seedlings of *pip1;2* (EGFP-PIP1;2) and *pip1;2 pip2;1 pip2;2* (EGFP-PIP1;2) utilizing the Maximum-intensity-projection function of the Zen software (1 μ m interval per Z-stack). (B) Quantification of EGFP-PIP1;2 fluorescence intensity in the root zone IV by using overlapped pictures as shown in A. (C) Quantification of a EGFP-PIP1;2 fluorescence signal from single Z-stack picture of around 20 μ m below the upper surface of the root zone IV. Expression levels relative to the levels quantified for the wild-type line. The data represent the mean \pm SD of at least three independent samples. The asterisks denote statistically significant differences between samples. (***) $p < 0.001$, (**) $p < 0.01$; two-tailed t test). Bars = 50 μ m. The experiment was independently repeated with similar results.

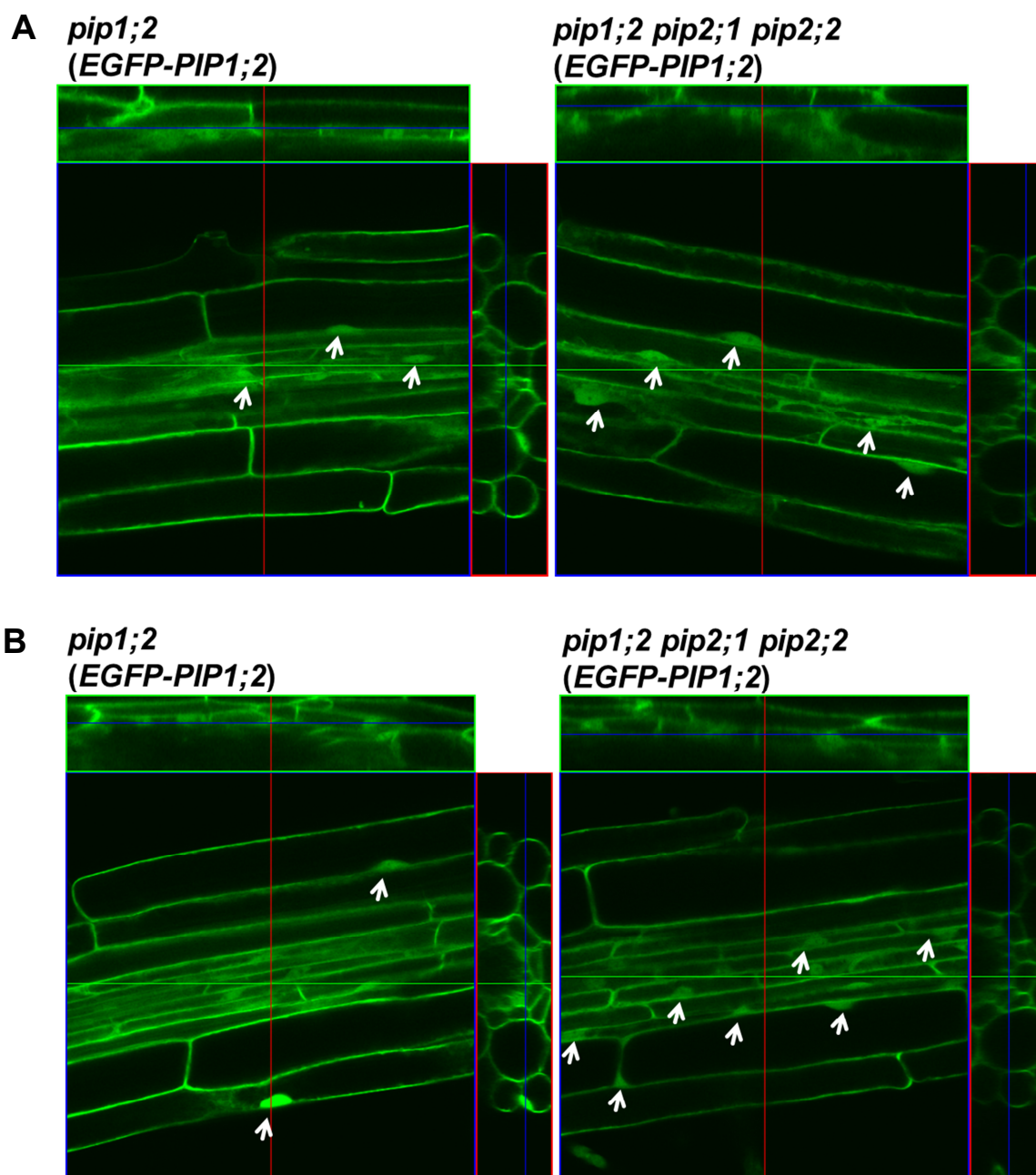


Figure 32. Unknown compartments of EGFP-PIP1;2 were observed in the root maturation zone of two transgenic lines.

(A) (B) EGFP-PIP1;2 fluorescence signal of the in root maturation zone II of two independent lines (seven-day-old seedlings). The images were selected from a Z-stack obtained from a similar position of *pip1;2* (EGFP-PIP1;2) and *pip1;2 pip2;1 pip2;2* (EGFP-PIP1;2).

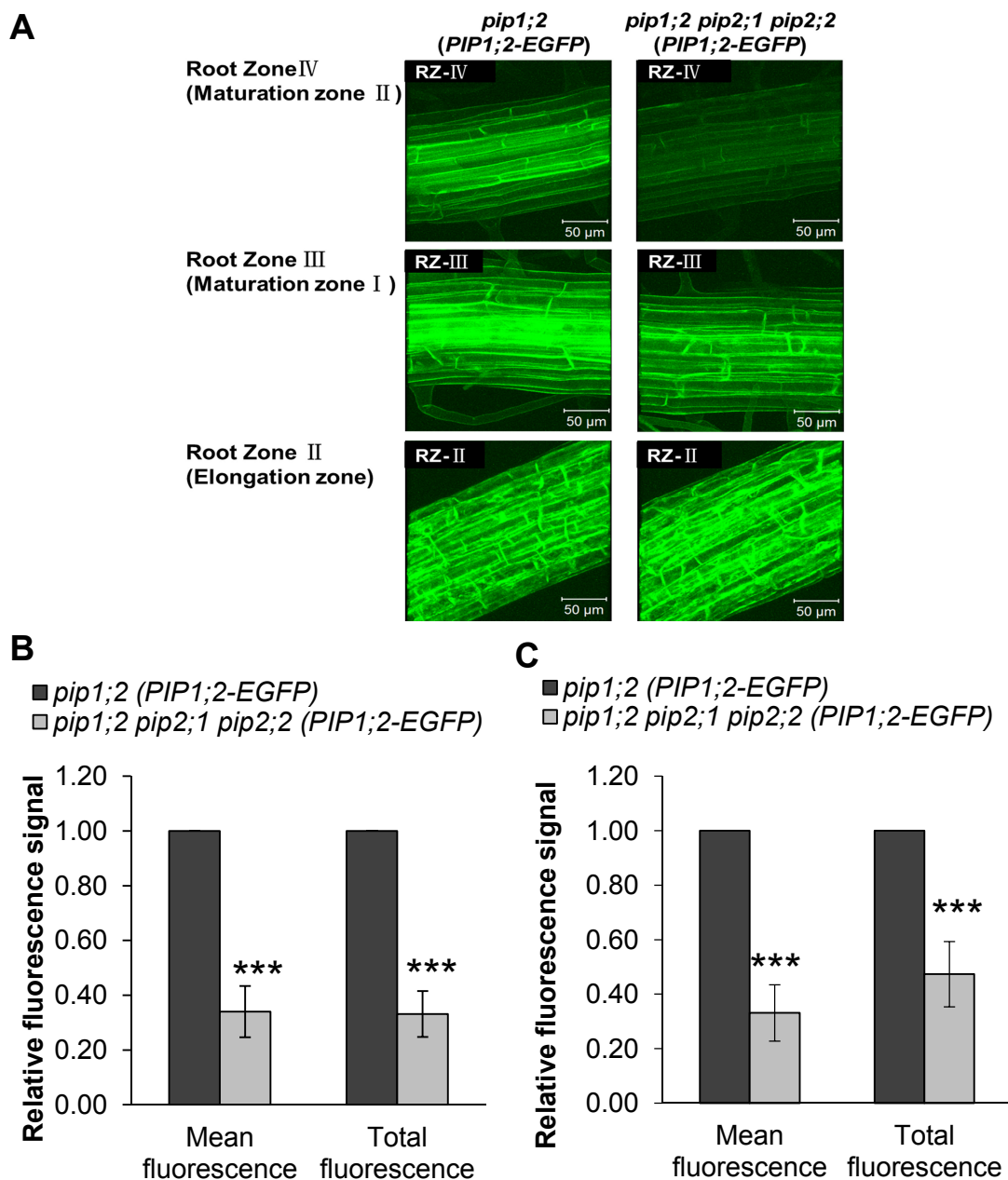


Figure 33. Fluorescence signals of PIP1;2-EGFP fusion protein in different root zones and quantification of fluorescence signal in the root zone IV.

(A) Overlapped 40 Z-stack pictures of different root zones in seven-day-old seedlings of *pip1;2* (PIP1;2-EGFP) and *pip1;2 pip2;1 pip2;2* (PIP1;2-EGFP) by using the Maximum-intensity-projection function of the Zen software (1 μ m interval per Z-stack). (B) Quantification of PIP1;2-EGFP fluorescence intensity in the root zone IV by using overlapped pictures as shown in A. (C) Quantification of a PIP1;2-EGFP fluorescence signal from single Z-stack picture of around 20 μ m below the upper surface of the root zone IV. Expression levels relative to the levels quantified for the wild-type line. The data represent the mean \pm SD of at least three independent samples. The asterisks denote statistically significant differences between samples. (***) $p < 0.001$; two-tailed t test). Bars = 50 μ m. The experiment was independently repeated with similar results.

RESULTS

In addition, another two sets of transgenic lines which possessed the small hemagglutinin tag fusion to *PIP1;2* were examined as an independent evidence for determining whether *PIP1;2* protein was affected in the *pip2;1 pip2;2* double mutant. Two lines which expressed the same transgenic insertion of *HA-PIP1;2* (in a thereby complemented/regenerated-wild type and *pip2;1 pip2;2* double mutant background) were examined by immunoblotting using an antibody against HA and an antibody against the *PIP1* protein, respectively. Western blot analysis revealed the correct size of the fusion protein: around 35 kDa (3 x HA tag: 4 kDa, *PIP1;1*: 28 kDa) in both transgenic lines (Figure 34A). The immunoblotting signal of *HA-PIP1;2* from *pip2;1 pip2;2* was apparently weaker than the signals from the wild-type line (Figure 34A), indicating that *PIP1;2* was affected in the *pip2;1 pip2;2* double mutant. Additionally, there was an extra band in this blot (above 55 kDa marker), which yielded a weaker signal in the *pip2;1 pip2;2* double mutant as compared to the wild-type line. This band could be the dimer of the *HA-PIP1;2* fusion protein, showing the same tendency of repression as the monomer of the *HA-PIP1;2* fusion protein. Furthermore, the weaker immunoblotting signal in the monomer position (between 25-35 kDa marker) suggested that the other four *PIP1* isoforms were also affected in the *pip2;1 pip2;2* double mutant as compared to the corresponding wild-type line in anti-*PIP1* Western blot analysis.

ELISA quantification analysis of two independent sets of transgenic lines was conducted to experimentally verify the Western blot result and to evaluate to what extent the repression level in *pip2;1 pip2;2* compared to the wild-type line. A strong reduction was detected in the rosettes of *pip2;1 pip2;2* as compared to the wild-type line (44-47%) of two independent sets of transgenic lines (Figure 34B). However, the repression of the *HA-PIP1;2* fusion protein was less affected in root (23-28%) (Figure 34B). In summary, these results therefore firmly established that *HA-PIP1;2* was strongly affected in the *pip2;1 pip2;2* double mutant as compared to the wild-type line, especially in the rosettes.

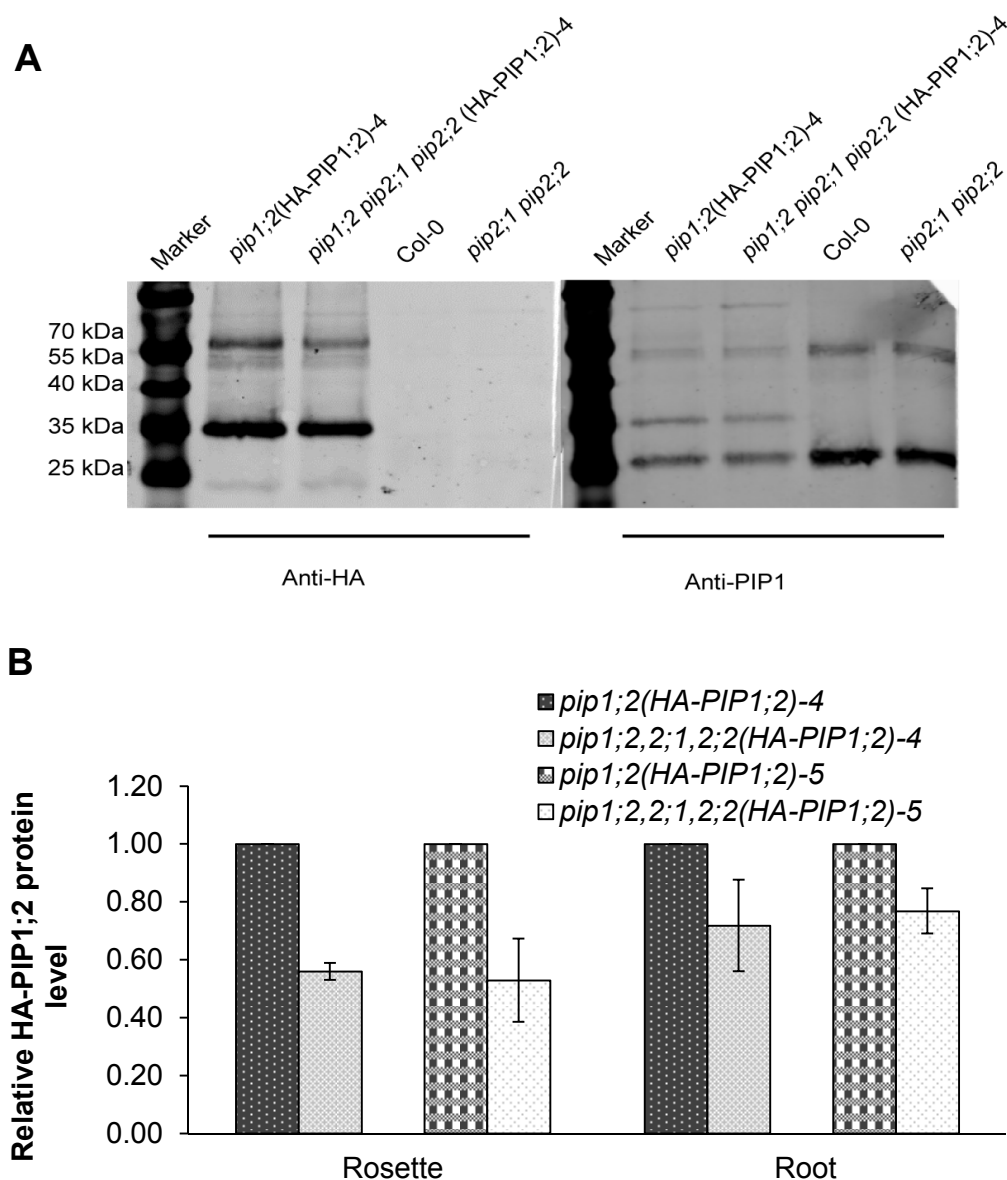


Figure 34. Immunoblot analysis and ELISA quantification of the HA-PIP1;2 fusion protein in transgenic lines.

A) Immunoblot analysis of microsomal fractions from 14-day-old rosettes of transgenic lines by an anti-HA and an anti-PIP1. Col-0 and the *pip2;1 pip2;2* double mutant as the negative control in anti-HA immunoblotting, and as the positive control in anti-PIP1 immunoblotting, respectively. B) ELISA quantification of microsomal membrane fractions from 14-day-old rosettes and roots of independent transgenic lines (60 seedlings pooled together for each sample) (with the help of Jessica Lutterbach). Expression levels relative to the levels quantified for pseudowild-type line *pip1;2 (HA-PIP1;2)*. The data represent the mean of three technical replicates. The experiment was independently repeated with similar results.

2.4.4.3.2 The PIP1;2 protein level is differently affected in specific tissues of the *pip2;1* and the *pip2;2* mutants

The transgenic lines which harboured the same *EGFP-PIP1;2* or *PIP1;2-EGFP* construct (listed in Table 5, which regenerated the *pip2;1* mutant and the *pip2;2* mutant) were utilized for observation of subcellular localization and for quantification of the fluorescence signal in order to assess whether PIP1;2 was differently affected in the rosettes and roots of the *pip2;1* and *pip2;2* mutants, similar to the approach followed for PIP1;1. The corresponding wild-type line and the *pip2;1 pip2;2* double mutant were used here as a relative control and for verification of the results demonstrated above (2.4.4.3.1). The mesophyll protoplasts from 28-day-old rosettes of four different transgenic lines were analyzed by using confocal microscopy. Confocal images showed that the fluorescence signal of PIP1;2-EGFP was relatively strong and uniformly distributed at the plasma membrane of wild type and *pip2;2* as compared to the protoplasts from *pip2;1* and *pip2;1 pip2;2*, which exhibited weak and relatively patchy distribution fluorescence signals of PIP1;2-EGFP at the plasma membrane (Figure 35A). More importantly, the EGFP-PIP1;2 protein showed evident repression in *pip2;1*, but less strong reduction in *pip2;2* (Figure 35A [b] [c]), as compared to the wild-type line and to *pip2;1 pip2;2* (Figure 35A [a] [d]). Relative quantification of the mean and the total fluorescence signals demonstrated a statistically significant reduction of EGFP-PIP1;2 in the *pip2;1* mutant and *pip2;1 pip2;2* double mutant as compared to the wild-type line. The tendency towards repression of EGFP-PIP1;2 was observed in the *pip2;2* mutant. The analysis of independent transgenic lines of PIP1;2-EGFP confirmed the result described above (Figure 36). Based on the quantitative results of EGFP-PIP1;2 and PIP1;2-EGFP in different mutant backgrounds, it became clear that PIP1;2 was significantly reduced in the rosettes of *pip2;1*. The repression of PIP1;2 was observed in the rosettes of *pip2;2*, however, it was not as evident as in the *pip2;1* mutant.

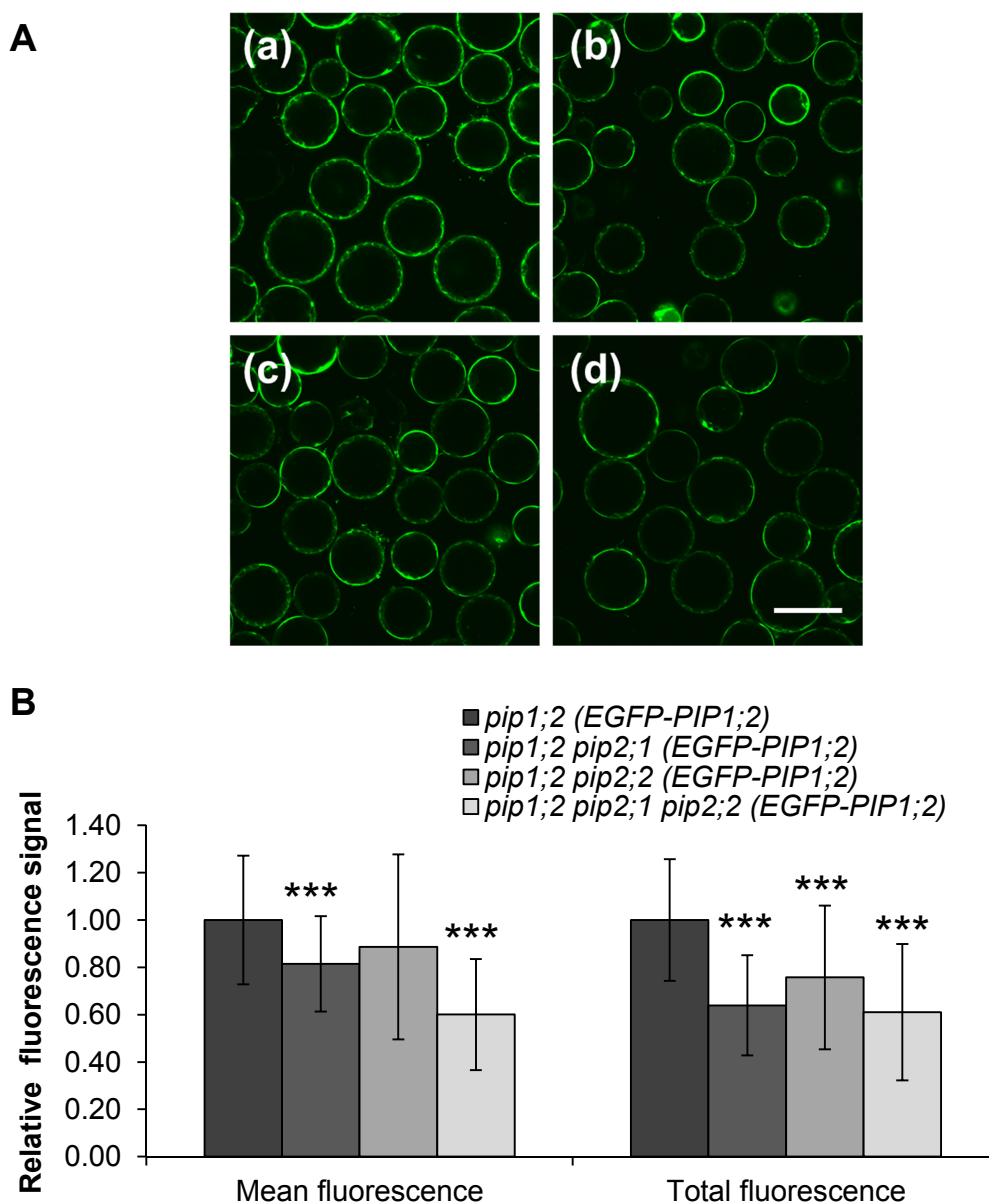


Figure 35. Fluorescence quantification of the EGFP-PIP1;2 fusion protein from mesophyll protoplasts of four different transgenic lines.

(A) Confocal pictures of mesophyll protoplasts from four different genotype backgrounds (a) *pip1;1* (EGFP-PIP1;2), (b) *pip1;2 pip2;1* (EGFP-PIP1;2), (c) *pip1;2 pip2;2* (EGFP-PIP1;2), (d) *pip1;2 pip2;1 pip2;2* (EGFP-PIP1;2). (B) Quantification of the mean and the total fluorescence signals of EGFP-PIP1;2 from individual protoplasts by the Image J software (as described before). Expression levels relative to the levels quantified for the wild-type line (mean value of at least 40 protoplast cells from three different confocal pictures with the same settings). The asterisks denote statistically significant differences between pseudowild-type line and corresponding mutant lines (*** $p < 0.001$; two-tailed t test). Bar = 50 μ m. The experiment was independently repeated with similar results.

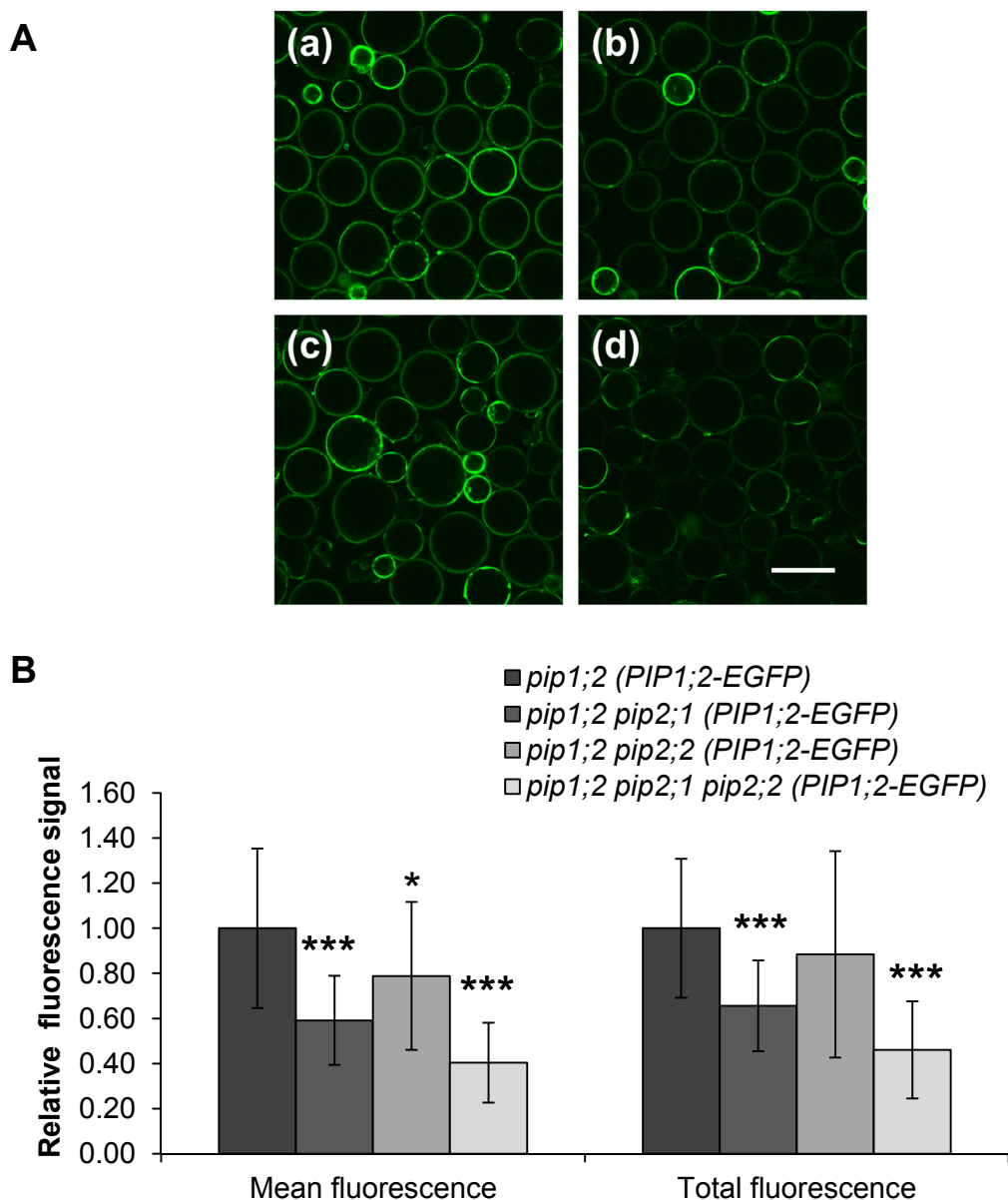


Figure 36. Fluorescence quantification of the PIP1;2-EGFP fusion protein from mesophyll protoplasts of four different transgenic lines.

(A) Confocal pictures of mesophyll protoplasts from four different genotype backgrounds (a) *pip1;2* (*PIP1;2-EGFP*), (b) *pip1;2 pip2;1* (*PIP1;2-EGFP*), (c) *pip1;2 pip2;2* (*PIP1;2-EGFP*), (d) *pip1;2 pip2;1 pip2;2* (*PIP1;2-EGFP*). (B) Quantification of the mean and the total fluorescence signals of PIP1;1-EGFP from individual protoplasts by the Image J software (as described before). Expression levels relative to the levels quantified for the wild-type line (mean value of at least 40 protoplast cells from three different confocal pictures with the same settings). The asterisks denote statistically significant differences between pseudowild-type line and corresponding mutant lines (***) $p < 0.001$, (*) $p < 0.05$; two-tailed t test). Bar = 50 μm . The experiment was independently repeated with similar results.

In addition, roots (of seven-day-old seedlings) of four different backgrounds of transgenic lines harbouring the same *EGFP-PIP1;2* or *PIP1;2-EGFP* were utilized for localization and fluorescence signal quantification analysis as before. Based on the observation of *EGFP-PIP1;2* fluorescence signals in the different root zones (Figure 31A), the root zone IV (maturation zone II) of these transgenic lines were selected for further investigation. Confocal microscopy observations of the root maturation zone in the wild-type line showed that the *EGFP-PIP1;2* was highly expressed in the epidermis, cortex, endodermis, pericycle, but less expressed in vascular tissue, mainly located in the plasma membrane (Figure 37A [a]). The pictures of the *pip2;1* mutant and of the *pip2;2* mutant both showed a slightly reduced fluorescence signal of the *EGFP-PIP1;2* fusion protein in general (Figure 37A [b] [c]). A strong decrease of the fluorescence signal of the *EGFP-PIP1;2* fusion protein in the *pip2;1 pip2;2* double mutant was observed (Figure 37A [d]). The overlapped Z-stack pictures of fluorescence signals of the *EGFP-PIP1;2* fusion protein in all four different backgrounds were used for further quantification analysis. Relative quantification of the mean and the total fluorescence signals from the overlapped pictures demonstrated the significant reduction of the *EGFP-PIP1;2* protein in the *pip2;1 pip2;2* double mutant as compared to the wild-type line. This result revealed that the *EGFP-PIP1;2* fusion protein was repressed in *pip2;1 pip2;2* by about 35% (Figure 37B). However, no statistically significant change was observed in the *pip2;1* and in the *pip2;2* mutants as compared to the wild-type line. On the other hand, the independent transgenic lines of *PIP1;2-EGFP* exhibited strong reduction in the *pip2* mutants (Figure 38A and 38B). The quantitative results of *PIP1;2-EGFP* transgenic lines in the root maturation zone not only confirmed the repression of the *EGFP-PIP1;2* fusion protein in *pip2;1 pip2;2* (roughly 70%), but also revealed an additional repression phenomenon in *pip2;1* (roughly 40%) and *pip2;2* (roughly 50%) (Figure 38C).

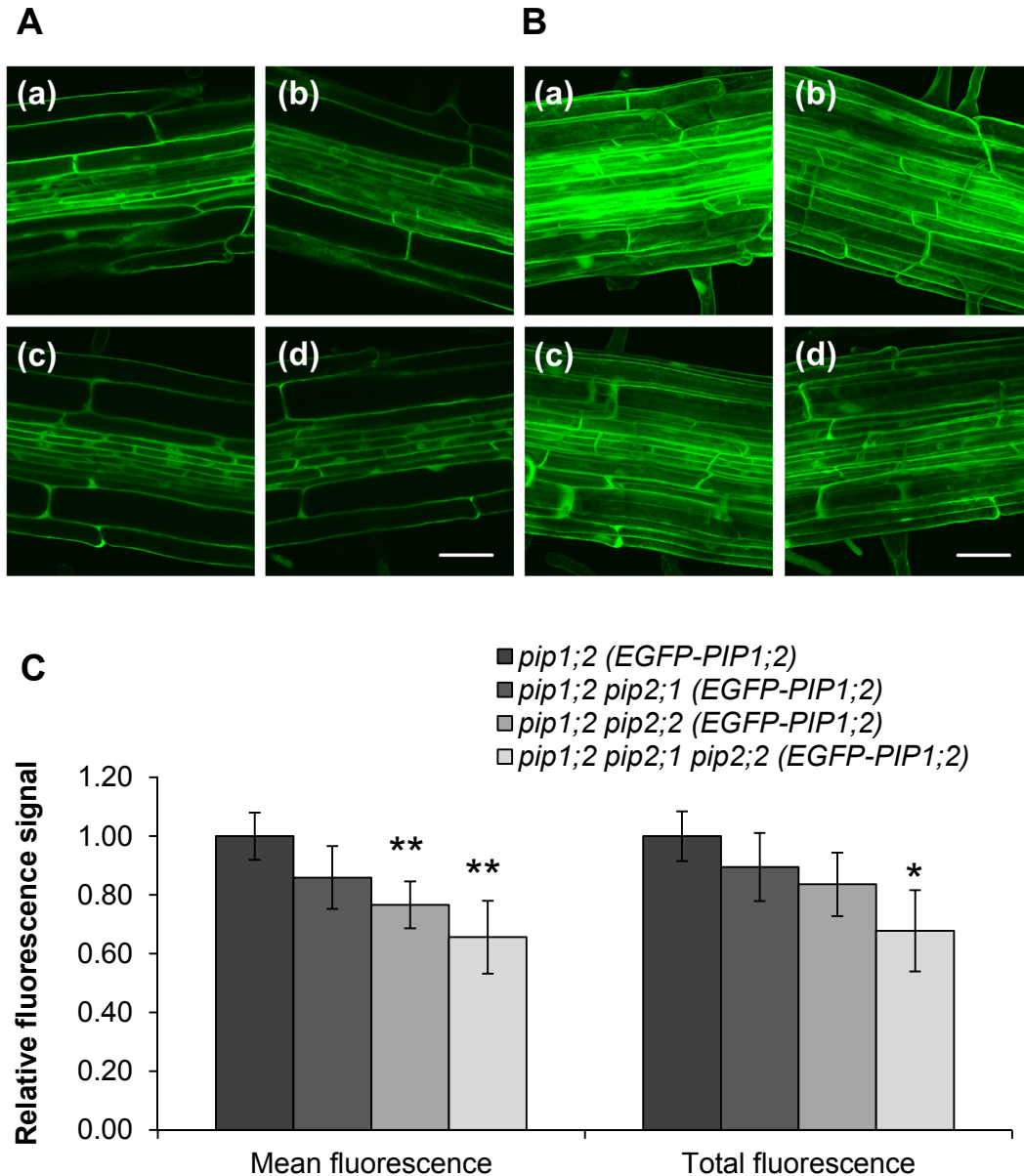


Figure 37. Fluorescence signals of EGFP-PIP1;2 in root zone IV and quantification of fluorescence signals in four different backgrounds.

(A) EGFP-PIP1;2 fluorescence of the root maturation zone of seven-day-old seedlings. The images were selected from a Z-stack from a similar position in (a) *pip1;2* (EGFP-PIP1;2), (b) *pip1;2 pip2;1*(EGFP-PIP1;2), (c) *pip1;2 pip2;2* (EGFP-PIP1;2), (d) *pip1;2 pip2;1 pip2;2* (EGFP-PIP1;2). (B) Maximum-intensity-projection of 40 Z-stack pictures of root maturation zone of EGFP-PIP1;2 in transgenic lines as in A (1 μm interval per Z-stack). (C) Quantification of fluorescence of images as presented in B. Expression levels relative to the levels quantified for the wild-type line. The data represent the mean \pm SD of at least three independent seedlings. The asterisks denote statistically significant differences between pseudowild-type line and corresponding mutant lines (** $p < 0.01$, * $p < 0.05$; two-tailed t test). Bars = 50 μm .

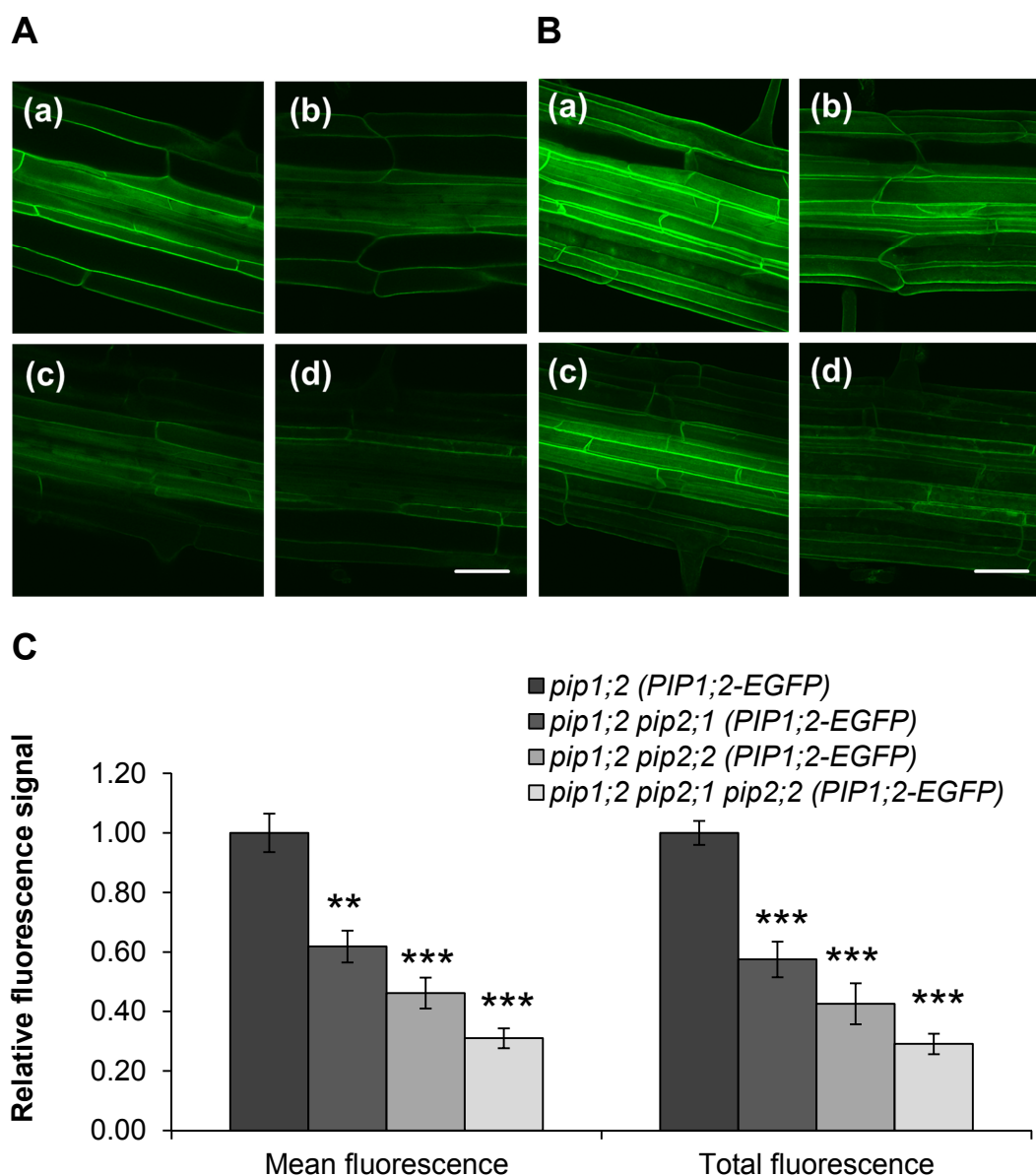


Figure 38. Fluorescence signals of PIP1;2-EGFP in root zone IV and quantification of fluorescence signals in four different backgrounds.

(A) PIP1;2-EGFP fluorescence of the root maturation zone of seven-day-old seedlings. The images were selected from a Z-stack from a similar position (a) *pip1;2* (*PIP1;2-EGFP*), (b) *pip1;2 pip2;1* (*PIP1;2-EGFP*), (c) *pip1;2 pip2;2* (*PIP1;2-EGFP*), (d) *pip1;2 pip2;1 pip2;2* (*PIP1;2-EGFP*). (B) Maximum-intensity-projection of 30 Z-stack pictures of root maturation zone of PIP1;2-EGFP in transgenic lines as in A (1 μm interval per Z-stack). (C) Quantification of fluorescence of images as presented in B. Expression levels relative to the levels quantified for the wild-type line. The data represent the mean \pm SD of at least three independent seedlings. The asterisks denote statistically significant differences between pseudowild-type line and corresponding mutant lines (** $p < 0.01$, *** $p < 0.001$; two-tailed t test). Bars = 50 μm .

2.5. All five *PIP1* genes are not changed at the transcriptional level

The ELISA quantification analysis revealed repression of the PIP1 protein in *pip2* mutants, especially evident in the *pip2;1 pip2;2* double mutant as compared to the wild-type line (Figure 6). Several independent experimental results have determined that PIP1;1 and PIP1;2 were differently affected in *pip2* mutants (detailed information in 2.4.4). To evaluate possible mechanisms behind the repression of the PIP1 protein in *pip2* mutants, all five *PIP1* genes were investigated by quantitative real-time PCR analysis to assess whether their transcriptional levels were altered in *pip2* mutants as compared to the wild-type line.

RNA extracts of the rosettes and the roots from 35-day-old plants were isolated and analyzed in consideration of the detailed demonstration of PIP1 protein repression in mature plant materials (Figure 6). The results of quantitative real-time PCR determined that *PIP1;1*, *PIP1;2* and *PIP1;5* showed relative highly abundant transcript levels compared to *PIP1;3* and *PIP1;4* (absolute CT value) in both rosettes and roots of each sample. This is consistent with previous studies on transcript analyses of *Arabidopsis thaliana*, which have indicated that *PIP1;1*, *PIP1;2*, *PIP1;5* are the main isoforms of the *PIP1* subfamily in the *Arabidopsis* rosettes. *PIP1;1* and *PIP1;2* are the main isoforms of *PIP1* subfamily in the *Arabidopsis* roots (Alexandersson *et al.*, 2005). This is also reflected at the protein level. The correlation between gene expression and protein accumulation was comparably high (Monneuse *et al.*, 2011). However, no statistically significant downregulation of any *PIP1* isoform transcripts in the *pip2;1* mutant, the *pip2;2* mutant and the *pip2;1 pip2;2* double mutant compared to the wild-type line in both rosettes and roots had been observed (Figure 39). Therefore, the repression of PIP1 proteins was not due to the influence at the transcriptional level, indicating that interference may occur at the post-transcriptional level.

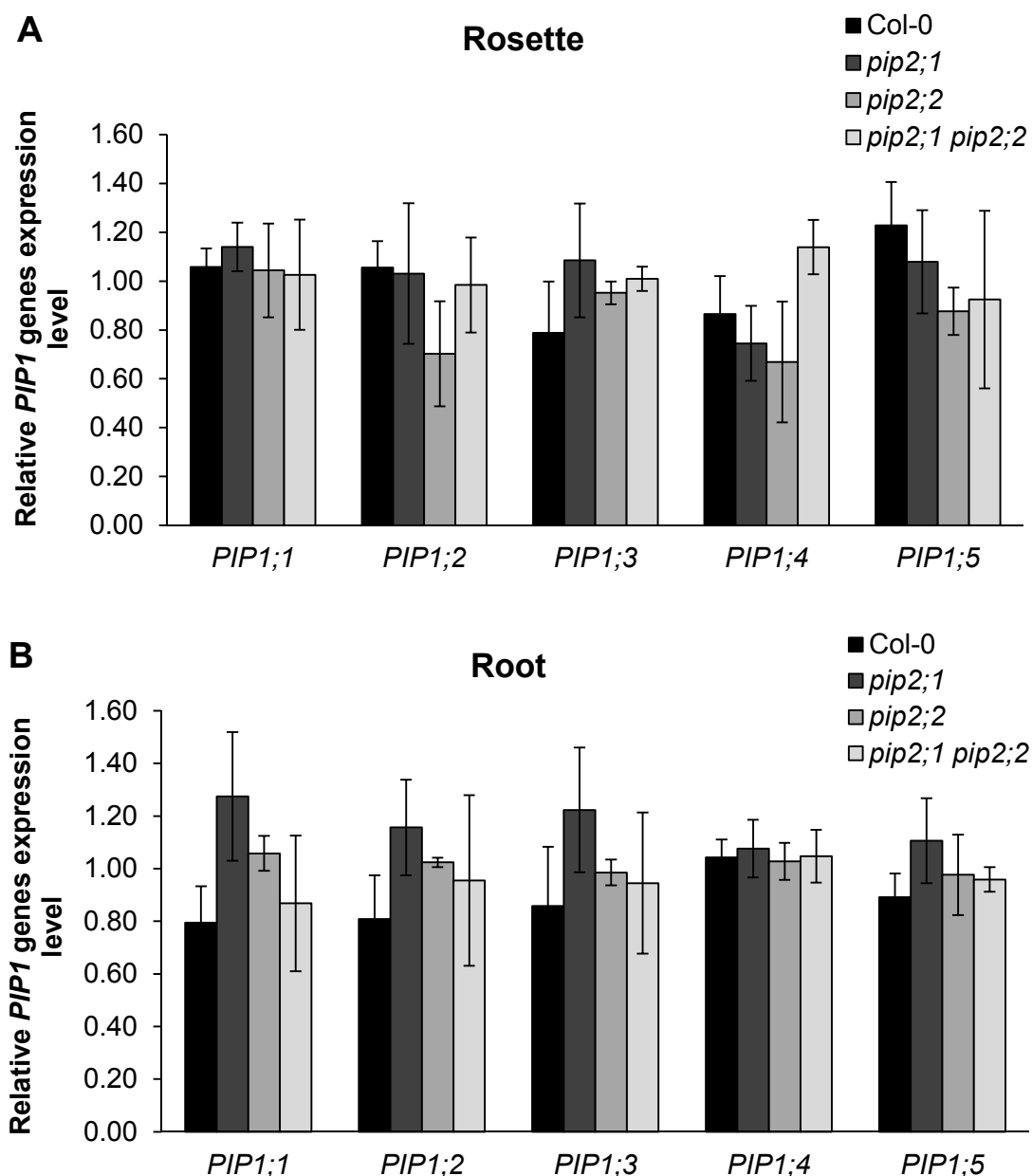


Figure 39. *PIP1* transcript levels were not altered in *pip2* mutants as shown by quantitative real-time PCR analysis.

Transcript levels of all five *PIP1* genes assessed by quantitative Real-time PCR analysis in the rosettes and roots from the 35-day-old plants grown in hydroponic culture (approximately 10-20 plants were pooled in one sample). Transcript levels were normalized by the endogenous content of *UBIQUITIN5* (At3g62250), and *S16* (At5g18380) transcripts (Vandesompele *et al.*, 2002). The data are given as means \pm SD of three biological replicates.

2.6. All five *PIP1* transcripts are not affected at the translational level

The unchanged steady-state transcript levels of all five *PIP1* isoforms suggested that the interference with PIP1 protein expression occurs at the post-transcriptional level. The abundance of total cytosolic mRNA does not necessarily reflect to the quantity of polypeptide synthesized (Nawy *et al.*, 2005). Actively translated mRNAs are associated with multiple ribosomes in large polyribosome (polysome) complexes, whereas other mRNAs can remain as ribonucleoprotein complexes to be either stored or degraded (Proud, 2007). Thus, the translational status of an mRNA could be evaluated by monitoring its association with polyribosomes. A quantitative comparison of actively translated mRNAs of all five *PIP1* genes between wild-type and the *pip2;1 pip2;2* double mutant could elucidate whether the translational state of their mRNAs were altered in the *pip2;1 pip2;2* double mutant.

The investigation of the expression profiles of *PIP2;1* and *PIP2;2* by promoter:*GUS* fusion transgenic lines had shown that these two genes displayed a widespread expression in roots and leaves with a similar expression pattern (Figure 3). To quantitatively evaluate whether the actively translated mRNAs are affected in the *PIP2;1/PIP2;2*-expressing cells, the polyribosomes from these specific cells were isolated for further analysis. To allow the isolation of ribosome-associated mRNA from *PIP2;1/PIP2;2*- expressing cells, transgenic lines were generated, which stably expressed the HIS-FLAG-tagged ribosomal protein L18 (HF-RPL18) under the control of the *PIP2;2* promoter in the wild-type plant and in *pip2;1 pip2;2*. Single insertion lines were selected in T3 generation in the wild-type line and in the *pip2;1 pip2;2* double mutant background.

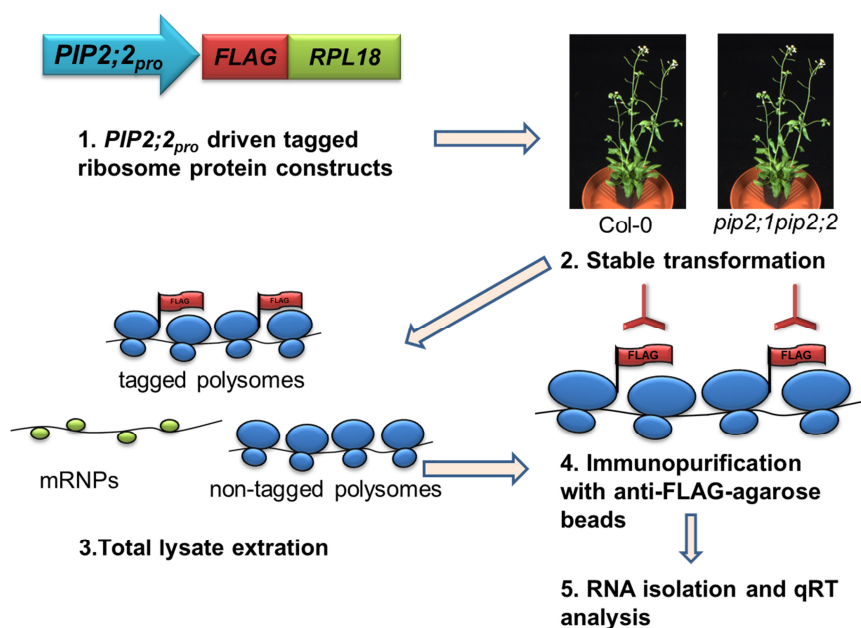


Figure 40. Immunopurification of ectopically expressed HIS-FLAG-tagged ribosomal proteins driven by $PIP2;2$ promoter.

Diagram of the transgenic ribosome tagging and transcriptome analysis [Modified from (Zanetti *et al.*, 2005)].

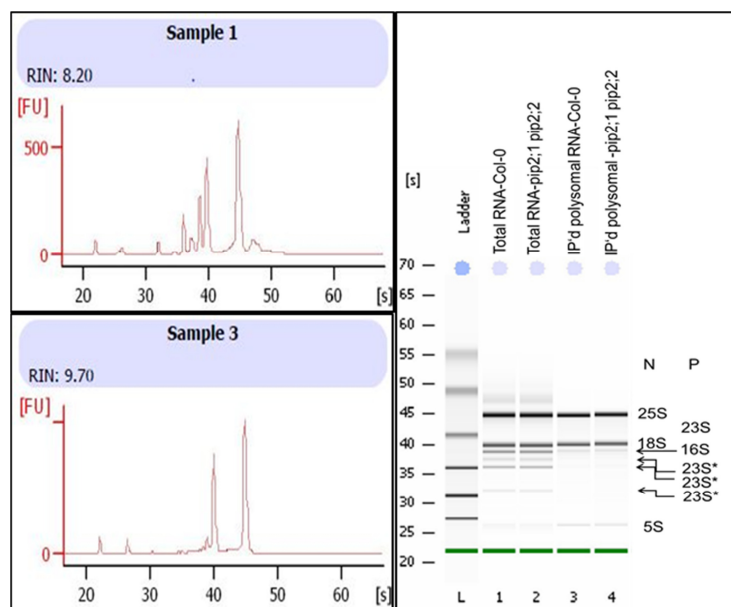


Figure 41. Quality control of total RNA and immunopurified polysomal RNA isolated from rosettes of transgenic lines by Bioanalyser™.

Polysomes were immunopurified from the cells expressing $PIP2;2_{pro}:HF:RPL18$ and RNA was isolated as described in 4.2.3.11 (Zanetti *et al.*, 2005; Muströph *et al.*, 2009a). An RNA Integrity Number (RIN score) represents the quality of RNAs. The quality of purified RNAs was controlled by Bioanalyser™ (Agilent). N, nuclear rRNAs (25S, 18S, 5S); P, plastid rRNAs (23S, 16S) and their degradation products (23S*).

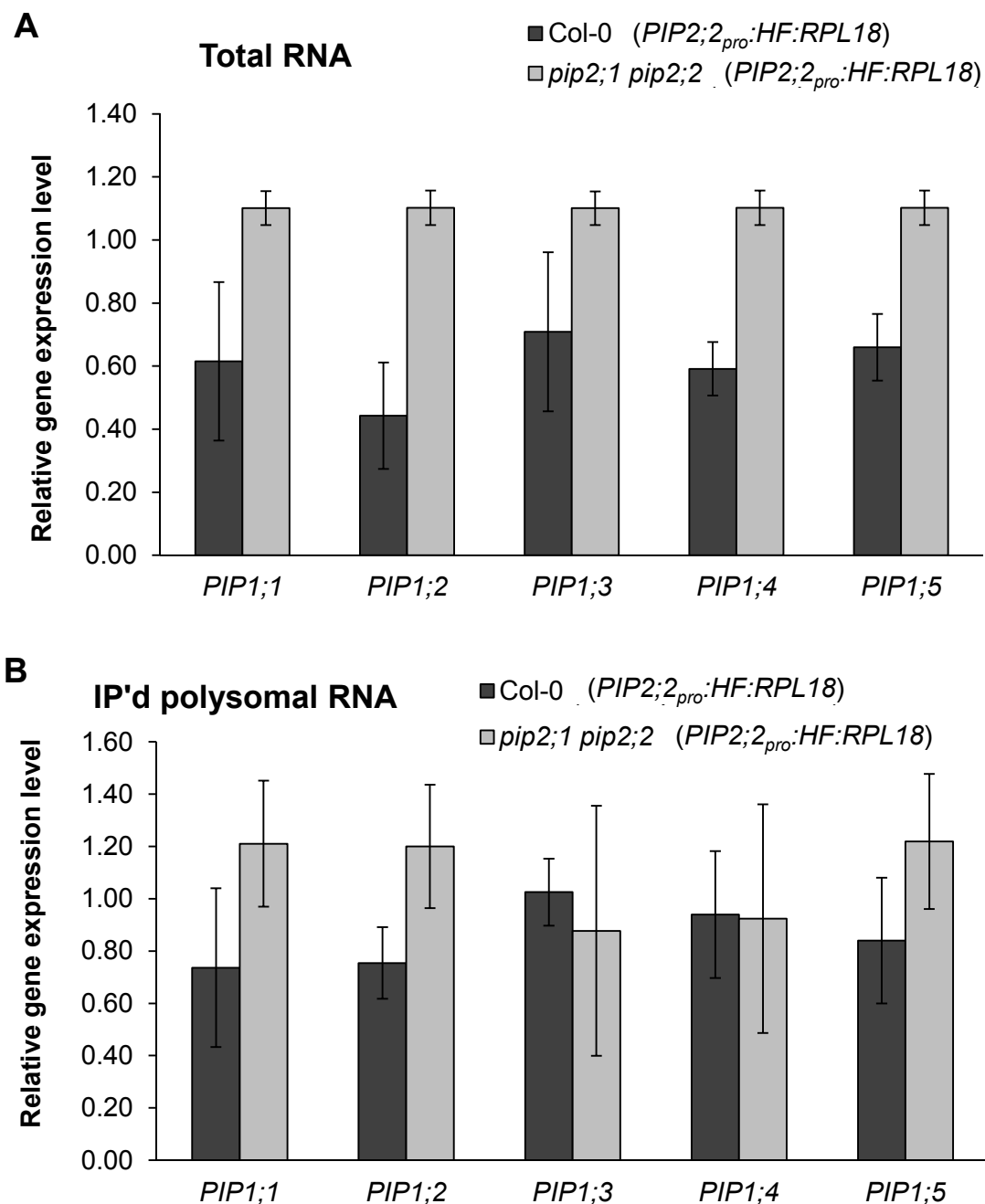


Figure 42. Transcriptional analysis of *PIP1s* and *PIP2s* of total RNA and immunopurified polysomal RNA from *PIP2;2*-expressing cells.

Polysomal RNA was isolated from the mRNA-ribosome complexes using the rosettes of 28-day-old plants grown on soil (~15-25 g plants pooled together for each sample) by the translating ribosome affinity immunopurification. Total RNA was isolated from the same cell homogenate. Transcript levels were normalized by the endogenous content of *UBIQUITIN5* (At3g62250) and *TUBULIN9* (At4g20890) transcripts (Vandesompele *et al.*, 2002). Mean values obtained from the two biological replicates with three technical replicates.

By using the translating ribosome affinity immunopurification (TRAP) method (Zanetti *et al.*, 2005) (Figure 40), polysomal mRNAs from *PIP2;2* expressing cell were extracted (Figure 41) and analyzed by quantitative Real-time PCR to assess whether the translational levels of PIP1 isoforms were affected in *pip2;1 pip2;2*. The quantitative Real-time PCR analysis of total RNA revealed that there was no down-regulation of *PIP1s* genes in the *pip2;1 pip2;2 double* mutant background as compared to the wild-type line. However, there was a tendency of up-regulation of *PIP1s* (Figure 42A). One experiment showed similar results like the transcriptional analysis demonstrated before (detailed in 2.5), another independent experiment exhibited relative high expression of *PIP1s* genes in the *pip2;1 pip2;2* background. An additional biological replicate needs to be done to verify this result. Subsequently, quantitative Real-time PCR analysis of immunopurified RNA revealed that transcripts of all five *PIP1* isoforms had not been down-regulated in the *pip2;1 pip2;2 double* mutant as compared to the wild-type line (Figure 42B). In summary, affinity isolation of cell-specific polyribosome and subsequent quantitative Real-time analysis of the bound mRNA indicated that approximately same levels of all five *PIP1* isoforms mRNAs had been actively translated in *PIP2;2*-expressing cells in wild-type and in the *pip2;1 pip2;2* double mutant backgrounds. This indicated that the repression of the PIP1 protein should be due to regulation at the post-translational level.

2.7. PIP1;1 and PIP1;2 may physically interact with PIP2;1/PIP2;2/PIP2;3

According to previous studies in maize, endoplasmic reticulum-retained ZmPIP1s could target to the plasma membrane by physically interacting with ZmPIP2s via forming hetero-oligomers (Fetter *et al.*, 2004; Zelazny *et al.*, 2007). There was no further experimental data of the interaction between PIP1s and PIP2s in *Arabidopsis thaliana* after the yeast-two hybrid analyses (Consortium, 2011; Jones *et al.*, 2014). The interaction between the major isoforms of AtPIP1 (PIP1;1 and PIP1;2) and major isoforms of AtPIP2 (PIP2;1 and PIP2;2) is still unknown. By investigating whether a physical interaction is present between major isoforms of PIP1 and major isoforms of PIP2, it could broaden our understanding of the mechanism behind the repression major PIP1 isoforms in the absence of PIP2;1 and PIP2;2. Thus, the interaction of PIP1 and PIP2 would provide a basis to understand the interplay of these two subfamilies. To assess whether such an interaction existed between PIP1 and PIP2 in *Arabidopsis*, stable transgenic lines *pip1;1 (HA-PIP1;1)*, *pip1;1 pip2;1 pip2;2 (HA-PIP1;1)*, *pip1;2 (HA-PIP1;2)*, and *pip1;2 pip2;1 pip2;2 (HA-PIP1;2)* (listed in Table 6) were employed for the analysis of protein-protein interaction by using co-immunoprecipitation.

The HA-PIP1;1 or HA-PIP1;2 protein was specifically immunoprecipitated with an anti-HA antibody. Due to the high sequence similarity, the antibody which was used in the Western blot analysis recognized PIP2;1/PIP2;2/PIP2;3 proteins. Preliminary results suggested a possible co-precipitation of PIP2;1/PIP2;2/PIP2;3, since weak signals were detected in both the HA-PIP1;1 and in the HA-PIP1;2 immunoprecipitation in the HA-PIP1-complemented wild-type lines (Figure 43 black arrows). The *pip1;1 pip2;1 pip2;2 (HA-PIP1;1)* was used as a negative control which indicated the specific immunoblotting signal of PIP2;1/PIP2;2/PIP2;3 (Figure 43). In this respect, PIP2;3 should be detected in this line. However, one possible

explanation of this result could be that there was no interaction between HA-PIP1;1 and PIP2;3. Another possibility would be that PIP2;3 was expressed at a low level, even if it was pulled down by immunoprecipitation. Such a low amount could not be recognized by this antibody. The latter possibility seemed to be more likely based on the transcriptional and proteomic analyses (Jang *et al.*, 2004; Alexandersson *et al.*, 2005; Monneuse *et al.*, 2011). There was one unspecific band (near 25 kDa) in the HA antibody lines, which could be the light chain of the antibody (Figure 43). This preliminary result raised the hypothesis that PIP2;1, PIP2;2 or PIP2;3 may physically interact with PIP1;1 and PIP1;2, very likely not only to facilitate their trafficking to the plasma membrane, but also to maintain or stabilize the protein level of PIP1;1 and PIP1;2.

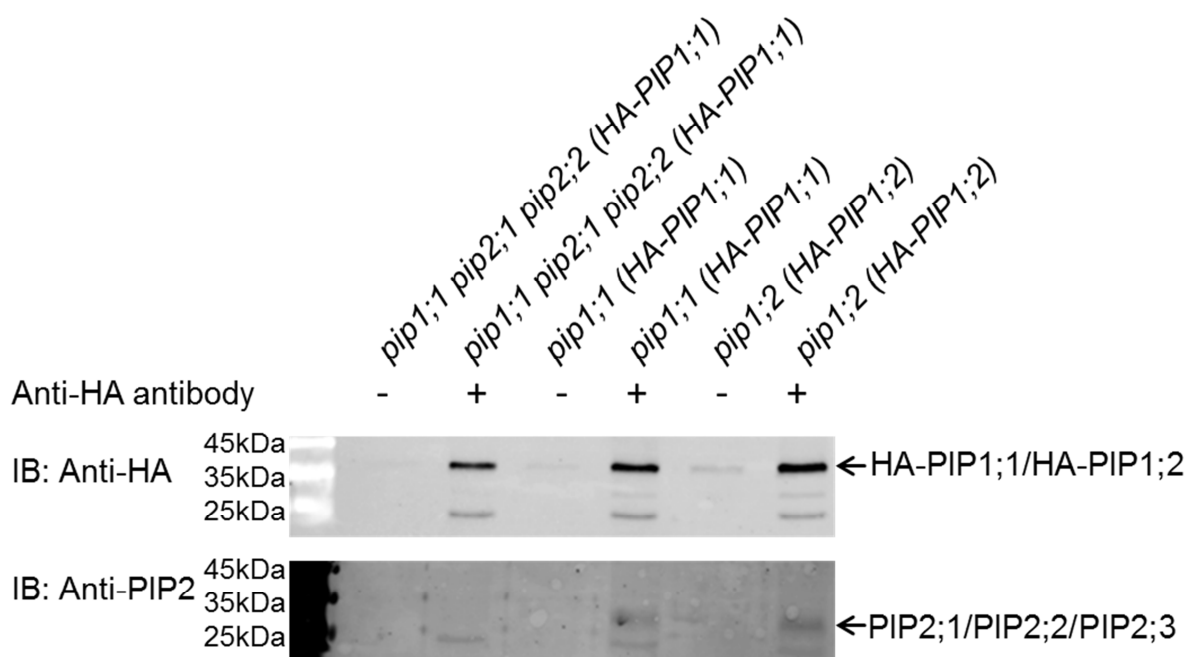


Figure 43. The Co-Immunoprecipitation experiment revealed the interaction between HA-PIP1;1 or HA-PIP1;2 and PIP2;1/PIP2;2/PIP2;3

Microsomal membrane fractions extracted from rosettes of 28-day-old transgenic lines grown on soil (~16-20 plants pooled together in one sample) were immunoprecipitated using an anti-HA antibody, separated on 15% SDS-PAGE gel, and probed with an anti-HA or an anti-PIP2;1/PIP2;2/PIP2;2 antibody, respectively (see 4.2.4.7 and 4.2.4.9).

2.8. Trafficking and/or stability of PIP1;1 and PIP1;2 proteins are influenced by PIP2;1 or PIP2;2

Based on the quantitative analyses of tagged PIP1;1 and PIP1;2 in different sets of transgenic lines, the repression of major PIP1 isoforms was particularly pronounced in the rosettes of *pip2;1*, in the root maturation zone of *pip2;1* and *pip2;2* mutants, as well as in the rosettes and roots of the *pip2;1 pip2;2* double mutant (described in 2.4.4). This revealed that these two major PIP1 isoforms were affected in the absence of PIP2;1 and PIP2;2. Since PIP2;1, PIP2;2 or PIP2;3 may physically interact with PIP1;1 and PIP1;2 (Figure 43), transient expression of PIP1;1 or PIP1;2 alone or co-expression with PIP2s (PIP2;1 or PIP2;2) were performed in mesophyll protoplasts in order to examine whether localization or stability of PIP1 isoforms were influenced by the presence of PIP2;1 or PIP2;2 in the same cell.

The *EGFP-PIP1;1* construct (*PIP1;1_{pro}:EGFP-PIP1;1:tPIP1;1*) alone or together with the *35S_{pro}:PIP2;2* construct (*35S_{pro}:PIP2;2-cDNA*) were transiently expressed in mesophyll protoplasts of *pip1;1*, *pip1;1 pip2;2*, or *pip1;1 pip2;1 pip2;2*, respectively. The fluorescence signal of EGFP-PIP1;1 was monitored by epifluorescence microscopy after overnight expression (Figure 44). When only transiently expressed in the mesophyll protoplast of these mutants (*pip1;1*, *pip1;1 pip2;2*, *pip1;1 pip2;1 pip2;2*) (Figure 44A, C and E), the EGFP-PIP1;1 fluorescence signals were observed to occur in four different patterns: 1) all-over localization; 2) spherical localization (accumulated in intracellular organelles); 3) spherical and plasma membrane localization (parts of the fluorescence signals accumulated in intracellular organelles while other parts were located at the plasma membrane); 4) The plasma membrane localization (Figure 42E from 1 to 4). The EGFP-PIP1;1 fluorescence signals in the co-expressed protoplasts were present in four different patterns similar to those in the singly expressed protoplasts. However, punctate-like fluorescence compartments were observed in co-transformed protoplasts (Figure

42F- 2, 3) instead of sphere-like compartments (Figure 42E- 2, 3). These observations suggested that ectopically expressed PIP2;2 might affect the trafficking pathway of EGFP-PIP1;1 to the plasma membrane by forming another targeting way (punctate vesicle) and then enhance or stabilize the expression level of the EGFP-PIP1;1 fusion protein.

The same approach was utilized to examine whether the expression or stability of PIP1;2 was influenced by the presence of PIP2;2 in the protoplast cells. *EGFP-PIP1;2* (*PIP1;2_{pro}:EGFP-PIP1;2:tPIP1;2*) alone or together with *35S_{pro}:PIP2;2* (*35S_{pro}:PIP2;2-cDNA*) were transiently expressed in protoplasts of *pip1;2*, *pip1;2 pip2;2*, or *pip1;2 pip2;1 pip2;2* mutants, respectively.

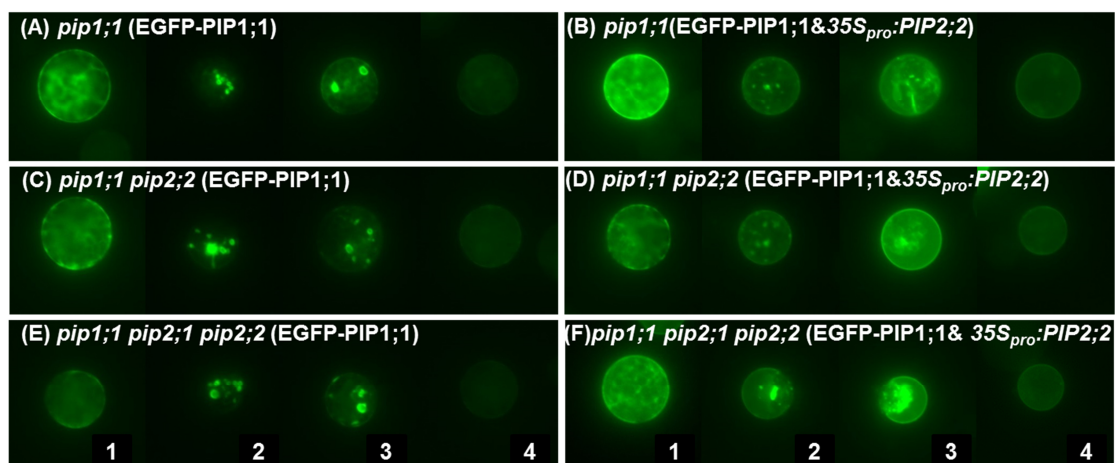


Figure 44. Transient expression of *EGFP-PIP1;1* singly (left) or co-expressed *EGFP-PIP1;1* with *35S_{pro}:PIP2;2* (right) in mesophyll protoplasts of different mutants.

The high copy plasmids of *EGFP-PIP1;1* (Green) alone, or in combination with *35S_{pro}:PIP2;2* were transiently expressed in *pip1;1* (A, B), *pip1;1 pip2;2* (C, D), *pip1;1 pip2;1 pip2;2* (E, F) by PEG transformation (see 4.2.3.14), respectively (For example, *pip1;1* (*EGFP-PIP1;1*) indicates that *EGFP-PIP1;1* has been transformed into protoplasts of the *pip1;1* mutant). Images were taken by epifluorescence microscopy of these protoplasts after overnight expression (18 h-22 h).

By comparing the fluorescence signals of EGFP-PIP1;2 in singly-transformed protoplasts (Figure 45A, C and E) and co-transformed protoplasts (Figure 45B, D and F), different expression patterns were also observed. A few sphere-like fluorescence compartments of EGFP-PIP1;2 were found in the singly-transformed

RESULTS

protoplasts (Figure 45E- 2), although not as many as in the case of EGFP-PIP1;1. In contrast, punctate-like fluorescence signals were detected in co-transformed protoplasts (Figure 45F- 2). The overall-localization combined with a patchy pattern was frequently observed in singly-transformed protoplasts, exhibiting high or low fluorescence intensity (Figure 45E- 1, 3, 4). However, a uniform PM-localized pattern of fluorescence signal was mostly found in co-expressed protoplasts (Figure 45F- 4). These different patterns suggested that the trafficking of EGFP-PIP1;2 might be changed when it co-expressed with PIP2;2.

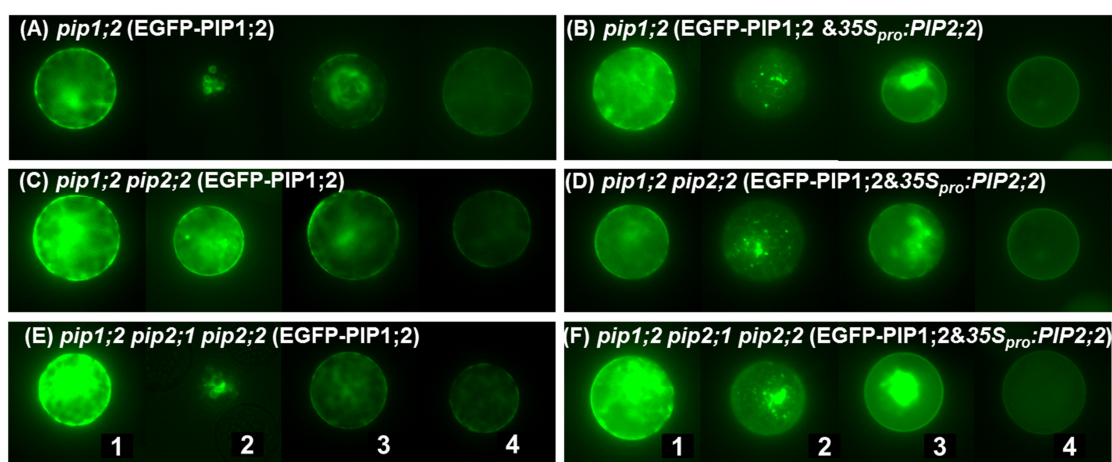


Figure 45. Transient expression of EGFP-PIP1;2 singly (left) or co-expressed EGFP-PIP1;2 with $35S_{pro}$:PIP2;2 (right) in mesophyll protoplasts of different mutants.

The high copy plasmids of EGFP-PIP1;2 (Green) alone, or combined with $35S_{pro}$:PIP2;2 were transiently expressed into *pip1;2* (a, b), *pip1;2 pip2;2* (c, d), *pip1;2 pip2;1 pip2;2* (e, f) by PEG transformation (see 4.2.3.14), respectively. Pictures were taken by epifluorescence microscopy of these protoplasts after overnight expression (18 h-22 h).

The similar fluorescence signal level and pattern of EGFP-PIP1;1 in singly transformed protoplasts of *pip1;1* and *pip1;1 pip2;2* (Figure 44 A, C) suggested that trafficking or stability of EGFP-PIP1;1 could be assisted by natively expressed PIP2;1 to a certain level. To examine whether the expression level or trafficking of EGFP-PIP1;1 is affected by PIP2;1, a transgenic line harbouring a mCherry labelled PIP2;1 which mimics the endogenous PIP2;1 expression (*PIP2;1_{pro}:PIP2;1-mCherry* cassette) (Peret *et al.*, 2012) was utilized as a host protoplast system to check the localization of the EGFP-PIP1;1 fluorescence signal. The EGFP-PIP1;1 construct

was transiently expressed in mesophyll protoplasts of the PIP2;1-mCherry line. The fluorescence signal of EGFP-PIP1;1 was observed to be partially localized at the plasma membrane when PIP2;1-mCherry fluorescence signal was visible in these protoplasts (Figure 46 A-[a], [b]). Additionally, an accumulated fluorescence signal of EGFP-PIP1;1 in the sphere-like intracellular compartments was frequently found when there was no or a very low level of PIP2;1-mCherry expression (Figure 46 A-[c], [d] white arrows). This suggested that EGFP-PIP1;1 might be affected by the expression level of PIP2;1. The partial plasma membrane localization of the EGFP-PIP1;1 fluorescence signal might be due to the mimic-endogenously expressed PIP2;1 in those protoplasts unable to support trafficking or stability of highly expressed EGFP-PIP1;1 (high copy number plasmid). Furthermore, to examine whether the accumulation of EGFP-PIP1;1 in the intracellular compartment or partial localization at the plasma membrane could be rescued or improved by constitutively expressed PIP2;1 or PIP2;2, the *EGFP-PIP1;1* construct and the *35S_{pro}:PIP2;2* construct were transiently expressed together in PIP2;1-mCherry protoplasts, since ectopic expression of PIP2;2 might influence the trafficking or stability of EGFP-PIP1;1 as indicated before (Figure 44). The fluorescence signal of EGFP-PIP1;1 was localized at the plasma membrane even though the expression of PIP2;1-mCherry was at a low level in these protoplasts (Figure 46B-e, f). In addition, in a short time series observation (thirty seconds to one minute), the sphere-like compartments which were observed in singly-transformed protoplasts exhibited no obvious or slow movement (Figure 47 A white arrows) under confocal microscopy. In contrast, the punctate compartments were rapidly moving for a short time along linear intracellular paths in co-expressed protoplasts in short time series under confocal microscopy (Figure 47B white arrows).

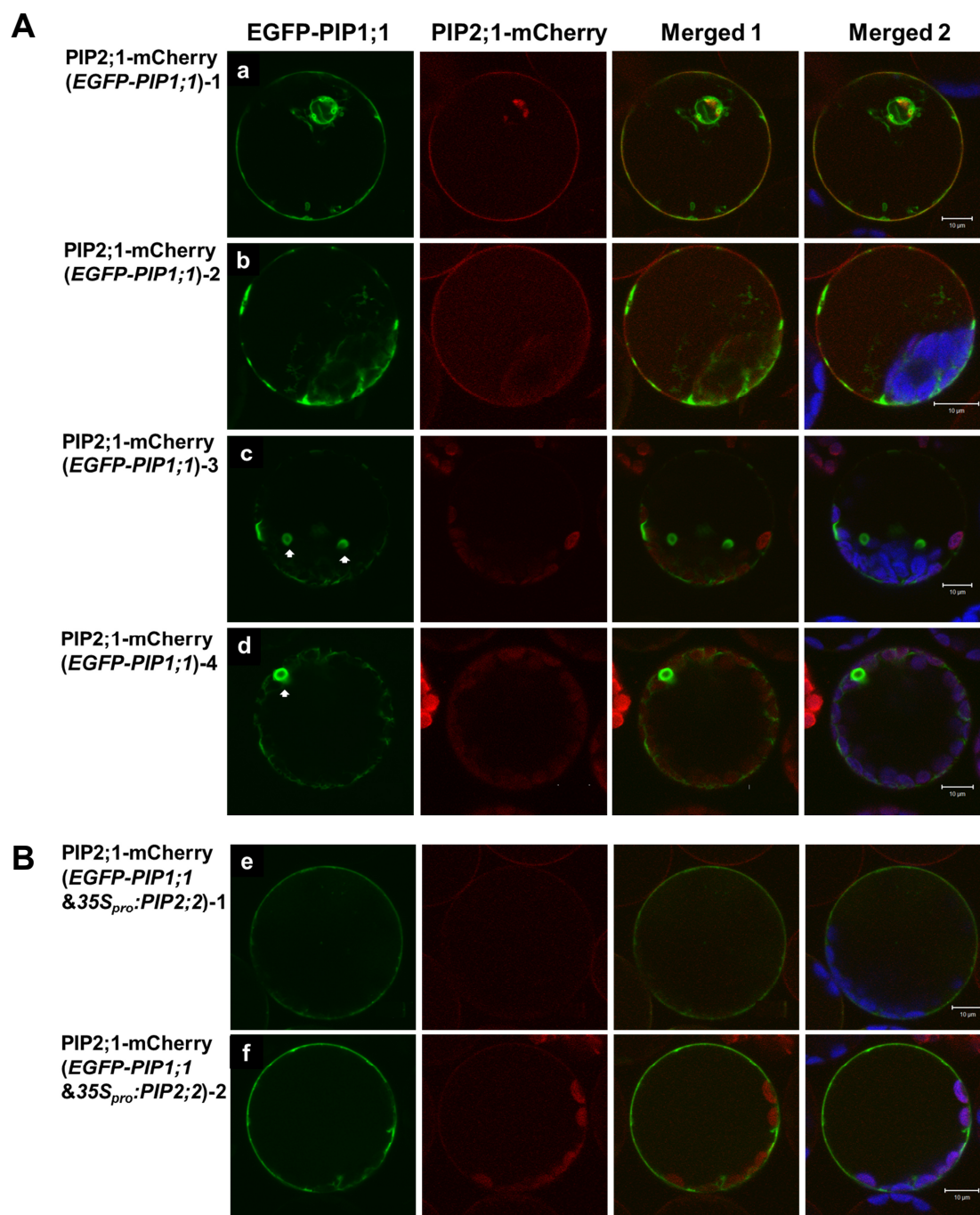


Figure 46. Localization and expression analysis of EGFP-PIP1;1 in protoplasts of PIP2;1-mCherry line.

(A) Transiently expressed *EGFP-PIP1;1* (Green) alone or (B) co-expressed with *35S_{pro}:PIP2;2* in PIP2;1-mCherry (Red) protoplasts as indicated (18-20 h after transformation). Images were collected using the optimal filters for each fluorescence protein by Confocal Laser Scanning Microscope (CLSM 510 META, Zeiss) as described in 4.2.5. The autofluorescence of chlorophyll was shown in blue. Merge 1 represented the EGFP merged with mCherry. Merge 2 represented EGFP, mCherry and autofluorescence (blue) merge together. Bars = 10 μ m.

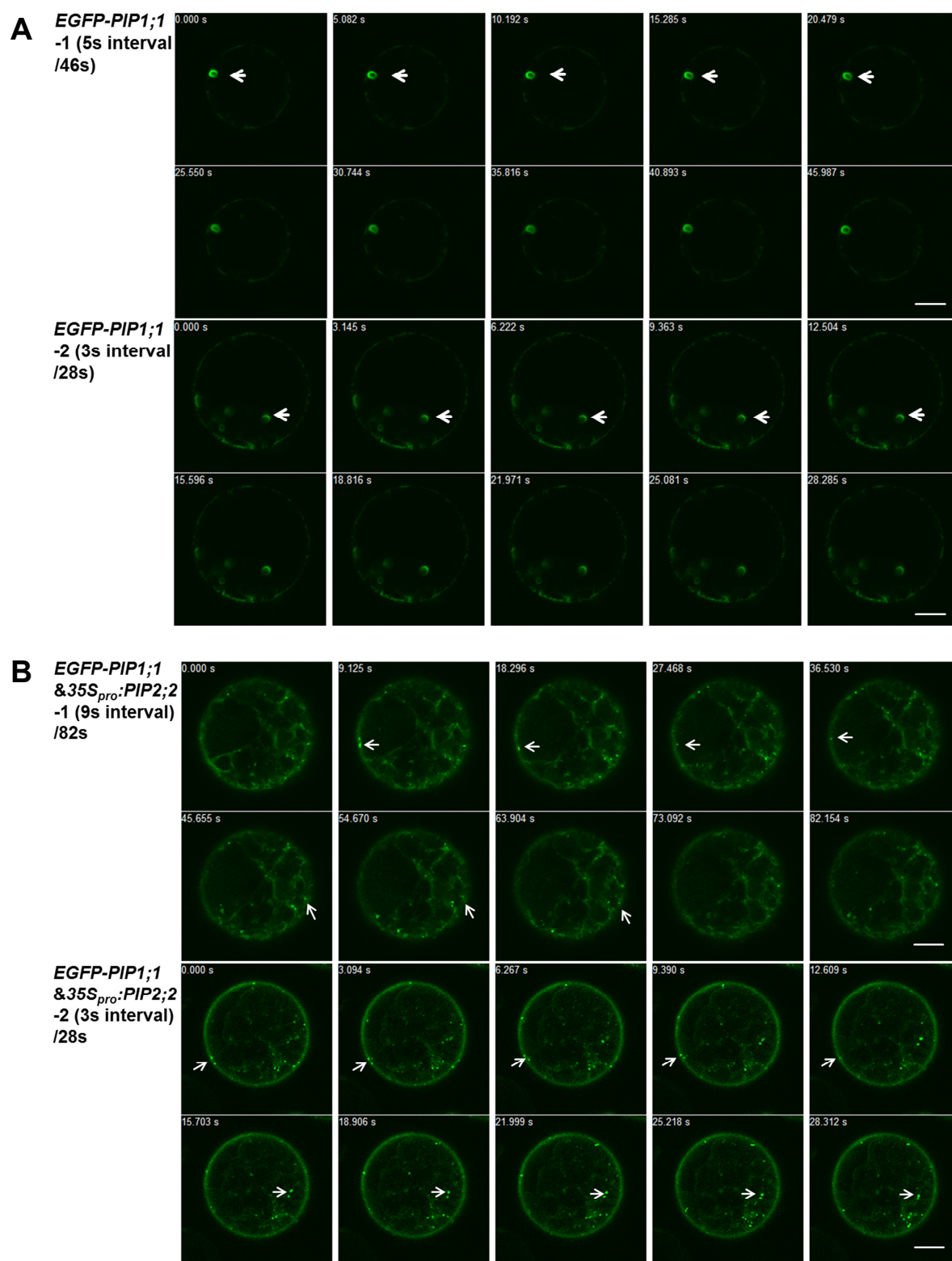


Figure 47. Time-lapse images of two different shapes and movements of fluorescence compartments of *EGFP-PIP1;1* in mesophyll protoplasts.

(A) Transiently expressed *EGFP-PIP1;1* alone in *PIP2;1-mCherry* protoplasts as indicated.
 (B) Co-expressed *EGFP-PIP1;1* with *35S_{pro}:PIP2;2* in *PIP2;1-mCherry* protoplasts as indicated. The images were taken at intervals as indicated.

RESULTS

This suggested that trafficking of EGFP-PIP1;1 might be different with the ectopic presence of PIP2;2 in the same protoplasts. To follow the fate of the sphere-like or punctate-like fluorescence signals of EGFP-PIP1;1 or EGFP-PIP1;2 and to better discriminate the influences of ectopically expressed PIP2;1 and PIP2;2 on the trafficking and/or stability of PIP1;1 and PIP1;2, the singly-transformed and co-transformed protoplasts were monitored at an earlier time point (8 h) and at a later time point (20 h) by confocal microscopy. To make sure the influence of trafficking or stability is derived from the ectopic expression of PIP2;1 or PIP2;2, the protoplasts of *pip1;1 pip2;1 pip2;2* or *pip1;2 pip2;1 pip2;2* were used for transient expression.

The fluorescence signals of EGFP-PIP1;1 and EGFP-PIP1;2 became visible 13-14 h after transformation. Z-stack pictures were collected at 14 h and 20 h after transformation at the same confocal setting with one hour intervals. When EGFP-PIP1;1 was expressed alone in protoplasts of *pip1;1 pip2;1 pip2;2*, sphere-like or ring-shaped compartments were observed 14 h after transformation (Figure 48A [a]). These compartments were still found 20 h after transformation (Figure 48A [b]). When the *EGFP-PIP1;1* construct was co-expressed with *35S_{pro}:PIP2;1* or *35S_{pro}:PIP2;2*, some punctate-like compartments appeared 14 h after transformation. The punctate compartments cumulatively increased. The fluorescence signals of EGFP-PIP1;1 located at the plasma membrane was apparently enhanced compared to the singly-transformed protoplasts 20 h after transformation (Figure 48 A-[b], B-[d], C-[f]). The same experiment was also accomplished with the protoplasts of *pip1;2 pip2;1 pip2;2*. The sphere-like compartments were not frequently observed in the protoplasts which expressed EGFP-PIP1;2 alone. In these protoplasts, the fluorescence signals of EGFP-PIP1;2 were detected at the plasma membrane 14 h-16 h after transformation.

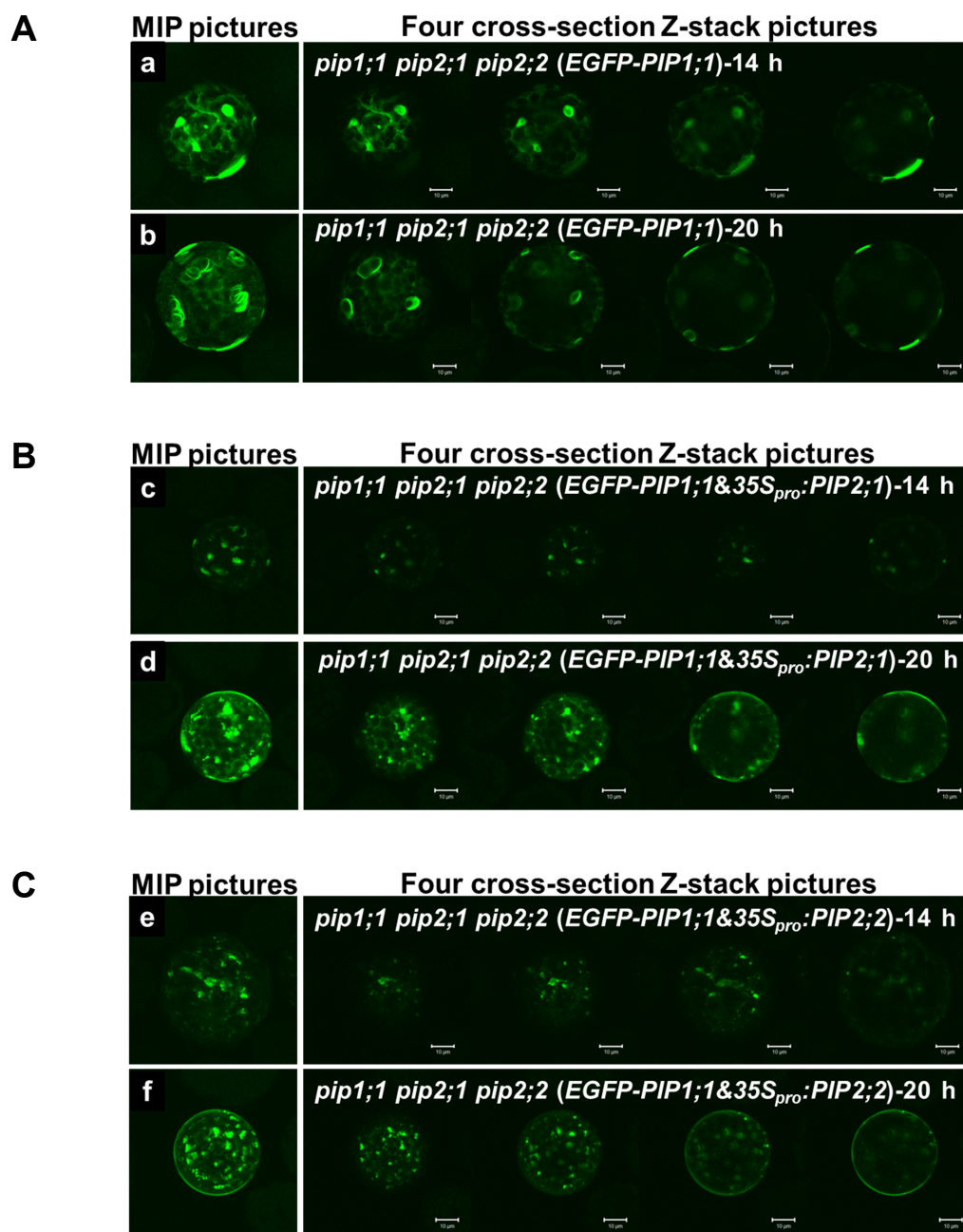


Figure 48. Confocal pictures of *pip1;1 pip2;1 pip2;2* triple mutant protoplasts 14 h and 20 h after transformation.

A) Transiently expressed *EGFP-PIP1;1* alone in *pip1;1 pip2;1 pip2;2* protoplasts as indicated. B) Co-expressed *EGFP-PIP1;1* with *35S_{pro}:PIP2;1* in *pip1;1 pip2;1 pip2;2* protoplasts as indicated. C) Co-expressed *EGFP-PIP1;1* with *35S_{pro}:PIP2;2* in *pip1;1 pip2;1 pip2;2* protoplasts as indicated. Images were collected using the Confocal Laser Scanning Microscope (CLSM 510 META, Zeiss) 14 h and 20 h after transformation as described in 4.2.5. MIP pictures represent approximately 20-30 Z-stack pictures overlapped by using the Maximum-intensity-projection function of the Zen software (1 μm interval per Z-section). Cross-section pictures represent a single Z-stack picture each taken from different positions. Bars = 10 μm .

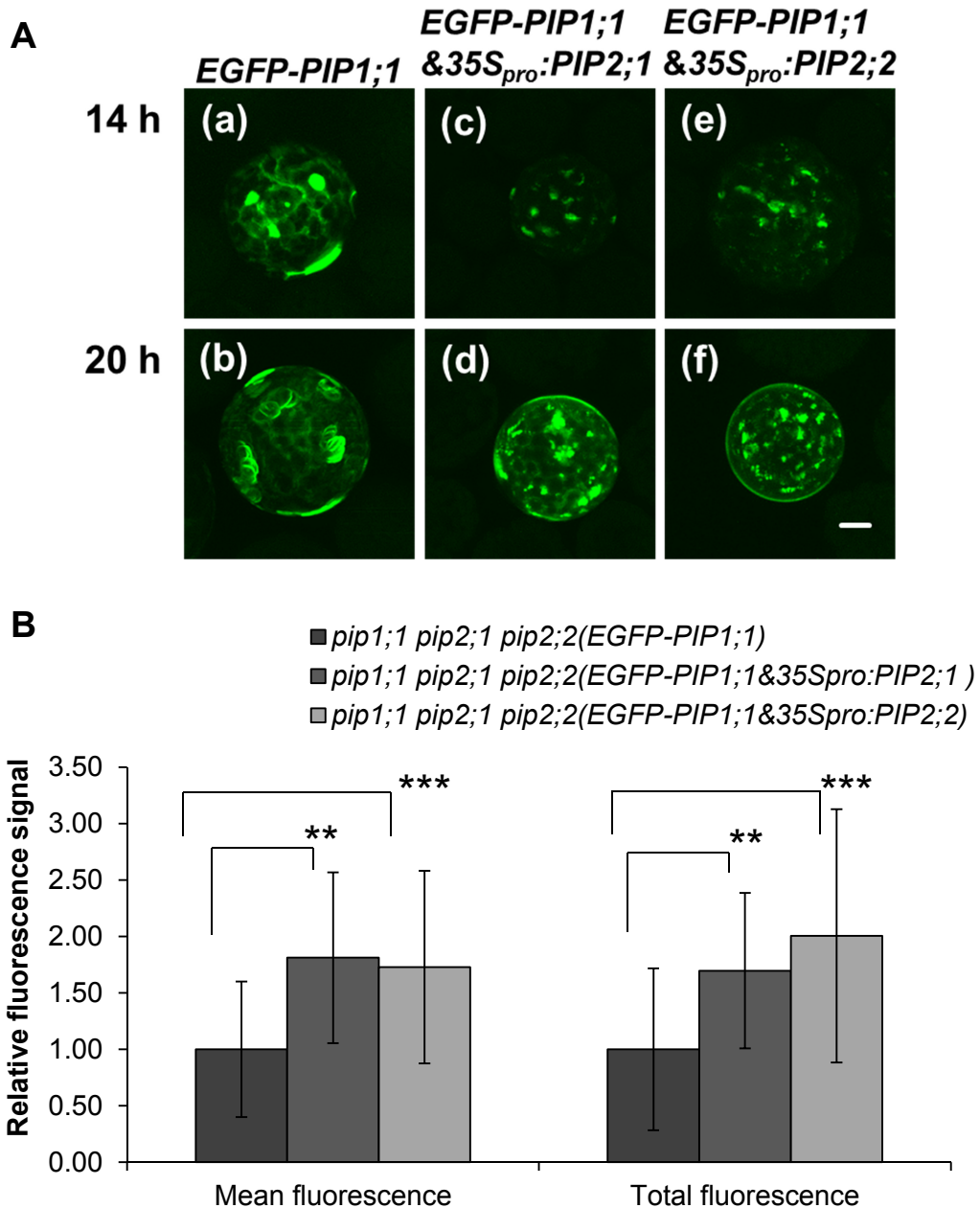


Figure 49. The stability of EGFP-PIP1;1 was influenced by the constitutive expression of PIP2;1 and PIP2;2.

A) Overlapped Z-stack pictures of transient expressions of *EGFP-PIP1;1* alone or co-expressed with $35S_{pro}:PIP2;1$ or $35S_{pro}:PIP2;2$ in the mesophyll protoplasts protoplasts of *pip1;1 pip2;1 pip2;2* are presented in Figure 48, which have been put here to provide an overview over representatives for further quantification. B) Quantification of fluorescence intensity of transformed protoplasts after 24 h using the pictures which were taken by epifluorescence microscopy. Expression levels relative to the levels quantified for singly-transformation of *EGFP-PIP1;1* (mean value of $n = 25, 17, 35$ protoplasts from different pictures at the same setting). The asterisks denote statistically significant differences between samples (*** $p < 0.001$, ** $p < 0.01$; two-tailed t test). Bar = 10 μm .

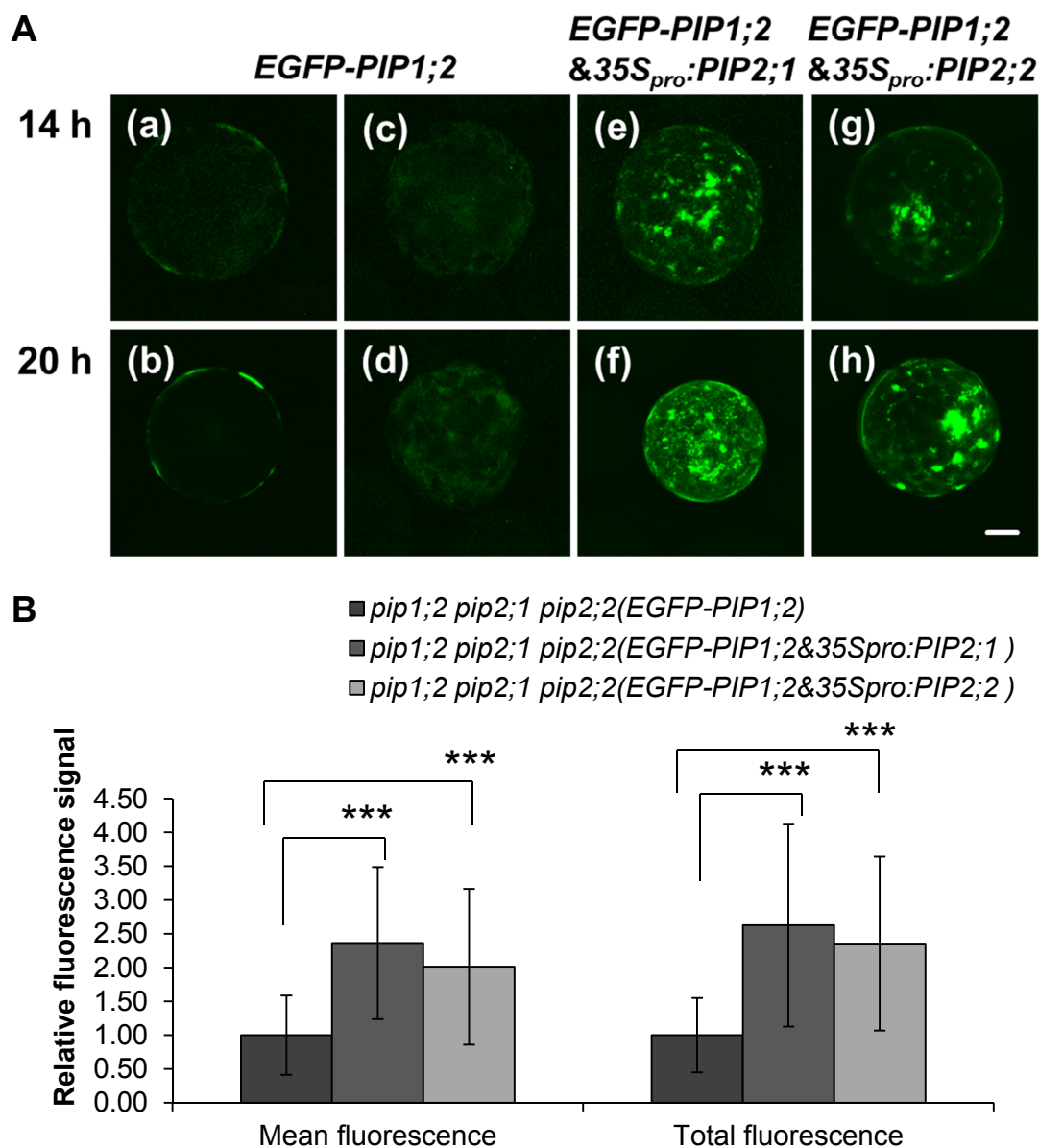


Figure 50. The stability of EGFP-PIP1;2 was influenced by the constitutive expression of PIP2;1 and PIP2;2.

A) Overlapped Z-stack pictures of transient expression of *EGFP-PIP1;2* alone, or co-expressed with *35S_{pro}:PIP2;1* or *35S_{pro}:PIP2;2* in the mesophyll protoplasts of *pip1;2 pip2;1 pip2;2* by using the Maximum-intensity-projection function of the Zen software (20 Z-stack images at 1 μ m intervals). B) Quantification of fluorescence intensity of transformed protoplasts after 24 h using the pictures which were taken by epifluorescence microscopy. Expression levels relative to the levels quantified for singly-transformation of EGFP-PIP1;2 (mean value of n = 17, 27, 23 protoplasts from different pictures at the same setting). The asterisks denote statistically significant differences between samples (***) $p < 0.001$; two-tailed *t* test). Bar = 10 μ m.

RESULTS

The punctate compartments were observed in co-transformed protoplasts (*EGFP-PIP1;2* with *35S_{pro}:PIP2;1*, *EGFP-PIP1;2* with *35S_{pro}:PIP2;2*). The fluorescence signals of *EGFP-PIP1;2* at the whole protoplast level seemed to be increased after 20 h transformation as compared to 14 h transformation (Figure 50 A).

Subsequently, the fluorescence signal of *EGFP-PIP1;1* or *EGFP-PIP1;2* from single-transformed and co-transformed protoplasts were quantified 24 h after transformation. The relative mean and total fluorescence signals were statistically significantly enhanced in the co-expressed protoplasts (*EGFP-PIP1;1* with *35S_{pro}:PIP2;1*, *EGFP-PIP1;1* with *35S_{pro}:PIP2;2*, *EGFP-PIP1;2* with *35S_{pro}:PIP2;1*, *EGFP-PIP1;2* with *35S_{pro}:PIP2;2*) as compared to the protoplasts which transiently expressed the *EGFP-PIP1;1* or *EGFP-PIP1;2* alone (Figure 49B and 50B).

The possible physically interaction between *PIP1;1* and *PIP1;2* with *PIP2;1*, *PIP2;2* or *PIP2;3* (Figure 43), together with these preliminary observations described above indicated that the trafficking and/or stability of the *PIP1;1* protein and the *PIP1;2* proteins might be influenced by the ectopic expression of *PIP2;1* and *PIP2;2* through a direct interaction. Further work will be required to identify the types and roles of different compartments and to understand the basic regulatory mechanism behind the observed phenomena.

2.9. Pilot experiments to address the degradation analysis of PIP1 protein in the *pip2;1 pip2;2* double mutant

All following experiments are to be considered as pilot experiments, which have not been reproduced so far. Nevertheless, several results can already give hints towards the localization or possible routes for degradation. In particular, several possibilities can be regarded as less likely, since e.g. co-localization of fluorescently labelled PIP1 isoform with a certain compartment has not been found.

2.9.1. Co-localization analysis of EGFP-PIP1;1 fluorescence with different compartments

Transiently expressed *EGFP-PIP1;1* was observed in several, so far unidentified compartments, e.g. the nearly immobile ring-shaped fluorescence compartments of protoplasts transformed with EGFP-PIP1;1 alone (Figure 48A). In contrast, rapidly moving punctate fluorescence compartments were detected in protoplasts co-expressing *EGFP-PIP1;1* with *35S_{pro}:PIP2;1* or *35S_{pro}:PIP2;2* (Figure 48B and 48C). These two different types of fluorescence compartments might reflect the existence of different systems controlling the trafficking or fate of EGFP-PIP1;1 with or without the presence of PIP2;1 or PIP2;2. Therefore, these transient expressions were repeated in protoplasts harbouring compartment-specific mCherry-labeled fluorescence. Marker lines (Geldner *et al.*, 2009) were employed to investigate potential co-localization with different EGFP-PIP1;1 fluorescence compartments: Wave 13R-VTI12 (trans-Golgi network/early endosome), Wave 27R-RabE1D (Post-Golgi/endosomal), Wave7R-RabF2a (Late endosome/pre-vacuolar compartment) and Wave 11 R-RabG3C (Late endosome/Vacuole). There was no clear evidence that the ring-shaped or punctate fluorescent compartments of EGFP-PIP1;1 prominently co-localize with any of these specific-fluorescent marker lines (Figure 51, 52 and 53 white arrows). However, punctate fluorescent compartments of EGFP-PIP1;1 exhibited rapid movement in the protoplasts which

RESULTS

co-expressed *EGFP-PIP1;1* with *35S_{pro}:PIP2;2* as described earlier (Figure 47B). A similar but not overlapping localization patterns of punctate fluorescent compartments of *EGFP-PIP1;1* and mCherry-labeled marker lines were observed (Figure 52 enlarged squares). This suggested that the co-localization might actually exist, but the rapid movement of punctate compartments renders it very difficult to obtain good pictures due to the long time intervals (1 to 3 seconds) required for sequentially scanning the specimen by confocal laser microscopy. Advanced settings of confocal scanning would be desirable to rapidly scan the specimen to confirm this possibility. Autofluorescence of chloroplasts were labelled in blue for controlling the crosstalk signal of the mCherry label.

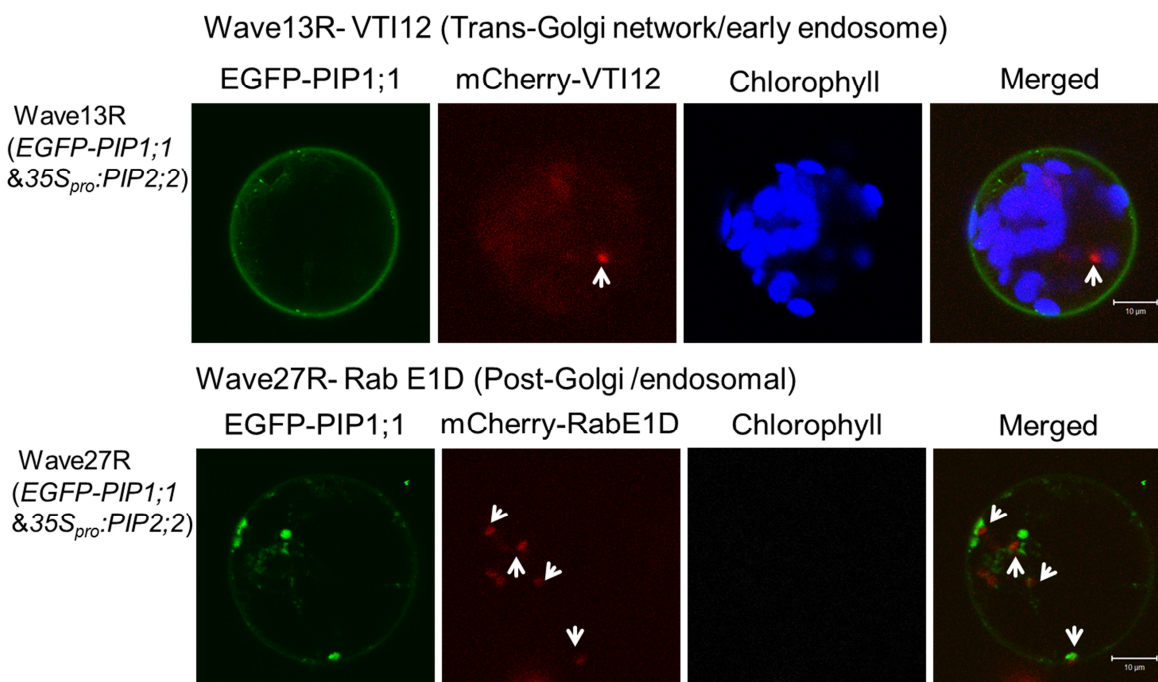


Figure 51. Co-localization analysis with Wave 13R (trans-Golgi network/early endosome) and Wave 27R (Post-Golgi/endosomal) and EGFP-PIP1;1.

Co-expressed *EGFP-PIP1;1* (Green) with *35S_{pro}:PIP2;2* into Wave13R (mCherry-VTI12) (Red, white arrow) protoplasts and Wave 27R (mCherry-RabE1D) (Red, white arrows) protoplasts as indicated (18-20 h after transformation), respectively. Images were collected using the optimal filters for each fluorescing protein by Confocal Laser Scanning Microscope (CLSM 510 META, Zeiss) as described in 4.2.5. The autofluorescence of chlorophyll is shown in blue. Merge represented EGFP, mCherry and autofluorescence merged together. Bars = 10 μ m. This experiment was performed only once.

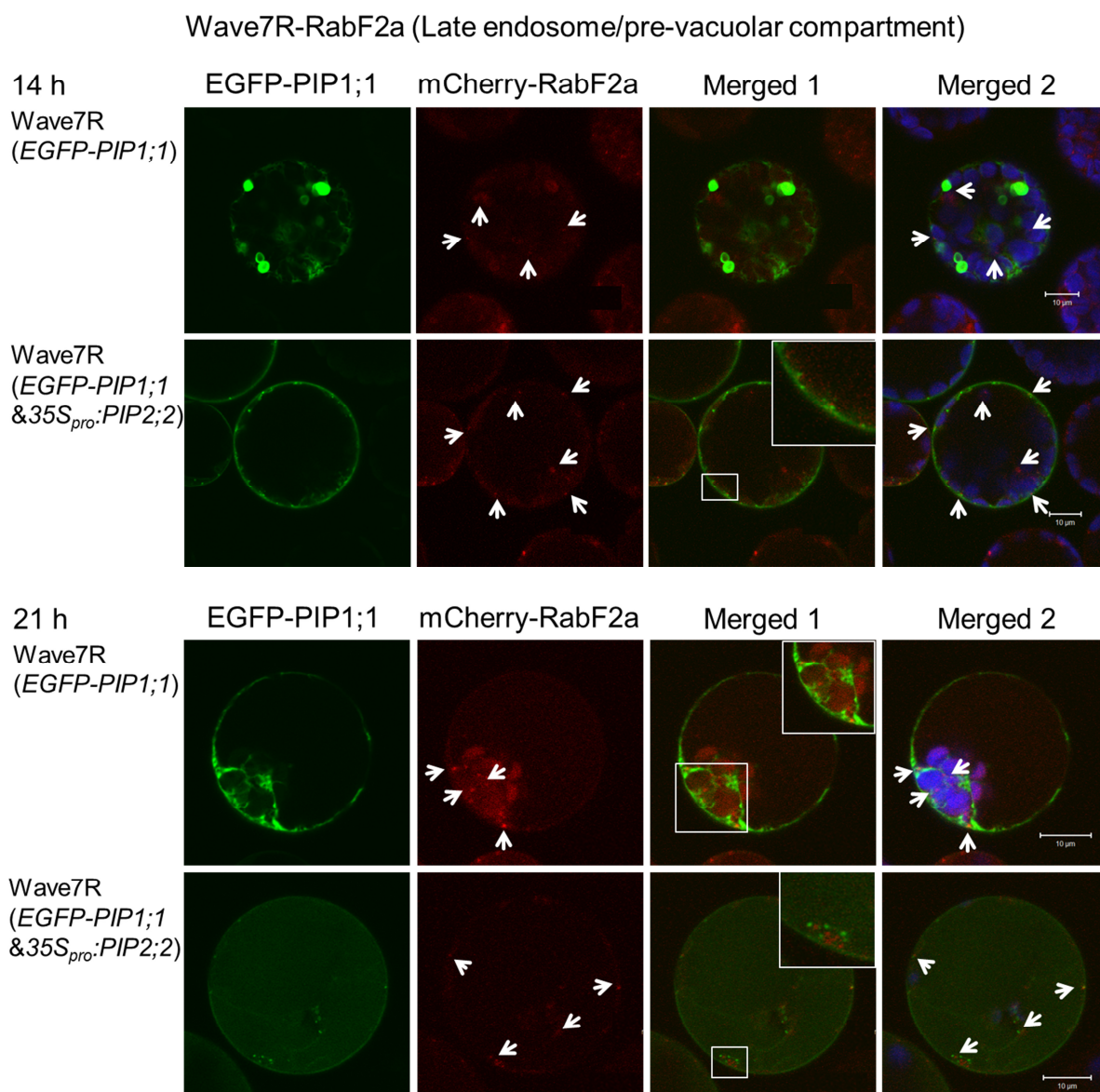


Figure 52. Co-localization analysis of Wave 7R (Late endosome/pre-vacuolar compartment) and EGFP-PIP1;1.

Transiently expressed *EGFP-PIP1;1* (Green) alone or co-expressed with *35S_{pro}:PIP2;2* into Wave 7R (mCherry-RabF2a) (Red, white arrows) protoplasts as indicated, respectively. Images were collected using the optimal filters for each fluorescing protein by Confocal Laser Scanning Microscope (CLSM 510 META, Zeiss) as described in 4.2.5. The autofluorescence of chlorophyll is shown in blue. Merge 1 represented the EGFP merged with mCherry. Merge 2 represented EGFP, mCherry and autofluorescence merged together. Bars = 10 μ m. This experiment was performed only once.

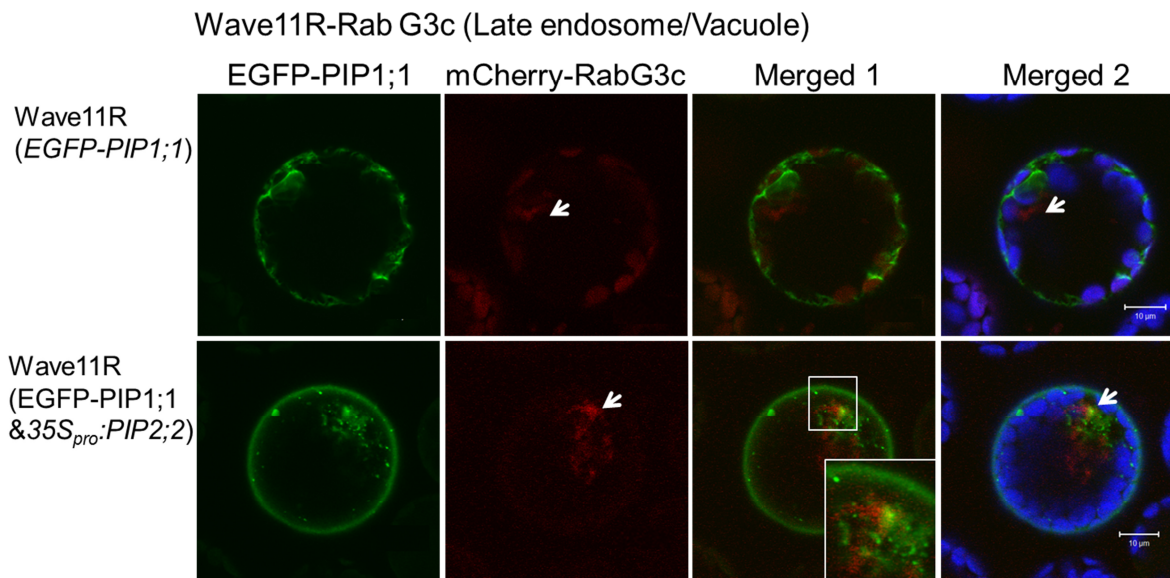


Figure 53. Live-cell fluorescence microscopy of co-localization analysis of Wave 11R (Late endosome/ Vacuole) and EGFP-PIP1;1.

Transiently expressed *EGFP-PIP1;1* (Green) alone or co-expressed with *35S_{pro}:PIP2;2* into Wave 11R (mCherry-Rab G3c) (Red, white arrows) protoplasts by PEG method as indicated (18-22 h after transformation), respectively. Images were collected using the optimal filters for each fluorescing protein by Confocal Laser Scanning Microscope (CLSM 510 META, Zeiss) as described in 4.2.5. Merge 1 represented the EGFP merged with mCherry. Merge 2 represented EGFP, mCherry and autofluorescence merged together. The autofluorescence of chlorophyll is shown in blue. Bars = 10 μ m. This experiment was performed only once.

2.9.2. Pilot experiment to check whether the ubiquitin-26S proteasome system is involved in the degradation of PIP1 protein

Previous studies demonstrated that Rma1, a pepper ubiquitin-protein ligase and 26S proteasome played a role in downregulation of AtPIP2;1 under drought stress (Lee *et al.*, 2009). MG132 (carbobenzoxy-Leu-Leu-leucinal) is usually applied as a proteasome inhibitor to examine whether the ubiquitin-proteasome system is involved in the degradation of a certain protein (Lee and Goldberg, 1996). To assess whether the ubiquitin-proteasome mediated degradation system is involved in repression of PIP1 protein in the *pip2;1 pip2;2* double mutant, PIP1 protein was determined after the treatment with or without MG132.

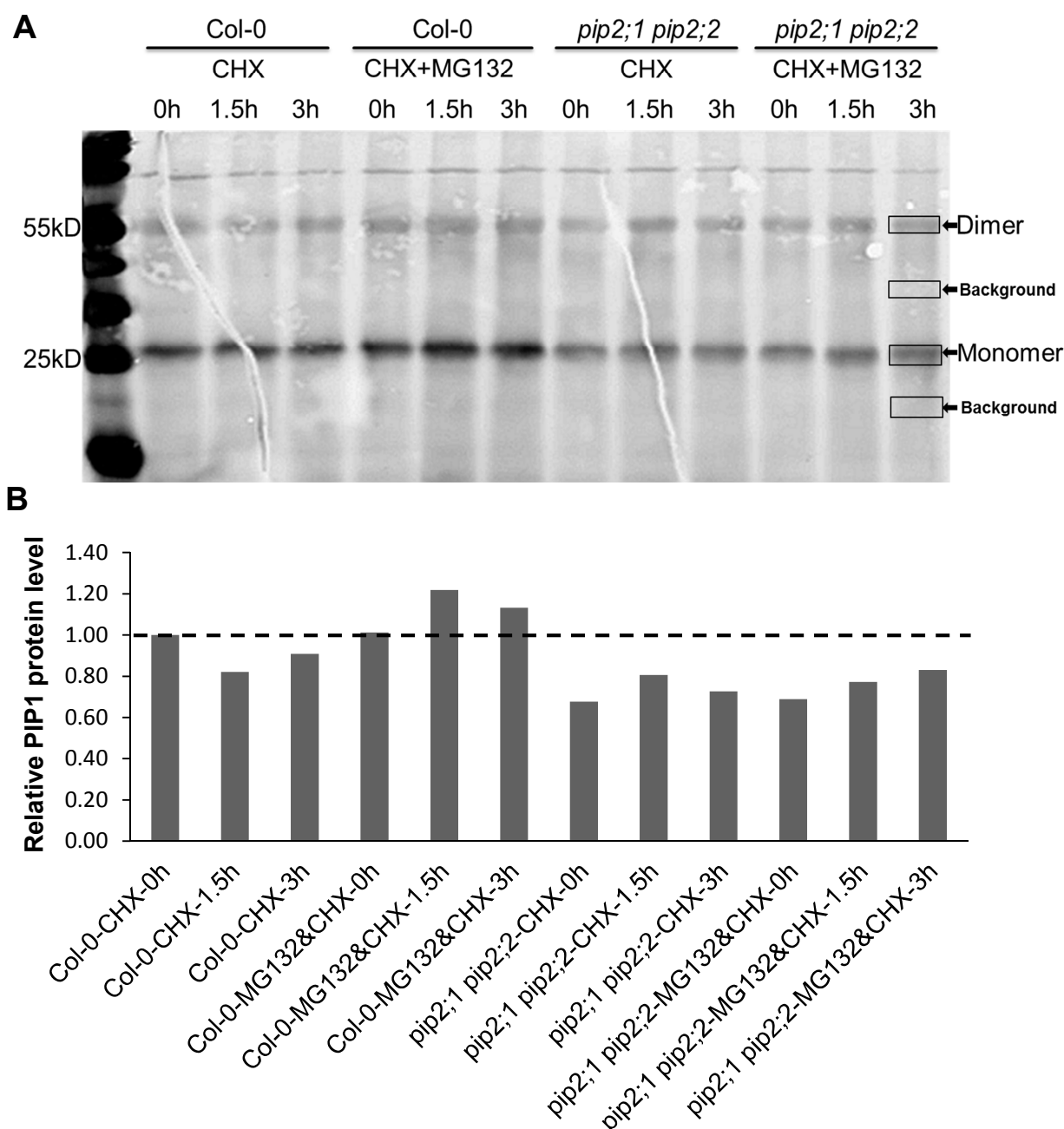


Figure 54. Immunoblotting and quantification analysis of MG132 treatment with mesophyll protoplasts of the wild-type line and the *pip2;1 pip2;2* double mutant.

(A) Protoplasts of Col-0 and *pip2;1 pip2;2* were treated with cycloheximide (100 μ M) or cycloheximide (100 μ M) plus MG132 (50 μ M). The cells were harvested, lysed at 0 h, 1.5 h, and 3 h and were evaluated via Western blot using an anti-PIP1 antibody (see 4.2.4.10). (B) Relative quantification of PIP1 protein was performed with the Image J software. The pixels in each line (including dimer and monomer which minus the backgrounds) are shown in (A) were measured and normalized to the levels quantified for the wild-type control (Col-0-CHX-0 h). This experiment was performed only once.

The whole protein extraction was examined after 0 h to 3 h after MG132 treatment in the protoplasts of the wild-type and the *pip2;1 pip2;2* double mutant, respectively (see 4.2.4.10). In addition, cycloheximide (CHX) was employed to block the protein synthesis. Later, the gray intensity of the specific band (monomer and dimer) of each time course in the immunoblotting picture was quantitatively analyzed by the Image J software and compared to the wild-type mock control (Figure 54).

After 3 h CHX treatment, there was no clear reduction of PIP1 proteins compared to the wild-type at the start time point (0 h) (Figure 54A), indicating that PIP1 proteins are long-lived. Since the PIP1 protein level was stable in both wild type and *pip2;1 pip2;2* after 3 h CHX treatment, a prolonged treatment with CHX is needed to determine the half-life of PIP1 protein in the wild-type line. The relatively increased protein level of PIP1 after the CHX and MG132 treatment may be due to experimental variation (Figure 54B). In conclusion, the question whether an ubiquitin-proteasome-mediated degradation system is involved in the repression of the PIP1 protein could not be deduced by applying CHX and MG132 for a short time period (i.e without creating artifacts) due to the temporal stability of PIP1 proteins.

2.9.3. Preliminary investigation of the degradation of the PIP1:1 and PIP1;2 protein

Potential mechanisms which could be involved in the degradation of PIP1;1 and PIP1;2 in *pip2* mutants should be investigated. Finding out when and where does this degradation happens would further our understanding of these process. Bioactive molecules are widely used to investigate the mechanisms of membrane protein trafficking, for instance, brefeldin A (BFA) blocking exocytosis and Wortmannin (Wm) blocking endocytosis and vacuolar trafficking, also known as an autophagy inhibitor (Robinson *et al.*, 2008; Li *et al.*, 2012). In this work, these chemical compounds were also employed to focus on the time and place of protein degradation. The roots of transgenic lines harbouring *EGFP-PIP1;1* and *PIP1;2-EGFP* (same lines as used in 2.4.4) were treated with these inhibitors (see 96

4.2.4.10). By comparing the change of fluorescence signals between wild type and *pip2;1 pip2;2*, it could provide certain information about the time and place of the degradation of PIP1;1 and PIP1;2 (e.g. similar amount BFA-induced compartments point out the degradation of PIP1;1 or PIP1;2 might happen after plasma membrane targeting, whereas less amount BFA-induced compartments indicate the degradation take place before plasma membrane targeting, probably at the ER). BFA-induced fluorescence compartments appeared in the root elongation zone 3 h after BFA treatment. The plasma membrane localization of the fluorescence signal of EGFP-PIP1;1 in the wild-type line was disturbed as compared to the mock control (DMSO) (Figure 55A). The same phenomenon was observed in *pip2;1 pip2;2* (Figure 55A). The approximately close fluorescence intensities of EGFP-PIP1;1 of these two lines suggested that the amount of newly synthesized EGFP-PIP1;1 were comparable in the root elongation zone in both genetic backgrounds (Figure 55A). This observation agreed that the mRNA level of PIP1;1 was not changed in *pip2;1 pip2;2* compared to the wild-type (Figure 42). However, it was difficult to quantify the size and number of fluorescence signals of BFA compartments in each cell of the wild-type and of *pip2;1 pip2;2* after BFA treatment. Therefore, the time and place of degradation of PIP1;1 could not be deduced by BFA-induced compartments. In contrast, almost no BFA-induced compartments were observed in the root maturation zone, indicating that there was nearly no newly synthesized PIP1;1 protein in this region (Figure 55B).

The application of endocytosis inhibitor Wortmannin is another independent method to deduce whether the degradation takes place before or after targeting to the plasma membrane by quantifying the fluorescence signal at the plasma membrane. The intracellular fluorescence signal of EGFP-PIP1;1 was decreased compared to the mock control 6 h after Wortmannin treatment (Figure 56A). This might indicate that endocytosis of EGFP-PIP1;1 was influenced by Wortmannin in the root elongation zone (Figure 56A).

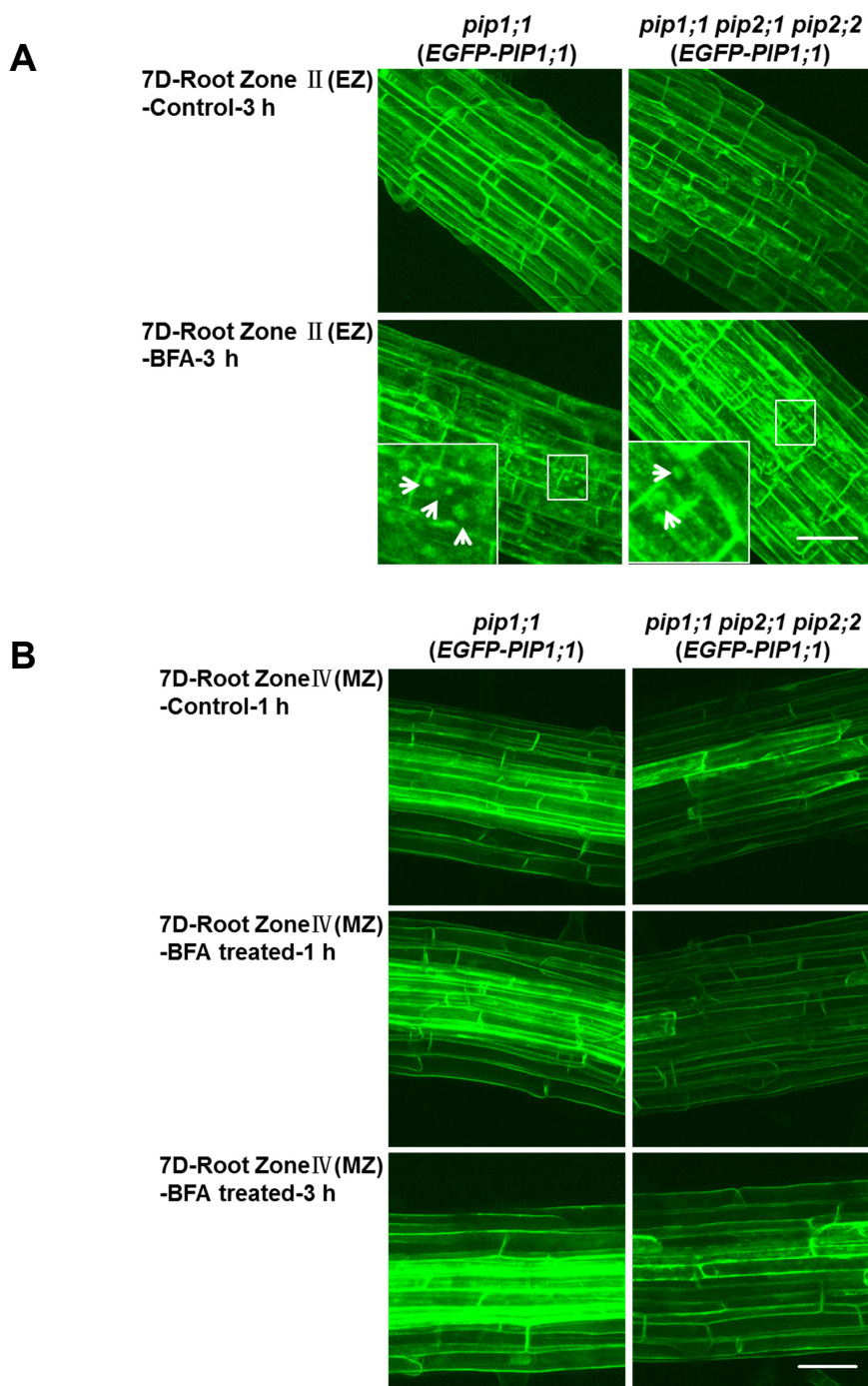


Figure 55. Confocal observation of BFA-induced compartments in the root elongation zones and the maturation zones of different transgenic lines.

(A) The fluorescence signals of EGFP-PIP1;1 were monitored by confocal in the root transition zone after a 3 h treatment with 50 μ M BFA or mock control (DMSO). (B) The fluorescence signals of EGFP-PIP1;1 were monitored by confocal laser microscopy in the root maturation zone 1 h or 3 h after treatment with 50 μ M BFA or mock control (with the help of Jessica Lutterbach). The Z-stack pictures were collected from the root top to 30 μ m (1 μ m interval per Z-stack). All pictures used for comparison were taken employing the same confocal settings (see 4.2.5). Bars = 50 μ m.

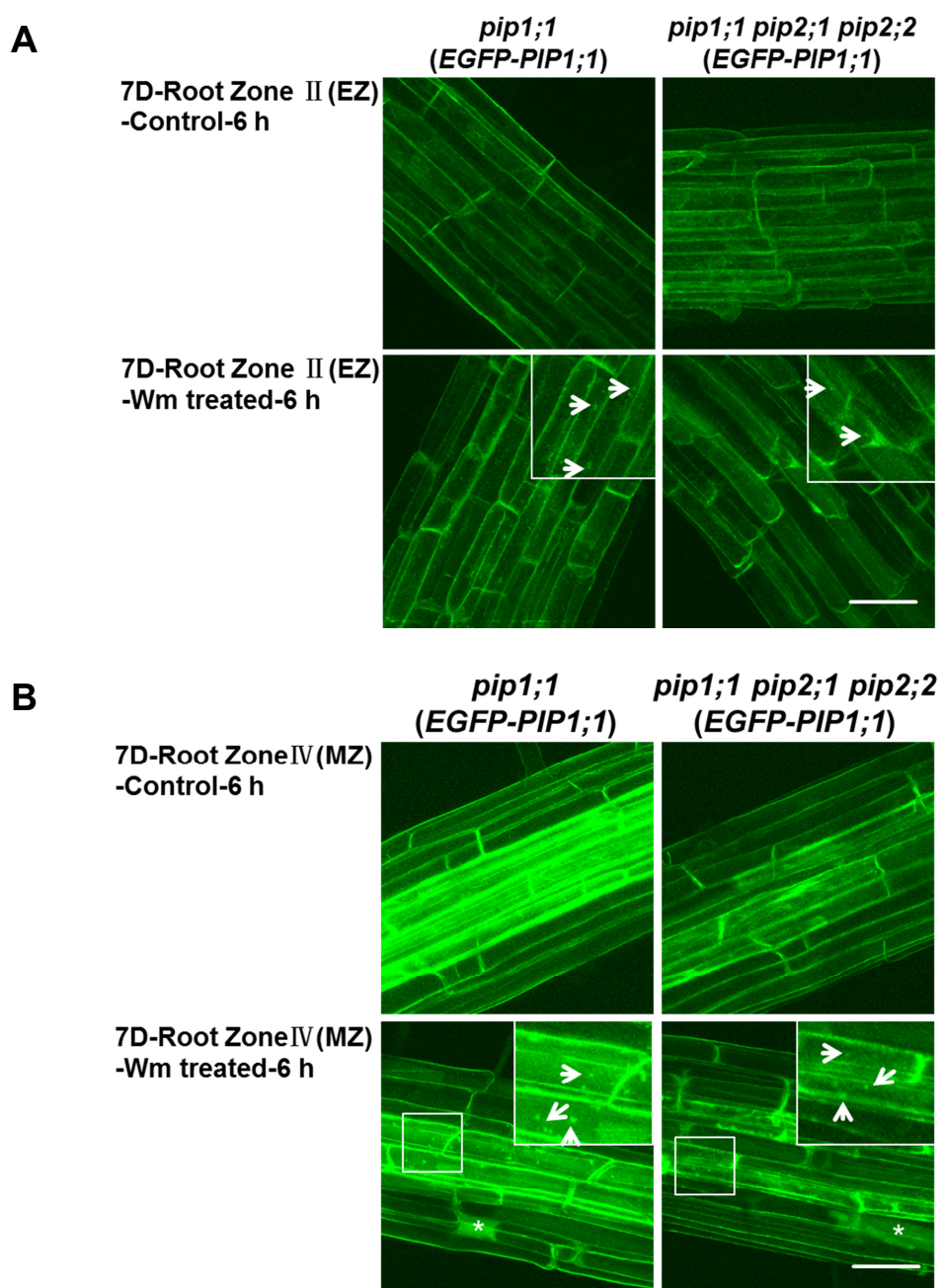


Figure 56. Confocal observation of Wortmannin-induced compartments (EGFP-PIP1;1) in the root elongation zones and the maturation zones of different transgenic lines.

(A) The fluorescence signals of EGFP-PIP1;1 were monitored by confocal in the root transition zone 6 h after treatment with 33 μ M Wortmannin or mock control (DMSO). (B) The fluorescence signals of EGFP-PIP1;1 were monitored by confocal laser microscopy in the root maturation zone 6 h after treatment with 33 μ M Wortmannin or mock control (DMSO) (with the help of Jessica Lutterbach). The Z-stack pictures were collected from the top to 30 μ m (1 μ m interval per Z-stack). All pictures used for comparison were taken employing the same confocal settings. The asterisks represent vacuole-like compartments. Bars = 50 μ m.

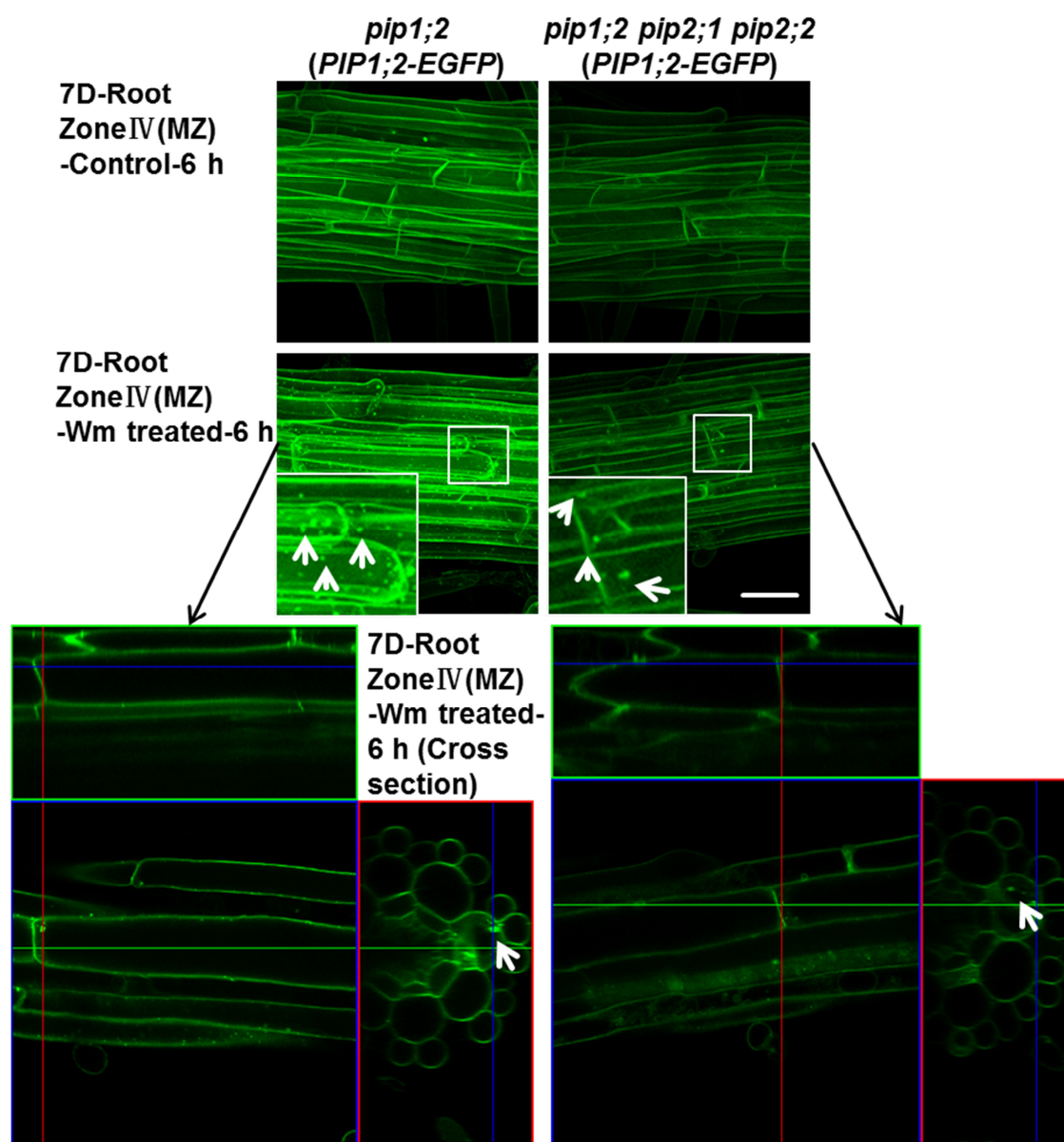


Figure 57. Confocal observation of Wortmannin-induced compartments (PIP1;2-EGFP) in root maturation zone of different transgenic lines.

Seven-day-old seedlings were used for Wortmannin treatment. The fluorescence signals of EGFP-PIP1;1 were monitored by confocal laser microscopy in the root maturation zone 6 h after treatment with 33 μ M Wortmannin or mock control (DMSO) (with the help of Jessica Lutterbach). The Z-stack pictures were collected from the top to 30 μ m (1 μ m interval per Z-stack). All pictures used for comparison were taken employing the same confocal settings. Bars = 50 μ m.

Dot-like fluorescence compartments of EGFP-PIP1;1 (white arrows) were observed in the elongation zone 6 h after Wortmannin treatment and compartments in the wild-type line seemed to be higher in number than in *pip2;1 pip2;2* (Figure 56A). In addition, more Wortmannin induced fluorescence compartments (white arrows) were observed in the wild-type line as compared to *pip2;1 pip2;2*, with regard to their root maturation zones (Figure 56B).

As indicated earlier, Wortmannin is a phosphatidylinositol 3 kinase inhibitor, in addition to its function of blocking the endocytosis, it also works as an autophagy inhibitor for blocking vacuolar trafficking and degradation. The dot-like fluorescence compartments induced by Wortmannin might suggest that an autophagy-vacuole associated (Wortmannin-dependent) degradation pathway is involved in the degradation of EGFP-PIP1;1 in both genetic backgrounds. The same phenomenon was observed in the PIP1;2-EGFP transgenic lines (white arrows), which exhibited the intracellular localization in the cross section images (Figure 57). This preliminary observation suggested that an autophagy-vacuole associated degradation pathway might also be involved in the degradation of EGFP-PIP1;2 in both genetic backgrounds.

Further replicates of drug experiments and additional inhibitors and other biochemical analysis are needed to get a deeper understanding of the mechanisms underlying degradation. However, the preliminary observations above might provide a new hint towards the regulation and degradation of the PIP1 protein in the wild-type line and in the *pip2;1 pip2;2* double mutant.

3. DISCUSSION

The model plant *Arabidopsis thaliana* harbors two PIP subgroups: there are five PIP1 and eight PIP2 members, which belong to the largest aquaporin subfamily under high evolutionary constraint. Previous studies in our lab had revealed that PIP1 protein was repressed in the roots of *pip2;2* and *pip2;1 pip2;2* mutants (Da Ines and Geist, unpublished; Figure 4). This finding has raised several new questions such as which isoform of PIP1 subgroup is affected and what mechanism is underlying this regulation. PIPs are presumed to be involved in cell water homeostasis and other small molecule (e.g.CO₂) transports in *Arabidopsis*. Activation, relocalization and post-translational modifications are all considered to be important for the regulation of the function of PIPs. However, the interaction and regulation between PIP1s and PIP2s and the mechanisms involved therein remain mostly obscure. The answers to the questions raised above might reveal a unique and important regulation between PIP1 and PIP2 subgroups and thus spark a further investigation of a possible mechanism underlying the specific dependence of PIP1 protein expression on PIP2;1/PIP2;2, even further elucidating the possible influence on the physiological function of PIPs.

3.1. Reduction of the PIP1 protein level in *pip2* mutants depends mainly on PIP2;1 and PIP2;2

3.1.1. PIP1 expression is dependent on both PIP2;1 and PIP2;2

Detailed determination of PIP1 proteins in specific tissues showed that PIP1 protein was significantly reduced in the rosettes of *pip2;1* mutant and in the roots of *pip2;2* mutant (Figure 6), which was further verified in EGFP-tagged transgenic lines (Figure 25-28 and 35-38). In agreement with previous studies in our lab (Da Ines and Geist, unpublished; Figure 4), this observation indicated that PIP1 protein was differently reduced in the absence of PIP2;1 and PIP2;2 in different tissues. PIP2;1 is the most abundance isoform of the PIP2 subfamily in 21-day-old leaves and

PIP2;2 is the most abundant isoform of the PIP2 subfamily in 49-day-old root according to a previous proteomic study (Monneuse *et al.*, 2011) (Figure 58). This indicates that the reduction of PIP1 may be associated with the protein abundance of PIP2;1 or PIP2;2 in different tissues. Accordingly, the significant reduction of PIP1 protein was stably observed in the *pip2;1 pip2;2* double mutant regardless of specific tissues and different development stages (Figure 7), supporting the additive effect of PIP2;1 and PIP2;2 on the PIP1 reduction. This suggested that PIP1 reduction is largely dependent on the specific expression level of PIP2;1 and PIP2;2 which share highly similar sequence. In addition, the hybrid transgenic lines which expressed the *PIP2;3* gene under the control of *PIP2;2* promoter were able to enhance the protein abundance of PIP1 in the *pip2;1 pip2;2* double mutant (Figure 9), indicating a functional similarity of PIP2;2 and PIP2;3 protein (96.8% identity) in affecting the expression of PIP1 protein. Nevertheless no PIP1 reduction was observed in the *pip2;3* mutant (Da Ines and Geist, unpublished; Figure 4), possibly due to the much lower abundance PIP2;3 compared to PIP2;1 and PIP2;2 under natural conditions (Monneuse *et al.*, 2011).

The approximately 40-50% reduction of the PIP1 protein level in *pip2;1 pip2;2* indicated that PIP1 expression was not exclusively dependent on PIP2;1 and PIP2;2 (Figure 6). However, there was no repressive effect on PIP1 protein abundance in other *pip2* mutants (Da Ines and Geist, unpublished; Figure 4). Nevertheless the total PIP1 protein content could be examined in the multiple mutants (e.g. *pip2;1 pip2;2 pip2;4* or *pip2;1 pip2;2 pip2;7*) to check whether there was any additive effect on the reduction of PIP1 protein since PIP2;4 and PIP2;7 were also highly expressed at transcript and protein levels in the roots or in the root and rosettes, respectively (Jang *et al.*, 2004; Alexandersson *et al.*, 2005; Hruz *et al.*, 2008; Monneuse *et al.*, 2011). In addition, hybrid transgenic lines which expressed the *PIP2;4* or *PIP2;7* gene under the promoter of *PIP2;1* or *PIP2;2* could be investigated whether these two isoforms could substitute the positive impact of PIP2;1 and

PIP2;2 in PIP2;1- or PIP2;2- expressing cells. Taken together, PIP1 protein level is mainly dependent on the presence of PIP2;1 and PIP2;2.

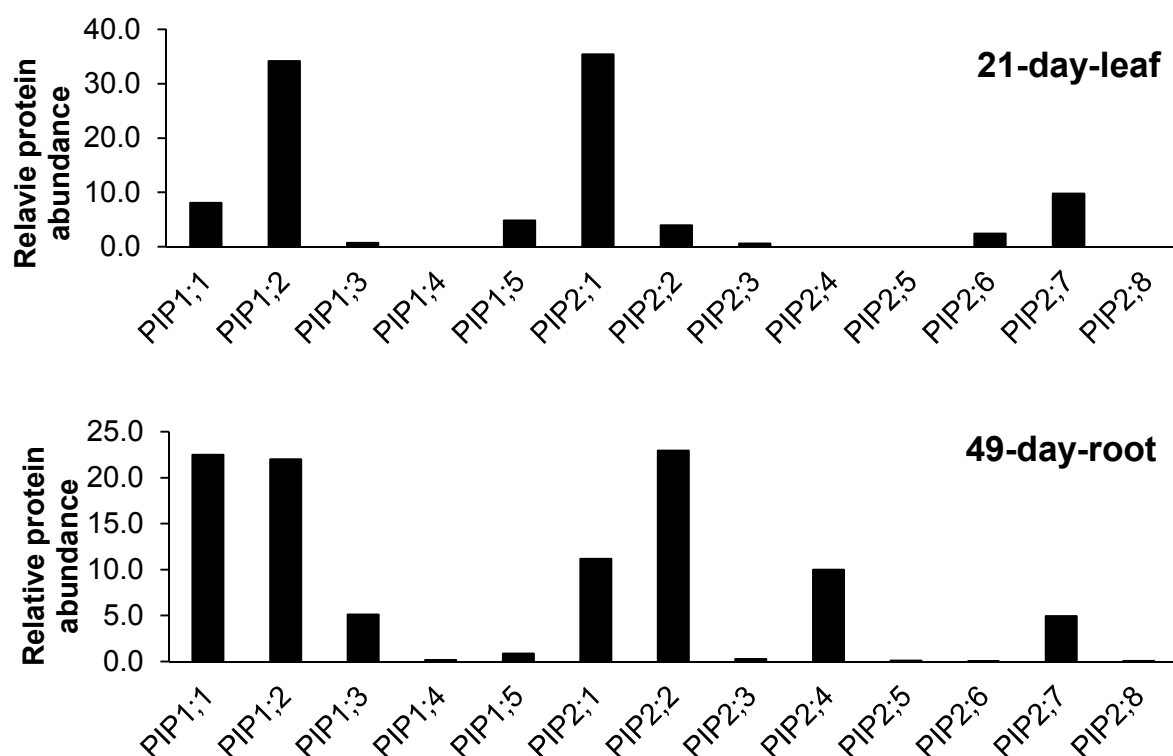


Figure 58. Relative protein abundance profile of five PIP1s and eight PIP2s in leaf and root of *Arabidopsis*.

PIP isoforms were quantified in 21-day-old leaves and 49-day-old roots, respectively, by a targeted proteomics approach in a previous proteomic study (Monneuse *et al.*, 2011). Relative protein abundance of 13 PIP isoforms was normalized according to the percentage of abundance of measurement, assuming the whole PIP protein as 100 %.

3.1.2. Multiple lines of evidence reveal that PIP1 isoforms are reduced in the *pip2;1 pip2;2* double mutant

Therefore, the question remained, which isoforms of PIP1 were affected by PIP2;1 and PIP2;2 expression, since an antiserum detecting all five PIP1 isoforms had been used and the production of isoform-specific antibodies was hampered by their high sequence similarity. A quantitative analysis of PIP1 protein levels in *pip1* single mutants compared to *pip1* mutations introgressed into the *pip2;1 pip2;2* background (Figure 13 and 14) suggested that both PIP1;1 and PIP1;2 were downregulated in *pip2;1 pip2;2*. These results were independently supported by EGFP- and HA-

tagged transgenic PIP1;1- and PIP1;2-expressing lines (Figure 19-38). However, it cannot be excluded that any of the other three PIP1 isoforms are affected in *pip2;1 pip2;2*. The same strategy of *pip1* mutant analysis and specifically tagged isoform experiments could be applied in the other three PIP1 isoforms to investigate whether there was a reduction of these isoforms in *pip2;1 pip2;2*. In fact, the results from protein quantification have suggested that the other three PIP1 isoforms may be influenced in the *pip2;1 pip2;2* double mutant compared to wild type (Figure 15). This result was in agreement with proteomics studies in our laboratory. A preparation of plasma membrane protein from wild-type and *pip2;1 pip2;2* rosettes (Jin Zhao, Anton Schäffner, Juliane Merl-Pham, personal communication) suggested that all five PIP1 isoforms were affected in *pip2;1 pip2;2*. In part, this could be independently confirmed by quantitative analyses of microsomal fractions obtained from 28-day-old wild-type and *pip2;1 pip2;2* rosettes, which revealed a similar repression of PIP1;1, PIP1;2, PIP1;3, PIP1;4 and PIP1;5 (Table 1, preliminary data, together with Jin Zhao).

The repression of total PIP1 protein may be mainly contributed by the reduction of PIP1;1 and PIP1;2, because PIP1;1 and PIP1;2 were the major isoforms of the PIP1 subfamily according to the analysis of the expression of PIPs homologues at both transcript and protein levels (Jang *et al.*, 2004; Alexandersson *et al.*, 2005; Monneuse *et al.*, 2011), and because both isoforms had been shown to be affected by the absence of PIP2;1 and PIP2;2. However, the other three PIP1 isoforms seemed to be affected in the *pip2;1 pip2;2* double mutant as well.

3.2. Possible mechanisms underlying the PIP2;1/PIP2;2-dependence of PIP1 expression

The data so far suggest a unidirectional regulation of PIP1 by PIP2;1 and PIP2;2, since no significant reduction of PIP2 was detected in *pip1;1* and *pip1;2* mutants (Danes and Geist, unpublished; Figure 4). The PIP2;1/PIP2;2-dependence of PIP1 expression was further elucidated by transient expression (Figure 49 and 50). The expression levels and/or stabilities of PIP1;1 and PIP1;2 as well as possibly other PIP1 proteins depend on these PIP2 isoforms. However, the mechanism underlying the dependence of PIP1 expression on these two PIP2 isoforms remain unclear. Several possible hypotheses will be proposed based on the results of this work and on the literature.

3.2.1. Potential interaction between PIP1s and PIP2s may be involved in regulation of PIP2;1/PIP2;2-dependence of PIP1 expression

Preliminary co-immunoprecipitation results of this study indicated that PIP1;1 or PIP1;2 may interact with PIP2;1/PIP2;2/PIP2;3 (Figure 43). It has been reported that the fluorescence signal intensity of the maize aquaporin ZmPIP1;2 expressed as a ZmPIP1;2-GFP fusion protein in *Xenopus* oocytes was increased three- to four-fold at the oocyte membranes when it was coexpressed with ZmPIP2;5 compared to ZmPIP1;2-GFP expression alone, indicating that the expression and/or stability of ZmPIP1;2 was affected by ZmPIP2;5 (Fetter *et al.*, 2004) due to a possible physical interaction.

A broad range of evidence supporting the interaction between PIP1s and PIP2s was reported by examining the translocation of fluorescence-labelled PIP1s or comparing the osmotic permeability in heterologous expression system which expressed PIP1s alone or co-expressed them with PIP2s (Fetter *et al.*, 2004; Zelazny *et al.*, 2007; Chen *et al.*, 2013; Jozefkowicz *et al.*, 2013; Yaneff *et al.*, 2014).

This interaction is supported by the co-evolution theory between PIP1s and PIP2s. It has been reported that certain proteins that are part of complexes tend to evolve at a relatively slow rate to assist the co-evolution with their interacting partner proteins (Mintseris and Weng, 2005). According to the evolutionary analysis of aquaporins, PIPs are under high evolutionary constraint (Soto *et al.*, 2012). The physical interaction of PIPs in a wide variety of species suggest that the high evolutionary constraint of PIPs may be also due to functional constraint between PIP1s and PIP2s (Soto *et al.*, 2012).

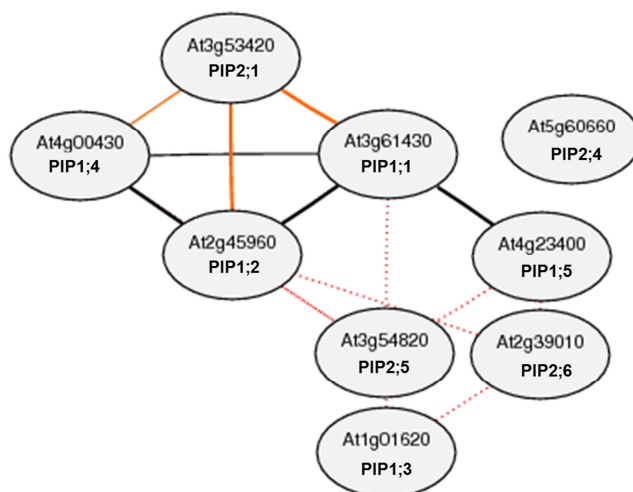
Based on previous studies, multiple interactions of AtPIP1s and AtPIP2s as well among AtPIP2s have been demonstrated by the yeast-two-hybrid system from a proteome-wide binary protein-protein interaction map analysis (Consortium, 2011) (e.g. PIP1;1 interacts with PIP2;3, PIP2;5, PIP2;7 in yeast cell-Figure 60A) and independently investigated by the split-ubiquitin system in yeast as well (e.g. PIP1;3 interacts with PIP1;2, PIP1,4, PIP1,5, PIP2;2 and PIP2;5) (Jones *et al.*, 2014) (listed in Figure 60B). In addition, PIP1;1, PIP1;2 and PIP1;3 exhibited a remarkably high correlation with PIP2;1, PIP2;2/2;3 and PIP2;7/2;8 in *Arabidopsis* based on transcriptional coexpression analysis (Da Ines, 2008) (Figure 59). The presence of PIP2;1, PIP2;6, PIP2;7 and PIP2;8 as well as PIP1;1, PIP1;2, PIP1;3 and PIP1;5 has been found in detergent resistant membranes (Bhat and Panstruga, 2005; Borner *et al.*, 2005; Shahollari *et al.*, 2005). These observations may provide further hints to the interaction between the PIP1s and PIP2s in *Arabidopsis*, although they do not directly show their interaction *in situ*.

If direct interactions of PIP2;1/PIP2;2-PIP1 are mechanistically important for the dependence of PIP1 expression on PIP2;1/PIP2;2, an overlapping spatial expression of these two subfamilies would be essential. According to the histochemical localization analysis of *PIP1s* and *PIP2s* via GUS-staining, certain *PIP1s* and *PIP2s* exhibited similar or overlapping expression patterns in specific cells or tissues (Javot *et al.*, 2003; Da Ines, 2008; Alexandersson *et al.*, 2010; Da

Ines *et al.*, 2010; Postaire *et al.*, 2010; Peret *et al.*, 2012; Prado *et al.*, 2013). For instance, *PIP1;2*, *PIP2;1*, *PIP2;2*, *PIP2;3* and *PIP2;7* were all expressed in the whole stele of GUS-stained root cross-section, whereas *PIP1;2* was also expressed in the other root cell layers (Zhao, Dissertation, 2013) and *PIP1;2*, *PIP2;1*, *PIP2;2*, *PIP2;6* and *PIP2;7* showed expression in the vein of leaves (xylem parenchyma and bundle sheath) (Da Ines *et al.*, 2010; Prado *et al.*, 2013). Again *PIP1;2* was also expressed in the other leaf cell types (Kaldenhoff *et al.*, 1995; Postaire *et al.*, 2010). These partially overlapping expression patterns between *PIP1;2* and *PIP2;1/PIP2;2* provided a hint for an interaction and the *PIP2;1/PIP2;2*-dependence of *PIP1* expression. The expression patterns of other *PIP1* isoforms need to be investigated to check whether an overlapping spatial expression exists between the rest of *PIP1* isoforms and *PIP2;1/PIP2;2*. These aspects highlight the possibility that *PIP2;1* and *PIP2;2* could act as positive regulators of certain *PIP1* isoforms when *PIP2;1* or *PIP2;2* are coexpressed in the same cell.

So far, a wide range of studies have been focussed on whether *PIP2*s could physically interact with *PIP1*s and thus facilitate the trafficking of *PIP1*s to reach the plasma membrane. However, a physical interaction could as well be part of mechanism by which *PIP2;1* and *PIP2;2* affect *PIP1* protein expression and stability. To fully understand the rules and the significance of *PIP* subfamily interplay, it remains crucial to dissect the mechanism which determines the *PIP1* protein stabilization as well as the reduction of *PIP1* protein in case of *PIP2;1/PIP2;2* deficiency.

A



B

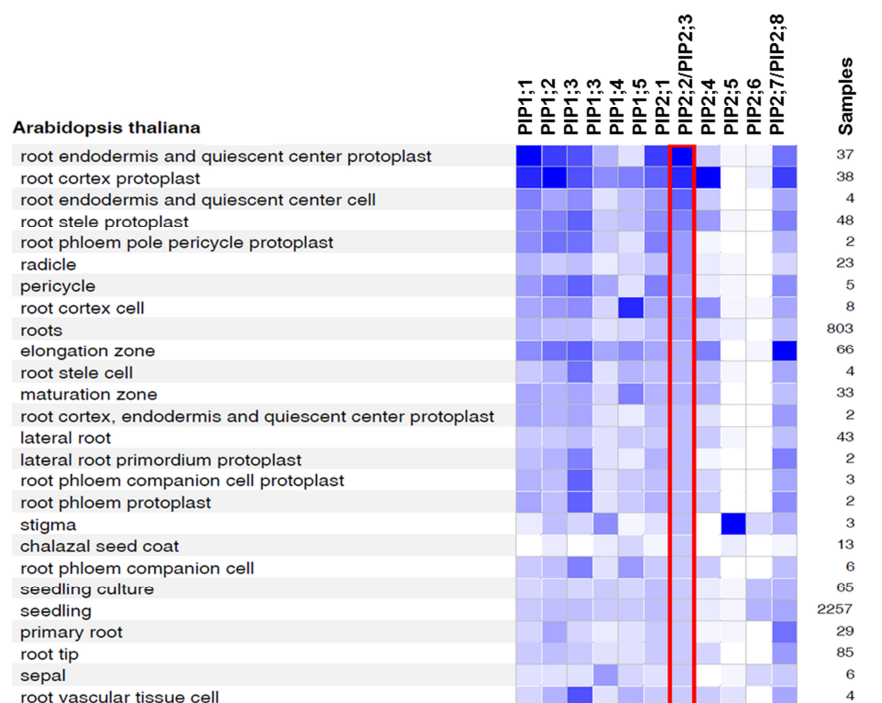


Figure 59. Coexpression analyses of aquaporin transcripts and protein-protein interaction (ATTED-II) and Genevestigator analysis of *PIPs* gene expression in different tissues.

(A) Integration of a coexpression network based on different correlation of *PIPs* transcripts and known protein-protein interactions between different *PIPs* in *Arabidopsis* by ATTED-II (solid edges represent gene coexpression and red dotted edges represent known protein-protein interactions) (Obayashi *et al.*, 2014). (B) The picture was adapted from Genevestigator (Hruz *et al.*, 2008). Red lines indicate that this linear heatmap is built from highest expression level to lowest expression level of PIP2;2/PIP2;3. The color key represents expression level of specific genes based on the absolute value scaled to the expression potential of each gene as indicated (darker blue represents higher expression level) <https://www.genevestigator.com>.

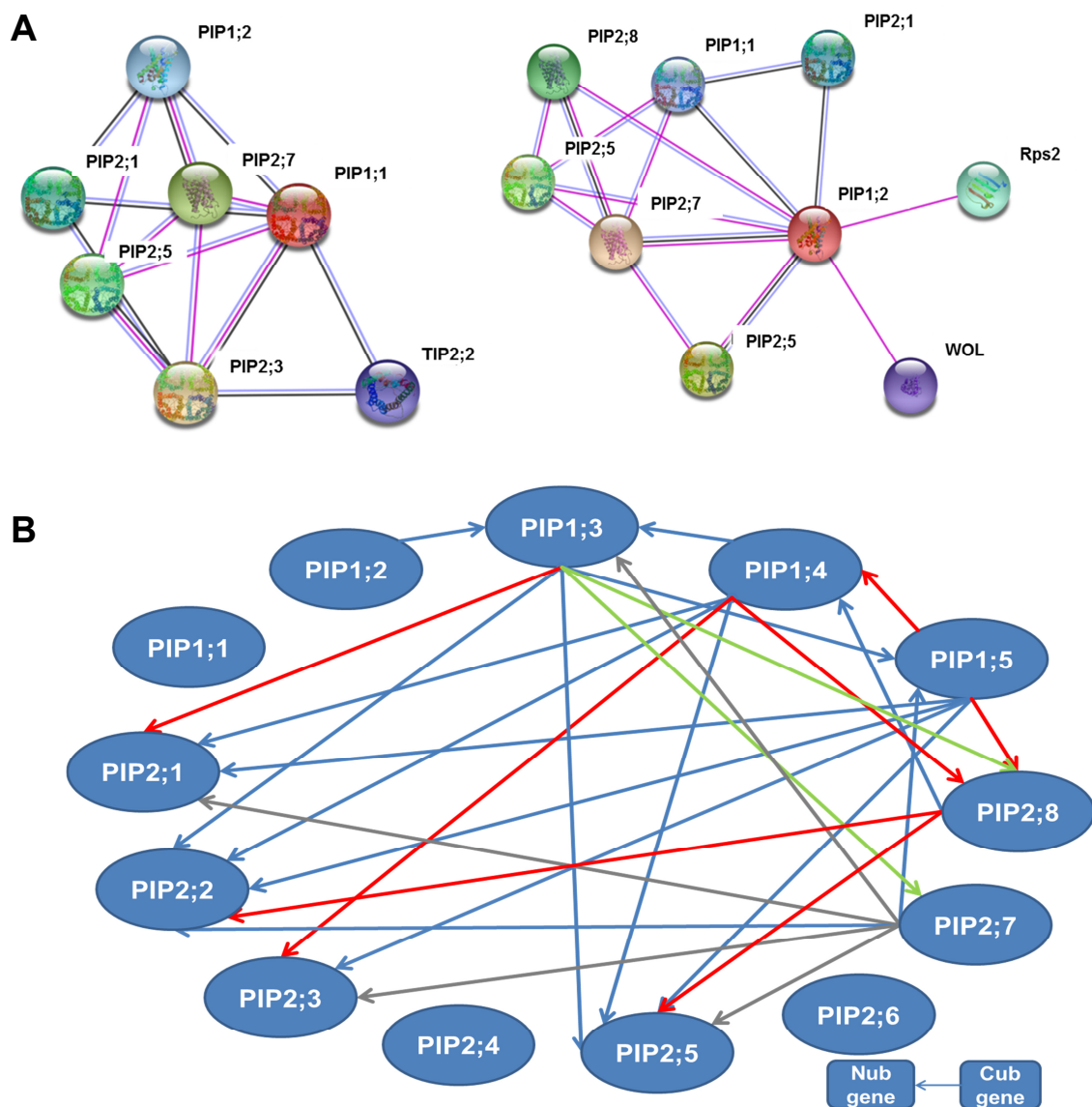


Figure 60. Protein-protein interaction network.

(A) Protein-protein interaction networks of PIP1;1 or PIP1;2 in *Arabidopsis* generated by STRING9.1 (Franceschini *et al.*, 2013) with high confidence greater than 0.7 (Red edges indicate experimental data, black edges indicate transcripts co-expression analysis and blue edges indicate whether there is homologous relationship). (B) Protein-protein interaction analysis of PIPs with membrane-based interaction database as described (Jones *et al.*, 2014). This figure was generated in this work based on the interaction of PIPs. Interaction tested positive in two split-ubiquitin assays in a primary interaction screen will be tested in another two split-ubiquitin assays in a secondary interaction screen. Different colors indicated different levels of interaction verification: blue lines represent four positive tests, red lines represent three positive tests, light Green lines represent two positive tests, gray lines represent one positive test in a primary screen which was not tested in the second screen. The arrows of each edges represented the gene used as Nub fusion in a split-ubiquitin assay.

3.2.2. Possible mechanisms underlying the dependence of PIP1 expression on PIP2;1 and PIP2;2

One possible target for regulating the PM-located PIPs *via* a physical interaction may be their intracellular trafficking. PIPs are synthesized at the ER and are exported from the ER through the secretory pathway to reach the plasma membrane (Hachez *et al.*, 2013; Luu and Maurel, 2013). Surprisingly, transiently expressed EGFP-PIP1;1 alone was observed in several, so far unidentified compartments, e.g. the relatively immobile ring-shaped fluorescence compartments in protoplasts (Figure 44, 46A and 47A). These spherical or ring-shaped fluorescence compartments are morphologically similar to organized smooth endoplasmic reticulum (OSER) whorls structures, a phenomenon which has been reported in many living organisms under physiological conditions or by overexpression of ER transmembrane proteins (Snapp *et al.*, 2003). The formation of OSER structures depends on a weak homotypic interaction (dimerization) of the cytoplasmic domain of certain proteins in opposing membranes regions (Snapp *et al.*, 2003).

Although the OSER structures were considered to be artifacts of overexpression of GFP-tagged ER transmembrane proteins which accumulated in the ER (Snapp *et al.*, 2003), these findings actually indicated that certain proteins were unable to be exported out of the ER due to a so far unknown mechanism. Recently, OSER structures were found to be produced by overexpressing Venus-AtPIP2;7 in *osm1* (mutant of SYP61 – a member of the SNARE family) but not in corresponding wild-type cells (Hachez *et al.*, 2014). This phenomenon can be rescued by complementation with SYP61, suggesting that the accumulation of Venus-AtPIP2;7 may be caused by the disturbance of secretion from the ER in the *osm1* mutant. This leads to the hypothesis that over-expressed EGFP-PIP1;1 may be deficient in its ability to be exported from the ER and instead accumulated there, forming OSER-like structures, possibly due to weak homotypic interactions of N-terminal

EGFP or the long N-terminal cytoplasmic domain of PIP1;1 or cytosolic loop D, which contain a number of predicted protein binding sites (Figure 61). On the other hand, OSER-like structures were less frequently observed when EGFP-PIP1;2 was expressed alone in mesophyll protoplasts compared to EGFP-PIP1;1 transient expression (Figure 45). This experiment has to be repeated to confirm this phenomenon. Although PIP1;1, PIP1;2 and PIP1;3 have been reported to have water permeability and therefore are predicted to reach the oocyte membrane (Kammerloher *et al.*, 1994), in another studies PIP1;2 was the only one among several PIP1 isoforms (PIP1;1/PIP1;2/PIP1;3/PIP1;4) which exhibited significant water transport activity and pH sensitivity in *Xenopus* oocytes (Tournaire-Roux *et al.*, 2003). Although these were heterologous expression studies in a non-plant system, they may indicate that the trafficking of PIP1;2 was different from PIP1;1 in *Arabidopsis* as well.

In addition, OSER-like structures formed by accumulation of EGFP-PIP1;1 disappeared and were replaced by the rapidly-moving punctate compartments when co-expressed with $35S_{pro}:PIP2;1$ or $35S_{pro}:PIP2;2$. This indicated that ectopic expression of PIP2;1 or PIP2;2 might assist the secretion of EGFP-PIP1;1 out of ER and targeting towards to the plasma membrane via these small unknown punctate compartments which move rapidly along linear intracellular paths (Figure 47B). Heterotetramerization via interaction between PIP1;1 or PIP1;2 and PIP2;1/PIP2;2/PIP2;3 which had been demonstrated at a preliminary level, could be a means to achieve this (Figure 43). It is known that aquaporins form homo- and/or hetero-tetramers in the membrane (Murata *et al.*, 2000; Fetter *et al.*, 2004), suggesting that aquaporin monomers possess the ability to interact with each other in different manners. However, the assembly of homo- and/or hetero-tetramers is still largely unknown.

PIP2s can be independently targeted to the plasma membrane as well which has been demonstrated by a plethora of experimental studies. An N-terminal diacidic

motif DXE acts as an ER export signal into COPII both in maize and *Arabidopsis* (Zelazny *et al.*, 2009; Sorieul *et al.*, 2011). LXXXA is another motif in the transmembrane helix3 of ZmPIP2;5, which is important for export from the ER and targeting to the PM in maize (Chevalier *et al.*, 2014). However, replacing these two motifs in ZmPIP1;2 with motifs of ZmPIP2;5 was not sufficient to mediate a plasma membrane localization of ZmPIP1;2, indicating the existence of other ER-retention signals in ZmPIP1;2 (Zelazny *et al.*, 2009; Chevalier *et al.*, 2014). Alternatively there is another additional requirement for ZmPIP1;2 export out of the ER. ER-retained ZmPIP1s were relocalized to the plasma membrane when ZmPIP2s (ZmPIP2;1 or ZmPIP2;5) were coexpressed with ZmPIP1s (ZmPIP1;1 or ZmPIP1;2) in *Xenopus* oocytes (Zelazny *et al.*, 2007). This highlighted the importance of heteromerization between PIP1s and PIP2s for ER-export of PIP1s. It has been reported that PIPs might assemble with each other in a random arrangement dependent on their abundance (Yanef *et al.*, 2014). The heterotetramerization between PIP1s and PIP2s was indicated by a growing number of experimental studies, which revealed that ER-retained PIP1s could be targeted to the plasma membrane by physically interacting with PIP2s forming hetero-oligomers thereby enhancing the water permeability in heterologous system (Fetter *et al.*, 2004; Zelazny *et al.*, 2007; Chen *et al.*, 2013; Jozefkowicz *et al.*, 2013; Yanef *et al.*, 2014).

A study of random heteromerization of PIPs demonstrated that a mutant form of strawberry FaPIP2;1N228D-EYFP could not reach the plasma membrane when expressed alone in *Xenopus laevis* oocytes. However when co-expressed with FaPIP1;1, or FaPIP2;1N228D coexpressed with FaPIP1;1-EYFP, both fluorescent signals could be detected at the plasma membrane (Yanef *et al.*, 2014). This indicated that not only PIP2s could facilitate the PM-targeting of ER-retained PIP1s as demonstrated in many studies, but PIP1s can also assist mistargeted or misfolded PIP2s to reach the plasma membrane.

Based on previous studies, oligomerization is regarded as an important mechanism for exporting signal directing membrane proteins without a known cytosolic export signal into COPII vesicles for the specific destinations (Sato and Nakano, 2003; Springer *et al.*, 2014). Normally, misfolded proteins tend to be retained in the ER by ER quality control (ERQC) (Hurtley and Helenius, 1989; Araki and Nagata, 2011), which could be assisted by chaperones via proper folding and targeting to the right localization. Therefore, this raises the hypothesis that chaperones are required to mediate the interaction of PIP2s (especially the highly abundant PIP2;1 and PIP2;2) with PIP1s lacking a known cytosolic export signal to exit the ER and reach the plasma membrane in certain cell types (in PIP2;1- and PIP2;2-expressing cells). Such an interaction possibly induces an allosteric functional conformation change via oligomerization and then results in the proper folding of PIP1s or *vice versa*, and forms the hetero-oligomer for exporting from the ER by facilitating the interaction of PIPs with a cargo receptor protein or other trafficking partners. For instance, the SNARE family (ZmPIP2;5 with SYP121, AtPIP2;7 with SYP121 and SYP61) is known to mediate vesicular trafficking and impact PIP2 targeting (Geelen *et al.*, 2002; Besserer *et al.*, 2012; Hachez *et al.*, 2014). It would also be interesting to know whether these trafficking partners were also involved in the trafficking and/or stability of PIP1s in *Arabidopsis*.

The study of PIP1/PIP2 heterotetramerization revealed possible contact points between PIP subfamily members (Otto *et al.*, 2010; Bienert *et al.*, 2012; Jozefkowicz *et al.*, 2013). A conserved cysteine residue in Loop A is involved in dimer stabilization of ZmPIP1s and ZmPIP2s by disulfide bond formation via a conformational arrangement (Bienert *et al.*, 2012). Loop E of maize ZmPIP1;2 and Loop A of bean BvPIP2;1 are considered to be important elements for the heterotetramerization which has been proven by different experiments (Fetter *et al.*, 2004; Jozefkowicz *et al.*, 2013). Loop E of AtPIP1s harbours several key amino acids of the essential element of ZmPIP1;2 with minor variance (Da Ines, 2008)

(Figure 62). Loop A of AtPIP2;1/PIP2;2/PIP2;3 possesses the IQ (isoleucine/glutamine) residues which are vital for the interaction according to the conserved region analysis for heterotetramerization between bean PIP1s and PIP2s (Jozefkowicz *et al.*, 2013) (Figure 62). Those possible contact points in AtPIPs, together with the preliminary interaction result (Figure 43) and different transient expression effects (Figure 44 to 50) in protoplasts indicating the trafficking and/or stability of PIP1s is affected by PIP2;1/PIP2;2 via a possible interaction. This supports the notion that all five AtPIP1 isoforms have the possibility to form hetero-oligomers with AtPIP2;1/PIP2;2/PIP2;3. An analysis using mutagenesis of these essential elements for interaction together with water transport assays and are required for a thorough mechanism investigation regarding such heterotetramerizations of PIPs in *Arabidopsis*.

Beside the heterotetramerization between PIP1s and PIP2s, there are several other aspects which need to be considered for further studies. For instance, heterooligomerization among PIP2s (ZmPIP2;1 and ZmPIP2;6) (Cavez *et al.*, 2009), or PIP1s (ZmPIP1;1 and ZmPIP1;2) (Fetter *et al.*, 2004), suggesting that heterotetramerization is more complicated and may contribute to multiple layers of regulation within the PIP subfamilies. ZmPIP1;1 or ZmPIP1;2 are inactive when it expressed alone in oocytes. However, when ZmPIP1;1 was coexpressed with ZmPIP1;2, a significantly increased osmotic water permeability of oocytes was detected, indicating a synergistic effect of these two isoforms to form a functional water channel. However, it has to be kept in mind that this has been only observed in a heterologous, non-plant system (Fetter *et al.*, 2004). There is evidence that this heterooligomerization of ZmPIP1s (ZmPIP1;1 and ZmPIP1;2) is not sufficient to relocalize ER-retained ZmPIP1s to the plasma membrane and that it results in no synergistic effect in maize protoplasts (Zelazny *et al.*, 2007). It was reported that one of the human aquaporins AQP4 formed heterotetramers between the two different truncated isoforms M1 and M3 by a random arrangement (Neely *et al.*, 1999). Yet, it

DISCUSSION

is unclear whether there is also interaction among AtPIP1s and whether there are different truncated AtPIP1 isoforms forming heterotramers in *Arabidopsis*. It is also important to know whether the interplay between PIP1s subfamily will affect the channel activity or modulate the trafficking or stability of PIP1 isoforms. A mathematic model and experimental data supported the random arrangement of PIP isoforms dependent on their abundance. The heteromerization of PIPs resulted in a cooperative effect on the function of PIP1 and PIP2 despite the fact that these two subfamilies may have distinct functions (Otto *et al.*, 2010; Yaneff *et al.*, 2014). The formation of heterotetramers may not just facilitate the trafficking of PIP1s, but may also be an important regulatory mechanism to stabilize PIPs or influence their function. Taken together, it is tempting to propose that PIP2s serve as indispensable partners, assisting the proper folding of PIP1s, and forming a heterodimer or heterotetramer (conformational stability, which form an allosteric cooperativity) which will then be recognized by the cargo receptor as an exporting signal and sorted into COPII vesicles for the correct targeting from ER to PM and then stabilize the PIP1 abundance. However, other mechanisms or a signal which was induced by the loss-of-function of PIP2;1 or PIP2;2 could be also involved in the reduction of PIP1 in the mutant situation.

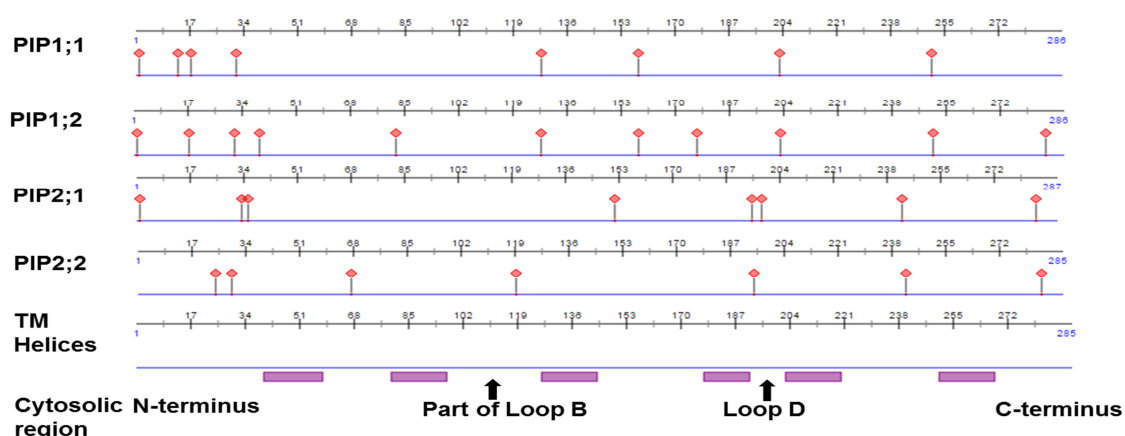


Figure 61. Protein-protein binding site prediction according to ISIS2 analysis.

Predicted protein-protein interaction sites of PIPs (amino acid sequences) were analyzed by the ISIS analysis at www.predictprotein.org (Ofran and Rost, 2007).

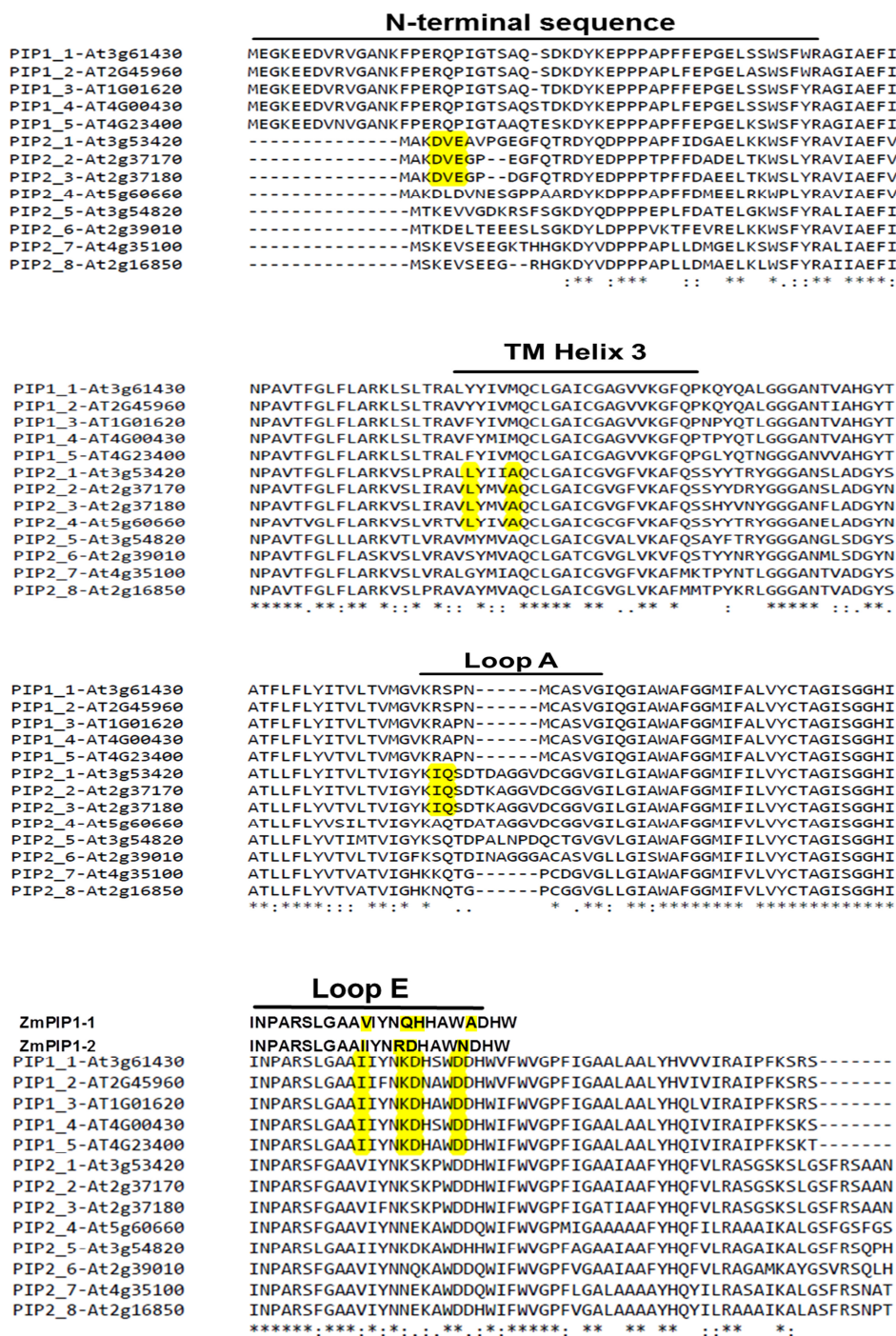


Figure 62. Clustal W multiple sequence alignment of PIP isoforms.

The important amino acids are labelled in yellow (Embnet.vital-it.ch/wwwtmp). An N-terminal diacidic motif DXE or an LXXXA motif in the transmembrane helix3 (acting as an ER export signal) is conserved in AtPIP2;1/PIP2;2/PIP2;3. IQ (isoleucine/glutamine) of Loop A could be found in AtPIP2;1/PIP2;2/PIP2;3 as indicated for heterotetramerization. Loop E of AtPIP1s harbors several key amino acids of the essential element for heterotetramerization of maize ZmPIP1;2 with minor variance (Interaction between maize PIP1s and PIP2s depends on the Loop E of ZmPIP1;2 instead of Zm PIP1;1).

3.3. Possible timing and localization of PIP1 protein degradation

Since PIP1 genes are properly transcribed and PIP1 proteins are synthesized in the *pip2;1 pip2;2* double mutant, but lost in the absence of PIP2;1 and PIP2;2 (Figure 39 and 42), it is of importance to investigate the post-translational mechanism behind this reduction. Furthermore, the reduction of PIP1 protein was analyzed with the microsomal fraction, implying that PIP1 protein is indeed degraded instead of being retained at the ER or mistargeted to any other membrane system in *pip2* mutants.

The reduced fluorescence signal of EGFP-tagged PIP1 isoforms clearly indicated that the abundance of PIP1;1 and PIP1;2 had been affected in the *pip2;1 pip2;2* double mutant (Figure 19, 21, 29 and 31). However, the process of downregulation remains unclear. It could either take place at the ER because of the first protein quality control procedure or by ER-phagy leading to the degradation of misfolded or unfolded PIP1s. Alternatively, it could also happen after PIP1s targeting to the plasma membrane and then associated with proteasomal or vacuolar degradation in an endocytic process.

3.3.1. ER-associated degradation or ER-phagy-related degradation of PIP1s in the *pip2;1 pip2;2* double mutant

There is evidence that a defect in the interplay of PIP1s and PIP2s may not only influence the targeting and water transport potential (Fetter *et al.*, 2004; Zelazny *et al.*, 2007; Chen *et al.*, 2013; Jozefkowicz *et al.*, 2013; Yaneff *et al.*, 2014), but may lead to an endoplasmic reticulum quality control process and an ER-stress situation when PIP1s are “stuck in traffic” in this study. ER associated degradation (ERAD) or selective autophagy directing the ER-to-vacuole degradation has been reported to be responsible for degradation of proteins in certain situations (Babst, 2014; Michaeli and Galili, 2014).

ER-associated degradation is a common pathway for eliminating misfolded proteins when they cannot be rescued via the ER quality control system (Ruggiano *et al.*, 2014). Normally the ERAD machinery is associated with the ubiquitin-26S proteasome system (Guerra and Callis, 2012). According to protein-protein interaction analysis of *Arabidopsis* protein using the split-ubiquitin system in yeast (Jones *et al.*, 2014), all five PIP1 isoforms may interact with ubiquitin-conjugating enzymes: UBC34 and UBC32. The latter one is an active ERAD component localized in the ER and thereby connected to ER-associated degradation during salt stress tolerance (Cui *et al.*, 2012; Liu and Li, 2014) (Figure 63). The speculation is that the folding status of PIP1 might be different in the cell with or without enough PIP2;1 or PIP2;2 acting as required interaction partner as discussed earlier. This points out the possibility that misfolded or ER-retained PIP1s might be controlled by the ERQC system, leading to the degradation via ERAD machinery or other ER-related degradation pathways. The involvement of the ubiquitin-26S proteasome system in the degradation of total PIP1 protein was assessed using a 26S-proteasome inhibitor MG132 and protein synthesis inhibitor cycloheximide. However, the total PIP1 protein level was stable both in wild type and *pip2;1 pip2;2* during a 3 h cycloheximide treatment (Figure 54), indicating that the turnover of PIP1 protein at this developmental stage might be relatively slow (protoplasts of 28-day-old rosette). However, at different developmental stages, the half-life of the PIP1 protein may be different (not tested). If a shorter half-lives of PIP1 protein were identified, a further experiment with MG132 may indicate whether ubiquitin-26S proteasome mediated degradation system were involved in reduction of PIP1 protein. AtPIP2;1 has been shown to be polyubiquitinated by the pepper ubiquitin ligase Rma1H1 at the ER, following by the degradation via the 26S-proteasome (Lee *et al.*, 2009). It would be interesting to check whether AtPIP1s could be ubiquitinated by the *Arabidopsis* homolog of this protein or whether the abundance of PIP1 proteins would change in the corresponding mutant. A possible

ubiquitination of PIP1;1 or PIP1;2 could also be determined with the transgenic lines expressing tagged PIP1;1 or PIP1;2 by immunoprecipitation and Western blot analysis using anti-ubiquitin antibodies. These transgenic lines can be further employed to investigate whether the ERAD machinery together with the ubiquitin-26S proteasome degradation system underlies the reduction of specific PIP1 isoforms.

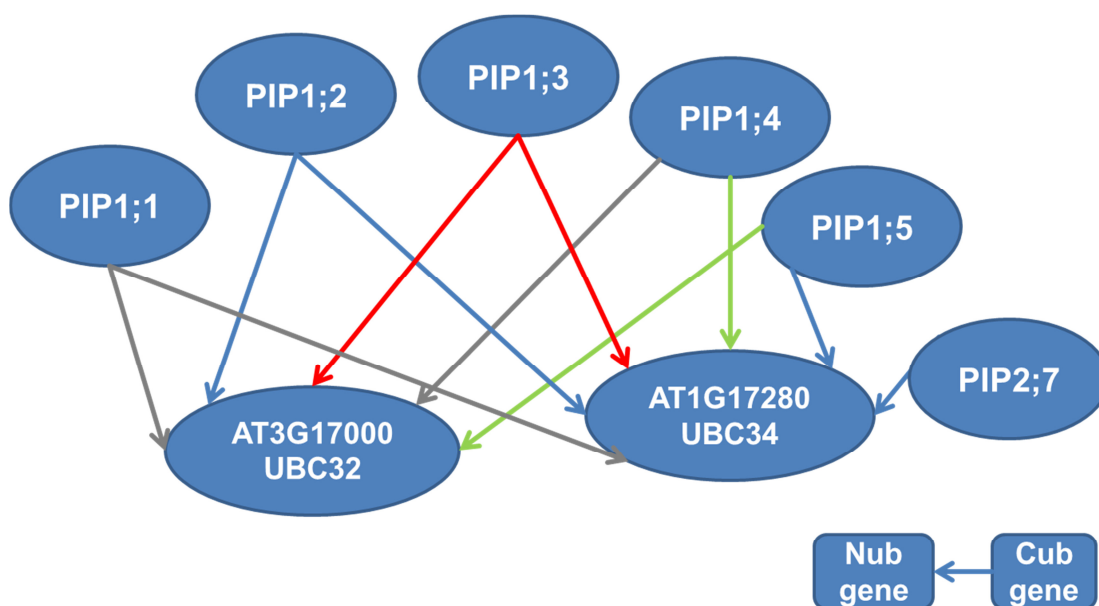


Figure 63. Protein-protein interaction analysis with membrane-based interactome database.

The picture generated in this work with information obtained from membrane-based interactome database as described (Jones *et al.*, 2014). Different colors indicate different levels of verification of interactions as indicated in Figure 60 B.

Pharmacological studies with the exocytosis inhibitor brefeldin A and the endocytosis inhibitor Wortmannin, functioning also as an autophagy inhibitor, were employed in pilot experiments to explore the time and place underlying the reduction of PIP1;1 and PIP1;2. The observed BFA-induced compartments indicated that trafficking of PIP1;1 and PIP1;2 are affected by BFA treatment in the wild-type line and the *pip2;1 pip2;2* double mutant. The comparison of the size and number of BFA-induced fluorescence compartments in single cells of the root between the wild type and *pip2;1 pip2;2* could be used for estimating whether the same amount of

PIP1;1 or PIP1;2 was exported from the ER, thus determining whether the degradation happened at the ER or after exporting from the ER. However, quantification of fluorescence signals from BFA-induced compartments between wild type and double mutant did not yet yield clear results because of several technical limitations. For instance, the size of one root cell was too large for a single picture taken by confocal. The quantification of the fluorescence signal at the plasma membrane by applying the endocytosis inhibitor Wortmannin is another independent method to deduce whether the degradation takes place before or after targeting to the plasma membrane. Further detailed and modified quantitative analysis is needed to estimate the time and place of degradation. On the other hand, the dot-like fluorescence compartments induced by Wortmannin might suggest that autophagy associated vacuolar degradation is involved in the degradation of EGFP-PIP1;1 and EGFP-PIP1;2 both in wild type and *pip2;1 pip2;2* because of the function of Wortmannin as an autophagy inhibitor. In addition, more Wortmannin-induced fluorescence compartments were observed in the wild type as compared to the *pip2;1 pip2;2* double mutant (Figure 56B and 57). One possible explanation of this observation is that the process of degradation happened before PIP1s were targeted to the plasma membrane, i.e. the observed fluorescence compartments were directly derived from the ER, which will be discussed later in the autophagy-related pathway. Another possibility is that there is already less PIP1s in the root cell of *pip2;1 pip2;2* due to another unknown process, and the fluorescence compartments observed just represented one pathway for degradation of PIP1;1 or PIP1;2 in general. Further replicates of drug experiments and other inhibitors like tyrphostin A23 (an inhibitor of clathrin-mediated endocytosis), concanamycin A (a specific V-ATPase inhibitor affecting vacuolar degradation) are needed for more detailed examination to get a deeper understanding of the underlying degradation mechanism.

In addition, ER-stress was induced when the clearance of overloaded misfolded proteins was beyond the ability of the ERAD machinery in the ER (Walter and Ron, 2011; Howell, 2013). Besides these classical ER-stress signaling pathways, it has been reported that autophagy is involved in the homeostasis or recovery after ER-stress. In ER-stress conditions, the components of the ER, which contain the accumulated and often misfolded proteins, are engulfed by autophagosomes and delivered to the vacuole or lysosome for degradation in both yeast and mammalian cells (Bernales *et al.*, 2006; Deegan *et al.*, 2013). In plants, autophagy has been reported to be induced by ER-stress, directing the ER membrane-derived vesicles for vacuolar degradation via stress-related selective autophagosome (Li and Vierstra, 2012; Liu *et al.*, 2012). Most intriguingly, the large ER whorls which are induced by ER stress in yeast are selectively engulfed by vacuoles via ER-phagy independent from autophagosomes or the core autophagy machinery (Schuck *et al.*, 2014). This provides a distinct type of autophagy which degrades the ER component. However, the existence of ER-phagy in higher eukaryotes remains unclear, although the ER whorls have been frequently reported in mammalian cells, either linked to an autophagic response (Lingwood *et al.*, 2009) or independently from the core autophagy machinery (Korkhov, 2009). There is no report on the ER-phagy in plants, even though OSER-whorls structures could also be observed in several cases in plants (Wang *et al.*, 2011). Previous studies pointed out the OSER structures might be artifacts produced by overexpression of membrane protein or low-affinity protein interaction. Hence, the possibility cannot be excluded that ER-whorls might be a novel autophagy mechanism (ER-phagy) which was possibly induced by ER-stress, directing the accumulating proteins towards vacuolar degradation to keep ER homeostasis. Therefore, the sphere-like or whorl structure and OSER-like fluorescence compartments of EGFP-PIP1;1 need to be further examined by electron microscopy or by colocalization analysis or vacuole visualization via staining to check whether this fluorescence compartments are still

localized at the ER or engulfed by vacuoles for degradation. Marker proteins of autophagy-related vacuolar degradation pathway should be utilized for co-localization analysis and their corresponding mutants, e.g. *atg7* (Hofius *et al.*, 2009) (blocking the autophagy-related vacuolar degradation) could be crossed with *pip2;1 pip2;2* double mutant to investigate whether this pathway is indeed involved in the degradation of PIP1;1 or PIP1;2.

3.3.2. Vesicle-associated vacuolar degradation of PIP1s in the *pip2;1 pip2;2* double mutant

Another possibility related to the downregulation of PIP1;1 and PIP1;2 is an altered turnover or stability of PIP1s in the absence of PIP2;1 and PIP2;2 after plasma membrane targeting. When different root regions were compared between wild type and *pip2;1 pip2;2*, the overall fluorescence intensity of EGFP-PIP1;1 or EGFP-PIP1;2 was reduced in the root maturation zone of *pip2;1 pip2;2* (Figure 21 and 31), whereas the targeting and/or the stability of EGFP-PIP1;1 or EGFP-PIP1;2 appeared to be less affected in the root elongation zone compared to the root maturation zone of *pip2;1 pip2;2*. In this case, the influence of PIP2;7 on PIP1s can not be excluded possibly due to the high transcriptional expression of PIP2;7/PIP2;8 in the root elongation zone (Figure 59B) and a possible interaction between PIP1;1 and PIP1;2 with PIP2;7 (Figure 60). This raises the possibility that EGFP-PIP1;1 or EGFP-PIP1;2 could be properly targeted to the plasma membrane, however, the stability of PIP1s may be changed after targeting in the *pip2;1 pip2;2* double mutant background when cells grew in the elongation region to fully develop and to become mature cells. Furthermore, some unknown fluorescence compartments (white arrows) of EGFP-PIP1;1 or EGFP-PIP1;2 seemed to be more frequently observed in the root maturation zone of the *pip2;1 pip2;2* double mutant compared to the wild-type background (Figure 22 and 32). Although the nature or destiny of these intracellular structures remains to be identified, it is possible that these fluorescence compartments may be related to the degradation of EGFP-PIP1;1 or EGFP-PIP1;2

in the *pip2;1 pip2;2* double mutant. This might provide a hint for further investigation. The colocalization analysis should be performed to check whether these unknown compartments are associated with prevacuolar compartments or multivesicular bodies. The staining of vacuoles may also provide a hint for the fate of these fluorescence compartments.

The unknown fluorescence compartments mentioned above could be EGFP-PIP1;1 or EGFP-PIP1;2 complexes endocytosed from the plasma membrane. Although the fate of endocytosed PIPs remains unclear, either the proteins could be directly recycled back to the plasma membrane or they are directed to multivesicular bodies to be recycled or degraded (Dhonukshe *et al.*, 2007). Nevertheless, an internalization of PIP1;1-GFP and PIP2;1-GFP had been already observed after salt stress, which showed that reactive oxygen species activated cell signaling cascades were involved in this regulation (Boursiac *et al.*, 2005; Boursiac *et al.*, 2008). Furthermore, the enhanced internalization and cycling of AtPIP2;1 and AtPIP1;2 was reported in response to salt stress (Li *et al.*, 2011; Luu *et al.*, 2012). The phosphorylation of the C-terminal tail of PIPs has been reported to be involved in the regulation of plasma membrane trafficking or their internalization, phosphorylation of Ser283 results in the intracellular accumulation of AtPIP2;1 in unknown compartments, possibly endosome or prevacuole under salt stress condition (Prak *et al.*, 2008). In mammals, both ubiquitination and phosphorylation have been demonstrated to be involved in the regulation of endocytosis of aquaporin-2 (Tamma *et al.*, 2011; Moeller *et al.*, 2014). It is important to know whether ubiquitination and phosphorylation may also play a role in the internalization and possibly in the degradation of EGFP-PIP1;1 or EGFP-PIP1;2 in the *pip2;1 pip2;2* double mutant backgrounds (Figure 22 and 32). In addition, vacuole-associated accumulation of AtPIP2;1-GFP signals after dark treatment in combination with lytic vacuole inhibitor treatment experiments indicated that AtPIP2;1-GFP was targeted to the vacuole for degradation in resting conditions

(Kleine-Vehn *et al.*, 2008). Recently, one of the human aquaporins AQP4 was significantly downregulated by its splicing variant form AQP4- $\Delta 4$ through proteasomal degradation via an heterodimerization (De Bellis *et al.*, 2014). Even though the regulation and degradation of PIPs still leaves open questions, these studies might provide the diverse possibilities for transient modification that mark them for different degradation or recycling processes. These diversification strategies might suggest that multiple layers or coordinative effects exist among different degradation pathways for efficiently regulating the activity and abundance of PIPs. The described possible degradation processes in this study might pose another specific regulation strategy linking PIP1 expression to the presence or abundance of PIP2;1 and PIP2;2.

3.4. Possible physiological role of dependence of PIP1s on PIP2;1 and PIP2;2

3.4.1. The dependence of PIP1s on PIP2;1 and PIP2;2 may prevent the ER stress

As described earlier, PIP1;1 and PIP1;2 are high abundant isoforms of PIP2 subfamily (Monneuse *et al.*, 2011). Based on the previous relocalization studies on PIP1s (Fetter *et al.*, 2004; Zelazny *et al.*, 2007; Chen *et al.*, 2013; Jozefkowicz *et al.*, 2013; Yaneff *et al.*, 2014) and the preliminary interaction result in this work, a possible mechanism that has been proposed for the interplay of PIPs is that PIP2s already participate in the folding of PIP1s and lead to or facilitate their export from the ER and targeting to the plasma membrane and thus keep their stability. It is tempting to speculate that a possible overload of PIP1s at the ER would be degraded via a yet unidentified mechanism in case of the loss-of-function PIP2;1 and PIP2;2 to avoid the ER-stress. In addition, the OSER structures observed in the transient expression system are regarded as a detoxification system in the cell (Snapp *et al.*, 2003). In yeast, the ER whorls structures are engulfed by vacuoles for

keeping the balance of the cell when ER-stress occurs (Schuck *et al.*, 2014). In this respect and combined with the transient expression experiment in *Arabidopsis* protoplasts in this work, it is interesting to note that the dependence of PIP1 protein level on the PIP2;1 and PIP2;2 might be a regulatory mechanism to reduce a possible detrimental accumulation of highly abundant PIP1 isoforms (PIP1;1 or PIP1;2) in the ER and thus provide a fast and convenient way to maintain ER homeostasis without provoking a further transcriptional response.

3.4.2. The dependence of PIP1s on PIP2;1 and PIP2;2 may influence water permeability or transport of other molecules (CO₂, NO, H₂O₂ or NH₃) in plants

Aquaporins are regarded as water channel proteins, especially PIPs which are localized at the plasma membrane are considered to be highly important for modulating membrane water permeability in response to different environmental conditions and water availability (Schäffner, 1998; Javot *et al.*, 2003; Chaumont *et al.*, 2005; Da Ines, 2008; Maurel *et al.*, 2008; Chaumont and Tyerman, 2014; Li *et al.*, 2014). In *Arabidopsis*, PIP2;1, PIP2;2, PIP2;3 all have been proven to be functional water channels which greatly enhanced the membrane water permeability in heterologous systems (Daniels *et al.*, 1994; Kammerloher *et al.*, 1994; Weig *et al.*, 1997). The utilization of *pip2;1* and *pip2;2* mutants indicates that these single abundant isoforms plays a role in leaf hydraulic conductivity and in root osmotic water transport, respectively (Javot *et al.*, 2003; Prado *et al.*, 2013). PIP1;1, PIP1;2 and PIP1;3 exhibited water transport activity in oocytes as well (Kammerloher *et al.*, 1994). *pip1;2* mutant analysis has demonstrated that PIP1;2 plays an important role in plant hydraulic conductivity (Postaire *et al.*, 2010). The dependence of PIP1 protein expression on PIP2;1 and PIP2;2 may reveal a new aspect of a rapid control of the water conductivity in the cell or at the tissue level by coupling the regulation of the abundance of PIP1 and PIP2, especially in response to different environmental challenges or specific plant development stages. For instance,

downregulation of root aquaporins together with stomatal closure under salt stress may play a role in preventing excessive water loss in *Arabidopsis*. Similarly, coordinated downregulation of PIP1 and PIP2 together with reduced root water transport in the evening may be essential for preventing the water flow back from plants into the soil (Steudle, 2000; Boursiac *et al.*, 2005). The coupled downregulation of PIP1-PIP2 might enhance this protective mechanism. Combined with the studies on the aquaporin expression or posttranslational modification in response to various environmental stimuli, the abundance and activity of PIPs tend to be reduced under drought, salinity, anoxia or chilling conditions (Tournaire-Roux *et al.*, 2003; Jang *et al.*, 2004; Boursiac *et al.*, 2005; Liu *et al.*, 2005; Boursiac *et al.*, 2008; Maurel *et al.*, 2008). This suggests that the coupling PIP1-PIP2 expression may play an important role in adaptation to environmental challenges in a short-term by changing the protein abundance in a combined manner. This could be also applied in circumstances when highly expressed PIPs are needed. Some studies have suggested that aquaporins may function as osmosensors, probably as part of feedback loops, signaling within the cell to modulate diverse processes (Hill *et al.*, 2004; Hill and Shachar-Hill, 2006; MacRobbie, 2006). Such a coupling of PIP1-PIP2 expression may be involved in raising the sensitivity to the osmotic changes and subsequently play a role in the signal transduction chain.

Loss-of-function of PIP2;1 and PIP2;2 not only exhibits a reduced water flux from roots to leaves but also results in defective lateral root emergence (Da Ines *et al.*, 2010; Peret *et al.*, 2012). It suggests that PIPs may play an essential role in plant development. The dependence of PIP1 protein on PIP2;1 and PIP2;2 may contribute to a proper temporal and spatial control of water transport in specific development stages, for instance, cell expansion, leaf movement, stomatal movement or diurnal and circadian regulation.

The dependence of the PIP1 protein level on PIP2;1 and PIP2;2 could also provide a means for the control of the channel selectivity or other related functions.

Based on the previous studies, PIP1s are postulated to be membrane transporters exhibiting different molecule channel activities (glycerol, urea or other volatile substrates like CO₂) or their functions depend on their expression or specific localization (Biela *et al.*, 1999; Moshelion *et al.*, 2002; Gaspar *et al.*, 2003; Uehlein *et al.*, 2003). For instance, AtPIP1 was reported to be highly expressed in plasmalemmasomes, and these structures invading the vacuolar lumen may facilitate the rapid water exchange between apoplast and vacuole (Robinson *et al.*, 1996). NtAQP1 localized both at the plasma membrane and chloroplast envelope may contribute in water transport and the CO₂ transport across the membrane (Uehlein *et al.*, 2003; Uehlein *et al.*, 2008). AtPIP1;2 was demonstrated to be involved in the transport of CO₂, thereby affecting the photosynthesis in leaves (Heckwolf *et al.*, 2011; Uehlein *et al.*, 2012). One hypothesis regarding this possible multifunctionality of PIP1s is that the dependence of PIP1 on the PIP2;1 and PIP2;2 may allow a tight regulation or coordination of uptake of other molecules together with the up- or downregulated water transport. This coupled regulation of PIP1-PIP2 may be essential to keep the balance of plants during certain circumstances, especially facing the conflict of the plant growth and stress response. In addition, it has been proposed that the function or intrinsic permeability of PIPs might be changed depending on the tetramer composition (Otto *et al.*, 2010; Yaneff *et al.*, 2014). The central fifth pore generated by the tetramer might exhibit different ion or gas transport activities in different homo- or hetero-tetrameric compositions (Muller *et al.*, 2002; Yool and Weinstein, 2002; Kruse *et al.*, 2006; Bertl and Kaldenhoff, 2007; Wang *et al.*, 2007). The coupled regulation of PIP1-PIP2 may change the network partners of aquaporins for generating different tetramers, and may thus alter the corresponding transport activities as well. Taken together, the coupled expression of PIP1 and PIP2 may reveal an additional function of heterotetramerization of PIP1s and PIP2s in affecting the substrate preference and transport activities in plants during plant growth or water stress conditions.

Since the major isoforms PIP1;1 and PIP1;2 are affected in the *pip2;1*, *pip2;2* and *pip2;1 pip2;2 double* mutant (Figure 18 to 37), it is reasonable to hypothesize that downregulation of PIP1 protein may contribute to the defects in the water transport and plant development of these mutants. This may raise a possible trade-in theory, i.e a possible PIP1-related ER-stress is avoided by PIP1 degradation, although this effect may reduce water-permeability even further in addition to the loss of PIP2;1 and PIP2;2. However, plants may keep the ER homeostasis as a most important aspect of major importance and therefore sacrifice a higher water permeability. Since there is no obvious detrimental growth effect observed in *pip2* mutants under controlled laboratory conditions, it is possible that other mechanisms may be activated or be involved in compensating the reduced water hydraulic conductivity in plants. It would also be interesting to know whether degradation of PIP1s was the outcome of a stress sensing system provoked in the *pip2;1 pip2;2* double mutant due to the loss-of-function of these two major isoforms.

As a conclusion of this work, we find that PIP1s are distinctly regulated in the absence of certain PIP2 isoforms (PIP2;1 and PIP2;2), both in the roots and leaves. We could prove that neither transcription nor translation of PIP1s is regulated in this situation, however, there is an indication of a so far not yet unravelled degradation process. In our view, it is important to further investigate, whether this kind of specific regulation might also play a role in specific instances in the wild type background when PIP2;1 and/ PIP2;2 are downregulated. e.g. in guard cells or vascular tissue during plant growth or stress situations.

4. MATERIALS AND METHODS

4.1. Materials

4.1.1. Plant materials

Wild-type plants and insertion lines used in this study are *Arabidopsis thaliana* ecotype Columbia (Col-0). Most of the seeds were obtained from the Nottingham *Arabidopsis* Stock Center (NASC) or from the *Arabidopsis* Biological Resource Center (ABRC, Ohio State University, USA). Single mutants of *pip1s* and *pip2s* used in this work were backcrossed with *Arabidopsis thaliana* ecotype Columbia (Col-0) (Table 2). Multiple mutants were generated by crossing and verified by PCR-based genotyping at the DNA level and by RT-PCR at the RNA level (Table 3). In addition, the seeds of *pip2;1-2* complemented with the *PIP2;1_{pro}:PIP2;1-mCHERRY* construct were provided by Professor Christophe Maurel (CNRS Montpellier) (Peret *et al.*, 2012). Wave lines transgenic plants used in this work were purchased from NASC (Geldner *et al.*, 2009). Transgenic complementation lines were utilized for PIP1 protein analysis. EGFP- or HA-tagged PIP1;1 or PIP1;2 transgenic lines in different mutant backgrounds were generated and used in this work (Table 4 and 5), additional transgenic lines generated in this work are listed in Table 6 and 7, respectively. Transgenic hybrid-lines (*PIP2;2_{pro}:PIP2;3:tPIP2;2*) in different mutant backgrounds were generated and used in this work (Table 8). Transgenic estradiol-inducible lines (*G10-90_{pro}:PIP2;2-cDNA*) were generated in this work (Table 8). Transgenic lines inserted with *PIP2;2_{pro}:HF-RPL18* constructs were screened and employed for translome analysis (Table 9) (4.2.3.11). The vectors used for generating these transgenic lines are listed in 4.1.2, the constructs generated in this work are depicted in 4.2.3.4, production of these transgenic lines is described in 4.2.1.7.

Table 7. List of transgenic lines of tagged-PIP1;1 generated in this work.

Construct	Mutant background
<i>PIP1;1_{pro}:EGFP-PIP1;1:tPIP1;1</i>	<i>pip1;1-1</i> (2/13/5)
	<i>pip1;1-1</i> (2/9/3)
	<i>pip1;1-1</i> (2/4/1)
	<i>pip1;1-1 pip2;2-4</i> (6/11/6)
	<i>pip1;1-1 pip2;2-4</i> (6/3/5)
	<i>pip1;1-1 pip2;2-4</i> (6/6/7)
	<i>pip1;1-1 pip2;1-2 pip2;2-3</i> (10/2/5)
	<i>pip1;1-1 pip2;1-2 pip2;2-3</i> (10/7/6)
	<i>pip1;1-1 pip2;1-2 pip2;2-3</i> (10/9/4)
<i>PIP1;1_{pro}:PIP1;1-EGFP:tPIP1;1</i>	<i>pip1;1-1</i> (4/3/2)
	<i>pip1;1-1</i> (4/7/5)
	<i>pip1;1-1</i> (4/11/7)
	<i>pip1;1-1 pip2;2-4</i> (8/14/8)
	<i>pip1;1-1 pip2;2-4</i> (8/8/5)
	<i>pip1;1-1 pip2;2-4</i> (8/6/7)
	<i>pip1;1-1 pip2;1-2 pip2;2-3</i> (12/1/1)
	<i>pip1;1-1 pip2;1-2 pip2;2-3</i> (12/4/8)
	<i>pip1;1-1 pip2;1-2 pip2;2-3</i> (12/10/6)
<i>PIP1;1_{pro}:HA-PIP1;1:tPIP1;1</i>	<i>pip1;1-1</i> (1/7/4)
	<i>pip1;1-1</i> (1/19/5)
	<i>pip1;1-1</i> (1/4/1)
	<i>pip1;1-1 pip2;2-4</i> (5/5/2)
	<i>pip1;1-1 pip2;2-4</i> (5/7/6)
	<i>pip1;1-1 pip2;2-4</i> (5/14/8)
	<i>pip1;1-1 pip2;1-2 pip2;2-3</i> (9/1/4)
	<i>pip1;1-1 pip2;1-2 pip2;2-3</i> (9/10/5)
	<i>pip1;1-1 pip2;1-2 pip2;2-3</i> (9/17/6)
<i>PIP1;1_{pro}:PIP1;1-HA:tPIP1;1</i>	<i>pip1;1-1</i> (3/17/4)
	<i>pip1;1-1</i> (3/8/3)
	<i>pip1;1-1</i> (3/16/4)
	<i>pip1;1-1 pip2;2-4</i> (7/14/4)
	<i>pip1;1-1 pip2;2-4</i> (7/12/5)
	<i>pip1;1-1 pip2;2-4</i> (7/6/4)
	<i>pip1;1-1 pip2;1-2 pip2;2-3</i> (11/1/7)
	<i>pip1;1-1 pip2;1-2 pip2;2-3</i> (11/6/2)
	<i>pip1;1-1 pip2;1-2 pip2;2-3</i> (11/4/6)

The number behind each transgenic line represents information documented in this work. For instance, 2/13/5: 2 indicates that the *pip1;1-1* mutant is inserted with the *PIP1;1_{pro}:EGFP-PIP1;1:tPIP1;1* construct, 13 represents the single insertion transgenic line

MATERIALS AND METHODS

after selection (ratio 3:1, see 4.2.1.7), 5 indicates the homozygous line obtained from T3 generation selection. For one transformation, two to three independent single insertion transgenic lines were selected. This nomenclature also was applied in the tables below.

Table 8. List of transgenic lines of tagged-PIP1;2 generated in this work.

Construct	Mutant background
<i>PIP1;2_{pro}:EGFP-PIP1;2:tPIP1;2</i>	<i>pip1;2-2</i> (2/2/7)
	<i>pip1;2-2</i> (2/5/3)
	<i>pip1;2-2</i> (2/1/4)
	<i>pip1;2-1 pip2;2-3</i> (6/12/4)
	<i>pip1;2-1 pip2;2-3</i> (6/15/3)
	<i>pip1;2-1 pip2;2-3</i> (6/9/6)
	<i>pip1;2-2 pip2;1-2 pip2;2-3</i> (10/8/7)
	<i>pip1;2-2 pip2;1-2 pip2;2-3</i> (10/2/4)
	<i>pip1;2-2 pip2;1-2 pip2;2-3</i> (10/7/7)
<i>PIP1;2_{pro}:PIP1;2-EGFP:tPIP1;2</i>	<i>pip1;2-2</i> (4/9/4)
	<i>pip1;2-2</i> (4/13/3)
	<i>pip1;2-2</i> (4/17/5)
	<i>pip1;2-1 pip2;2-3</i> (8/8/7)
	<i>pip1;2-1 pip2;2-3</i> (8/4/7)
	<i>pip1;2-1 pip2;2-3</i> (8/9/2)
	<i>pip1;2-2 pip2;1-2 pip2;2-3</i> (12/1/7)
	<i>pip1;2-2 pip2;1-2 pip2;2-3</i> (12/10/6)
	<i>pip1;2-2 pip2;1-2 pip2;2-3</i> (12/11/1)
<i>PIP1;2_{pro}:HA-PIP1;2:tPIP1;2</i>	<i>pip1;2-2</i> (1/4/1)
	<i>pip1;2-2</i> (1/5/3)
	<i>pip1;2-2</i> (1/8/6)
	<i>pip1;2-1 pip2;2-3</i> (5/5/5)
	<i>pip1;2-1 pip2;2-3</i> (5/6/2)
	<i>pip1;2-1 pip2;2-3</i> (5/4/5)
	<i>pip1;2-2 pip2;1-2 pip2;2-3</i> (9/1/4)
	<i>pip1;2-2 pip2;1-2 pip2;2-3</i> (9/11/4)
	<i>pip1;2-2 pip2;1-2 pip2;2-3</i> (9/15/8)
<i>PIP1;2_{pro}:PIP1;2-HA:tPIP1;2</i>	<i>pip1;2-2</i> (3/12/2)
	<i>pip1;2-2</i> (3/6/6)
	<i>pip1;2-2</i> (3/1/1)
	<i>pip1;2-1 pip2;2-3</i> (7/3/3)
	<i>pip1;2-1 pip2;2-3</i> (7/14/3)
	<i>pip1;2-1 pip2;2-3</i> (7/7/5)
	<i>pip1;2-2 pip2;1-2 pip2;2-3</i> (11/6/4)
	<i>pip1;2-2 pip2;1-2 pip2;2-3</i> (11/11/6)
	<i>pip1;2-2 pip2;1-2 pip2;2-3</i> (11/13/3)

Table 9. List of transgenic lines of hybrid-lines and inducible-lines in different mutant backgrounds generated in this work.

Construct	Mutant background
<i>PIP2;2_{pro}:PIP2;3:tPIP2;2</i>	<i>pip2;2-3</i> (1/17/1)
	<i>pip2;2-3</i> (1/11/6)
	<i>pip2;2-3</i> (1/2/4)
	<i>pip2;2-4</i> (2/15/5)
	<i>pip2;2-4</i> (2/8/2)
	<i>pip2;2-4</i> (2/6/1)
	<i>pip2;1-2 pip2;2-3</i> (3/10/1)
	<i>pip2;1-2 pip2;2-3</i> (3/13/1)
	<i>pip2;1-2 pip2;2-3</i> (3/18/3)
<i>G10-90_{pro}:PIP2;2-cDNA</i>	<i>pip2;2-3</i> (1/8/1)
	<i>pip2;2-3</i> (1/7/2)
	<i>pip2;2-3</i> (1/19/5)
	<i>pip2;2-4</i> (2/16/3)
	<i>pip2;2-4</i> (2/15/6)
	<i>pip2;2-4</i> (2/11/2)
	<i>pip2;1-2 pip2;2-3</i> (3/11/3)
	<i>pip2;1-2 pip2;2-3</i> (3/20/5)
	<i>pip2;1-2 pip2;2-3</i> (3/2/1)

Table 10. List of transgenic lines selected and used for translatoome analysis.

Construct	Mutant background
<i>PIP2;2_{pro}:HF-GFP-RPL18</i>	Col-0 (1/5/4)
	Col-0 (1/6/3)
	Col-0 (1/16/6)
	<i>pip2;2-3</i> (2/3/1)
	<i>pip2;2-3</i> (2/5/3)
	<i>pip2;2-3</i> (2/7/1)
	<i>pip2;1-2 pip2;2-3</i> (3/4/1)
	<i>pip2;1-2 pip2;2-3</i> (3/5/2)
	<i>pip2;1-2 pip2;2-3</i> (3/3/1)
<i>PIP2;2_{pro}:HF -RPL18</i>	Col-0 (4/6/2)
	Col-0 (4/5/9)
	Col-0 (4/8/3)
	<i>pip2;2-3</i> (5/2/4)
	<i>pip2;2-3</i> (5/8/6)
	<i>pip2;2-3</i> (5/3)
	<i>pip2;1-2 pip2;2-3</i> (6/5/4)
	<i>pip2;1-2 pip2;2-3</i> (6/11/7)
	<i>pip2;1-2 pip2;2-3</i> (6/12/1)

4.1.2. Vectors

Table 11. Vectors

Name	Application	Source	Reference
pDONR221 TM	Gateway TM	Gent	
pDONRP4P1R TM	cloning, Donor vector	University, Belgium	
pEN-R2-3XHA-L3	3XHA fragment cloning	Gent University, Belgium	(Van Leene <i>et al.</i> , 2007)
pBGWFS7	EGFP fragment cloning	Gent University, Belgium	(Karimi <i>et al.</i> , 2002)
pAlligator2	At2S3pro:GFP fragment cloning	Francois Parcy, France	(Bensmihen <i>et al.</i> , 2004)
pm42GW7,3	High copy number vector	Gent University, Belgium	(Karimi <i>et al.</i> , 2007b)
pBS-2x35s-HA-GW	High copy number vector	pBS-KS& pAlligator2	(Geist and Schäffner ,unpublished)
pKGW	Gateway TM cloning, binary vector	Gent University, Belgium	(Karimi <i>et al.</i> , 2002)
pHm42GW	MultiSite Gateway vectors, binary vector	Gent University, Belgium	(Karimi <i>et al.</i> , 2007b)
pPm42GW	MultiSite Gateway vectors, binary vector	Gent University, Belgium	(Karimi <i>et al.</i> , 2007b)
pER8-GW-3XHA	estradiol- inducible binary vector	Jaqueline Bautor, Germany	(Zuo <i>et al.</i> , 2000)

4.1.3. Plasmids

Table 12. Plasmids generated in this work.

Construct	Destination vector
<i>PIP1;1_{pro}:HA-PIP1;1:tPIP1;1</i>	pm42GW7,3
<i>35S_{pro}:HA-PIP1;1:tPIP1;1</i>	
<i>PIP1;1_{pro}:EGFP-PIP1;1:tPIP1;1</i>	pHm42GW3
<i>35S_{pro}:EGFP-PIP1;1:tPIP1;1</i>	
<i>PIP1;1_{pro}:PIP1;1-HA:tPIP1;1</i>	pPm42GW3-At2s3pro:GFP
<i>PIP1;1_{pro}:PIP1;1-EGFP:PIP1;1</i>	
<i>35S_{pro}:PIP1;1-HA:tPIP1;1</i>	
<i>35S_{pro}:EGFP-PIP1;1:tPIP1;1</i>	
<i>PIP1;2_{pro}:HA-PIP1;2:tPIP1;2</i>	
<i>35S_{pro}:HA-PIP1;2:tPIP1;2</i>	
<i>PIP1;2_{pro}:EGFP-PIP1;2:tPIP1;2</i>	
<i>35S_{pro}:EGFP-PIP1;2:tPIP1;2</i>	
<i>PIP1;2_{pro}:PIP1;2-HA:tPIP1;2</i>	
<i>PIP1;2_{pro}:PIP1;2-EGFP:tPIP1;2</i>	
<i>35S_{pro}:PIP1;2-HA:tPIP1;2</i>	
<i>35S_{pro}:EGFP-PIP1;2:tPIP1;2</i>	
<i>PIP2;1-cDNA</i>	pBS-2x35s-HA-GW
<i>PIP2;2-cDNA</i>	
<i>PIP2;3-cDNA</i>	

4.1.4. Bacterial strains

Table 13. Bacterial strains.

Species	Strain
<i>Escherichia coli</i>	DH-5 α
	DB-3.1
<i>Agrobacterium tumefaciens</i>	GV3101 (pMP90)

4.1.5. Antibiotics

Table 14. Antibiotics.

Name	Source	Stock solution (mg / mL)	Working concentration (μ g / mL)
Ampicillin	Roche, Mannheim (Germany)	100	100
Kanamycin	Sigma, Deisenhofen (Germany)	50	50
Gentamicin	Roche, Mannheim (Germany)	50	25
Spectinomycin	Sigma, Deisenhofen (Germany)	10	100
Rifampicin	Sigma, Deisenhofen (Germany)	10	100
Hygromycin B	Sigma, Deisenhofen (Germany)	15	15

All stock solutions were dissolved in water except rifampicin which was dissolved in methanol and kept at -20°C.

4.1.6. Chemicals

All commonly used media chemicals utilized in this study were of molecular biology grade and purchased from commercial sources: Amersham Pharmacia (Freiburg), Bio-Rad Lab GmbH (München), Gibco-BRL (Eggenstein), Merck (Darmstadt), Roche (Mannheim), Roth (Karlsruhe), Serva (Heidelberg) and Sigma (Deisenhofen). Detergent Silwet L-77 was purchased from Lehle Seeds (Round Rock, Texas, USA). PCR purification kits, agarose gel extraction and plasmid isolation kits used in this work were obtained from Qiagen (Hilden) or Amersham Pharmacia (Freiburg). Special chemicals are listed in the corresponding methods below.

4.1.7. Medium and solutions

Common media, buffers and solutions were prepared according to the recipe and information obtained from the laboratory manual *Current Protocols in Molecular Biology* (Ausubel *et al.*, 1987 with quarterly updates). Special media and solutions are listed in the corresponding methods below.

Table 15. Chemicals

Name	Source	Stock solution (mg/mL)	Working concentration (µg/mL)
MG132	Sigma, Deisenhofen (Germany)	100	50
Cycloheximide	Sigma, Deisenhofen (Germany)	100	100
Brefeldin A	VWR/ Applichem (Germany)	50	25
Wortmannin	Biomol, Adipogen (Germany)	33	33

All stock solutions were prepared in DMSO except for cycloheximide, which was dissolved in water and kept at -20°C.

4.1.8. Oligonucleotide primers

Table 16. The primers used for the characterization of mutants.

Name	Sequence
AtTUB9 f	<i>gtacctgaagcttgctaataccta</i>
AtTUB9 r	<i>gttctggacggtcatcatctgttc</i>
AtPIP1;1f	<i>cagagctttacaatttctctctaca</i>
AtPIP1;1r	<i>cacagtgttagctcctcctcct</i>
AtPIP1;2f	<i>ctggtttctccgatctaacga</i>
AtPIP1;2r	<i>gcattttgatccgatgttataa</i>
AtPIP1;3f	<i>aattggcttttgttgcatgc</i>
AtPIP1;3r	<i>taacgtggcccataaagagtg</i>
AtPIP1;4f	<i>ttgttgattcaattcggttctgt</i>
AtPIP1;4r	<i>ctcagctattccggctctgt</i>
LBa1 mod	<i>ggttcacgtagtgggcatc</i>
GABI_LB2	<i>ccatttgacgtgaatgtagacac</i>
SAIL_L	<i>ttcataaccaatctcgatacac</i>

Table 17. The primer sequences of reference genes used for RT-qPCR.

Gene	Name	Sequence	Reference
<i>UBIQUITIN5</i> (At3g62250)	AtUBQ5qRT_f	<i>gtaccttgaagcttgctaataccta</i>	
	AtUBQ5qRT_r	<i>gttctggacgttcatcatctgttc</i>	
<i>S16</i> (At5g18380)	AtS16qRT_f	<i>tttacgccatccgtcagagtat</i>	
	AtS16qRT_r	<i>tctggtaacgagaacgagcac</i>	
<i>TUBULIN9</i> (At4g20890)	AtTUB9 qRT_f	<i>gtaccttgaagcttgctaataccta</i>	
	AtTUB9 qRT_r	<i>gtcaaagggtgcaaaaccaac</i>	
<i>AtPIP1;1</i> (At3g61430)	AtPIP1;1qRT_f	<i>ctggccttgtccttagttgcttc</i>	(Postaire et al., 2010)
	AtPIP1;1qRT_r	<i>tctcctttggaacttcttccttg</i>	
<i>AtPIP1;2</i> (At2G45960)	AtPIP1;2qRT_f	<i>tctcttctttgcctaattggagac</i>	
	AtPIP1;2qRT_r	<i>agttgcctgcttgagataaac</i>	
<i>AtPIP1;3</i> (At1G01620)	AtPIP1;3qRT_f	<i>gctgtggatgatctggttttatcg</i>	
	AtPIP1;3qRT_r	<i>gccgaaacaatatggatcttactc</i>	
<i>AtPIP1;4</i> (At4G00430)	AtPIP1;4qRT_f	<i>ctctgaagtctaagggtgattagtg</i>	
	AtPIP1;4qRT_r	<i>caacccgagaacttgatgttga</i>	
<i>AtPIP1;5</i> (At4G23400)	AtPIP1;5qRT_f	<i>gtttcctatgtcatgtgtgatg</i>	
	AtPIP1;5qRT_r	<i>gtacacaatgtattcttcattgac</i>	

Table 18. The primers used for the production of transgenic lines using Gateway™ recombination

Name	Sequence
PIP1;1_Pro_GW_B4_F	<i>ggggacaactttgatagaaaagttgaaagcatggtaaaattgggtg</i>
PIP1;1_Pro_GW_B1R_R	<i>ggggactgctttttgtacaaaacttgatcttcgatctctgtagagagaaaat</i>
EGFP_GW_B1_f	<i>ggggacaagttttgtacaaaaaagcaggctatggtgagcaagggcg</i>
EGFP_PIP1;1_ORF_Hy_R	<i>gtcttctccttgccctccatagcgcccttgacagctcgtccatg</i>
EGFP_PIP1;1_ORF_Hy_F	<i>catggacgagctgtacaagggcgctatggaaggcaaggaagaagac</i>
PIP1;1_TER_GW_B2_R	<i>ggggaccactttgtacaagaagctgggtctcgtggaatgatcaactt</i>
HA_ATG_GW_B1_F	<i>ggggacaagttttgtacaaaaaagcaggctatggcatacccttacgatg</i>
HA_PIP1;1_ORF_Hy_R	<i>gtcttctccttgccctccatagcgccagcgtaatctggaacgtcg</i>
HA_PIP1;1_ORF_Hy_F	<i>cgacgttccagattacgctggcgctatggaaggcaaggaagaag</i>
EGFP_PIP1;2_ORF_Hy_R	<i>acatcttctctttaccttccatagcgcccttgacagctcgtccatg</i>
EGFP_PIP1;2_ORF_Hy_F	<i>catggacgagctgtacaagggcgctatggaaggtaagaagaagaatgt</i>
PIP1;2_Pro_GW_B4_F	<i>ggggacaactttgatagaaaagttgtcgaatcttctcatttgaa</i>
PIP1;2_Pro_GW_B1R_R	<i>ggggactgctttttgtacaaaacttgctctctctcttctctcttagagc</i>
HA_PIP1;2_ORF_Hy_R	<i>acatcttctctttaccttccatagcgccagcgtaatctggaacgtcg</i>
HA_PIP1;2_ORF_Hy_F	<i>cgacgttccagattacgctggcgctatggaaggtaagaagaagaatgt</i>
PIP1;2_TER_GW_B2_R	<i>ggggaccactttgtacaagaagctgggtatgccttggaattcagaca</i>
PIP1;1_ORF_EGFP_Hy_F	<i>tcccctcaagtccagaagcggcgctatggtgagcaagggcg</i>

PIP1:1_ORF_EGFP_Hy_R	<i>cgcccttgctcaccatagcgccgcttctggacttgaagggga</i>
EGFP_STOP_GW_B1R_R	<i>ggggactgctttttgtacaaaactgttactgtacagctcgtccat</i>
PIP1;1_pA_GW_B1_F	<i>ggggacaagtttgtacaaaaaagcaggctgtaaaaacaagacatcaagtcc</i> <i>tc</i>
PIP1:1_ORF_HA_Hy_R	<i>tcaggaacatcgtaagggttaagcgccgcttctggacttgaaggg</i>
PIP1:1_ORF_HA_Hy_F	<i>cccttcaagtccagaagcggcgcttacccttacgatgttcctga</i>
HA_STOP_GW_B1R_R	<i>ggggactgctttttgtacaaaactgttaagcgtaatctggaacgt</i>
PIP1;2_ORF_HA_Hy_R	<i>tcaggaacatcgtaagggttaagcgccagaacaaaagccagattttaa</i>
PIP1;2_ORF_HA_Hy_F	<i>attttaaactctggcttttctggcgcttacccttacgatgttcctga</i>
PIP1;2_pA_GW_B1_F	<i>ggggacaagtttgtacaaaaaagcaggcttttctttctttgtgaatctacta</i>
PIP1:2_ORF_EGFP_Hy_R	<i>cgcccttgctcaccatagcgccgagaacaaaagccagattttaa</i>
PIP1;2_ORF_EGFP_Hy_F	<i>attttaaactctggcttttctggcgctatggtgagcaagggcg</i>
35S_Pro_GW_B4_F	<i>ggggacaactttgtatagaaaagttgatttaggtgacactatagaataactcaag</i>
PIP1:1_ORF_35S_Hy_R	<i>gtcttcttcttgccttccatcgactagaatagtaaattgtaattgtt</i>
PIP1:1_ORF_35S_Hy_F	<i>caacattacaatttactattctagtcgatggaaggcaaggaagaagac</i>
PIP1:2_ORF_35S_Hy_R	<i>acatcttcttcttacccttccatcgactagaatagtaaattgtaattgtt</i>
PIP1:2_ORF_35S_Hy_F	<i>caacattacaatttactattctagtcgatggaaggtaaagaagaagatgt</i>
At2S3_GFP_pA_Sac_f	<i>ggttgagctcgcccttgaaccaa</i>
At2S3_GFP_pA_Sac_r	<i>ccccgagctccactggatttttgg</i>

Table 19. The primers used for the production of PIP2;1/PIP2;2-cDNA constructs using Gateway™ recombination.

Gene	Name	Sequence
<i>AtPIP2;1</i> (At3g53420)	AtPIP2;1_f	<i>ggggacaagtttgtacaaaaaagcaggctccatggcaaaggatgtgg</i> <i>aagc</i>
	AtPIP2;1_r	<i>ggggaccactttgtacaagaagctgggttagacggtggcagcacttc</i>
<i>AtPIP2;2</i> (At2g37170)	AtPIP2;2_f	<i>ggggacaagtttgtacaaaaaagcaggctccatggcceaagacgtgg</i> <i>aag</i>
	AtPIP2;2_r	<i>ggggaccactttgtacaagaagctgggttcaaacggtggctgcac</i>

All primers were obtained from Thermo Electron (Ulm, Germany). Stock solutions were prepared at 200 µM and stored at -20°C. Primer sequences are given from 5' to 3'.

4.2. Methods

4.2.1. Plant methods

4.2.1.1. Growth conditions

Plants were grown on half strength MS (Murashige and Skoog) plate under the 16 h light / 8 h dark cycle at $200 \mu\text{E m}^{-2} \text{ s}^{-1}$ light intensity at 22°C and 60% relative humidity for 7-day-old root confocal observation and 14-day-old plant materials prepared for microsomal membrane fractions isolation. Plants were grown on soil under a 10 h light / 14 h dark cycle at $200 \mu\text{E m}^{-2} \text{ s}^{-1}$ light intensity at 22°C and 60% relative humidity for RT-qPCR analysis, tranlatome analysis, protein analysis, protoplasts isolation and stable transformation. Plants were grown in hydroponic culture under a 10 h light / 14 h cycle at $200 \mu\text{E m}^{-2} \text{ s}^{-1}$ light intensity at 20°C and 70% relative humidity for 35-day-old plant materials used for microsomal membrane fractions isolation.

4.2.1.2. Plant growth on soil

Soil (Floragard) was mixed with silica sand in a ratio of 5:1 and poured in 6-well pots aligned in the trays for normal plant growth. After the soil-sand mixture was wetted with water, seeds were placed with a toothpick on the surface of wet soil and stratified for 2 days at 4°C before transfer into the plant chamber.

4.2.1.3. Seed surface sterilization

Seeds were dropped within 80% (v/v) ethanol on filter paper in sterile Petri dishes and dried under a sterile hood. This procedure was repeated once for seed surface sterilization.

4.2.1.4. Sterile culture on solid medium

Surface-sterilized seeds were placed with a sterile toothpick on squared Petri dishes (120 mm x 120 mm x 17 mm Greiner bio-one Germany) containing 75 mL half strength MS medium (1% sucrose, 0.5% (w/v) Gelrite). Plates were then sealed with

parafilm and kept for 2 days at 4°C for stratification before being transferred to a plant chamber in a vertical orientation.

4.2.1.5. Plant growth in hydroponic culture

For analysis of both rosettes and root materials, surface-sterilized seeds were placed with a sterile toothpick on agar-filled black microcentrifuge lids with germination medium (GM) and kept for 2 days at 4°C for stratification as indicated (Conn *et al.*, 2013). Seedlings were transplanted after 7 days into a hydroponic system and further grown for 28 days in grey boxes containing the hydroponic medium as described (Da Ines *et al.*, 2010).

4.2.1.6. Generation of double/triple/quadruple mutants and backcrossing of single mutants

For the new multiple mutants, individual mutant lines grown on soil until the stage of developing 5-6 inflorescences were used for crossing (Table 2). All the immature anthers around stigmata of the recipient flowers (ovaries) were removed completely to avoid self-fertilization. The pollen obtained from mature flowers of donor plants was transferred to the stigmata of the emasculated plants by dabbing. This step was repeated at least twice to ensure proper pollination. T-DNA insertion lines (see 2.2.1 for more information) were backcrossed three or four times with the wild-type line (Col-0) using the same method as described above. When several crosses were done in a row, forceps had to be cleaned in between by washing with 80% ethanol (v/v) followed by rinsing with sterile distilled water. Each pollinated inflorescence was independently labeled, successful ovaries were allowed to develop and generate new siliques. Siliques were harvested after they had turned completely yellow, the seeds were dried and planted again for segregation to get the F2 generation. Afterwards, homozygous plants were selected by genotyping-PCR (see 4.2.3.2) using the same primers used for amplification of the mutant allele and by the absence of amplification of the wild-type allele using gene specific primers (Table 16). Lack of the functional transcript in those multiple lines and single mutant

lines was confirmed by RT-PCR (see 4.2.3.12) using the same gene specific primers.

4.2.1.7. Production and/or characterization of transgenic lines

The constructs for PIP1 isoforms were generated using a PCR-based joining of fragments method (4.2.3.2) and a GATEWAY™ two-fragment vector recombination cloning system (Invitrogen, Germany) (see 2.2.4.1 for more information). The fragments of EGFP or 3xHA, endogenous promoter of *PIP1;1* or *PIP1;2* and/or genomic fragments of *PIP1;1* or *PIP1;2* were amplified by PCR using specific primers (see Table 18) with high fidelity DNA polymerase. N- or C-terminal EGFP or HA labelled genomic DNA were generated by PCR-based joining of fragments method to avoid improper protein folding (see 4.2.3.2). Fragments were first cloned into the pDONRP4P1R and pDONR221 vectors accordingly, and then transformed into *E. coli* DH5 α (see 4.2.2.2). After verification by sequencing (4.2.3.9), the fragment was further recombined and cloned into the destination vector pPm42GW inserted with seed coat specifically expressed GFP (*At2S3_{pro}:GFP* fragment cloned from pAlligator2) and transformed into *Agrobacterium tumefaciens* (see 4.2.2.5). The *Agrobacterium tumefaciens*-mediated transformation into several different mutants (Table 6 and 7) was performed using the floral dip method (Clough and Bent, 1998). Selection was carried out by a visible marker using seed coat specifically expressed GFP. After selection of transformants, segregation analysis was used for identification of single insertion lines (3:1 ratio) in the T2 generation. Three independent and homozygous single insertion lines were selected for each transformation for further molecular characterization (see Table 7 and 8). Constructs used for translome analysis were generated by Birgit Geist (Helmholtz Zentrum München) and transformants were selected due to their resistance to kanamycin in this work (see Table 9). Transgenic hybrid-lines and estradiol-inducible lines were generated in this work by their resistance to kanamycin and hygromycin B as indicated (Harrison *et al.*, 2006), respectively (see 4.2.3.4).

4.2.1.8. Seed harvesting and storage

Seeds of different mutant lines and transgenic lines were harvested into individual paper packets and dried for one week in a desiccator before being stored at room temperature.

4.2.2. Microbiological methods

4.2.2.1. Competent cells of *E. coli*

A single colony of *E. coli* DH5 α and *E. coli* DB3.1, respectively, were inoculated into Lysogeny broth (LB) medium and cultivated overnight at 37°C with agitation at a speed of 200 rpm to be further used to produce competent cells. The overnight-culture was then subcultured in 250 mL LB medium containing 20 mM MgSO₄. The cells were grown to an OD₅₉₅ of 0.4-0.6, and were then collected by centrifugation at 4°C and at 5,000 rpm for 5 min. The supernatants were discarded and the bacterial pellets resuspended carefully in 100 mL of ice-cold TFB1 and kept on ice for 5 min. The bacterial suspensions were then centrifuged at 4°C and at 5,000 rpm for 5 min. The new pellets were resuspended gently in 10 mL cold TFB2 and incubated on ice for 30 min. The 60 μ L bacterial suspensions were aliquoted in ice-cold Eppendorf tubes, frozen in liquid nitrogen and stored at -80°C.

Solution	Concentration	Component
TBF1	30 mM	KOAc (potassium acetate)
	100 mM	RbCl
	10 mM	CaCl ₂
	50 mM	MnCl ₂
	15 %	Glycerol
		pH adjusted to 5.8 with acetic acid
TBF2	10 mM	MOPS
	75 mM	CaCl ₂
	10 mM	RbCl
	15 %	glycerol
		pH adjusted to 6.5 with KOH

Both solutions were filter sterilized using 0.45 μ m filter (Millipore Germany).

4.2.2.2. Heat shock transformation of *E. coli*

An aliquot of competent *E. coli* cells (DH5 α or DB3.1) was thawed on ice, mixed with approximately 100-200 ng plasmid DNA (1-2 μ L), incubated for 20 min on ice and then transferred in a 42°C water bath for 45 sec incubation and subsequently cooled on ice for 2 min. After addition of 950 mL normal LB medium, cells were incubated 1 h at 37°C with gentle agitation. Cells were then centrifuged at 5,000 rpm for 2 min at room temperature. The pellets were resuspended with 50-80 μ L LB medium and plated on the selective LB medium containing corresponding antibiotics.

4.2.2.3. Competent cells of *Agrobacterium tumefaciens*

A single colony *Agrobacterium tumefaciens* (GV3101) was inoculated into Lysogeny broth (LB) medium and cultivated overnight at 28°C at a speed of 200 rpm to be further used to produce competent cells. The overnight-culture was then subcultured in 300 mL LB medium containing appropriate antibiotics. The cells were grown at 28°C until an OD₆₀₀ of 0.5-0.7. Then the cells were incubated on ice for 30 min and collected by centrifugation at 4°C and at 400 rpm for 20 min. The supernatant was discarded and the pellet was resuspended in 125 mL ice cold water and then incubated on ice for 30 min. The resuspension and centrifugation procedures were repeated with a subsequent incubation on ice for 60 min. After another centrifugation, the pellet was resuspended in 3 mL of ice-cold glycerol (15%), aliquoted in 50 μ L portions, immediately frozen in liquid nitrogen and stored at -80°C.

4.2.2.4. Electroporation of competent *Agrobacterium tumefaciens* cells

An aliquot of electrocompetent cells of *Agrobacterium tumefaciens* GV3101 containing an appropriate helper Ti plasmid (pMP90) was thawed on ice and mixed with approximately 100 ng (1 μ L) of plasmid DNA for electroporation. The mixture was then transferred to a dry, pre-chilled 0.1 cm electroporation cuvette. Electroporation was performed with the BioRad Gene-Pulser using the following

conditions: Capacitance 25 μ F, Voltage 1.25 kV and Resistance 400 Ω . After an electroporation, 1 mL of LB medium (without antibiotics) was immediately added to the cuvette, and the bacterial was gently resuspended and transferred to a 1.5 mL Eppendorf tube. The culture was incubated for 2 h at 28°C with gentle agitation. The cells were collected by centrifugation at 5000 rpm for 2 min, the pellet was resuspended in 50-80 μ L LB medium and plated on the selective LB medium (Rifampicin and gentamicin for agrobacteria and appropriate antibiotic for T-DNA vector) and incubated at 28°C for 2 days.

4.2.2.5. *Agrobacterium tumefaciens* mediated plant transformation

The transformation of *Arabidopsis thaliana* was carried out by the floral dip procedure (Clough and Bent, 1998). *Arabidopsis* plants were grown in a short day light period (10 h, 22°C) in big pots to the flowering stage. Siliques of plants were removed before transformation in order to increase the transformation rate. A single colony of *Agrobacterium tumefaciens* strain GV3101 containing a construct of interest was used for a 2 mL preculture with appropriate antibiotics (overnight, 28°C, 200 rpm). 250 mL of LB medium were inoculated with 1 mL of the preculture and grown overnight (200 rpm) until stationary phase (OD_{600} 1.5-1.6). Cells were collected by centrifugation at 4°C, 5,500 $\times g$ for 10 min and the pellet was resuspended in 5% (w/v) sucrose solution to a final OD_{600} of approximately 0.8. Silwet L-77 was freshly added to the suspension to a final concentration of 0.05%. Inflorescence shoots from 10-15 *Arabidopsis* plants, were dipped into the suspension and soaked for 45 sec. Dipped plants were then covered with a transparent plastic bag to maintain the humidity and kept in a low light intensity location for 24 h. The plastic cover was then removed and the plants were subjected to normal growth conditions. After about 4-5 weeks seeds were harvested when the siliques had turned yellow and dry. The first-generation seeds (T0) were collected and transformants were selected either by visible markers using seed coat specifically expressed GFP (*At2S3_{pro}:GFP*) or hygromycin B (pER8-GW-3XHA) or

kanamycin (pKGW) resistance 1-2 weeks after sowing on half strength MS medium with appropriate antibiotics.

4.2.2.6. Miniprep plasmid DNA preparation

Plasmid DNA from *E. coli* or *Agrobacterium tumefaciens* was isolated with Qiaprep[®] Spin Miniprep Kit (Qiagen, Hilden, Germany), following the manufacturer's instructions. This procedure is based on alkaline lysis of bacterial cells followed by adsorption of the DNA onto a silica membrane in the presence of high salt-binding conditions.

4.2.2.7. Midiprep plasmid DNA preparation

Plasmid DNA from *E. coli* was isolated with Qiaprep[®] Spin Midiprep Kit (Qiagen, Hilden, Germany), following the manufacturer's instructions. This procedure is based on alkaline lysis of bacterial cells followed by adsorption of the DNA onto a silica membrane in the presence of high salt-binding conditions.

4.2.3. Molecular biology methods

4.2.3.1. PCR (Polymerase Chain Reaction)

To amplify short DNA sequences (approximately 300 bp to 5 kb) from a double stranded DNA template, polymerase chain reaction (PCR) was performed by repeated cycles of denaturation, primer annealing and elongation. The temperatures of annealing and the length of elongation steps depend on the melting temperature of primers and the size of the interested DNA fragment. The elongation in vitro was catalysed by Taq DNA Polymerase (6805-P) from Agrobiogen GmbH (Germany) or the Polymerase Phusion[®] (M0530L) from Thermo Fisher Scientific (Germany) to decrease the mismatch rate. The systems for both polymerases were employed as follows:

The PCR mixture for AgrobioGen Taq polymerase (20 μ L reaction volume):

Component	Concentration	Volume (μ L)
Template DNA	~2 ng - 20 ng	1-2
10x reaction buffer	1x	2
2 mM MgCl ₂	0.12 mM	1.2
10 μ M Forward Primer	0.5 μ M	1
10 μ M Reverse Primer	0.5 μ M	1
10 mM dNTPs	200 μ M	0.4
AgrobioGen Taq	0.5 units	0.1
Sterile ddH ₂ O		Up to volume of 20 μ L

The PCR mixture for Phusion PCR (20 μ L reaction volume):

Component	Concentration	Volume (μ L)
Template DNA	~2 ng - 20 ng	1-2
5x Phusion HF buffer	1x	4
10 μ M Forward Primer	0.5 μ M	1
10 μ M Reverse Primer	0.5 μ M	1
10 mM dNTPs	200 μ M	0.4
Phusion HF Polymerase	0.4 units	0.2
Sterile ddH ₂ O		Up to volume of 20 μ L

PCR reaction was carried out using an automated Multicycler PTC-500 (Biozym, Germany) with the following standard program (with some adjustments for optimizing each reaction according to different properties):

Step	Temperature	Time
1	95°C	5 min
2	95°C (denaturation)	20 sec
3	X°C (annealing)	30 sec
4	72°C (extension)	1min / 1kb
5	Step 2 to step 4, 34 cycles	
6	72°C	10 min
7	8°C	∞

4.2.3.2. PCR-based joining of fragments

PCR-based joining of fragments was performed to fuse the epitope tag (EGFP or HA) protein to the N- or C-terminal of the gene of interest (*PIP1;1* and *PIP1;2*) in order to avoid the influence of the extra amino acids linker encoded by the att

recombination sites of the Gateway system. Primer pairs were specifically designed for generating the gene of interest and the epitope tag with the approximately 50-100bp overlapped region by PCR (Table 18). After obtaining the two fragments, another PCR was carried out using these two fragments as templates to get a complete long fragment linking the epitope tag with the gene of interest together within two amino acid (Glycine and Alanine).

4.2.3.3. PCR-based genotyping

To identify or verify the homozygous mutants by PCR-based genotyping with specific primer pairs, an Extract-N-Amp™ plant PCR kit (sigma, Germany) was employed following the manufacturer's instructions.

4.2.3.4. Molecular cloning using single fragment or multisites two fragment Gateway™ recombination technology

The Gateway™ recombination technology was employed for cloning all constructs in this work. The cloning of the fragment of interest into the destination vector was achieved by two steps of site-specific recombination reactions, BP and LR cloning. The BP cloning is achieved with an attB-flanked DNA fragment and an attP containing donor vector and then an entry clone is generated. The LR cloning is achieved with an attL-containing entry clone and an attR-containing destination vector and then the final vector is generated.

For single fragment cloning using the Gateway™ recombination technology, the full-length cDNAs encoding *PIP2;1* and *PIP2;2* were amplified by PCR (see 4.2.3.1) from total cDNA using primers containing specific attachment sites allowing recombination reactions (Invitrogen, Germany) (Table 19). PCR fragments were recombined into a pDONR221 vector via BP cloning (Invitrogen) and further recombined into the pBS-2x35s-HA-GW destination vector (high copy number vector for transient expression) or estradiol-inducible pER8 vector (pER8-GW-3xHA, Jaqueline Bautor, Germany) (The β -Estradiol inducible vector for stable transgenic lines) via LR cloning (Invitrogen).

The multisites two fragment Gateway™ recombination technology was performed according to the following instructions. The 35S promoter or the endogenous promoter with or without specific genomic DNA (PIP1;1 or PIP1;2), the genomic DNA fragments with N or C terminal epitope EGFP or HA tags and 3' terminator of specific genes were amplified via PCR (see 4.2.3.1) (EGFP, HA fragments were cloned from the corresponding vectors [see 4.1.3]) or PCR-based joining fragments (see 4.2.3.2) accordingly with BP cloning-compatible primers from the a genomic DNA extract or plasmid DNA. These fragments were inserted into pDONR P4-P1R (Invitrogen) and pDONR 221 (Invitrogen) via BP cloning (Invitrogen), respectively (as described in Figure 16). These two vectors containing the different fragments were then recombined using the multiSite Gateway technology (Invitrogen) with the destination vectors pm42GW, pHm42GW and pPm42GW3-At2s3_{pro}:GFP (generated in this work) (Karimi *et al.*, 2005; Karimi *et al.*, 2007a) (Table 11).

4.2.3.5. DNA gel electrophoresis

Nucleic acids were separated on 0.5 to 2% agarose gels (agarose dissolved in 1x Tris-acetate-EDTA [TAE] buffer) containing 0.5 µg/mL ethidium bromide with an appropriate standard size marker (pUC 19 and λ / Hind III DNA ladders). Samples were mixed with 6x DNA loading buffer and loaded on the gels. Then gels were run in 1x TAE buffer at 5-10 V/cm for 30 min to 1 h. After electrophoresis, DNA fragments were visualized under UV light and recorded with Bio-Rad Gel Doc 2000 (Bio-Rad, Munich, Germany).

Solution	Concentration	Component
1x TAE buffer	40 mM	Tris
	5 mM	Sodium acetate
	1 mM	EDTA
		pH adjusted to 5.8 with glacial acetic acid
6 x Loading buffer	30% (v/v)	Glycerol
	0.25% (w/v)	Orange G
	1x	TAE buffer

4.2.3.6. Purification of PCR product and DNA gel extraction

Purification of DNA fragments from primers, nucleotides, polymerase and salts of previous enzymatic reactions was performed with the QIAquick[®] PCR Purification Kit (Qiagen, Hilden, Germany) following manufacturer's instructions before DNA sequencing.

To purify PCR products from the agarose gels, target DNA bands were excised from the gel with a scalpel after electrophoresis and transferred into a sterile Eppendorf tube. The extraction was carried out with the Qiaquick[®] Gel Extraction Kit (Qiagen, Hilden, Germany) following the manufacturer's manual.

4.2.3.7. Determination of nucleic acids concentration

The concentrations of DNA and RNA were determined by measuring the absorption at 260 nm and 280 nm using the Nanodrop ND-1000 spectrophotometer (Kisker-biotech, Germany). Double distilled water or corresponding buffer was used to zero the spectrophotometer and a volume of 1.5 μ L was used for each measurement. The purity of total DNA or RNA was evaluated by the ratio of A_{260}/A_{280} yielding information about the contaminants that absorb UV light (e.g. proteins absorb at 280 nm). A ratio of approximately 1.8 or 2.0 is considered to be an indication of high quality of DNA or RNA, respectively. The purity was further controlled by the ratio of A_{260}/A_{230} , which should be in the range of 2.0 to 2.2 (a lower ratio may reflect the presence of contaminants absorbing at 230 nm).

4.2.3.8. Digestion by restriction endonucleases

Plasmids were verified by restriction digests performed with restriction enzymes from New England Biolabs (Frankfurt am Main, Germany) or Fermentas (Thermo Scientific, Germany) using the appropriate buffer and temperature according to the manufacturer's recommendations. 0.5-1 μ g plasmid DNA or PCR products were digested in a mixture containing 1 x reaction buffer and 5 units of restriction endonuclease (s). The mixture was incubated at 37°C for about 2-4 h in a

thermoblock or water bath. After digestion, the enzymes were deactivated for 10 min at 65°C and fragment sizes were checked by agarose gel electrophoresis.

4.2.3.9. DNA sequencing

To assess the precise order of nucleotides within a DNA fragment, the isolated plasmid DNA (4.2.2.6) and the purified DNA sequences (4.2.3.5) were prepared according to the manufacturer's instructions and processed by Eurofins MWG GmbH (Ebersberg, Germany).

4.2.3.10. Isolation of total RNA using Qiagen RNeasy Plant Mini Kit

Total RNA was extracted using the RNeasy Plant Mini Kit (Qiagen, Hilden, Germany). Plant material was prepared with a FastPrep[®]-24 homogenisator (MP Biomedicals, Germany) and 100-120 mg were used for RNA extraction following the manufacturer's instructions. DNase treatment was performed on the column as recommended to avoid genomic DNA contamination.

4.2.3.11. Affinity isolation of ribosomes and extraction of RNA

Epitope-tagged polyribosomes (HIS-FLAG-tagged ribosomal protein L18 [HF-RPL18]) driven by PIP2;2 promoter were isolated from different transgenic lines (see Table 10) by using the translating ribosome affinity immunopurification (TRAP) method following the protocol published with small modifications (Zanetti *et al.*, 2005; Mustroph *et al.*, 2009b; Mustroph *et al.*, 2013) for translome analysis. All solutions and equipments used in this method should be free of RNase (pretreated with DEPC water and autoclaved or fresh, separate reagents). Fifteen to 25 g of 28-day-old rosettes of plants grown on soil were harvested and pulverized to a fine powder with a Mixer Mill MM400 (Retsch, Germany) in liquid nitrogen. 30-40 mL pre-cooled polysome extraction buffer (PEB) were added to the powder and left to thaw on ice for 2-5 min. The mixtures were vortexed vigorously for 5 min and incubated on ice for 10-15 min. The supernatant was collected by centrifugation at 4°C, 16,000 x g for 15 min and transferred to a new pre-cooled 50 mL Falcon tube on ice. 150 µL FLAG M₂ agarose beads (Sigma, Germany) were washed twice with

MATERIALS AND METHODS

washing buffer and then added to the supernatant for immunocapture of epitope-tagged ribosomes for 4 h at 4°C with gentle back-and-forth shaking on a rocking platform. Then beads were collected by centrifugation at 4°C, 8,200 x *g* for 3 min and subsequently resuspended in 6 mL PEB and then transferred into a new 15 mL Falcon tube. The mixture was incubated at 4°C for 5 min with gentle shaking. The beads were collected again by centrifugation at 4°C, 8,200 x *g* for 3 min and incubated with 6 mL washing buffer at 4°C for 5 min with gentle shaking. After another four washing steps, the beads were eluted with 400 µL washing buffer containing 200 ng/µL FLAG₃ peptide (Sigma, Germany) and 20 U/mL RNase inhibitor (MBI Fermentas, Germany) at 4°C for 1 h with gentle shaking. The supernatant (approximately 300 µL) was collected by centrifugation at 4°C, 13,000 x *g* for 2 min and transferred to a new 2 mL Eppendorf tube. 600 µL 8 M guanidine-HCl were added to the supernatant and vortexed for 1 min. 900 µL of 99% ethanol were added to the mixture and vortexed for 1 min. Then, the mixture was precipitated at -20°C overnight. The pellet was obtained by centrifugation at 4°C, 16,000 x *g* for 45 min and dried for 20 min. The RNA was extracted for RT-qPCR analysis using the RNeasy Plant Mini Kit (Qiagen, Hilden, Germany) from the pellet. The quality of purified RNAs was controlled using Agilent RNA 6000 Pico kit by BioanalyserTM (Agilent, Germany) following the manufacturer's instructions.

Solution	Concentration	Component
Polysome extraction buffer	200 mM	Tris (pH 9.0)
	200 mM	KCl
	25 mM	EGTA (pH8.0)
	35 mM	MgCl ₂
	1%	Detergent mix
	1%	DOC
	1%	PTE
	5 mM	DTT
	1 mM	PMSF
	50 µg/mL	Cycloheximide
	50 µg/mL	Chloramphenicol

Washing buffer	200 mM	Tris (pH 9.0)
	200 mM	KCl
	25 mM	EGTA
	35 mM	MgCl ₂
	5 mM	DTT
	1 mM	PMSF
	50 µg/mL	Cycloheximide
	50 µg/mL	Chloramphenicol
	20 U/mL	RNAse inhibitor

The buffer mentioned above should be prepared freshly and kept on ice.

4.2.3.12. Reverse Transcription Polymerase Chain Reaction (RT-PCR)

1 µg of total RNA extracted from the plant material or 100 ng RNA isolated from polyribosomes was reverse transcribed using the QuantiTect Rev Transcription Kit (Qiagen, Germany) and SuperScript II of the reverse transcription-PCR kit (Invitrogen, Germany), respectively. For each sample a negative RT reaction without enzyme (-RT) was prepared to check afterwards for contaminations with genomic DNA. The two different first strand synthesis systems were employed as followed:

The mixture system of QuantiTect Rev Transcription Kit:

Component	Concentration	Volume (µL)
Total RNA	1 µg	1-2 µL
7x gDNA wipeout buffer	1x	2
Rnase-free water		Up to volume of 14 µL
The mixture was incubated at 42°C for 2 min and immediately placed on ice		
Mixture		14
5x Quantiscript RT buffer	1x	4
RT Primer mix		1
Quantiscript-Reverse transcriptase		1
		Up to volume of 20 µL

MATERIALS AND METHODS

The cDNA was synthesized as follows in a Multicycler PTC-200 (Biozym, Germany):

Step	Temperature	Time
1	42°C	15 min
2	95°C	3 min
3	4°C	∞

The mixture system of SuperScript II (reverse transcription-PCR kit):

Component	Concentration	Volume (µL)
RNA	100 µg	10-20 µL
5 x first-strand-synthesis buffer	1x	10
dNTP Mix (MBI Fermentas)	20 mM	2.5
Oligo (dT)15 (Promega)	0.5 µM	0.85
0.1 M DTT	10 µM	5
40 U/ µL RNase Inhibitor	2 units/µL	2.5
SuperScript II	8 units/µL	2
Sterile ddH ₂ O		Up to volume of 50 µL

The cDNA was synthesized as follows in a Multicycler PTC-200 (Biozym, Germany):

Step	Temperature	Time
1	42°C	30 min
2	50°C	40 min
3	95°C	5 min
4	4°C	∞

A PCR reaction with *TUBULIN* primers (Table 16) was performed in a Multicycler PTC-200 (Biozym, Germany) using 1 µL cDNA to verify the results of RT-PCR and to monitor the -RT control for contamination with genomic DNA. PCR fragments were then separated and visualized on agarose gels (4.2.3.5). A positive band for the +RT reaction and no band in the negative control (-RT) was considered proof for a successful RNA isolation and cDNA synthesis.

4.2.3.13. Quantitative real time polymerase chain reaction (qRT-PCR)

Plant materials from different organs were harvested for the qRT-PCR analysis as indicated. Total RNA and polysome RNA were isolated as described in 4.2.3.10 and 4.2.3.11. cDNA was prepared as in 4.2.3.12 and diluted 1:15 with HPLC grade water (Merck, Germany). Primer pairs of specific and reference genes used for qRT-PCR

analysis are listed in Table 17. Real time quantification was performed using a 7500 real time PCR system (Applied Biosystems, Germany).

Individual PCR reaction mixtures were prepared as follows:

Component	Volume (μL)
Diluted cDNA	4
10 μM forward primer	0.5
10 μM reverse primer	0.5
HPLC water	5
2 x SYBR Green Mastermix (Thermo Scientific, Germany)	10
	Final volume of 20 μL

The program was performed as follows using a 7500 real time PCR system

Step	Temperature	Time
1	95°C	15 min
2	95°C	3 min
3	95°C	15 sec
4	55°C	35 sec
5	72°C (data collection)	45 sec
6	Step 2 to step 5, 40 cycle	∞
7	95°C	15 sec
8	60°C	1 min
9	95°C	15 sec
	(Dissociation stage)	

Five *PIP1* genes were normalized by the endogenous content of *UBIQUITIN5* (At3g62250) and *S16* (At5g18380, At2g09990) transcripts for the transcriptional analysis. The data are given as means \pm SD of three biological replicates. For the translome analysis, five *PIP1* genes were normalized by the endogenous content of *UBIQUITIN5* (At3g62250), *TUBULIN9* (At4g20890) transcripts. Mean values were derived from the two biological replicates with three technical replicates. The stability of the reference genes was tested and normalization was performed using GeNorm (Vandesompele *et al.*, 2002)

4.2.3.14. Protoplast isolation and PEG-mediated transient expression

Twentyeight-day-old plants grown on soil were used for isolation of mesophyll protoplasts using the 'Tape-*Arabidopsis* Sandwich' method as described (Wu *et al.*, 2009). The upper epidermal surface of suitable leaves was first fixed by affixing a strip of Time tape (TimeMed labeling, Burr Ridge), and then the lower epidermal surface was affixed to a strip of Magic tape (3 M, Scotch[®]). After a few seconds, the Magic tape was carefully pulled away from the Time tape. The lower epidermal surface cell layer was peeled away along with the Magic tape. Several peeled leaves (depending on the experiments) were transferred to a flask containing 5-25 mL of enzyme solution. The mixture was gently shaken (40 rpm on a platform shaker) in light for 1-2 h to make sure the protoplasts were released into the solution. The protoplasts were collected by centrifugation at 4°C, 100 × *g* for 3 min. The pellet was washed twice with 25 mL of pre-chilled W5 solution as indicated (Yoo *et al.*, 2007) and incubated on ice for 30 min. During the incubation period, protoplasts were counted using a hemocytometer under a light microscope. The protoplasts were then centrifuged and resuspended in MMg solution to a final concentration of 2 × 10⁶ cells/mL.

Protoplasts were transfected by a modified PEG-mediated method as described (Yoo *et al.*, 2007). Approximately 4 × 10⁵ protoplasts in 200 µL of MMg solution were mixed with approximately 10 µL (10-20 µg) of plasmid DNA at room temperature. An equal volume of a freshly prepared solution of PEG was added, and the mixture was incubated at room temperature for 20 min. After incubation, 1 mL of W5 solution was slowly added and gently mixed with the solution. Then protoplasts were pelleted by centrifugation at 100 × *g* for 1 min. This wash step with 2 mL W5 solution was repeated twice. The protoplasts were resuspended gently in 1 mL of W5 and were incubated in 6-well plates coated with 1% BSA at room temperature in the dark for 14-24 h as indicated.

Solution	Concentration	Component
*Enzyme solution	1-1.5% (w/v)	Cellulase R10 (Serva,Germany)
	0.2-0.4% (w/v)	Macerozyme R10 (Serva,Germany)
	0.4 M	Mannitol
	20 mM	KCl
	20 mM	MES (pH 5.7)
		The enzyme solution was heated at 55°C for 10 min and cooled to room temperature before adding
	10 mM	CaCl ₂
	0.1%	BSA
*PEG solution	40% (w/v)	PEG 4000 (Fluka, 81240)
	40% (v/v)	CaCl ₂
		Mannitol
		Add ddH ₂ O up to 10 mL
W5 solution	154 mM	NaCl
	125 mM	CaCl ₂
	5 mM	KCl
	2 mM	MES (pH 5.7)
MMg solution	0.4 M	Mannitol
	15 mM	MgCl ₂
	4 mM	MES (pH 5.7)

*The enzyme solution and PEG solution are freshly prepared and passed through a 0.45 µm filter.

4.2.4. Protein methods

4.2.4.1. Whole protein extraction

Approximately 4×10^5 protoplasts were pelleted by centrifugation at $2000 \times g$ for 2 min according to each time point of the MG132 experiment and stored at -80°C . After collecting all of the samples, the pellets were thawed on ice and 100 µL extraction buffer were added to each tube. The mixtures were vortexed vigorously for 2 min and incubated at 56°C , for 20 min with gentle shaking. After incubation, the supernatant was collected by centrifugation at $16,000 \times g$ for 5 min, and then transferred to a new Eppendorf tube and stored at -80°C .

Solution	Concentration	Component
4 x laemmli buffer	250 mM	Tris (pH6.8)
	8% (w/v)	SDS
	10% (v/v)	Glycerol
Extraction buffer	1 x	4 x laemmli buffer
	2%	SDS
	100 mM	DTT
	1%	β -Mercaptoethanol

4.2.4.2. RC-DC for determination of protein concentration

The protein concentration of whole protein extractions from the protoplasts was determined with the RC DC™ (reducing agent and detergent compatible) Protein Assay kit (Bio-Rad) following the manufacturer's instructions.

4.2.4.3. Microsomal fractions preparation

All of the solution, tubes and equipments were pre-cooled at 4°C before use. Approximately 0.5 to 1 g plant material (roots or rosettes) were ground to a fine powder and mixed with 8 mL homogenization buffer. The homogenate was filtered through 2 layers of Miracloth into a pre-chilled tube. Mortar and pestle were washed with 2 mL homogenization buffer which were filtered as well and added to the homogenate for a final volume of 10 mL. After centrifugation at 8,000 × *g* for 10 min at 4°C (Sorvall RC 5B+), the supernatant was filtered through a layer of Miracloth into Beckman-ultra-clear tubes (rotor SW 28). After centrifugation at 110,000 × *g* for 40 min at 4°C (Ultracentrifuge LE-70), the pellet was harvested and 100 μ L of resuspension buffer was added to the pellet for incubation on ice for 30 min. The pellet was resuspended using a douncer after addition of 200 μ L resuspension buffer. Microsomal fractions were transferred to a fresh Eppendorf tube and stored at -80°C.

Solution	Concentration	Component
Homogenization buffer	50 mM	Hepes-KOH (pH 7.5)
	5 mM	EDTA (pH 8.0)
	0.1 mg / mL	BHT (Sigma, 47168)
	0.5 M	Sucrose
	1 mM	PMSF (freshly added)
	2 mM	DTT (freshly added)
	0.1%	PVPP (freshly added)
	1tablet / 10 mL	Protease Inhibitor Cocktail (Roche)
Resuspension buffer	0.33 M	Sucrose
	5 mM	K-phosphate buffer (pH 7.8)
	4 mM	KCl
	2 mM	DTT

4.2.4.4. Bradford determination of protein concentration

The protein concentration of microsomal fractions was determined with the Quick Start™ Bradford Protein Assay kit (Bio-Rad) following the manufacturer's instructions.

4.2.4.5. LC-MS and LC-MS/MS-based label-free quantification

Microsomal membrane fractions of 28-day-old rosettes from the wild type and the *pip2;1 pip2;2* double mutant were isolated together with Jin Zhao (Helmholtz München Zentrum). Each sample (5 µg) was digested with trypsin, mass spectrometry analyses were performed, and LC-MS/MS-based label-free quantification of microsomal membrane fractions was analyzed by Juliane Merl-Pham (Helmholtz München Zentrum) as previously described with a long gradient elution process (5 h) (Wisniewski *et al.*, 2009; Hauck *et al.*, 2010; Merl *et al.*, 2012; Vanzo *et al.*, 2014). Statistic analysis of the proteomic data was performed by Elisabeth Georgii based on a paired sample test that has been designed for count data (Pham and Jimenez, 2012).

4.2.4.6. SDS polyacrylamide gel electrophoresis (SDS-PAGE)

SDS polyacrylamide gel electrophoresis was carried out with the classical method as described (Laemmli, 1970). An Amersham biosciences Mighty Small II unit for 8 x 7 cm gels with a thickness of about 0.75 mm was used for preparation of SDS polyacrylamide gel and electrophoretic separation. Plates and combs were completely cleaned and the plates were placed on the rack. The bottom of assembled plates was sealed with gel to make sure there is no leakage. Separating gel (15%) was prepared following the recipe listed below and poured into assembled plates, leaving sufficient space at the top for the stacking gel and comb. The top was covered with water saturated butanol and the gel was allowed to polymerize at room temperature for 30 min. After removing the butanol, a comb was placed in between the assembled plates and 6% stacking gel was prepared and poured above the separating gel.

Approximately 0.5-1 cm of stacking gel should be present between the bottoms of the loading wells and the separating gel. After 10 min polymerization of stacking gel, 1 x SDS-PAGE running buffer was poured into the apparatus up to the top of the wells and the comb was slowly removed under running buffer. The 30 µg whole protein extractions or 3 µg microsomal membrane fractions denatured at 56°C for 20 min (or 70°C for 10 min) were loaded on the prepared 15% SDS polyacrylamide gel. The samples were separated by electrophoresis together with PageRuler Prestained Protein Ladder (10-170 kDa, Thermo Scientific, Germany, denatured like as samples) for estimation of molecular masses of the proteins. Electrophoresis was performed at 25 mA per gel till completion.

Solution	Concentration	Component
4x separate buffer	1.5 M 0.4% (w/v)	Tris (pH 8.8) SDS
4x stock buffer	0.5 M 0.4% (w/v)	Tris (pH 6.8) SDS
1x running buffer	25 mM 190 mM 0.1% (w/v)	Tris Glycine SDS
Gel	Volume	Component
15% Separating gel (10 mL)	2.39 mL 2.5 mL 5 mL 100 μ L 100 μ L 10 μ L	ddH ₂ O 4x separate buffer 30% acrylamide 10% Ammonium persulfate 10% SDS TEMED
6% Stacking gel (5 mL)	2.6 mL 1.25 mL 1 mL 50 μ L 50 μ L 5 μ L	ddH ₂ O 4x stock buffer 30% acrylamide 10% Ammonium persulfate 10% SDS TEMED

4.2.4.7. Western blot

A semi-dry transfer unit (Milliblot-Graphite Electroblotter I, Millipore, USA) was used for transferring proteins to a PVDF membrane (Amersham Biosciences, Germany). The separating gel containing the proteins was cut and the size was measured. The PVDF membrane and 9 blotter sheets (Whatman, 3MM paper) were cut to the same size as the gel. The PVDF membrane was soaked in methanol for 20 sec and washed in ddH₂O for 1 min. The gel, PVDF membrane and blotter sheets were pre-wetted in transfer buffer. The apparatus was rinsed with transfer buffer. Six sheets of presoaked blotting paper were placed in the middle of the transfer unit, they were then covered with the PVDF membrane, the gel and three sheets of presoaked blotting papers in order. The transfer sandwich was carefully assembled to remove air bubbles with a pipette by rolling over the sandwich. The transfer was performed based on the size of the gel (2.5 MA per cm²) for 60 min. After

MATERIALS AND METHODS

transferring, the PVDF membrane was blocked in the blocking solution at room temperature for 1-2 h with gentle shaking.

Then the PVDF membrane was incubated with the primary antibody solution for 2 h at room temperature (or overnight at 4°C). After incubation, the blot was rinsed with 1x Tris-buffered saline Tween-20 (TBST) solution 2-3 times for 5 min to remove the unbound antibody. The membrane was incubated with the second antibody solution for 1-2 h. After incubation, the membrane was washed with 1x TBST 3 times for 5 min and was subsequently washed with 1x Tris-buffered saline (TBS) solution 3 times for 5 min at room temperature with gentle shaking. After the PVDF membrane was dried, it was scanned at 532 nm (Cy3 detection) or 635 nm (Cy5 detection) using a Typhoon Scanner (Amersham Biosciences, Germany). For quantification of the immunoblot signals, the intensity of each band was corrected for background and measured using Image J software (version 1.37v; <http://rsb.info.nih.gov/ij/>).

Solution	Concentration	Component
Transfer buffer	80% 20%	1 x running buffer Methanol
1x TBS buffer	10 mM 150 mM	Tris (pH 7.5) NaCl
1x TBST buffer	1x 0.05%	TBS buffer Tween 20
Blocking buffer	1%	Milk powder In TBST buffer
*Antibody buffer	1:5000 dilution 1:2000 dilution 1:2000 dilution 1:2000 dilution 1:2500 dilution 1:2500 dilution	anti-PIP1 (antiserum from rabbit) anti-PIP2;1/PIP2;2/PIP2;3 (antiserum from rabbit) anti-HA (antiserum from mouse) anti-GFP (antiserum from mouse) anti-mouse cy3-linked (from goat) anti-rabbit cy5-linked (from goat)

*All antibody solutions were diluted in 1x TBST buffer. The primary antibodies of anti-PIP1 and anti-PIP2;1/PIP2;2/PIP2;3 were generated in our lab (Henzler *et al.*, 1999; Da Ines, 2008). The primary and secondary commercial antibodies were purchased from different companies: anti-HA (H3663, Sigma, Germany), anti-GFP (BIOZOL, Germany), anti-mouse cy3-linked and anti-rabbit cy5-linked antibodies (Amersham Biosciences, Germany).

4.2.4.8. Enzyme-linked immunosorbent assay (ELISA)

The quantification of protein expression of microsomal membrane fractions (PIP1s, PIP2;1/PIP2;2/PIP2;3, HA-PIP1;1 and HA-PIP1;2) was performed using the methods described previously (Santoni *et al.*, 2006) with some modifications. Isolated microsomal membrane fractions were diluted six times in 2-fold serial in a 0.1 M carbonate buffer and were loaded in triplicate on 96-well Maxisorp immunoplates (Nunc) overnight at 37°C for 1-2 h (0.1 µg in 200 µL 0.1 M carbonate buffer was the concentration of first well). The plate was emptied and rinsed with 200 µL 1x Phosphate-buffered saline (PBS) buffer for 5 min with gentle shaking. The blocking step and three times washing steps were carried out according to the manufacturer's instructions with 1x PBS with Tween 20 and BSA (PBS-TB) buffer for 30 min and 1x PBS with Tween 20 (PBST) buffer for 5 min, respectively. 100 µL primary antibody (listed below) were loaded in each well and incubated overnight at 4°C. The plate was emptied and rinsed five times with 200 µL 1 x PBST buffer for 5 min with gentle shaking. 100 µL secondary HRP-conjugated anti-rabbit antibody (Promega, Germany) was loaded in each well and incubated at 37°C for 2 h. The plate was emptied and rinsed five times with 200 µL 1 x PBS buffer for 5 min with gentle shaking.

An aliquot 10 mL 2,2'-azino-bis (3-ethylbenzothiazoline-6-sulphonic acid) diammonium salt (ABTS buffer) was thawed at room temperature. 10 µL 30% H₂O₂ were added into ABTS buffer and mixed well. Then 100 µL of the mixture were added to each well and incubated at room temperature for 20 min with gentle shaking. The absorbance signal was read with a multi-plate reader at 405nm (Infinite[®] M1000 PRO; TECAN). A linear regression was obtained according to the dilution series and the amount of proteins was estimated for each sample and used for relative comparison between samples.

MATERIALS AND METHODS

Solution	Concentration	Component
0.1 M Carbonate buffer (pH 9.5)	30mM 60mM	Na ₂ CO ₃ NaHCO ₃
1x PBS buffer	4 mM 16 mM 115 mM	KH ₂ PO ₄ Na ₂ HPO ₄ NaCl
1x PBST buffer	1x 0.1%	PBS buffer Tween 20
1x PBSTB buffer	1x 1%	PBST buffer BSA
Antibody buffer	1:10000 dilution 1:2500 dilution 1:30,000 dilution 1:2500 dilution	anti-PIP1 (antiserum from rabbit) anti-PIP2;1/PIP2;2/PIP2;3 (antiserum from rabbit) *anti-HA (antiserum from rabbit) anti-rabbit (HRP-conjugated antiserum from goat) All in 1x PBSTB buffer
ABTS buffer	5% (w/v) 100 mM	ABTS Citric acid buffer Adjust pH 4.35 with NaOH and aliquot into 10 ml portions and store at -20°C

*This anti-HA primary antibody was purchased from Bethyl Ranch.

4.2.4.9. Co-Immunoprecipitation

The co-immunoprecipitation method was performed as described (Zelazny *et al.*, 2007) with small modifications. Approximately 150 µg microsomal fractions were prepared as described (see 4.2.4.3) and solubilized in 250 µL of solubilization buffer at room temperature for 4 h on a rotating wheel (20 rpm). The supernatant was collected after centrifugation at 169,000 x *g* for 40 min at 4°C and was incubated with 25 µl Protein A-Agarose (Roche, Germany) for 1 h at 4°C to allow unspecific binding of Protein A-Agarose and solubilized proteins and used as the negative control. The samples were centrifuged at 12,000 x *g* for 1 min at 4°C. The supernatant was carefully transferred to a fresh 2 mL Eppendorf tube and incubated with 1 µL of anti-HA antiserum (H3663, Sigma, Germany) overnight at 4°C on a rotating wheel (20 rpm). Then 50 µL of Protein A-Agarose were added to each

sample. The mixtures were incubated for 4 h at 4°C on a rotating wheel (20 rpm). The agarose-antibody-antigen complexes were collected by centrifugation at 12,000 x g for 1 min at 4°C. After four times washing with 400 µL of solubilization buffer and four times washing with 800 µL of 1x TBS buffer, the resin was recovered and incubated in 60 µL of extraction buffer as indicated before (see 4.2.4.1) for 10 min at 70°C. Proteins were separated by 15% SDS-PAGE gel electrophoresis (see 4.2.4.5) and transferred to a PVDF membrane as described previously (see 4.2.4.8). Western blot analysis was performed by using a primary anti-HA antiserum (H3663, Sigma, Germany) and other primary anti-PIP2;1/PIP2;2/PIP2;3 antiserum, respectively (see 4.2.4.8).

Solution	Concentration	Component
1 x TBS buffer	20 mM 136 mM	Tris NaCl
Solubilization buffer (pH7.6)	1 x 3.5% 1 tablet /10 mL	TBS buffer n-octyl-β-D-thioglucopyranoside Protease Inhibitor Cocktail (Roche)

4.2.4.10. Degradation assay

For MG132 experiments, mesophyll protoplasts were isolated from the 28-day-old plants grown on soil as described (see 4.2.3.14). Mesophyll protoplasts were resuspended gently in W5 buffer containing 100 µM cycloheximide in the absence or presence of 50 µM MG132 and were incubated in 6-well plates coated with 1% BSA under light with gentle shaking (20-40 rpm). Approximately 4×10^5 protoplasts (200 µL) were collected for different time courses (0-3 h) and then were used for whole protein extraction (see 4.2.4.1) and Western blot analysis (see 4.2.4.7).

For the Brefeldin A and Wortmannin experiments, seven-day-old seedlings were immersed in 2 mL MS liquid medium with 50 µM Brefeldin A and 33 µM Wortmannin, respectively (with DMSO as mock control). The fluorescence signals of different root regions were monitored by confocal microscopy (see 4.2.5) after treatment.

4.2.5. Microscopy

For the selection of transgenic lines with seed coat specifically expressed GFP, some roots and protoplasts images were taken with an epifluorescence microscopy (Olympus BX61) using 488 nm (GFP) excitation lines. Those pictures used for quantification of fluorescence signals were taken under the same settings. Some pictures were further processed using Cell image software (Olympus Imaging). Some plant pictures were taken by the digital camera (Nikon D300).

For the most of the observations and quantifications of fluorescence signals (EGFP) from roots and protoplasts, pictures were taken with a Zeiss LSM 510 META confocal laser scanning microscopy using a C-APOCHROMAT ($\times 40/1.2w$ numerical aperture water immersion) with Excitation/emission wavelengths of 488/505 to 530 nm for EGFP. When the fluorescence signal intensity between the wild type and mutant lines needed to be compared in each experiment, calibration of the laser beam intensity, gain, and offset parameters were obtained from each of the appropriate control wild type backgrounds. The same parameters were applied to images which were used for the comparison between wild type and mutant backgrounds. A Z- (1 μ m/stack) and Time-series (3-10s/scan) pictures were achieved following the manufacturer's instructions. An approximately same position and distance were used for acquiring the Z-stacks of images and performing z-projection image processing by the function of Maximum-intensity-projection in the Zen 2009 software (Carl Zeiss MicroImaging). The fluorescence signal intensities of the roots and protoplasts of the wild type and the mutant lines were quantified with the Image J software.

The transient expression experiment and the colocalization analysis used the PIP2;1-mCherry line (Peret *et al.*, 2012) and different mCherry-labelled compartments marker lines (Geldner *et al.*, 2009), respectively. Protoplasts were examined with a Zeiss LSM 510 META laser scanning confocal microscope using a C-APOCHROMAT ($\times 40/1.2w$ numerical aperture water immersion) lens by frame

switching in multitrack mode. The pinhole diameter (1 Airy unit) was adjusted for every channel in most of the cases. The cLSM settings of the multitrack mode for GFP, chlorophyll fluorescence and mCherry were listed below (images were presented in pseudocolor: green for EGFP, red for mCherry, and blue for chlorophyll):

Channel	Fluorophore	Excitation (laser line) / filter set	Primary dichroic mirror (HFT)	Secondary dichroic mirror1 (NFT)	Secondary dichroic mirror2 (NFT)
Ch1	EGFP	488 nm (Argon2) / BP 500- 530	488/543	635 VIS	545
	Chlorophyll	488 nm (argon2) / META 650-704			
Ch2	mCherry ChD	543 nm (He/Ne 1) / BP 565-615	488/543	635 VIS	545

5. REFERENCES

- Agre, P., Saboori, A.M., Asimos, A., and Smith, B.L.** (1987). Purification and partial characterization of the Mr 30,000 integral membrane protein associated with the erythrocyte Rh(D) antigen. *J Biol Chem* **262**: 17497-17503.
- Alexandersson, E., Danielson, J.A., Råde, J., Moparhi, V.K., Fontes, M., Kjellbom, P., and Johanson, U.** (2010). Transcriptional regulation of aquaporins in accessions of *Arabidopsis* in response to drought stress. *Plant J* **61**: 650-660.
- Alexandersson, E., Fraysse, L., Sjövall-Larsen, S., Gustavsson, S., Fellert, M., Karlsson, M., Johanson, U., and Kjellbom, P.** (2005). Whole gene family expression and drought stress regulation of aquaporins. *Plant Mol Biol* **59**: 469-484.
- Alleva, K., Chara, O., and Amodeo, G.** (2012). Aquaporins: another piece in the osmotic puzzle. *FEBS Lett* **586**: 2991-2999.
- Araki, K., and Nagata, K.** (2011). Protein folding and quality control in the ER. *Cold Spring Harb Perspect Biol* **3**: a007526.
- Babst, M.** (2014). Quality control: quality control at the plasma membrane: one mechanism does not fit all. *J Cell Biol* **205**: 11-20.
- Bensmihen, S., To, A., Lambert, G., Kroj, T., Giraudat, J., and Parcy, F.** (2004). Analysis of an activated ABI5 allele using a new selection method for transgenic *Arabidopsis* seeds. *FEBS Lett* **561**: 127-131.
- Bernales, S., McDonald, K.L., and Walter, P.** (2006). Autophagy counterbalances endoplasmic reticulum expansion during the unfolded protein response. *PLoS Biol* **4**: e423.
- Bertl, A., and Kaldenhoff, R.** (2007). Function of a separate NH₃-pore in Aquaporin TIP2;2 from wheat. *FEBS Lett* **581**: 5413-5417.
- Besserer, A., Burnotte, E., Bienert, G.P., Chevalier, A.S., Errachid, A., Grefen, C., Blatt, M.R., and Chaumont, F.** (2012). Selective regulation of maize plasma membrane aquaporin trafficking and activity by the SNARE SYP121. *Plant Cell* **24**: 3463-3481.
- Bhat, R.A., and Panstruga, R.** (2005). Lipid rafts in plants. *Planta* **223**: 5-19.
- Biela, A., Grote, K., Otto, B., Hoth, S., Hedrich, R., and Kaldenhoff, R.** (1999). The *Nicotiana tabacum* plasma membrane aquaporin NtAQP1 is mercury-insensitive and permeable for glycerol. *Plant J* **18**: 565-570.
- Bienert, G.P., and Jahn, T.P.** (2010). Major intrinsic proteins and arsenic transport in plants: new players and their potential role. *Adv Exp Med Biol* **679**: 111-125.
- Bienert, G.P., Schussler, M.D., and Jahn, T.P.** (2008). Metalloids: essential, beneficial or toxic? Major intrinsic proteins sort it out. *Trends Biochem Sci* **33**: 20-26.

- Bienert, G.P., Bienert, M.D., Jahn, T.P., Boutry, M., and Chaumont, F.** (2011). Solanaceae XIPs are plasma membrane aquaporins that facilitate the transport of many uncharged substrates. *Plant J* **66**: 306-317.
- Bienert, G.P., Moller, A.L., Kristiansen, K.A., Schulz, A., Moller, I.M., Schjoerring, J.K., and Jahn, T.P.** (2007). Specific aquaporins facilitate the diffusion of hydrogen peroxide across membranes. *J Biol Chem* **282**: 1183-1192.
- Bienert, G.P., Cavez, D., Besserer, A., Berny, M.C., Gilis, D., Rooman, M., and Chaumont, F.** (2012). A conserved cysteine residue is involved in disulfide bond formation between plant plasma membrane aquaporin monomers. *Biochem J* **445**: 101-111.
- Borner, G.H., Sherrier, D.J., Weimar, T., Michaelson, L.V., Hawkins, N.D., Macaskill, A., Napier, J.A., Beale, M.H., Lilley, K.S., and Dupree, P.** (2005). Analysis of detergent-resistant membranes in *Arabidopsis*. Evidence for plasma membrane lipid rafts. *Plant Physiol* **137**: 104-116.
- Borstlap, A.C.** (2002). Early diversification of plant aquaporins. *Trends Plant Sci* **7**: 529-530.
- Boursiac, Y., Chen, S., Luu, D.T., Sorieul, M., van den Dries, N., and Maurel, C.** (2005). Early effects of salinity on water transport in *Arabidopsis* roots. Molecular and cellular features of aquaporin expression. *Plant Physiol* **139**: 790-805.
- Boursiac, Y., Boudet, J., Postaire, O., Luu, D.T., Tournaire-Roux, C., and Maurel, C.** (2008). Stimulus-induced downregulation of root water transport involves reactive oxygen species-activated cell signalling and plasma membrane intrinsic protein internalization. *Plant J* **56**: 207-218.
- Cavez, D., Hachez, C., and Chaumont, F.** (2009). Maize black Mexican sweet suspension cultured cells are a convenient tool for studying aquaporin activity and regulation. *Plant Signal Behav* **4**: 890-892.
- Chaumont, F., and Tyerman, S.D.** (2014). Aquaporins: highly regulated channels controlling plant water relations. *Plant Physiol* **164**: 1600-1618.
- Chaumont, F., Moshelion, M., and Daniels, M.J.** (2005). Regulation of plant aquaporin activity. *Biol Cell* **97**: 749-764.
- Chaumont, F., Barrieu, F., Jung, R., and Chrispeels, M.J.** (2000). Plasma membrane intrinsic proteins from maize cluster in two sequence subgroups with differential aquaporin activity. *Plant Physiol* **122**: 1025-1034.
- Chen, W., Yin, X., Wang, L., Tian, J., Yang, R., Liu, D., Yu, Z., Ma, N., and Gao, J.** (2013). Involvement of rose aquaporin RhPIP1;1 in ethylene-regulated petal expansion through interaction with RhPIP2;1. *Plant Mol Biol* **83**: 219-233.
- Chevalier, A.S., Bienert, G.P., and Chaumont, F.** (2014). A New LxxxA Motif in the Transmembrane Helix3 of Maize Aquaporins Belonging to the Plasma

REFERENCES

- Membrane Intrinsic Protein PIP2 Group Is Required for Their Trafficking to the Plasma Membrane. *Plant Physiol* **166**: 125-138.
- Clough, S.J., and Bent, A.F.** (1998). Floral dip: a simplified method for *Agrobacterium*-mediated transformation of *Arabidopsis thaliana*. *Plant J* **16**: 735-743.
- Conn, S.J., Hocking, B., Dayod, M., Xu, B., Athman, A., Henderson, S., Aukett, L., Conn, V., Shearer, M.K., Fuentes, S., Tyerman, S.D., and Gilliam, M.** (2013). Protocol: optimising hydroponic growth systems for nutritional and physiological analysis of *Arabidopsis thaliana* and other plants. *Plant Methods* **9**: 4.
- Consortium, A.I.M.** (2011). Evidence for network evolution in an *Arabidopsis* interactome map. *Science* **333**: 601-607.
- Cui, F., Liu, L., Zhao, Q., Zhang, Z., Li, Q., Lin, B., Wu, Y., Tang, S., and Xie, Q.** (2012). *Arabidopsis* ubiquitin conjugase UBC32 is an ERAD component that functions in brassinosteroid-mediated salt stress tolerance. *Plant Cell* **24**: 233-244.
- Da Ines, O.** (2008). Functional analysis of PIP2 aquaporins in *Arabidopsis thaliana* (Imu).
- Da Ines, O., Graf, W., Franck, K.I., Albert, A., Winkler, J.B., Scherb, H., Stichler, W., and Schäffner, A.R.** (2010). Kinetic analyses of plant water relocation using deuterium as tracer-reduced water flux of *Arabidopsis pip2* aquaporin knockout mutants. *Plant Biol (Stuttg)* **12 Suppl 1**: 129-139.
- Daniels, M.J., and Yeager, M.** (2005). Phosphorylation of aquaporin PvTIP3;1 defined by mass spectrometry and molecular modeling. *Biochemistry* **44**: 14443-14454.
- Daniels, M.J., Mirkov, T.E., and Chrispeels, M.J.** (1994). The plasma membrane of *Arabidopsis thaliana* contains a mercury-insensitive aquaporin that is a homolog of the tonoplast water channel protein TIP. *Plant Physiol* **106**: 1325-1333.
- Danielson, J.A., and Johanson, U.** (2008). Unexpected complexity of the aquaporin gene family in the moss *Physcomitrella patens*. *BMC Plant Biol* **8**: 45.
- De Bellis, M., Pisani, F., Mola, M.G., Basco, D., Catalano, F., Nicchia, G.P., Svelto, M., and Frigeri, A.** (2014). A novel human aquaporin-4 splice variant exhibits a dominant-negative activity: a new mechanism to regulate water permeability. *Mol Biol Cell* **25**: 470-480.
- Deegan, S., Saveljeva, S., Gorman, A.M., and Samali, A.** (2013). Stress-induced self-cannibalism: on the regulation of autophagy by endoplasmic reticulum stress. *Cell Mol Life Sci* **70**: 2425-2441.
- Dhonukshe, P., Aniento, F., Hwang, I., Robinson, D.G., Mravec, J., Stierhof, Y.D., and Friml, J.** (2007). Clathrin-mediated constitutive endocytosis of PIN auxin efflux carriers in *Arabidopsis*. *Curr Biol* **17**: 520-527.

- di Pietro, M., Vialaret, J., Li, G.W., Hem, S., Prado, K., Rossignol, M., Maurel, C., and Santoni, V. (2013). Coordinated post-translational responses of aquaporins to abiotic and nutritional stimuli in *Arabidopsis* roots. *Mol Cell Proteomics* **12**: 3886-3897.
- Dynowski, M., Schaaf, G., Loque, D., Moran, O., and Ludewig, U. (2008). Plant plasma membrane water channels conduct the signalling molecule H₂O₂. *Biochem J* **414**: 53-61.
- Feraru, E., Feraru, M.I., Asaoka, R., Paciorek, T., De Rycke, R., Tanaka, H., Nakano, A., and Friml, J. (2012). BEX5/RabA1b regulates trans-Golgi network-to-plasma membrane protein trafficking in *Arabidopsis*. *Plant Cell* **24**: 3074-3086.
- Fetter, K., Van Wilder, V., Moshelion, M., and Chaumont, F. (2004). Interactions between plasma membrane aquaporins modulate their water channel activity. *Plant Cell* **16**: 215-228.
- Fotiadis, D., Jenö, P., Mini, T., Wirtz, S., Müller, S.A., Fraysse, L., Kjellbom, P., and Engel, A. (2001). Structural characterization of two aquaporins isolated from native spinach leaf plasma membranes. *J Biol Chem* **276**: 1707-1714.
- Franceschini, A., Szklarczyk, D., Frankild, S., Kuhn, M., Simonovic, M., Roth, A., Lin, J., Minguez, P., Bork, P., von Mering, C., and Jensen, L.J. (2013). STRING v9.1: protein-protein interaction networks, with increased coverage and integration. *Nucleic Acids Res* **41**: D808-815.
- Frick, A., Järvå, M., and Törnroth-Horsefield, S. (2013). Structural basis for pH gating of plant aquaporins. *FEBS Lett* **587**: 989-993.
- Fu, D., Libson, A., Miercke, L.J., Weitzman, C., Nollert, P., Krucinski, J., and Stroud, R.M. (2000). Structure of a glycerol-conducting channel and the basis for its selectivity. *Science* **290**: 481-486.
- Fujiyoshi, Y., Mitsuoka, K., de Groot, B.L., Philippsen, A., Grubmuller, H., Agre, P., and Engel, A. (2002). Structure and function of water channels. *Curr Opin Struct Biol* **12**: 509-515.
- Gaspar, M., amp, x, lia, Bousser, A., Sissoëff, I., Roche, O., Hoarau, J., and Mahé, A. (2003). Cloning and characterization of ZmPIP1-5b, an aquaporin transporting water and urea. *Plant Science* **165**: 21-31.
- Geelen, D., Leyman, B., Batoko, H., Di Sanebastiano, G.P., Moore, I., and Blatt, M.R. (2002). The abscisic acid-related SNARE homolog NtSyr1 contributes to secretion and growth: evidence from competition with its cytosolic domain. *Plant Cell* **14**: 387-406.
- Geldner, N., Déneraud-Tendon, V., Hyman, D.L., Mayer, U., Stierhof, Y.D., and Chory, J. (2009). Rapid, combinatorial analysis of membrane compartments in intact plants with a multicolor marker set. *Plant J* **59**: 169-178.
- Gerbeau, P., Güclü, J., Ripoche, P., and Maurel, C. (1999). Aquaporin Nt-TIPa can account for the high permeability of tobacco cell vacuolar membrane to small neutral solutes. *Plant J* **18**: 577-587.

- Gerbeau, P., Amodeo, G., Henzler, T., Santoni, V., Ripoche, P., and Maurel, C.** (2002). The water permeability of *Arabidopsis* plasma membrane is regulated by divalent cations and pH. *Plant J* **30**: 71-81.
- Gomes, D., Agasse, A., Thiébaud, P., Delrot, S., Gerós, H., and Chaumont, F.** (2009). Aquaporins are multifunctional water and solute transporters highly divergent in living organisms. *Biochim Biophys Acta* **1788**: 1213-1228.
- Guerra, D.D., and Callis, J.** (2012). Ubiquitin on the move: the ubiquitin modification system plays diverse roles in the regulation of endoplasmic reticulum- and plasma membrane-localized proteins. *Plant Physiol* **160**: 56-64.
- Gupta, A.B., and Sankararamkrishnan, R.** (2009). Genome-wide analysis of major intrinsic proteins in the tree plant *Populus trichocarpa*: characterization of XIP subfamily of aquaporins from evolutionary perspective. *BMC Plant Biol* **9**: 134.
- Gustavsson, S., Lebrun, A.S., Nordén, K., Chaumont, F., and Johanson, U.** (2005). A novel plant major intrinsic protein in *Physcomitrella patens* most similar to bacterial glycerol channels. *Plant Physiol* **139**: 287-295.
- Hachez, C., and Chaumont, F.** (2010). Aquaporins: a family of highly regulated multifunctional channels. *Adv Exp Med Biol* **679**: 1-17.
- Hachez, C., Heinen, R.B., Draye, X., and Chaumont, F.** (2008). The expression pattern of plasma membrane aquaporins in maize leaf highlights their role in hydraulic regulation. *Plant Mol Biol* **68**: 337-353.
- Hachez, C., Besserer, A., Chevalier, A.S., and Chaumont, F.** (2013). Insights into plant plasma membrane aquaporin trafficking. *Trends Plant Sci* **18**: 344-352.
- Hachez, C., Veselov, D., Ye, Q., Reinhardt, H., Knipfer, T., Fricke, W., and Chaumont, F.** (2012). Short-term control of maize cell and root water permeability through plasma membrane aquaporin isoforms. *Plant Cell Environ* **35**: 185-198.
- Hachez, C., Laloux, T., Reinhardt, H., Cavez, D., Degand, H., Grefen, C., De Rycke, R., Inzé, D., Blatt, M.R., Russinova, E., and Chaumont, F.** (2014). *Arabidopsis* SNAREs SYP61 and SYP121 coordinate the trafficking of plasma membrane aquaporin PIP2;7 to modulate the cell membrane water permeability. *Plant Cell* **26**: 3132-3147.
- Harrison, S.J., Mott, E.K., Parsley, K., Aspinall, S., Gray, J.C., and Cottage, A.** (2006). A rapid and robust method of identifying transformed *Arabidopsis thaliana* seedlings following floral dip transformation. *Plant Methods* **2**: 19.
- Harvengt, P., Vlerick, A., Fuks, B., Wattiez, R., Ruyschaert, J.M., and Homble, F.** (2000). Lentil seed aquaporins form a hetero-oligomer which is phosphorylated by a Mg²⁺-dependent and Ca²⁺-regulated kinase. *Biochem J* **352 Pt 1**: 183-190.
- Hauck, S.M., Dietter, J., Kramer, R.L., Hofmaier, F., Zipplies, J.K., Amann, B., Feuchtinger, A., Deeg, C.A., and Ueffing, M.** (2010). Deciphering

- membrane-associated molecular processes in target tissue of autoimmune uveitis by label-free quantitative mass spectrometry. *Mol Cell Proteomics* **9**: 2292-2305.
- Heckwolf, M., Pater, D., Hanson, D.T., and Kaldenhoff, R.** (2011). The *Arabidopsis thaliana* aquaporin AtPIP1;2 is a physiologically relevant CO(2) transport facilitator. *Plant J* **67**: 795-804.
- Hemsley, P.A., Weimar, T., Lilley, K.S., Dupree, P., and Grierson, C.S.** (2013). A proteomic approach identifies many novel palmitoylated proteins in *Arabidopsis*. *New Phytol* **197**: 805-814.
- Henzler, T., Waterhouse, R.N., Smyth, A.J., Carvajal, M., Cooke, D.T., Schäffner, A.R., Steudle, E., and Clarkson, D.T.** (1999). Diurnal variations in hydraulic conductivity and root pressure can be correlated with the expression of putative aquaporins in the roots of lotus japonicus. *Planta* **210**: 50-60.
- Hill, A.E., and Shachar-Hill, B.** (2006). A new approach to epithelial isotonic fluid transport: an osmosensor feedback model. *J Membr Biol* **210**: 77-90.
- Hill, A.E., Shachar-Hill, B., and Shachar-Hill, Y.** (2004). What are aquaporins for? *J Membr Biol* **197**: 1-32.
- Hofius, D., Schultz-Larsen, T., Joensen, J., Tsitsigiannis, D.I., Petersen, N.H., Mattsson, O., Jorgensen, L.B., Jones, J.D., Mundy, J., and Petersen, M.** (2009). Autophagic components contribute to hypersensitive cell death in *Arabidopsis*. *Cell* **137**: 773-783.
- Holm, L.M., Jahn, T.P., Moller, A.L., Schjoerring, J.K., Ferri, D., Klaerke, D.A., and Zeuthen, T.** (2005). NH₃ and NH₄⁺ permeability in aquaporin-expressing *Xenopus* oocytes. *Pflugers Arch* **450**: 415-428.
- Howell, S.H.** (2013). Endoplasmic reticulum stress responses in plants. *Annu Rev Plant Biol* **64**: 477-499.
- Hruz, T., Laule, O., Szabo, G., Wessendorp, F., Bleuler, S., Oertle, L., Widmayer, P., Gruissem, W., and Zimmermann, P.** (2008). Genevestigator v3: a reference expression database for the meta-analysis of transcriptomes. *Adv Bioinformatics* **2008**: 420747.
- Hurtley, S.M., and Helenius, A.** (1989). Protein oligomerization in the endoplasmic reticulum. *Annu Rev Cell Biol* **5**: 277-307.
- Ishikawa, F., Suga, S., Uemura, T., Sato, M.H., and Maeshima, M.** (2005). Novel type aquaporin SIPs are mainly localized to the ER membrane and show cell-specific expression in *Arabidopsis thaliana*. *FEBS Lett* **579**: 5814-5820.
- Jang, J.Y., Kim, D.G., Kim, Y.O., Kim, J.S., and Kang, H.** (2004). An expression analysis of a gene family encoding plasma membrane aquaporins in response to abiotic stresses in *Arabidopsis thaliana*. *Plant Mol Biol* **54**: 713-725.
- Javot, H., Lauvergeat, V., Santoni, V., Martin-Laurent, F., Güclü, J., Vinh, J., Heyes, J., Franck, K.I., Schäffner, A.R., Bouchez, D., and Maurel, C.**

- (2003). Role of a single aquaporin isoform in root water uptake. *Plant Cell* **15**: 509-522.
- Johanson, U., and Gustavsson, S.** (2002). A new subfamily of major intrinsic proteins in plants. *Mol Biol Evol* **19**: 456-461.
- Johanson, U., Karlsson, M., Johansson, I., Gustavsson, S., Sjövall, S., Fraysse, L., Weig, A.R., and Kjellbom, P.** (2001). The complete set of genes encoding major intrinsic proteins in *Arabidopsis* provides a framework for a new nomenclature for major intrinsic proteins in plants. *Plant Physiol* **126**: 1358-1369.
- Johansson, I., Karlsson, M., Shukla, V.K., Chrispeels, M.J., Larsson, C., and Kjellbom, P.** (1998). Water transport activity of the plasma membrane aquaporin PM28A is regulated by phosphorylation. *Plant Cell* **10**: 451-459.
- Jones, A.M., Xuan, Y., Xu, M., Wang, R.S., Ho, C.H., Lalonde, S., You, C.H., Sardi, M.I., Parsa, S.A., Smith-Valle, E., Su, T., Frazer, K.A., Pilot, G., Pratelli, R., Grossmann, G., Acharya, B.R., Hu, H.C., Engineer, C., Villiers, F., Ju, C., Takeda, K., Su, Z., Dong, Q., Assmann, S.M., Chen, J., Kwak, J.M., Schroeder, J.I., Albert, R., Rhee, S.Y., and Frommer, W.B.** (2014). Border control--a membrane-linked interactome of *Arabidopsis*. *Science* **344**: 711-716.
- Jozefkowicz, C., Rosi, P., Sigaut, L., Soto, G., Pietrasanta, L.I., Amodeo, G., and Alleva, K.** (2013). Loop A is critical for the functional interaction of two *Beta vulgaris* PIP aquaporins. *PLoS One* **8**: e57993.
- Kaldenhoff, R., Kölling, A., Meyers, J., Karmann, U., Ruppel, G., and Richter, G.** (1995). The blue light-responsive *AthH2* gene of *Arabidopsis thaliana* is primarily expressed in expanding as well as in differentiating cells and encodes a putative channel protein of the plasmalemma. *Plant J* **7**: 87-95.
- Kammerloher, W., Fischer, U., Piechottka, G.P., and Schäffner, A.R.** (1994). Water channels in the plant plasma membrane cloned by immunoselection from a mammalian expression system. *Plant J* **6**: 187-199.
- Karimi, M., Inzé, D., and Depicker, A.** (2002). GATEWAY vectors for *Agrobacterium*-mediated plant transformation. *Trends Plant Sci* **7**: 193-195.
- Karimi, M., De Meyer, B., and Hilson, P.** (2005). Modular cloning in plant cells. *Trends Plant Sci* **10**: 103-105.
- Karimi, M., Depicker, A., and Hilson, P.** (2007a). Recombinational cloning with plant gateway vectors. *Plant Physiol* **145**: 1144-1154.
- Karimi, M., Bleys, A., Vanderhaeghen, R., and Hilson, P.** (2007b). Building blocks for plant gene assembly. *Plant Physiol* **145**: 1183-1191.
- Kleine-Vehn, J., Leitner, J., Zwiewka, M., Sauer, M., Abas, L., Luschig, C., and Friml, J.** (2008). Differential degradation of PIN2 auxin efflux carrier by retromer-dependent vacuolar targeting. *Proc Natl Acad Sci U S A* **105**: 17812-17817.

- Korkhov, V.M.** (2009). GFP-LC3 labels organised smooth endoplasmic reticulum membranes independently of autophagy. *J Cell Biochem* **107**: 86-95.
- Kosinska Eriksson, U., Fischer, G., Friemann, R., Enkavi, G., Tajkhorshid, E., and Neutze, R.** (2013). Subangstrom resolution X-ray structure details aquaporin-water interactions. *Science* **340**: 1346-1349.
- Kruse, E., Uehlein, N., and Kaldenhoff, R.** (2006). The aquaporins. *Genome Biol* **7**: 206.
- Laemmli, U.K.** (1970). Cleavage of structural proteins during the assembly of the head of bacteriophage T4. *Nature* **227**: 680-685.
- Lee, D.H., and Goldberg, A.L.** (1996). Selective inhibitors of the proteasome-dependent and vacuolar pathways of protein degradation in *Saccharomyces cerevisiae*. *J Biol Chem* **271**: 27280-27284.
- Lee, H.K., Cho, S.K., Son, O., Xu, Z., Hwang, I., and Kim, W.T.** (2009). Drought stress-induced Rma1H1, a RING membrane-anchor E3 ubiquitin ligase homolog, regulates aquaporin levels via ubiquitination in transgenic *Arabidopsis* plants. *Plant Cell* **21**: 622-641.
- Li, F., and Vierstra, R.D.** (2012). Autophagy: a multifaceted intracellular system for bulk and selective recycling. *Trends Plant Sci* **17**: 526-537.
- Li, G., Santoni, V., and Maurel, C.** (2014). Plant aquaporins: roles in plant physiology. *Biochim Biophys Acta* **1840**: 1574-1582.
- Li, R., Raikhel, N.V., and Hicks, G.R.** (2012). Chemical Effectors of Plant Endocytosis and Endomembrane Trafficking: 37-61.
- Li, X., Wang, X., Yang, Y., Li, R., He, Q., Fang, X., Luu, D.T., Maurel, C., and Lin, J.** (2011). Single-molecule analysis of PIP2;1 dynamics and partitioning reveals multiple modes of *Arabidopsis* plasma membrane aquaporin regulation. *Plant Cell* **23**: 3780-3797.
- Lingwood, D., Schuck, S., Ferguson, C., Gerl, M.J., and Simons, K.** (2009). Generation of cubic membranes by controlled homotypic interaction of membrane proteins in the endoplasmic reticulum. *J Biol Chem* **284**: 12041-12048.
- Liu, F., Vantoai, T., Moy, L.P., Bock, G., Linfoord, L.D., and Quackenbush, J.** (2005). Global transcription profiling reveals comprehensive insights into hypoxic response in *Arabidopsis*. *Plant Physiol* **137**: 1115-1129.
- Liu, Y., and Li, J.** (2014). Endoplasmic reticulum-mediated protein quality control in *Arabidopsis*. *Front Plant Sci* **5**: 162.
- Liu, Y., Burgos, J.S., Deng, Y., Srivastava, R., Howell, S.H., and Bassham, D.C.** (2012). Degradation of the endoplasmic reticulum by autophagy during endoplasmic reticulum stress in *Arabidopsis*. *Plant Cell* **24**: 4635-4651.
- Lopez, D., Bronner, G., Brunel, N., Auguin, D., Bourgerie, S., Brignolas, F., Carpin, S., Tournaire-Roux, C., Maurel, C., Fumanal, B., Martin, F., Sakr, S., Label, P., Julien, J.L., Gousset-Dupont, A., and Venisse, J.S.** (2012).

REFERENCES

- Insights into Populus XIP aquaporins: evolutionary expansion, protein functionality, and environmental regulation. *J Exp Bot* **63**: 2217-2230.
- Luu, D.T., and Maurel, C.** (2013). Aquaporin trafficking in plant cells: an emerging membrane-protein model. *Traffic* **14**: 629-635.
- Luu, D.T., Martinière, A., Sorieul, M., Runions, J., and Maurel, C.** (2012). Fluorescence recovery after photobleaching reveals high cycling dynamics of plasma membrane aquaporins in *Arabidopsis* roots under salt stress. *Plant J* **69**: 894-905.
- Ma, J.F., Tamai, K., Yamaji, N., Mitani, N., Konishi, S., Katsuhara, M., Ishiguro, M., Murata, Y., and Yano, M.** (2006). A silicon transporter in rice. *Nature* **440**: 688-691.
- MacRobbie, E.A.** (2006). Osmotic effects on vacuolar ion release in guard cells. *Proc Natl Acad Sci U S A* **103**: 1135-1140.
- Martinière, A., Li, X., Runions, J., Lin, J., Maurel, C., and Luu, D.T.** (2012). Salt stress triggers enhanced cycling of *Arabidopsis* root plasma-membrane aquaporins. *Plant Signal Behav* **7**: 529-532.
- Matsumoto, T., Lian, H.L., Su, W.A., Tanaka, D., Liu, C., Iwasaki, I., and Kitagawa, Y.** (2009). Role of the aquaporin PIP1 subfamily in the chilling tolerance of rice. *Plant Cell Physiol* **50**: 216-229.
- Maurel, C.** (2007). Plant aquaporins: novel functions and regulation properties. *FEBS Lett* **581**: 2227-2236.
- Maurel, C., Verdoucq, L., Luu, D.T., and Santoni, V.** (2008). Plant aquaporins: membrane channels with multiple integrated functions. *Annu Rev Plant Biol* **59**: 595-624.
- Merl, J., Ueffing, M., Hauck, S.M., and von Toerne, C.** (2012). Direct comparison of MS-based label-free and SILAC quantitative proteome profiling strategies in primary retinal Muller cells. *Proteomics* **12**: 1902-1911.
- Michaeli, S., and Galili, G.** (2014). Degradation of organelles or specific organelle components via selective autophagy in plant cells. *Int J Mol Sci* **15**: 7624-7638.
- Miller, E.A., Beilharz, T.H., Malkus, P.N., Lee, M.C., Hamamoto, S., Orci, L., and Schekman, R.** (2003). Multiple cargo binding sites on the COPII subunit Sec24p ensure capture of diverse membrane proteins into transport vesicles. *Cell* **114**: 497-509.
- Mintseris, J., and Weng, Z.** (2005). Structure, function, and evolution of transient and obligate protein-protein interactions. *Proc Natl Acad Sci U S A* **102**: 10930-10935.
- Mitsuoka, K., Murata, K., Walz, T., Hirai, T., Agre, P., Heymann, J.B., Engel, A., and Fujiyoshi, Y.** (1999). The structure of aquaporin-1 at 4.5-Å resolution reveals short alpha-helices in the center of the monomer. *J Struct Biol* **128**: 34-43.

- Mizutani, M., Watanabe, S., Nakagawa, T., and Maeshima, M.** (2006). Aquaporin NIP2;1 is mainly localized to the ER membrane and shows root-specific accumulation in *Arabidopsis thaliana*. *Plant Cell Physiol* **47**: 1420-1426.
- Moeller, H.B., Aroankins, T.S., Slengerik-Hansen, J., Pisitkun, T., and Fenton, R.A.** (2014). Phosphorylation and ubiquitylation are opposing processes that regulate endocytosis of the water channel aquaporin-2. *J Cell Sci* **127**: 3174-3183.
- Monneuse, J.M., Sugano, M., Becue, T., Santoni, V., Hem, S., and Rossignol, M.** (2011). Towards the profiling of the *Arabidopsis thaliana* plasma membrane transportome by targeted proteomics. *Proteomics* **11**: 1789-1797.
- Moshelion, M., Becker, D., Biela, A., Uehlein, N., Hedrich, R., Otto, B., Levi, H., Moran, N., and Kaldenhoff, R.** (2002). Plasma membrane aquaporins in the motor cells of *Samanea saman*: diurnal and circadian regulation. *Plant Cell* **14**: 727-739.
- Müller, D.J., Janovjak, H., Lehto, T., Kuerschner, L., and Anderson, K.** (2002). Observing structure, function and assembly of single proteins by AFM. *Prog Biophys Mol Biol* **79**: 1-43.
- Murata, K., Mitsuoka, K., Hirai, T., Walz, T., Agre, P., Heymann, J.B., Engel, A., and Fujiyoshi, Y.** (2000). Structural determinants of water permeation through aquaporin-1. *Nature* **407**: 599-605.
- Mustroph, A., Juntawong, P., and Bailey-Serres, J.** (2009a). Isolation of plant polysomal mRNA by differential centrifugation and ribosome immunopurification methods. *Methods Mol Biol* **553**: 109-126.
- Mustroph, A., Zanetti, M.E., Girke, T., and Bailey-Serres, J.** (2013). Isolation and analysis of mRNAs from specific cell types of plants by ribosome immunopurification. *Methods Mol Biol* **959**: 277-302.
- Mustroph, A., Zanetti, M.E., Jang, C.J., Holtan, H.E., Repetti, P.P., Galbraith, D.W., Girke, T., and Bailey-Serres, J.** (2009b). Profiling translatoemes of discrete cell populations resolves altered cellular priorities during hypoxia in *Arabidopsis*. *Proc Natl Acad Sci U S A* **106**: 18843-18848.
- Mut, P., Bustamante, C., Martínez, G., Alleva, K., Sutka, M., Civello, M., and Amodeo, G.** (2008). A fruit-specific plasma membrane aquaporin subtype PIP1;1 is regulated during strawberry (*Fragaria x ananassa*) fruit ripening. *Physiol Plant* **132**: 538-551.
- Nawy, T., Lee, J.Y., Colinas, J., Wang, J.Y., Thongrod, S.C., Malamy, J.E., Birnbaum, K., and Benfey, P.N.** (2005). Transcriptional profile of the *Arabidopsis* root quiescent center. *Plant Cell* **17**: 1908-1925.
- Neely, J.D., Christensen, B.M., Nielsen, S., and Agre, P.** (1999). Heterotetrameric composition of aquaporin-4 water channels. *Biochemistry* **38**: 11156-11163.
- Nyblom, M., Frick, A., Wang, Y., Ekvall, M., Hallgren, K., Hedfalk, K., Neutze, R., Tajkhorshid, E., and Törnroth-Horsefield, S.** (2009). Structural and

REFERENCES

- functional analysis of SoPIP2;1 mutants adds insight into plant aquaporin gating. *J Mol Biol* **387**: 653-668.
- Obayashi, T., Okamura, Y., Ito, S., Tadaka, S., Aoki, Y., Shirota, M., and Kinoshita, K.** (2014). ATTED-II in 2014: evaluation of gene coexpression in agriculturally important plants. *Plant Cell Physiol* **55**: e6.
- Ofran, Y., and Rost, B.** (2007). ISIS: interaction sites identified from sequence. *Bioinformatics* **23**: e13-16.
- Otto, B., Uehlein, N., Sdorra, S., Fischer, M., Ayaz, M., Belastegui-Macadam, X., Heckwolf, M., Lachnit, M., Pede, N., Priem, N., Reinhard, A., Siegfart, S., Urban, M., and Kaldenhoff, R.** (2010). Aquaporin tetramer composition modifies the function of tobacco aquaporins. *J Biol Chem* **285**: 31253-31260.
- Park, W., Scheffler, B.E., Bauer, P.J., and Campbell, B.T.** (2010). Identification of the family of aquaporin genes and their expression in upland cotton (*Gossypium hirsutum* L.). *BMC Plant Biol* **10**: 142.
- Peret, B., Li, G., Zhao, J., Band, L.R., Voss, U., Postaire, O., Luu, D.T., Da Ines, O., Casimiro, I., Lucas, M., Wells, D.M., Lazzerini, L., Nacry, P., King, J.R., Jensen, O.E., Schäffner, A.R., Maurel, C., and Bennett, M.J.** (2012). Auxin regulates aquaporin function to facilitate lateral root emergence. *Nat Cell Biol* **14**: 991-998.
- Pham, T.V., and Jimenez, C.R.** (2012). An accurate paired sample test for count data. *Bioinformatics* **28**: i596-i602.
- Postaire, O., Tournaire-Roux, C., Grondin, A., Boursiac, Y., Morillon, R., Schäffner, A.R., and Maurel, C.** (2010). A PIP1 aquaporin contributes to hydrostatic pressure-induced water transport in both the root and rosette of *Arabidopsis*. *Plant Physiol* **152**: 1418-1430.
- Prado, K., Boursiac, Y., Tournaire-Roux, C., Monneuse, J.M., Postaire, O., Da Ines, O., Schäffner, A.R., Hem, S., Santoni, V., and Maurel, C.** (2013). Regulation of *Arabidopsis* leaf hydraulics involves light-dependent phosphorylation of aquaporins in veins. *Plant Cell* **25**: 1029-1039.
- Prak, S., Hem, S., Boudet, J., Viennois, G., Sommerer, N., Rossignol, M., Maurel, C., and Santoni, V.** (2008). Multiple phosphorylations in the C-terminal tail of plant plasma membrane aquaporins: role in subcellular trafficking of AtPIP2;1 in response to salt stress. *Mol Cell Proteomics* **7**: 1019-1030.
- Preston, G.M., and Agre, P.** (1991). Isolation of the cDNA for erythrocyte integral membrane protein of 28 kilodaltons: member of an ancient channel family. *Proc Natl Acad Sci U S A* **88**: 11110-11114.
- Preston, G.M., Carroll, T.P., Guggino, W.B., and Agre, P.** (1992). Appearance of water channels in *Xenopus* oocytes expressing red cell CHIP28 protein. *Science* **256**: 385-387.
- Proud, C.G.** (2007). Signalling to translation: how signal transduction pathways control the protein synthetic machinery. *Biochem J* **403**: 217-234.

- Quigley, F., Rosenberg, J.M., Shachar-Hill, Y., and Bohnert, H.J.** (2002). From genome to function: the *Arabidopsis* aquaporins. *Genome Biol* **3**: RESEARCH0001.
- Ray, P.M.** (1960). On the Theory of Osmotic Water Movement. *Plant Physiol* **35**: 783-795.
- Robinson, D.G., Jiang, L., and Schumacher, K.** (2008). The endosomal system of plants: charting new and familiar territories. *Plant Physiol* **147**: 1482-1492.
- Robinson, D.G., Sieber, H., Kammerloher, W., and Schäffner, A.R.** (1996). PIP1 Aquaporins Are Concentrated in Plasmalemmasomes of *Arabidopsis thaliana* Mesophyll. *Plant Physiol* **111**: 645-649.
- Ruggiano, A., Foresti, O., and Carvalho, P.** (2014). Quality control: ER-associated degradation: protein quality control and beyond. *J Cell Biol* **204**: 869-879.
- Sade, N., Vinocur, B.J., Diber, A., Shatil, A., Ronen, G., Nissan, H., Wallach, R., Karchi, H., and Moshelion, M.** (2009). Improving plant stress tolerance and yield production: is the tonoplast aquaporin SITIP2;2 a key to isohydric to anisohydric conversion? *New Phytol* **181**: 651-661.
- Santoni, V., Vinh, J., Pflieger, D., Sommerer, N., and Maurel, C.** (2003). A proteomic study reveals novel insights into the diversity of aquaporin forms expressed in the plasma membrane of plant roots. *Biochem J* **373**: 289-296.
- Santoni, V., Verdoucq, L., Sommerer, N., Vinh, J., Pflieger, D., and Maurel, C.** (2006). Methylation of aquaporins in plant plasma membrane. *Biochem J* **400**: 189-197.
- Sato, K., and Nakano, A.** (2003). Oligomerization of a cargo receptor directs protein sorting into COPII-coated transport vesicles. *Mol Biol Cell* **14**: 3055-3063.
- Schäffner, A.R.** (1998). Aquaporin function, structure, and expression: are there more surprises to surface in water relations? *Planta* **204**: 131-139.
- Schuck, S., Gallagher, C.M., and Walter, P.** (2014). ER-phagy mediates selective degradation of endoplasmic reticulum independently of the core autophagy machinery. *J Cell Sci* **127**: 4078-4088.
- Shahollari, B., Varma, A., and Oelmuller, R.** (2005). Expression of a receptor kinase in *Arabidopsis* roots is stimulated by the basidiomycete *Piriformospora indica* and the protein accumulates in Triton X-100 insoluble plasma membrane microdomains. *J Plant Physiol* **162**: 945-958.
- Snapp, E.L., Hegde, R.S., Francolini, M., Lombardo, F., Colombo, S., Pedrazzini, E., Borgese, N., and Lippincott-Schwartz, J.** (2003). Formation of stacked ER cisternae by low affinity protein interactions. *J Cell Biol* **163**: 257-269.
- Sorieul, M., Santoni, V., Maurel, C., and Luu, D.T.** (2011). Mechanisms and effects of retention of over-expressed aquaporin AtPIP2;1 in the endoplasmic reticulum. *Traffic* **12**: 473-482.

- Soto, G., Alleva, K., Amodeo, G., Muschietti, J., and Ayub, N.D.** (2012). New insight into the evolution of aquaporins from flowering plants and vertebrates: orthologous identification and functional transfer is possible. *Gene* **503**: 165-176.
- Springer, S., Malkus, P., Borchert, B., Wellbrock, U., Duden, R., and Schekman, R.** (2014). Regulated oligomerization induces uptake of a membrane protein into COPII vesicles independent of its cytosolic tail. *Traffic* **15**: 531-545.
- Steudle, E.** (2000). Water uptake by roots: effects of water deficit. *J Exp Bot* **51**: 1531-1542.
- Steudle, E.** (2001). THE COHESION-TENSION MECHANISM AND THE ACQUISITION OF WATER BY PLANT ROOTS. *Annu Rev Plant Physiol Plant Mol Biol* **52**: 847-875.
- Steudle, E., and Peterson, C.** (1998). How does water get through roots. *J. exp. Bot* **49**: 775-788.
- Suga, S., Murai, M., Kuwagata, T., and Maeshima, M.** (2003). Differences in aquaporin levels among cell types of radish and measurement of osmotic water permeability of individual protoplasts. *Plant Cell Physiol* **44**: 277-286.
- Sui, H., Han, B.G., Lee, J.K., Walian, P., and Jap, B.K.** (2001). Structural basis of water-specific transport through the AQP1 water channel. *Nature* **414**: 872-878.
- Takano, J., Wada, M., Ludewig, U., Schaaf, G., von Wirén, N., and Fujiwara, T.** (2006). The *Arabidopsis* major intrinsic protein NIP5;1 is essential for efficient boron uptake and plant development under boron limitation. *Plant Cell* **18**: 1498-1509.
- Tamma, G., Robben, J.H., Trimpert, C., Boone, M., and Deen, P.M.** (2011). Regulation of AQP2 localization by S256 and S261 phosphorylation and ubiquitination. *Am J Physiol Cell Physiol* **300**: C636-646.
- Temmei, Y., Uchida, S., Hoshino, D., Kanzawa, N., Kuwahara, M., Sasaki, S., and Tsuchiya, T.** (2005). Water channel activities of *Mimosa pudica* plasma membrane intrinsic proteins are regulated by direct interaction and phosphorylation. *FEBS Lett* **579**: 4417-4422.
- Törnroth-Horsefield, S., Wang, Y., Hedfalk, K., Johanson, U., Karlsson, M., Tajkhorshid, E., Neutze, R., and Kjellbom, P.** (2006). Structural mechanism of plant aquaporin gating. *Nature* **439**: 688-694.
- Tournaire-Roux, C., Sutka, M., Javot, H., Gout, E., Gerbeau, P., Luu, D.T., Bligny, R., and Maurel, C.** (2003). Cytosolic pH regulates root water transport during anoxic stress through gating of aquaporins. *Nature* **425**: 393-397.
- Uehlein, N., Lovisolo, C., Siefritz, F., and Kaldenhoff, R.** (2003). The tobacco aquaporin NtAQP1 is a membrane CO₂ pore with physiological functions. *Nature* **425**: 734-737.

- Uehlein, N., Sperling, H., Heckwolf, M., and Kaldenhoff, R.** (2012). The *Arabidopsis* aquaporin PIP1;2 rules cellular CO₂ uptake. *Plant Cell Environ* **35**: 1077-1083.
- Uehlein, N., Otto, B., Hanson, D.T., Fischer, M., McDowell, N., and Kaldenhoff, R.** (2008). Function of *Nicotiana tabacum* aquaporins as chloroplast gas pores challenges the concept of membrane CO₂ permeability. *Plant Cell* **20**: 648-657.
- Van Leene, J., Stals, H., Eeckhout, D., Persiau, G., Van De Slijke, E., Van Isterdael, G., De Clercq, A., Bonnet, E., Laukens, K., Remmerie, N., Henderickx, K., De Vijlder, T., Abdelkrim, A., Pharazyn, A., Van Onckelen, H., Inze, D., Witters, E., and De Jaeger, G.** (2007). A tandem affinity purification-based technology platform to study the cell cycle interactome in *Arabidopsis thaliana*. *Mol Cell Proteomics* **6**: 1226-1238.
- Vandeleur, R.K., Mayo, G., Shelden, M.C., Gilliam, M., Kaiser, B.N., and Tyerman, S.D.** (2009). The role of plasma membrane intrinsic protein aquaporins in water transport through roots: diurnal and drought stress responses reveal different strategies between isohydric and anisohydric cultivars of grapevine. *Plant Physiol* **149**: 445-460.
- Vander Willigen, C., Postaire, O., Tournaire-Roux, C., Boursiac, Y., and Maurel, C.** (2006). Expression and inhibition of aquaporins in germinating *Arabidopsis* seeds. *Plant Cell Physiol* **47**: 1241-1250.
- Vandesompele, J., De Preter, K., Pattyn, F., Poppe, B., Van Roy, N., De Paepe, A., and Speleman, F.** (2002). Accurate normalization of real-time quantitative RT-PCR data by geometric averaging of multiple internal control genes. *Genome Biol* **3**: Research0034.
- Vanzo, E., Ghirardo, A., Merl-Pham, J., Lindermayr, C., Heller, W., Hauck, S.M., Durner, J., and Schnitzler, J.P.** (2014). S-nitroso-proteome in poplar leaves in response to acute ozone stress. *PLoS One* **9**: e106886.
- Verdoucq, L., Grondin, A., and Maurel, C.** (2008). Structure-function analysis of plant aquaporin AtPIP2;1 gating by divalent cations and protons. *Biochem J* **415**: 409-416.
- Verkman, A.S., and Mitra, A.K.** (2000). Structure and function of aquaporin water channels.
- Walter, P., and Ron, D.** (2011). The unfolded protein response: from stress pathway to homeostatic regulation. *Science* **334**: 1081-1086.
- Wang, P., Hummel, E., Osterrieder, A., Meyer, A.J., Frigerio, L., Sparkes, I., and Hawes, C.** (2011). KMS1 and KMS2, two plant endoplasmic reticulum proteins involved in the early secretory pathway. *Plant J* **66**: 613-628.
- Wang, Y., Cohen, J., Boron, W.F., Schulten, K., and Tajkhorshid, E.** (2007). Exploring gas permeability of cellular membranes and membrane channels with molecular dynamics. *J Struct Biol* **157**: 534-544.

- Weig, A., Deswarte, C., and Chrispeels, M.J.** (1997). The major intrinsic protein family of *Arabidopsis* has 23 members that form three distinct groups with functional aquaporins in each group. *Plant Physiol* **114**: 1347-1357.
- Wiśniewski, J.R., Zougman, A., Nagaraj, N., and Mann, M.** (2009). Universal sample preparation method for proteome analysis. *Nat Methods* **6**: 359-362.
- Wu, F.H., Shen, S.C., Lee, L.Y., Lee, S.H., Chan, M.T., and Lin, C.S.** (2009). Tape-*Arabidopsis* Sandwich - a simpler *Arabidopsis* protoplast isolation method. *Plant Methods* **5**: 16.
- Yanef, A., Sigaut, L., Marquez, M., Alleva, K., Pietrasanta, L.I., and Amodeo, G.** (2014). Heteromerization of PIP aquaporins affects their intrinsic permeability. *Proc Natl Acad Sci U S A* **111**: 231-236.
- Yoo, S.D., Cho, Y.H., and Sheen, J.** (2007). *Arabidopsis* mesophyll protoplasts: a versatile cell system for transient gene expression analysis. *Nat Protoc* **2**: 1565-1572.
- Yool, A.J., and Weinstein, A.M.** (2002). New roles for old holes: ion channel function in aquaporin-1. *News Physiol Sci* **17**: 68-72.
- Zanetti, M.E., Chang, I.F., Gong, F., Galbraith, D.W., and Bailey-Serres, J.** (2005). Immunopurification of polyribosomal complexes of *Arabidopsis* for global analysis of gene expression. *Plant Physiol* **138**: 624-635.
- Zelazny, E., Miecielica, U., Borst, J.W., Hemminga, M.A., and Chaumont, F.** (2009). An N-terminal diacidic motif is required for the trafficking of maize aquaporins ZmPIP2;4 and ZmPIP2;5 to the plasma membrane. *Plant J* **57**: 346-355.
- Zelazny, E., Borst, J.W., Muylaert, M., Batoko, H., Hemminga, M.A., and Chaumont, F.** (2007). FRET imaging in living maize cells reveals that plasma membrane aquaporins interact to regulate their subcellular localization. *Proc Natl Acad Sci U S A* **104**: 12359-12364.
- Zhao, J.** (2013). Roles of PIP aquaporins in lateral root development and stress responses in *Arabidopsis thaliana*, (Imu).
- Zuo, J., Niu, Q.W., and Chua, N.H.** (2000). Technical advance: An estrogen receptor-based transactivator XVE mediates highly inducible gene expression in transgenic plants. *Plant J* **24**: 265-273.

ACKNOWLEDGEMENTS

First and foremost, I would like to thank my supervisor PD Dr. Anton R. Schäffner for his excellent guidance and permanent support during my whole PhD study. His invaluable constructive criticism, aspiring advice and encouragement always supported me facing all the difficulties in this work. Moreover, his broad knowledge, scientific enthusiasm and rigorous scientific attitude have deeply inspired and encouraged me for pursuing the future scientific career.

I am sincerely grateful to Prof. Dr. Jörg Durner, Prof. Dr. Klaus Förstemann and PD Dr. Dietmar E. Martin and the other members of the examination committee for their willingness to review this work. I would like to especially acknowledge to Prof. Dr. Jörg Durner's support and valuable advices to my projects during three thesis committee meetings and our Tuesday institute seminars.

I am deeply thankful to Dr. Olivier Da Ines. This thesis would not have been possible without the initial work done by him. I am very much grateful also to Dr. Jin Zhao for the excellent cooperative work with mass spectrometry. Her valuable advices supported me to carry on this project. I also would like to thank Dr. Elisabeth Georgii for statistical analyses and statistical advices. Many thanks to Jessica Lutterbach for providing her kind help at the end of my PhD work. I wish to express my sincere thanks to Birgit Geist. Without her excellent assistance to ELISA quantification, this work would never have been finished.

Thanks also to Dr. Corina Vlot for providing the valuable plasmids. I wish to thank Dr. Sanjukta Dey for sharing the experience and providing kind help in ribosome isolation. I would also like to thank Dr. Angelika Mustroph for her valuable discussion related to ribosome experiments. My thanks also go to Mr. Andreas Voss and Dr. Jan Erik Heil for introducing me to the confocal laser scanning microscope and providing access as well as help with the Zen software, respectively. I also wish

ACKNOWLEDGEMENTS

to express my thanks to all of the students who contributed to this work in different aspects during their practical course.

I wish to express my warm and sincere gratitude to Dr. Stephan Dräxl for providing the scientific suggestion on protoplast isolation and for his excellent advice and critical reading and correction of this work. Thanks also go to Dr. Günter Bahnweg for English proofreading of this work. My special thanks go to Karoline Stoll for her kind help with documents and for providing the office supplies, whatever I needed. Thanks also go to Evi Bieber for fixing all kinds of computer problems.

I would also like to thank Ming Jin for scientific discussions and encouragement through my PdD. My thanks also go to Dr. Wei Zhang for valuable advices and open discussions. Special thanks also go to Rafał Maksym for his positive life attitude towards everything, thereby inspiring and encouraging me to fight with difficulties. I am thankful to Azam Shekariesfahlan for her support during my whole thesis writing. I am thankful to Dr. Werner Heller for several interesting discussions about the science and beyond. Special thanks go to all other former and current BIOP colleagues for several advices, interesting discussions and useful life tips, including Dr. Ruohe Yin, Dr. Malay Das, Dr. Veronica von Saint Paul, Kerstin Schuster, Dr. Gitto Kuruthukulangarakoola, Dr. Antonie Sophie Bernhard, Dr. Feng Zhao, Dr. Izabella Kovacs, Alexander Mengel, Felicitas Groß, Alexandra Ageeva, Eva Esther König and all other BIOP and EUS colleagues. I wish to express my sincere appreciation to my other friends in Germany: Jian, Weijia, Xin and so on, who have supported and encouraged me during the hard times of my PhD.

I would also like to thank the 'China Scholarship Council' (CSC) and Helmholtz Zentrum München for their financial support.

Finally, I want to thank all my friends and family in China. Especially deepest gratitude to my parents and my sister Jia for their endless love and support.

CURRICULUM VITAE

Name: Chen Liu
Date of birth: 15/06/1985
Place of birth: Hunan, China
Nationality: Chinese

EDUCATION & RESEARCH EXPERIENCES

- 10/2010-now Graduate student in Biochemistry at Ludwig-Maximilians Universität, München, Germany
Research topic: The PIP1 protein expression is positively regulated by PIP2;1 and PIP2;2 in *Arabidopsis thaliana*.
Supervisor: PD Dr. Anton Schäffner, Institute of Biochemical Plant Pathology, Helmholtz Zentrum München, Neuherberg, Germany
- 09/2007-08/2010 Master in Genetics at Sun Yat-Sen University, China
Research topic: Gene Clone and Function Analysis of a Peanut Lysophosphatidic acid Acyltransferase.
Supervisor: Prof. Shangzhi Huang, Department of Bioscience, Sun Yat-Sen University, China
- 09/2003-06/2007 Bachelor in Biology at Hunan Agricultural University, China
Research topic: The Random Mutagenesis Studies on β -1, 4-D-Mannanase Gene by PCR.
Supervisor: Prof. Xuwen Zhang, Department of Bioscience, Hunan Agricultural University, China
- 09/2004-10/2006 Undergraduate Graduation Program at Hunan Agricultural University, China
Supervisor: Dr. Yuanshan Lin, Department of Bioscience, Hunan Agricultural University, China

FELLOWSHIP

- 10/2010-09/2014 China Scholarship Council (CSC)
- 09/2007-06/2010 Sun Yat-sen Graduate Scholarship
- 11/2006 Provincial Government Scholarship of Hunan

PUBLICATIONS

Liu, Chen., Olivier, Da Ines., Zhao, Jin., Geist, Birgit., Lutterbach Jessica., Jin, Ming., Juliane Merl-Pham., Georgii, Elisabeth., Schäffner AR: The PIP1 protein expression is positively regulated by PIP2;1 and PIP2;2 in *Arabidopsis thaliana* (Manuscript in preparation).

Zhou, Y., Tan, B., Luo, M., Li, Y., **Liu, C.**, Chen, C., Yu, C.W., Yang, S., Dong, S., Ruan, J., Yuan, L., Zhang, Z., Zhao, L., Li, C., Chen, H., Cui, Y., Wu, K., and Huang, S. (2013): HISTONE DEACETYLASE19 interacts with HSL1 and participates in the repression of seed maturation genes in *Arabidopsis* seedlings. *Plant cell* 25: 134-148.

MEETING/WORKSHOP PRESENTATIONS

Liu, Chen., Jin, Ming., Olivier, Da Ines., Zhao, Jin., Geist, Birgit., Georgii, Elisabeth., Winkler, J. Barbro., Schäffner, AR: Loss of two major PIP2 isoforms leads to additional repression of PIP1 proteins but only to a limited impact on plant water relations. 9th Tri-National *Arabidopsis* Meeting, Heidelberg (Germany), September, 2014 (Poster presentation).

Attendance of 5th plant NO club meeting, Munich (Germany), July, 2014.

Attendance of conference "Plant Biology for the Next Generation", the International Symposium of the SFB924 "Molecular mechanisms regulating yield and yield stability in plants", Freising (Germany), September, 2013.